
Characterisation of synaptic proteins and their complexes using structural mass spectrometry

Dissertation
zur Erlangung des
Doktorgrades der Naturwissenschaften (Dr. rer. nat.)

der
Naturwissenschaftlichen Fakultät I
- Biowissenschaften -
der Martin-Luther-Universität
Halle-Wittenberg,

vorgelegt
von Frau **Julia Bieber**, geb. Hesselbarth

eingereicht am: 09.12.2024

verteidigt am: 09.05.2025

Gutachter*innen:

1. Prof. Dr. Carla Schmidt, Johannes-Gutenberg-Universität Mainz
2. Prof. Dr. Jochen Balbach, Martin-Luther-Universität Halle-Wittenberg
3. Prof. Dr. Nina Morgner, Goethe-Universität Frankfurt am Main

Table of contents

List of abbreviations	IV
List of figures	VII
List of tables	IX
Zusammenfassung	XI
Summary	XIII
1 Introduction	1
1.1 SNARE complex-mediated signal transmission in neurons	1
1.1.1 Synaptic exocytosis.....	1
1.1.2 SNARE proteins – the key players of membrane fusion	2
1.1.3 Regulation of SNARE complex assembly by Cpx1	7
1.2 Mass spectrometry for structure elucidation of proteins.....	9
1.2.1 Identification of proteins by MS	9
1.2.2 Chemical cross-linking combined with MS.....	12
1.2.3 Native MS	14
1.3 Aim of the study	17
2 Materials and methods	19
2.1 Materials	19
2.1.1 Chemicals	19
2.1.2 Consumables	20
2.1.3 Ready-to-use kits, solutions and buffers.....	21
2.1.4 Antibodies	21
2.1.5 Enzymes	21
2.1.6 Lipids	22
2.1.7 Plasmids and proteins	22
2.1.8 Instruments	23
2.1.9 Software.....	23
2.2 Molecular biological methods	24
2.2.1 Transformation of <i>Escherichia coli</i> cells.....	24
2.2.2 Cell culture and protein expression	24
2.3 Protein biochemical methods	25
2.3.1 Cell lysis.....	25
2.3.2 Protein purification of SNARE proteins	25
2.3.3 Protein purification of Cpx1	27
2.3.4 Determination of the protein concentration	28

2.3.5	Formation of protein complexes	29
2.3.6	Gel electrophoresis and western blotting.....	29
2.3.7	Chemical cross-linking	30
2.3.8	Lipid overlay assay.....	30
2.3.9	Preparation of proteoliposomes and flotation assay	31
2.4	Biophysical methods	32
2.4.1	Circular dichroism (CD) spectroscopy	32
2.4.2	Dynamic light scattering (DLS).....	32
2.5	Mass spectrometric methods	33
2.5.1	Precipitation with ethanol	33
2.5.2	In-solution hydrolysis of (cross-linked) proteins	33
2.5.3	Enrichment of cross-linked peptide pairs.....	33
2.5.4	LC-MS/MS analysis.....	34
2.5.5	Native MS	35
2.6	Database search and data analysis	35
2.6.1	Identification of proteins	35
2.6.2	Identification of cross-linked peptide pairs.....	36
2.6.3	Validation of identified cross-linking sites	36
2.6.4	SNARE:Cpx1 model building.....	37
2.6.5	Analysis of native mass spectra	37
2.6.6	Data availability	37
2.6.7	Statistics and Reproducibility.....	38
3	Results	39
3.1	Expression, purification and identification of SNARE proteins and Cpx1	39
3.2	Structural characterisation of individual synaptic proteins in solution.....	42
3.2.1	Oligomerisation of different Synaptobrevin-2 variants.....	42
3.2.2	Structural characterisation of SNAP25(CtoS)	45
3.2.3	Characterisation of Stx(1-262) in 'open' and 'closed' conformation.....	49
3.2.4	Oligomerisation of the SNARE regulator Cpx1	53
3.3	Assembly of the SNARE complex and its regulation by Cpx1	55
3.3.1	Formation of binary complexes and reorganisation into the SNARE complex..	55
3.3.2	Characterising interactions of Cpx1 with the SNARE proteins	67
3.4	Structural characterisation of Syb(1-96) and Cpx1 in a lipid environment.....	76
3.4.1	Interactions of Syb(1-96) with lipids.....	76
3.4.2	Interactions of Cpx1 with lipids	80
4	Discussion and outlook	84

4.1	Methodological aspects.....	84
4.2	Structural characterisation of individual synaptic proteins	88
4.3	Analysis of the SNARE complex assembly	91
4.4	Interactions of Cpx1 with SNARE proteins.	98
4.5	Structural characterisation of synaptic proteins in lipid environment.....	101
5	References.....	104
6	Supplement.....	121
	Acknowledgment.....	160
	Curriculum vitae	161
	Publication list.....	163
	Affidavit.....	167

List of abbreviations

ACN	acetonitrile
AEC	anion exchange chromatography
AH	accessory helix
BS3	bis-(sulfosuccinimidyl) suberate
C8E4	tetraethylene glycol monoethyl ether
CD	circular dichroism
CEM	chain ejection model
CH	central helix
CHAPS	3-[(3-Cholamidopropyl)-dimethyl ammonio]-1-propane sulphonate
CID	collision-induced dissociation
CL	cardiolipin
Cpx1	complexin-1
CRM	charged residue model
CTD	C-terminal domain
DOPC	di-oleyl-phosphatidylcholine
DOPE	di-oleyl-phosphatidylethanolamine
DOPG	di-oleyl-phosphatidylglycerol
DOPS	di-oleyl-phosphatidylserine
DHSO	dihydrazide sulfoxide
DSSO	disuccinimidyl sulfoxide
DTT	dithiothreitol
EDC	1-ethyl-3-(3-dimethylaminopropyl)-carbodiimide
EDTA	ethylenediamine tetra acetic acid disodium dihydrate
EM	electron microscopy
EPR	electron paramagnetic resonance
ESI	electrospray ionisation
FA	formic acid
FAIMS	field asymmetric ion mobility spectrometry
FDR	false discovery rate
HCD	high-energy collisional dissociation
HEPES	4-(2-hydroxyethyl)-1-piperazine ethanesulfonic acid
HPLC	high-performance liquid chromatography
IEM	ion evaporation model
IMAC	immobilized metal affinity chromatography
IPTG	Isopropyl- β -D-thiogalactopyranoside

LC	liquid chromatography
LC-MS/MS	liquid chromatography-coupled mass spectrometry
MCP	multichannel plate
MES	2-(N morpholino)ethansulfonic acid
MS	mass spectrometry
Munc13	mammalian Unc-13
Munc18	mammalian Unc-18
m/z	mass-to-charge
NHS	N-hydroxysuccinimide
NMR	nuclear magnetic resonance
NSF	N-ethylmaleimide sensitive factor
NTD	N-terminal domain
PBS	phosphate buffered saline
PA	phosphatidic acid
PC	phosphatidylcholine
PE	phosphatidylethanolamine
PG	phosphatidylglycerol
PI	phosphatidylinositol
PI(4)P	phosphatidylinositol-(4)-phosphate
PI(4,5)P ₂	phosphatidylinositol-(4,5)-bisphosphate
PI(3,4,5)P ₃	phosphatidylinositol-(3,4,5)-trisphosphate
PMSF	phenylmethylsulphonyl fluoride
PS	phosphatidylserine
PSM	peptide spectrum match
SCX	strong cation exchange chromatography
SEC	size exclusion chromatography
α-SNAP	α-Soluble NSF attachment protein
SNAP25	synaptosome associated protein of 25 kDa
SNARE	soluble N-ethylmaleimide-sensitive-factor attachment receptor
Stx1	syntaxin-1
Syb2	synaptobrevin-2
Syt1	synaptotagmin-1
TFA	trifluoroacetic acid
TCEP	tris(2-carboxyethyl) phosphine hydrochloride
ToF	time-of-flight
Tween-20	polyoxyethylen-20-sorbitanmonolaurat
VAMP	vesicle associated membrane protein

One letter code of amino acids

alanine	A
arginine	R
asparagine	N
aspartic acid	D
cysteine	C
glutamic acid	E
glutamine	Q
glycine	G
histidine	H
isoleucine	I
leucine	L
lysine	K
methionine	M
phenylalanine	F
proline	P
serine	S
threonine	T
tryptophan	W
tyrosine	Y
valine	V

List of figures

Figure 1. Signal transmission in neurons.....	2
Figure 2. Structure of the SNARE complex.....	3
Figure 3. Mechanisms of SNARE complex formation.....	5
Figure 4. Structural properties of Syb2 in the presence of lipids.....	6
Figure 5. Structural properties and models for the regulatory mechanism of Cpx1.....	8
Figure 6. Protein identification workflow.....	10
Figure 7. Chemical cross-linking.....	12
Figure 8. Native MS workflow.....	15
Figure 9. Purification of Syb(1-96).....	40
Figure 10. SDS-PAGE and Western Blot of the protein variants.....	41
Figure 11. Oligomerisation of Syb2 variants.....	43
Figure 12. Secondary structure content of Syb2 variants.....	44
Figure 13. Cross-linking analysis of SNAP25(CtoS).....	45
Figure 14. Example spectra of SNAP25(CtoS) cross-links.....	47
Figure 15. Validation of inter- and intramolecular interactions of SNAP25(CtoS).....	48
Figure 16. Native MS and CD spectroscopy of SNAP25(CtoS).....	49
Figure 17. Cross-linking analysis of Stx(1-262).....	50
Figure 18. Validation of inter- and intramolecular interactions of Stx(1-262).....	51
Figure 19. Native MS and CD spectroscopy of Stx(1-262).....	52
Figure 20. Cross-linking analysis of Cpx1.....	53
Figure 21. Validation of inter- and intramolecular interactions of Cpx1.....	54
Figure 22. Native MS and CD spectroscopy of Cpx1.....	55
Figure 23. Formation and reorganisation of SNAP25(CtoS):Stx(1-262) complexes.....	56
Figure 24. Collision induced dissociation of the ternary SNARE complex.....	58
Figure 25. Formation and reorganisation of SNAP25(CtoS):Syb(1-96) complexes.....	59
Figure 26. Collision induced dissociation of SNAP25(CtoS):Syb(1-96) complexes.....	60
Figure 27. CD spectra of SNAP25(CtoS), Syb(1-96) and binary SNARE complexes.....	61
Figure 28. Complex formation involving SNAP25(1-83).....	63
Figure 29. Stabilisation of the binary Syb(1-96):Stx(1-262) complex by Cpx1.....	64
Figure 30. CD spectra of Stx(1-262), Syb(1-96) and binary SNARE complexes.....	65
Figure 31. Individual SNARE proteins do not interact with Cpx1.....	67
Figure 32. Binary complexes do not interact with Cpx1.....	68
Figure 33. Disassembly of SNARE complex oligomers by Cpx1.....	69
Figure 34. Collision induced dissociation of the SNARE:Cpx1 complex.....	70
Figure 35. Cross-linking analysis of the SNARE:Cpx1 complex.....	71

Figure 36. Validation of intermolecular interactions between SNARE proteins.	72
Figure 37. Validation of intermolecular interactions of Cpx1 within the SNARE:Cpx1 complex.	73
Figure 38. Model of the SNARE:Cpx1 complex.	75
Figure 39. Lipid overlay assay of Syb(1-96).....	77
Figure 40. Native MS of Syb(1-96) interacting with lipids of different classes.....	78
Figure 41. Binding of Syb(1-96) to liposomes.	79
Figure 42. Lipid overlay assay of Cpx1.....	80
Figure 43. Native MS of Cpx1 interacting with lipids of different classes.....	81
Figure 44. Binding of Cpx1 to liposomes.	83
Supplementary Figure 1. Plasmid map of pET28a.....	121
Supplementary Figure 2. Purification of Syb(FL).	122
Supplementary Figure 3. Purification of Stx(1-262).	123
Supplementary Figure 4. Purification of SNAP25(1-83).....	124
Supplementary Figure 5. Purification of SNAP25(CtoS).	125
Supplementary Figure 6. Purification of Cpx1.....	126
Supplementary Figure 7. Rearrangement of the ternary Syb(1-96):Stx(1-262):Cpx1 complex.	127
Supplementary Figure 8. DOPS and DOPE binding of Syb(1-96) analysed by native MS. .	128
Supplementary Figure 9. DOPG and DOPC binding of Syb(1-96) analysed by native MS..	129
Supplementary Figure 10. DOPS and DOPE binding of Cpx1 analysed by native MS.....	130
Supplementary Figure 11. DOPG and DOPC binding of Cpx1 analysed by native MS.	131

List of tables

Table 1. Plasmids and protein variants.....	22
Table 2. Composition of media for bacterial cultivation.....	25
Table 3. Buffers for purification of SNARE proteins.....	26
Table 4. Buffers for purification of Cpx1.....	27
Table 5. Protein properties of SNARE proteins and Cpx1.....	28
Table 6. Buffers and solutions for western blotting.....	30
Table 7. Buffers and solutions for lipid overlay assay.....	31
Table 8. Gradients for liquid-chromatography.....	34
Supplementary Table 1. Incubation ratios of SNARE proteins and Cpx1.....	132
Supplementary Table 2. Protein identification.....	133
Supplementary Table 3. Cross-links identified in SNAP25(CtoS).....	135
Supplementary Table 4. Cross-links identified in Stx(1-262).....	139
Supplementary Table 5. Cross-links identified in Cpx1.....	146
Supplementary Table 6. Cross-links identified in SNARE:Cpx1 complex.....	149

Zusammenfassung

Die Proteine Synaptobrevin-2 (Syb2), Syntaxin-1 (Stx1) und SNAP25 (engl. *synaptosome associated protein of 25 kDa*) bilden den sogenannten SNARE (engl. *soluble N-ethylmaleimide-sensitive-factor attachment receptor*)-Komplex, der die Signalweiterleitung zwischen Neuronen durch Exozytose synaptischer Vesikel vermittelt. Während der generelle Ablauf der SNARE-vermittelten Membranfusion bekannt ist, sind die Details der zugrundeliegenden Mechanismen weitestgehend ungeklärt. Dies beinhaltet die Bildung potenzieller Intermediate und möglicher „off-pathway“-Komplexe, die Interaktionen mit regulatorischen Proteinen wie Complexin-1 (Cpx1) sowie den Einfluss von Protein-Lipid- und Protein-Membran-Wechselwirkungen auf die SNARE-Assemblierung.

In dieser Arbeit wurden die einzelnen SNARE-Proteine, binäre SNARE-Teilkomplexe und Intermediate sowie der vollständig assemblierte SNARE-Komplex strukturell charakterisiert. Zudem wurden die Interaktionen mit Cpx1 in allen Phasen der SNARE-Assemblierung untersucht. Hierfür wurden lösliche Varianten der Proteine (Syb(1-96), Stx(1-262), SNAP25(CtoS)) in *Escherichia coli* exprimiert und aus diesen isoliert und gereinigt. Unter Verwendung der nativen Massenspektrometrie (MS) wurde die Bildung, Stöchiometrie und Stabilität von Oligomeren und Komplexen analysiert. Mittels chemischer Quervernetzung wurden anschließend die spezifischen Interaktionsstellen zwischen den interagierenden Proteinen identifiziert. Es konnte gezeigt werden, dass die einzelnen SNARE-Proteine Syb(1-96), SNAP25(CtoS) und Stx(1-262) sowie das regulatorische Protein Cpx1 in Abwesenheit von Interaktionspartnern multimerisieren. Die Proteine nehmen dabei keinen definierten Oligomerisierungszustand ein, sondern lagern sich „aggregationsähnlich“ zu Oligomeren zusammen. Die Analyse der Proteine mittels Zirkulardichroismus (engl. *circular dichroism*, CD)-Spektroskopie bestätigte, dass der Grad der Multimerisierung mit dem Gehalt an flexiblen Strukturen korreliert. Darüber hinaus wurden die Interaktionen zwischen Untereinheiten innerhalb der Homooligomere mittels chemischer Quervernetzung identifiziert. Die Validierung der Interaktionen durch Visualisierung in Strukturmodellen zeigte, dass sich die Untereinheiten in paralleler und antiparalleler Orientierung zusammenlagern. Für Stx(1-262) wurde zudem eine „offene“ als auch eine „geschlossene“ Konformation nachgewiesen. Des Weiteren wurden zur Analyse der Komplexbildung mehrere SNARE-Proteine miteinander inkubiert. Es wurde gezeigt, dass in Gegenwart eines weiteren SNAREs die Proteine bevorzugt miteinander interagieren und die Multimerisierung zugunsten der Komplexbildung aufgeben. Die gebildeten binären SNARE-Komplexe nehmen dabei eine Stöchiometrie ein, die den SNARE Komplex imitiert. Die Bildung helikaler Strukturen konnte mittels CD-Spektroskopie bestätigt werden. In Abwesenheit von Syb(1-96) wird die zur Verfügung stehende Bindestelle durch ein weiteres vorhandenes Stx(1-262)- oder SNAP25(CtoS)-Molekül eingenommen. Binäre Komplexe, an

denen Syb(1-96) beteiligt ist, beinhalten ausschließlich ein Syb(1-96)-Molekül. Diese Stöchiometrie konnte durch Variieren der Mischungsverhältnisse nicht beeinflusst werden. Die gebildeten Komplexe wiesen zudem eine unterschiedliche Stabilität auf, die durch das Dissoziieren der Komplexe ermittelt wurde. Während sich der Stx(1-262):SNAP25(CtoS)-Komplex stabil bildete, dissoziierte der Syb(1-96):SNAP25(CtoS)-Komplex bei vergleichbarer Kollisionsenergie. Syb(1-96) erwies sich insgesamt als die am schwächsten eingebaute Untereinheit. Ein binärer Komplex bestehend aus Syb(1-96) und Stx(1-262) konnte mittels nativer MS nicht erfasst werden. Durch Zugabe des jeweils dritten SNARE-Interaktionspartners konnten bestehende binäre Komplexe umgelagert werden, sodass sich in allen Fällen der SNARE-Komplex bildete. Native MS und chemisches Quervernetzen zeigten darüber hinaus, dass sich der SNARE-Komplex antiparallel zu Oligomeren zusammenlagert und die Interaktionen zwischen den Komplexen durch interagierende SNAP25-Moleküle hervorgerufen werden.

Bindungsanalysen von Cpx1 an einzelne SNARE-Proteine und binäre SNARE-Teilkomplexe zeigten, dass Cpx1 eine Interaktionsfläche, die durch Syb2 und Stx1 gebildet wird, benötigt. Interaktionen mit einzelnen SNARE-Proteinen oder binären Komplexen, die entweder Syb2 oder Stx1 enthalten, konnten nicht nachgewiesen werden. Jedoch wurde gezeigt, dass Cpx1 den binären Syb(1-96):Stx(1-262)-Teilkomplex stabilisiert und peripher an den SNARE-Komplex bindet, sodass die Multimerisierung des Komplexes inhibiert wird. Die identifizierten Interaktionen innerhalb des SNARE:Cpx1-Komplexes wurden in einem Model zusammengefasst und zeigen, dass Cpx1 den C-terminalen Teil des SNARE-Komplexes umklammert, wodurch die Bildung von Multimeren verhindert wird. Dadurch ergibt sich eine regulatorische Funktion von Cpx1 in den finalen Schritten der Assemblierung.

Zusätzlich zu den Proteininteraktionsstudien wurden mit Syb(1-96) und Cpx1 Lipidbindestudien durchgeführt, um Präferenzen für spezifische Lipide zu identifizieren. Hierfür wurde zunächst die Bindung an immobilisierte Lipide mittels Antikörperfärbung untersucht. Es zeigte sich, dass sowohl Syb(1-96) als auch Cpx1 bevorzugt mit negativ geladenen Lipiden, die einfach zugängliche Phosphatgruppen enthalten, interagieren. Durch Analyse der Bindungsaffinitäten der Proteine an gelöste Lipide mittels nativer MS sowie die Bindung an Lipidmembranen in Form von Liposomen, konnte die Präferenz von Syb(1-96) für negativ geladene Lipide bestätigt werden. Für Cpx1 wurde gezeigt, dass dieses auch zwitterionische Lipide mit hoher Affinität bindet und damit eine geringere Spezifität für Lipide aufweist.

Summary

The synaptic proteins Synaptobrevin-2 (Syb2), Syntaxin-1 (Stx1) and Synaptosome associated protein of 25 kDa (SNAP25) assemble into the soluble N-ethylmaleimide-sensitive-factor attachment receptor (SNARE) complex, which mediates signal transmission between neurons through exocytosis of synaptic vesicles. While the general sequence of SNARE-mediated membrane fusion is established, the exact underlying mechanisms are largely unknown. This includes the formation of potential intermediates and possible “off-pathway” complexes, the interactions with regulatory proteins such as Complexin-1 (Cpx1) as well as the influence of protein-lipid and protein-membrane interactions on the SNARE complex assembly.

In this thesis, individual SNARE proteins, binary SNARE sub-complexes and intermediates as well as the fully assembled SNARE complex were structurally characterised. In addition, interactions of the SNAREs with Cpx1 at all stages of the SNARE complex assembly were investigated. For this, soluble variants of the proteins (Syb(1-96), Stx(1-262), SNAP25(CtoS)) were expressed in *Escherichia coli*, isolated and purified. Using native mass spectrometry (MS), formation, stoichiometry and stability of oligomers and complexes were analysed. Specific interaction sites between the interacting proteins were further identified by chemical cross-linking. The individual SNARE proteins Syb(1-96), SNAP25(CtoS) and Stx(1-262) as well as the regulatory protein Cpx1 multimerised in the absence of interaction partners. The proteins do not adopt a defined oligomeric state but assemble into oligomers in an 'aggregation-like' manner. Analysis of the proteins using circular dichroism (CD) spectroscopy confirmed that the degree of multimerisation correlates with the intrinsic disorder of the proteins. In addition, using chemical cross-linking interactions between the subunits within the homooligomers were identified. Validation of the observed interactions using structure predictions revealed parallel and antiparallel orientations of the subunits. Furthermore, Stx(1-262) was shown to adopt both 'open' and 'closed' conformations. In addition, to analyse formation of complexes, SNARE proteins were incubated with each other. In the presence of an interaction partner, the SNAREs preferentially interact with each other forming complexes rather than multimers. The observed binary complexes adopt a stoichiometry resembling the SNARE complex. Formation of helical arrangements was further confirmed by CD spectroscopy. In the absence of Syb(1-96), the available binding site is occupied by an additional copy of Stx(1-262) or SNAP25(CtoS). Binary complexes involving Syb(1-96) exclusively incorporated only one Syb(1-96) molecule. This stoichiometry could not be challenged by varying protein mixing ratios. Furthermore, the stability of the complexes was determined by gas phase dissociation revealing that the Stx(1-262):SNAP25(CtoS) complex stably formed, while the Syb(1-96):SNAP25(CtoS) complex dissociated at comparable

dissociation energy. Syb(1-96) was shown to be the least stably integrated subunit. A binary complex composed of Syb(1-96) and Stx(1-262) was, however, not detected by native MS. Addition of the third SNARE interaction partner immediately rearranged existing binary complexes, thereby, forming the SNARE complex. Native MS and chemical cross-linking further revealed oligomerisation of the SNARE complex in antiparallel orientation resulting from interacting SNAP25 molecules.

When studying interactions between Cpx1 and individual SNARE proteins as well as binary SNARE sub-complexes, Cpx1 requires an interaction surface formed by Syb2 and Stx1. Interactions with individual SNAREs or binary complexes containing either Syb(1-96) or Stx(1-262) were not observed. However, Cpx1 stabilised the binary Syb(1-96):Stx(1-262) sub-complex and bound peripherally to the SNARE complex, thus, inhibiting multimerisation of the complex. The interaction sites identified within the SNARE:Cpx1 complex were visualised in a model revealing Cpx1 to clamp the C-terminal part of the SNARE core complex, thereby, preventing multimer formation. Accordingly, the regulatory function of Cpx1 takes place in the final steps of the SNARE complex assembly.

In addition to the protein interaction studies, lipid binding was analysed to identify preferences of Syb(1-96) and Cpx1 for specific lipids. First, binding to immobilised lipids was investigated using antibody staining revealing both, Syb(1-96) and Cpx1, to preferentially interact with negatively charged lipids containing accessible phosphate groups. Analysing the binding affinities of the proteins to solubilised lipids by native MS and validating the binding by making use of membranes in form of liposomes confirmed interactions of Syb(1-96) with negatively charged lipids. In the case of Cpx1, high-affinity binding to zwitterionic lipids was also observed suggesting a lower specificity for lipids.

1 Introduction¹

1.1 SNARE complex-mediated signal transmission in neurons

The nervous system is an interactive network of neurons that communicate via synapses. Most of the processes involved in neuronal signal transmission are still elusive and the underlying mechanisms such as formation of thoughts or storage of memories are still unknown. In addition, neurodegenerative diseases such as dementia are related to dysfunctional synaptic proteins. Elucidating the structures of synaptic proteins and their interactions in protein assemblies involved in signal transmission are, therefore, crucial to understand their function. Consequently, a deeper understanding of the overall pathway will be explored in this thesis.

1.1.1 Synaptic exocytosis

Signal transmission between neurons takes place at synapses, specialised neuronal contact sites, which are organised in the presynaptic and the postsynaptic nerve terminal separated by the synaptic cleft. For this, synaptic vesicles undergo a trafficking cycle resulting in fusion with the presynaptic membrane and release of neurotransmitters into the synaptic cleft (**Figure 1**) [2]. Synaptic vesicles are the storage organelles of neurotransmitters, which are densely packed with proteins of varying function. For instance, the neurotransmitter transporter VGlu1 mediates the uptake of glutamic acid into the vesicles driven by a proton gradient provided by the vesicular proton-pump V-ATPase, while Synaptotagmin-1 (Syt1) and Synaptobrevin-2 (Syb2) are directly involved in calcium-dependent membrane fusion [3]. During the trafficking cycle, synaptic vesicles migrate to the so-called 'active zone', a highly organised protein network that is directly located at the presynaptic membrane (**Figure 1**). The vesicles then dock at the presynaptic membrane in immediate vicinity of Ca²⁺ channels, thereby, forming a pool of readily releasable vesicles ('docking'), which are subsequently transferred into a fusion-competent state ('priming') (**Figure 1**) [2]. The soluble N-ethylmaleimide-sensitive-factor attachment receptor (SNARE) proteins as well as their regulators mammalian Unc-18 (Munc18) and Unc-13 (Munc13) are involved in this process. Upon arrival of an action potential, the plasma membrane depolarises leading to the influx of Ca²⁺ ions, which results in rapid membrane fusion [4]. The assembly of SNARE proteins forming the SNARE complex mediates fusion of the vesicles with the plasma membrane, which is additionally regulated by the calcium sensor Syt1 as well as Complexin-1 (Cpx1) [2]. Neurotransmitters are then released into the synaptic cleft and migrate to the postsynaptic

¹ Figures shown in this chapter are adopted from J. Hesselbarth, C. Schmidt (2022) *Disorder-to-order transition of Synaptobrevin-2: Tracing the conformational diversity of a synaptic SNARE protein*. *Journal of structural biology* 214 (1):107824 [1].

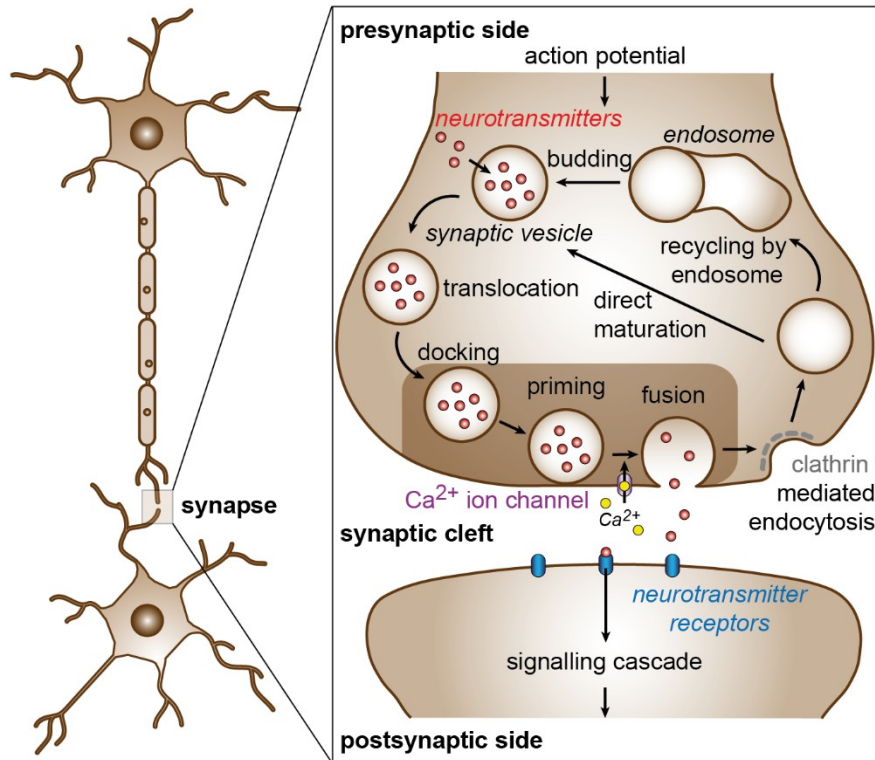


Figure 1. Signal transmission in neurons.

Synaptic vesicles are loaded with neurotransmitters (red circles) in the cytosol of the presynaptic terminal and migrate to the 'active zone' (brown shading), where they dock to the presynaptic membrane (docking) and are activated by SNARE complex assembly (priming). Upon arrival of an action potential, influx of Ca²⁺ ions (yellow circles) leads to fusion of the membranes resulting in release of neurotransmitters into the synaptic cleft. Neurotransmitters migrate to the postsynaptic terminal, bind to neurotransmitter receptors and initiate a signalling cascade. Vesicles are e.g regenerated by clathrin-mediated endocytosis by directly loading with neurotransmitters or by budding from the endosome. (Figure adapted from [1].)

terminal where they bind neurotransmitter receptors inducing a downstream signalling cascade (**Figure 1**). Following exocytosis, degradation of the SNARE complex is mediated by a machinery composed of the N-ethylmaleimide sensitive factor (NSF) and the α -soluble NSF attachment protein (α -SNAP) to rapidly regenerate functional vesicles [5]. Synaptic vesicles are recycled through different mechanisms, for instance clathrin-mediated endocytosis, in which vesicles are formed by invagination and either mature directly into functional synaptic vesicles or fuse with an intermediate endosomal compartment and emerge from these by budding (**Figure 1**) [6].

1.1.2 SNARE proteins – the key players of membrane fusion

Synaptic SNARE proteins. SNARE proteins represent a protein family of small, mostly membrane-anchored proteins. They are characterised by an evolutionarily conserved sequence of 60 to 70 amino acids, the so-called SNARE motif [7]. The SNARE proteins that are involved in exocytosis of synaptic vesicles are the 25 kDa Synaptosome associated protein

(SNAP25) and Syntaxin-1 (Stx1), which are both anchored to the presynaptic membrane, as well as the vesicular-anchored Synaptobrevin-2 (Syb2) [8]. SNAP25 contains two SNARE motifs connected by a flexible linker and is anchored to the membrane by palmitoylation of cysteine residues in its linker region (**Figure 2A**). Stx1 and Syb2, on the other hand, are anchored to their membranes by C-terminal transmembrane domains, which are attached to the SNARE motifs through a short and flexible linker, referred to as juxtamembrane domain [7]. While Syb2 has a highly flexible N-terminal peptide, Stx1 contains an independently folded N-terminal domain consisting of an antiparallel three-helix bundle, the Habc domain (**Figure 2A**) [9]. In the absence of other SNARE proteins, the Habc domain reversibly interacts with the SNARE motif of Stx1 leading to formation of an ‘open’ or ‘closed’ conformation [10–12]. In the ‘closed’ conformation, intercalation of the SNARE motif in the Habc domain results in a four-helix bundle inhibiting formation of the SNARE complex [12]. The three neuronal SNARE proteins assemble into the SNARE complex through interactions of complementary SNARE motifs. Zippering of the SNAREs proceeds from the N-terminus towards the membrane-proximal C-terminus and is proposed to provide the required energy to initiate membrane fusion [13,14]. While the SNARE motifs of monomeric SNAREs are mainly unstructured, the presence of other SNAREs induces conformational changes resulting

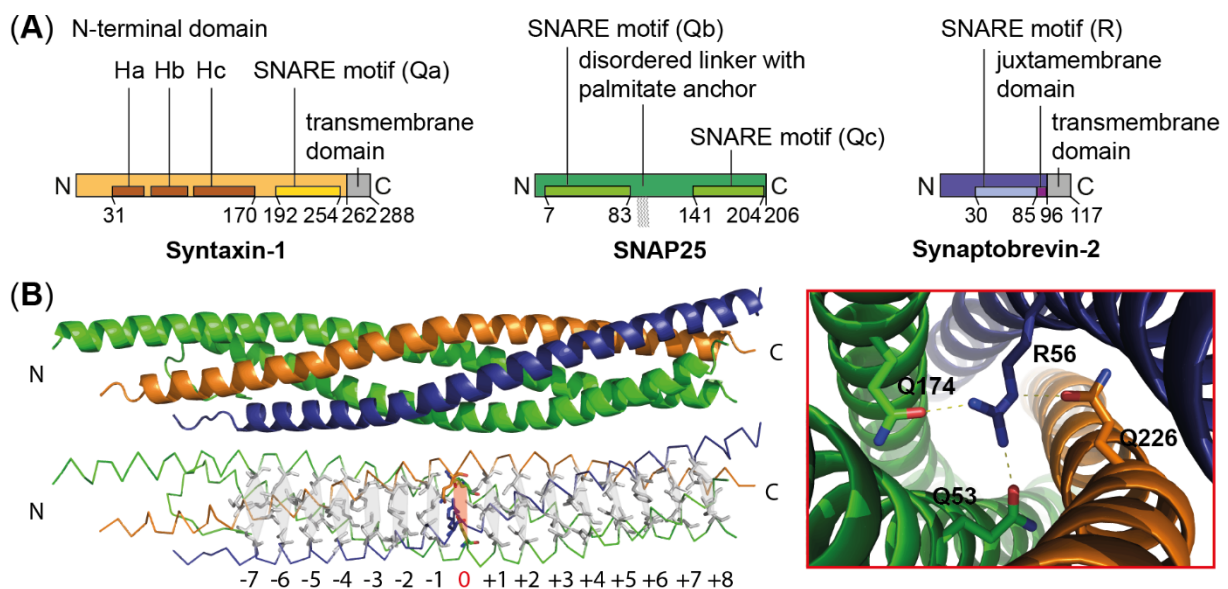


Figure 2. Structure of the SNARE complex.

(A) Schematic representation of the three neuronal SNARE proteins Syb2 (blue), Stx1 (orange) and SNAP25 (green). Syb2 and Stx1 each contain one SNARE motif (R and Qa) as well as a C-terminal transmembrane domain, while SNAP25 contains two SNARE motifs (Qb and Qc), which are connected through a linker that is anchored to the plasma membrane by palmitoylation (zig zag lines). Stx1 additionally contains an N-terminal folded domain consisting of an antiparallel three-helix bundle (Habc, brown). **(B)** Cartoon (top, lhs) and skeleton (bottom, lhs) representation of the high-resolution structure of the neuronal SNARE core complex formed by the QabcR SNARE motifs (PDB ID: 1SFC [17]). Position of the central ionic layer (red square) and hydrophobic layers (grey squares) of interacting side chains are indicated. The ‘zero layer’ (rhs) is formed by three glutamine and one arginine residues.

in a stable four-helix bundle of parallel α -helices (**Figure 2B**) [15–18]. The core complex of this bundle contains 16 parallel layers of interacting amino acid side chains. With the exception of the central ionic layer (the so-called ‘zero layer’), which is formed by three highly conserved glutamine (Q) and one arginine (R) residues, all layers are formed by hydrophobic residues (**Figure 2B**) [17]. Based on the composition of the ‘zero layer’, the SNARE proteins are classified as Qa- (Stx1), Qb- and Qc- (SNAP25) or R-SNAREs (Syb2) resulting in formation of the ternary QabcR (3Q:1R) SNARE complex [19].

Mechanisms of SNARE complex formation. Fusion of synaptic vesicles with the presynaptic membrane requires energy, which is provided by the assembly of the SNARE proteins into the four-helix bundle [13,14]. This process is mediated by regulatory proteins such as Munc18 and Munc13, providing a scaffold for the ordered and sequential alignment of the SNARE motifs and preventing SNAREs to enter ‘off-pathway’ complexes [5,10,20,21]. The formed complexes are helical homo- and heterooligomeric bundles of SNARE motifs, which are kinetically and thermodynamically “trapped” [22–26]. In these assemblies, SNARE proteins associate in parallel and antiparallel orientation mimicking the helical arrangement of the SNARE core complex, however, are less stable and impede membrane fusion [27,28].

The initiation and the exact pathway of the SNARE complex assembly are still elusive; and different mechanisms have been described (**Figure 3**): In the absence of interaction partners SNAP25 and Syb2 are mainly disordered, while Stx1 is kept in a ‘closed’ conformation by binding to a U-shaped binding pocket of Munc18 [10,11,23]. In this assembly, the N-terminal peptide of Stx1 binds to the outer surface of the regulator [29]. Recruitment of Munc13 converts Stx1 into an ‘open’ conformation [21,20,30], thereby enabling association of SNAP25 through its complementary SNARE motifs and formation of an ‘acceptor’ complex containing Stx1 and SNAP25 (**Figure 3i**) [31,32]. This complex is considered to be the starting point of the SNARE complex assembly, providing a binding site for Syb2 [32]. Rapid association of Syb2 through N- to C-terminal zippering forms the partially assembled trans-SNARE complex, an activated intermediate keeping synaptic vesicles in immediate proximity of the plasma membrane without inducing membrane fusion. An alternative pathway describes Syb2 binding to a metastable Munc18:Munc13:Stx1 complex, thereby connecting the membranes and initiating formation of a trans-SNARE complex by providing a ‘template’ complex for subsequent binding of SNAP25 (**Figure 3ii**) [33–36]. In this mechanism, Munc13 cooperates with Munc18 to chaperone SNARE assembly by stabilising the ‘open’ conformation of Stx1, while binding and aligning Syb2 in the proper parallel orientation and recruiting SNAP25 for a fast assembly [37,38].

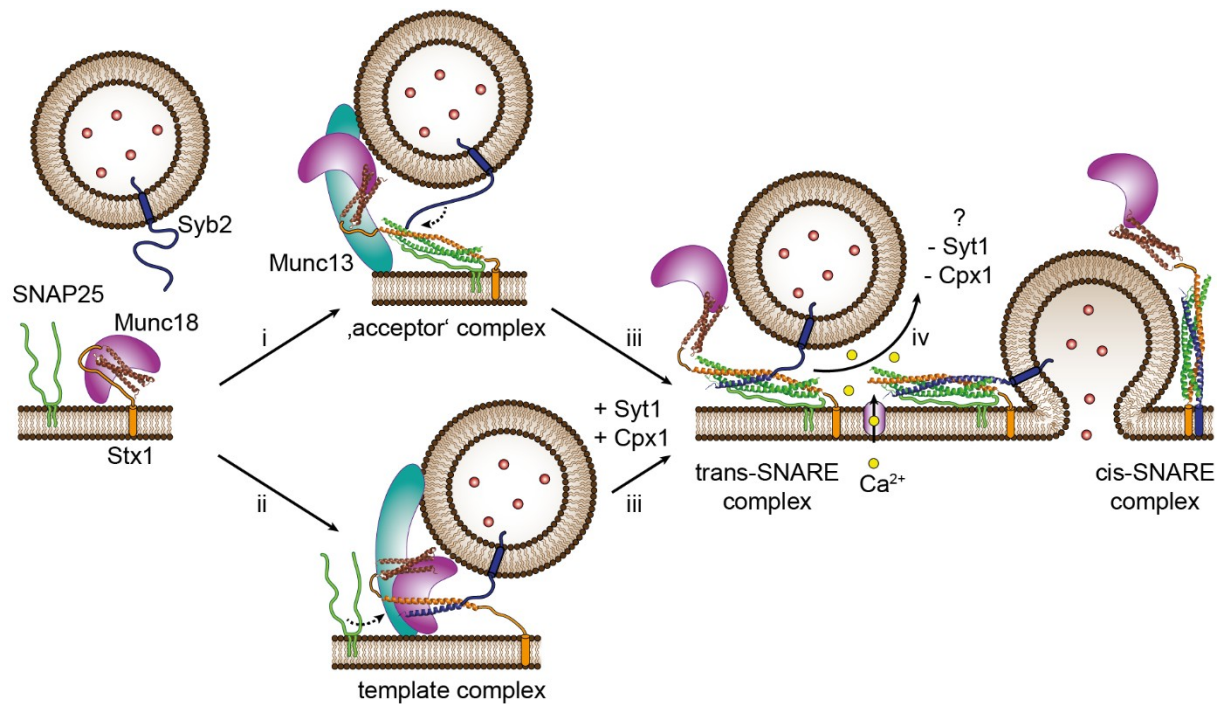


Figure 3. Mechanisms of SNARE complex formation.

Synaptic vesicles dock at the presynaptic membrane. The vesicular Syb2 (blue) and plasma membrane-anchored SNAP25 (green) are unstructured, while Munc18 (purple) stabilises the 'closed' conformation of Stx1 (orange). (i) Recruitment of Munc13 (cyan) converts Stx1 to an 'open' conformation enabling binding of SNAP25 and formation of the 'acceptor' complex that provides a binding site for Syb2. (ii) Alternatively, Munc13 and Munc18 convert Stx1 to an 'open' conformation enabling simultaneous binding of Syb2, thereby, forming a template complex for association of SNAP25. (iii) SNARE assembly takes place from the N- to the C-terminus forming the trans-SNARE complex. This activated intermediate state is regulated by Syt1 and Cpx1 following unknown mechanisms. (iv) Upon influx of Ca²⁺ ions (yellow), the membranes fuse, neurotransmitters are released, and the cis-SNARE complex is formed. (Figure adapted from [1].)

The final step of SNARE-mediated membrane fusion is regulated by the vesicular-anchored calcium sensor Syt1 as well as the cytosolic Cpx1, which associate with the partially zippered SNARE complex and stabilise the complex in an NSF/ α -SNAP-resistant, primed state (**Figure 3iii**) [39–41]. Although the underlying mechanism of these final regulators is unclear, they appear to support calcium-dependent membrane fusion. Following an action potential, calcium ions are transported into the cytosol of the presynaptic terminal resulting in the full assembly of the SNARE proteins, thereby, fusing the membranes and releasing neurotransmitters into the synaptic cleft (**Figure 3iv**). All SNAREs finally align in parallel orientation at the presynaptic membrane forming the so-called cis-SNARE complex.

Structural properties of Syb2 in a lipid environment. Protein-protein interactions involved in SNARE complex assembly were extensively studied, and a general knowledge about the procedure is established. On the contrary, less is known about protein-lipid interactions and how these influence the formation of the pre-fusion state and consequently membrane fusion. Indeed, structure formation and lipid interactions of SNARE proteins in a variety of membrane

mimetics were controversially discussed. For instance, in the presence of DPC micelles, helical structures were observed for Syb2 including the transmembrane domain, the juxtamembrane domain as well as some residues of the C-terminal SNARE motif [42]. In addition, the N-terminal half of the SNARE motif was shown to form a helix, which was proposed to function as ‘nucleation’ site for rapid SNARE zippering (**Figure 4A**) [42]. For Stx1 and SNAP25, similar helical structures, N-terminal of the SNARE motif, were observed and speculated to induce SNARE assembly [43,44]. On the contrary, the cytosolic domain of Syb2 was found to be disordered in lipid bilayers such as liposomes and nanodiscs and even described to be reluctant to the membrane (**Figure 4A**) [45,46]. However, an equilibrium between a lipid-bound conformation and a dissociated, disordered conformation was suggested, in which the lipid binding affinity decreases with decreasing curvature of the membrane mimetic used [47,48]. Interactions with lipids increase towards the C-terminus of the cytosolic domain and were found to mainly form due to electrostatic attraction of positively charged residues in the juxtamembrane domains of the SNAREs with anionic lipids of the membrane (**Figure 4B**) [48–51]. Supported by insertion of aromatic residues into the membrane, this was further hypothesized to perturb and bend the membranes and properly position the SNARE complex in membrane proximity, thereby, facilitating fusion of the membranes (**Figure 4C**) [51–55]. The negatively charged SNARE motifs, on the other hand, were described to experience

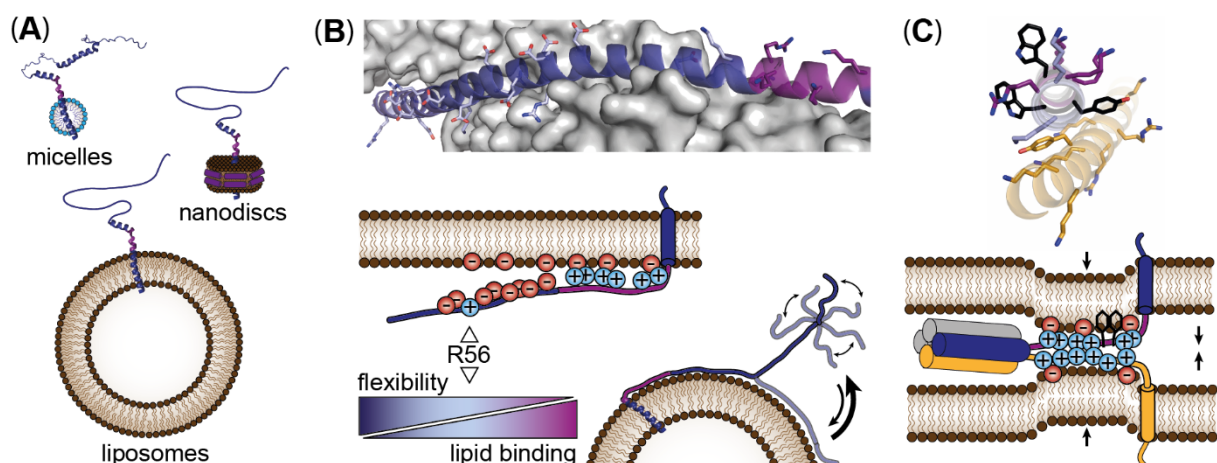


Figure 4. Structural properties of Syb2 in the presence of lipids.

(A) Syb2 forms a helix in the presence of DPC micelles (PDB ID: 2KOG [42]), which is absent in the presence of nanodiscs and liposomes. (B) High-resolution structure of Syb2 (top) in complex with SNAP25 and Stx1 (grey surface, PDB ID: 3HD7 [18]) highlighting charged residues (positively charged, blue; negatively charged, red) of the SNARE motif (blue) and the juxtamembrane domain (purple). A cartoon (middle) representing electrostatic attraction and repulsion of the cytosolic domain of Syb2 with the membrane is visualised. The cytosolic domain of Syb2 shows decreasing flexibility towards the C-terminus, which correlates with an increase in lipid binding (bottom). (C) High-resolution structure of the juxtamembrane domains of Syb2 and Stx1 (top) highlighting the aromatic motif (black) of Syb2 and the positively charged linker of Stx1 (orange, PDB-ID: 3HD7). A cartoon (bottom) visualises membrane protrusion induced by the positively charged linkers of Syb2 and Stx1 and insertion of aromatic residues into the membrane. The trans-SNARE complex is repositioned in the proximity of the membrane. (Figure adapted from [1].)

electrostatic repulsion and consequently be available for complementary SNARE motifs to assemble (**Figure 4B**) [45,48,51].

1.1.3 Regulation of SNARE complex assembly by Cpx1

Structural properties and functions of Cpx1. Complexins are a family of small soluble, highly charged and evolutionary conserved neuronal proteins that co-localise with the SNARE complex and regulate membrane fusion. The mechanisms of Cpx1-mediated regulation of the SNARE assembly are still elusive, however, stimulatory and inhibitory functions for different domains have been discussed [56–58]. Accordingly, Cpx1 is composed of an unstructured N-terminal domain (NTD), a dynamic accessory helix (AH), a central helix (CH) including the SNARE complex binding motif as well as a highly disordered C-terminal domain (CTD) (**Figure 5A**) [59]. Binding of Cpx1 to the core SNARE complex occurs through the CH, which binds in antiparallel orientation to the groove formed by Syb2 and Stx1 (**Figure 5A**) [60,61]. Binding of the CH is crucial for all regulatory functions of Cpx1 including stabilisation of the SNARE complex and preventing degradation by the NSF/ α -SNAP machinery [59,61–64]. The disordered NTD of Cpx1 is located at the membrane proximal part of the SNARE complex consecutive to the AH. The NTD potentially forms a positively charged amphipathic helix and is therefore likely involved in membrane binding [65,66]. Deletion of the NTD was shown to abolish the function of Cpx1, which was restored by deletion of the AH [59]. Accordingly, the AH inhibits membrane fusion, which is presumably relieved by the NTD [59]. The CTD contains a tandem lipid binding motif composed of two consecutive amphipathic helical motifs to bind the vesicular membrane (**Figure 5A**) [67,68]. Binding of the CTD to the membrane was described to play both stimulatory and inhibitory functions in membrane fusion by properly guiding Cpx1 to the fusion site, while blocking the proceeding of the fusion [69–71].

Models of regulatory mechanisms of Cpx1. To explain the function of Cpx1, several models were proposed that are not mutually exclusive. In the ‘fusogenicity model’, Cpx1 facilitates spontaneous and Ca^{2+} /Syt1-triggered membrane fusion by decreasing the energy needed to transfer the primed SNARE complex into the fully assembled complex [56]. The ‘clamping model’, on the other hand, describes Cpx1 binding to the SNARE complex, thus, inhibiting spontaneous membrane fusion by clamping the SNARE complex in its primed state. Upon Ca^{2+} -mediated Syt1 binding to the SNARE complex, Cpx1 disassembles from the trans-SNARE complex resulting in complete SNARE complex assembly and membrane fusion [72]. According to the ‘cooperativity model’, Syt1 binds to the SNARE complex regardless of the presence of Cpx1 and removes an inhibitory domain of Cpx1 without displacing Cpx1 from the SNARE complex [73].

However, none of these models involves all functional domains of Cpx1, which were shown to be either inhibitory or stimulating. Therefore, different models focussing on the domain structure of Cpx1 were proposed; Cpx1 can adopt two conformations when associated to the SNARE complex. In trans-conformation Cpx1 binds to the core of the SNARE complex through interactions with its CH, while the NTD and AH are unbound and exposed for other interactions, e.g. binding an additional ‘acceptor’ complex (**Figure 5Bi**) [74]. On the contrary, in cis-conformation, the AH binds to the SNARE core complex and the NTD clamps the C-terminal part of the complex (**Figure 5Bii**) [74]. While the NTD might interact with the vesicular or plasma membrane, the CTD of Cpx1 undergoes a disorder-to-order transition in the presence of lipids forming amphipathic helices, which then bind to the vesicular membrane after recognising the curvature of the vesicles (**Figure 5B**) [68,75,76]. The AH plays a central role in the inhibition of spontaneous neurotransmitter release, however, the mechanism is controversially discussed. Inhibition of the membrane fusion by the AH was hypothesised to be achieved through (i) insertion into a neighbouring ‘acceptor’ complex and leading to a zigzag array [59,77], (ii) clamping the C-terminal SNARE complex [65,78], (iii) occupying the binding site of the C-terminal SNARE motif of Syb2, thus, preventing full zippering [59,79],

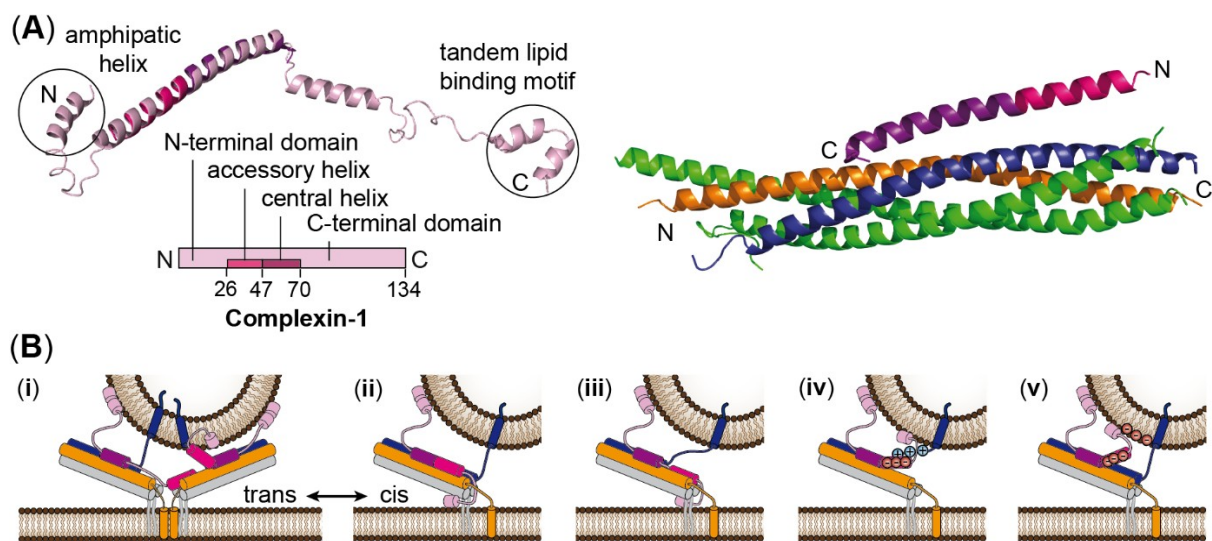


Figure 5. Structural properties and models for the regulatory mechanism of Cpx1.

(A) Schematic representation and AlphaFold structure prediction (lhs) of Cpx1 (light pink). Cpx1 is composed of the disordered NTD and CTD containing amphipathic helices, an AH (magenta) as well as a CH (purple). Cartoon representation of the high-resolution structure of the neuronal SNARE complex co-crystallised with Cpx1 (rhs, PDB ID: 1KIL [61]). Cpx1 binds through its CH to the groove formed by Stx1 (orange) and Syb2 (blue), while the AH is not interacting with the SNAREs. (B) Inhibition was proposed to arise from the following structural models: (i) The AH inserts into a second ‘acceptor’ complex, thereby, blocking the assembly of Syb2. Cpx1 adopts trans-conformation. (ii) The AH binds to the SNARE complex and the NTD clamps the C-termini of the SNAREs. Cpx1 adopts cis-conformation. (iii) The AH occupies the Syb2 binding site of the same SNARE complex. (iv) The negatively charged AH binds the SNARE motif and the positively charged linker of Syb2 and prevents binding of Syb2 to the SNARE complex. (v) Electrostatic repulsion and steric hindrance resulting from the negatively charged AH and the negatively charged membrane prevent fusion.

(iv) interacting with the C-terminal SNARE motif of Syb2 inhibiting its incorporation into the SNARE complex [80] or (iv) electrostatic repulsion or sterical hindrance with the negatively charged membranes (**Figure 5Bi-iv**) [80,81]. Regardless of the underlying mechanism, there is strong evidence that Cpx1 binds to trans-SNARE complexes interfering with the C-terminal zippering of SNARE proteins [78,82–84].

1.2 Mass spectrometry for structure elucidation of proteins

For understanding the biological function of protein assemblies, a detailed understanding of their structure and dynamics is essential. To date, x-ray crystallography, nuclear magnetic resonance (NMR) spectroscopy and cryo-electron microscopy (EM) provided the majority of high-resolution structural models. However, these techniques are limited and, for instance, the analysis of disordered proteins or membrane proteins remains difficult. Mass spectrometry (MS) is a suitable technique to provide complementary structural information to overcome the limitations of these conventional approaches. In combination with cross-linking of proteins (cross-linking MS) and the analysis of intact proteins and protein complexes (native MS), additional structural information for the characterisation of proteins and protein complexes is available.

1.2.1 Identification of proteins by MS

Identification of proteins established through the analysis of peptides. Two general approaches are commonly used: (i) 'top-down' MS, in which the intact protein is transferred into the gas phase and peptides are generated through fragmentation of the protein within the mass spectrometer or (ii) 'bottom up' approaches, in which the protein is enzymatically hydrolysed, e.g. using trypsin, prior to the MS analysis (**Figure 6A**). To reduce the complexity of the resulting peptide mixture, peptides are separated by high-performance liquid chromatography (HPLC) system. For this, the peptides are separated according to their hydrophobicity using a reversed phase LC column and directly eluted into the mass spectrometer. The individual steps of bottom-up MS analysis are described in the following paragraphs.

Ionisation of peptides. Peptides are often ionised by electrospray ionization (ESI) [85]. For this, the peptides pass through a capillary to which a high voltage (1-3 kV) is applied. The peptide solution is sprayed under atmospheric pressure into an electric field, the 'Taylor cone' is formed, charged droplets emit from the tip and are accelerated towards the counter electrode [86]. Continuous solvent evaporation leads to an increase in the charge density on the surface of the droplets resulting in repeated spontaneous decay into smaller droplets as soon as the 'Rayleigh limit' is reached. The final ionisation of peptides is best described by the ion evaporation model (IEM), which is based on the electric field emanating from a Rayleigh-

charged nanodroplet causing the ejection of small, solvated ions from the droplet surface (**Figure 6B**) [87]. The remaining solvent shell evaporates at the interface of the mass spectrometer. ESI is commonly used in nanoflow (nanoESI). The advantages of nanoESI are smaller droplets resulting from smaller sample volumes, enabling the use of aqueous solutions, tolerating higher salt concentrations and requiring lower sample amounts [88].

Ion separation and detection. The generated ions are then transferred into the gas phase of the mass spectrometer. Often hybrid instruments, e.g. quadrupole-orbitrap [89] (**Figure 6C**) or quadrupole time-of-flight (ToF) [90] mass spectrometers are used. The mass of the ions is determined by their mass-to-charge ratio (m/z) in high vacuum using mass analysers, e.g. quadrupole [91], ToF [92] or orbitrap [93] mass analysers as well as mass detectors. The commonly used quadrupole mass analyser is composed of four rods to which a radio frequency and direct current potential is applied. Note that adjacent rods have a radio frequency voltage out of phase by 180° and a direct current voltage of opposite polarity. The resulting electric field stabilises the ions on a trajectory to pass through the analyser. Depending on the applied

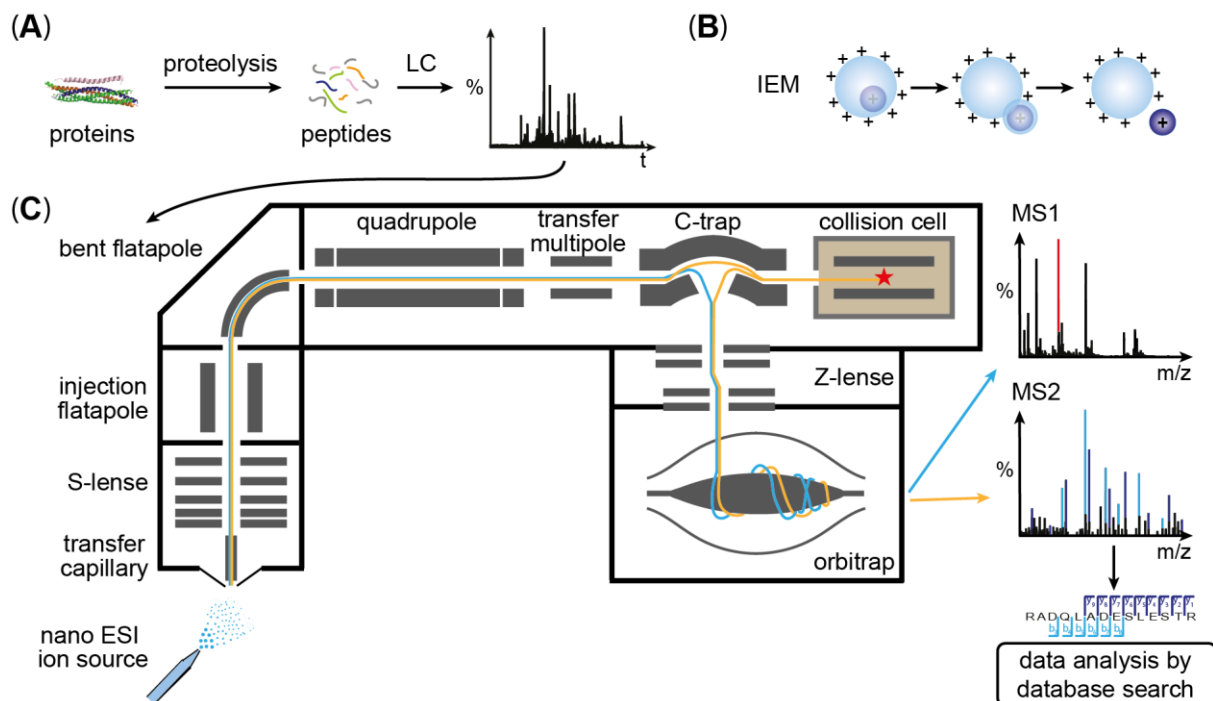


Figure 6. Protein identification workflow.

(A) Protein (complexes) are hydrolysed using specific proteases and resulting peptides are subsequently separated by LC and processed by tandem MS. (B) Peptides are ionised by nanoESI following the IEM mechanism and transferred into (C) a Q Exactive Plus Hybrid Quadrupole-Orbitrap mass spectrometer. In MS1 mode (blue path) all ions are guided through the lenses and flatapoles into the quadrupole and are forwarded through the C-trap into the orbitrap, where they are analysed and detected. An overview MS1 spectrum of all peptides is acquired. In MS2 mode (orange path) a specific m/z is selected (red) in the quadrupole and transmitted through the C-trap into the collision cell. Peptides are fragmented by HCD with inert gas molecules (red star) and fragment ions are guided back into the C-trap and forwarded into the orbitrap. The fragment ions are analysed, detected and an MS2 spectrum is acquired. Acquired data are further searched against databases and analysed by specific software.

potential, the quadrupole is operated in 'scanning mode', guiding all ions on stable trajectories, or in 'filter mode' by selecting and stabilising only one specific m/z value. The ToF analyser separates ions of different m/z values, which have been accelerated to the same kinetic energy, in a field free drift tube. The flight-time of the ions to the detector is analysed. As the velocity of the ions correlates with their m/z value, ions of smaller molecular weight will reach the detector first, while ions of higher molecular weight arrive later. ToF analysers are often combined with a multichannel plate (MCP) detector to record the induced current resulting from the arriving ions [94,95]. Compared to the quadrupole and the ToF analysers, the orbitrap operates as analyser and detector. Ions axially oscillate onto stable orbits around a central electrode depending on their m/z value [93]. Thereby, the ions induce a current in the outer electrode, which is converted into m/z values by Fourier transformation.

LC-MS/MS of peptides. In this thesis, the Q Exactive Plus Hybrid Quadrupole-Orbitrap mass spectrometer was used for protein identification (**Figure 6C**). In the mass spectrometer, the ionised peptides are first focussed by ion lenses and forwarded to the quadrupole analyser. In an MS1 experiment, the quadrupole operates in 'scanning mode' transmitting all ions through the analyser. Subsequently, the ions pass the C-trap, enter the orbitrap and an 'overview' spectrum of all peptides (MS1) is acquired (**Figure 6C**). During the acquisition, peptides continuously elute from the HPLC and ionise. Consequently, previously detected peptides with a specific m/z value can now be selected in the quadrupole when operated in 'filter mode'. The peptides pass the C-trap and are forwarded to the collision cell for fragmentation, which is achieved by high-energy collisional dissociation (HCD) [96]. For this, precursor ions are accelerated in the collision cell and collide with inert gas molecules, e.g. nitrogen, resulting in specific fragment ions that are guided to the C-trap and injected into the orbitrap. Within the orbitrap, the fragment ions are analysed, and a fragment ion spectrum (MS2) is detected (**Figure 6C**).

Database search. For identification of proteins, experimentally determined m/z values and intensities of the precursor and fragment ions are compared with theoretical values of *in silico* calculated peptides and their fragments from a target database. For matching peptide and fragment ion spectra, specialised software such as MaxQuant [97] is used. The obtained peptide spectrum matches (PSM) are used to estimate the false discovery rate (FDR), which is applied while data base search to limit identification of false positive peptides. The FDR is a measure of the incorrect PSMs amongst all accepted PSMs [98].

1.2.2 Chemical cross-linking combined with MS

Chemical cross-linking is used to obtain structural information on protein conformations and protein-protein interactions. It is a versatile tool to validate protein structures or derive models of protein complexes by integrative structural biology approaches complementing high-resolution structural information from traditional structural biology techniques. Accordingly, it was successfully applied to obtain models of large protein assemblies, e.g. the nuclear pore complex [99] or entire cell organelles, e.g. mitochondria [100]. It can be applied to characterise protein interactions in whole cells [101] or tissue [102].

Cross-linking workflow. By incubating proteins with a chemical cross-linker, functional groups of amino acid side chains in proximity are covalently linked, thereby, conserving non-covalent interactions of proteins and capturing their conformations. Cross-links are formed within a protein (intramolecular) or between two proteins (intermolecular). If the cross-linking reagent interacts with the protein through one functional group while the second is hydrolysed, a so-called ‘dead-end’ cross-link is formed (**Figure 7A**). Loop cross-links represent a special case of intramolecular cross-links, which connect amino acids within the same peptide [103]. Based on the cross-linked positions, the three-dimensional structure of proteins can be identified, thereby, providing information on subunit arrangement as well as solvent accessibility. After introducing covalent linkages, the cross-linked proteins are enzymatically hydrolysed. Traditionally, trypsin is used for hydrolysis; however, to increase sequence coverage of the cross-linked proteins, sequential hydrolysis using additional proteases, e.g. LysC or chymotrypsin, was established [104,105]. Cross-linked peptide pairs are then enriched

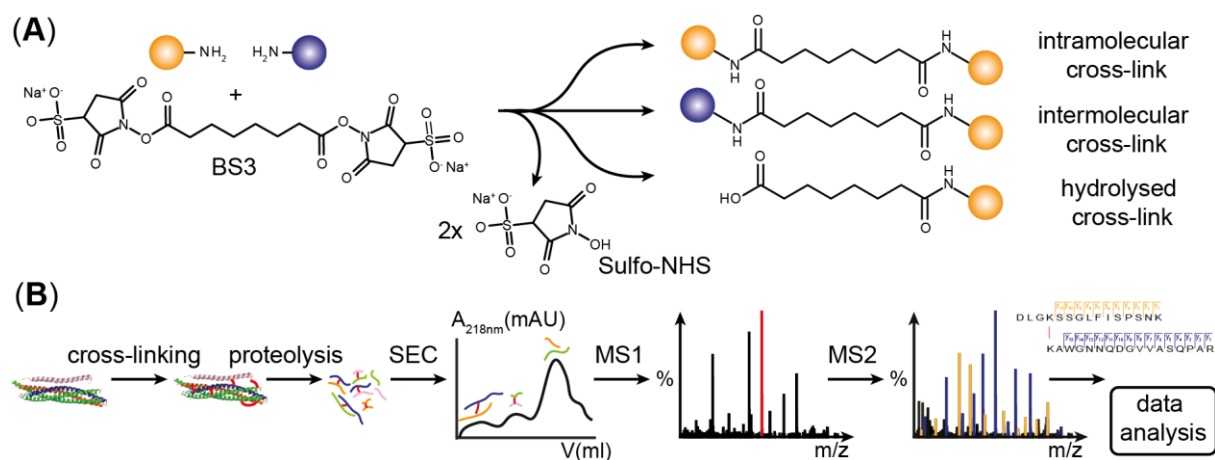


Figure 7. Chemical cross-linking.

(A) BS3 covalently links primary amines in proximity resulting in release of Sulfo-NHS forming inter-, intra- or partially hydrolysed cross-links. **(B)** Proteins are chemically cross-linked and hydrolysed using proteases. Obtained cross-linked dipeptides are separated from non-cross-linked linear peptides using SEC and analysed by LC-MS/MS. Acquired data are further processed using specific software.

from non-cross-linked linear peptides and analysed by LC-MS/MS as described above (**Figure 7B**).

Cross-linking reagents. A large number of cross-linkers is available for interaction studies. Most cross-linkers contain of two functional groups, which are connected through a flexible linker varying in length. Depending on the functional groups of the cross-linking reagent, primary amines as well as carboxyl groups, hydroxyl groups and thiol groups of the amino acid side chains can be targeted. Homobifunctional cross-linkers based on N-hydroxysuccinimide (NHS) esters such as bis-(sulfosuccinimidyl) suberate (BS3) are often used to link primary amines of lysine side chains and the proteins' N-termini [106]. After release of NHS, a stable amide bond is formed (**Figure 7A**). However, side reactions with less reactive hydroxyl groups of serine, threonine and tyrosine are also possible [107]. Cross-linking reagents such as 1-ethyl-3-(3-dimethylaminopropyl)-carbodiimide (EDC) covalently link carboxyl groups of the side chains of aspartic acid and glutamic acid with primary amines [108]. EDC mediates the reaction, however, is not integrated into the structure and, therefore, called 'zero-length' cross-linker.

Strategies for improved identification of cross-links. Cross-linked peptide pairs are low abundant compared to non-cross-linked linear peptides and their identification is challenging due to complex data sets. To reduce the complexity of the samples and increase the identification rate, several approaches were introduced such as chromatographic enrichment prior to LC-MS/MS acquisition. For this, size exclusion chromatography (SEC) [105], strong cation exchange chromatography (SCX) [109], hydrophilic strong anion exchange chromatography [110] or affinity chromatography using trifunctional cross-linking reagents [111,112] are often performed. For whole cell cross-linking studies, a multidimensional fractionation was established [101]. In addition, cleavable cross-linkers, e.g. disuccinimidyl sulfoxide (DSSO) [113] or dihydrazide sulfoxide (DHSO) [114], which contain labile bonds in their linker region, are used. These cross-linkers can be cleaved by collisions in the gas phase, resulting in a characteristic doublet of fragment ions. Another approach is the use of isotopically labelled cross-linkers e.g. BS3-d4, which bases on the substitution of several atoms of the linker region by stable isotopes such as deuterium. The use of 'heavy' (deuterated, dx) and 'light' (non-deuterated, d0) cross-linkers at equimolar ratio results in characteristic peak pairs in the MS1 spectrum. The mass difference of these peaks allows the unambiguous identification of the less abundant cross-links and is used for quantitative and comparative experiments [115,116]. Adjustments during the LC-MS/MS acquisition, such as optimized fragmentation parameters were also used to increase the identification [117]. In addition, charge state selection is used, as cross-linked dipeptides contain higher charges compared to

linear peptides. The recent development of field asymmetric ion mobility spectrometry (FAIMS) further enables multidimensional separation and filtering of higher charged peptides during the measurement [118].

Identification and validation of identified cross-links. Cross-links are in principle identified in a similar fashion as linear peptides; however, specialised software, e.g. xQuest [119], pLink2 [120], StavroX [121], MeroX [122] or XiSearch [104] is necessary. During the data base search, an FDR is estimated from a target-decoy database, followed by manual validation of the mass spectra to reduce the identification of false positives. Identified cross-linking positions are visualised in bar, circle or network plots [123] and will be further validated by mapping onto high-resolution structures or structure predictions using e.g. the visualisation software UCSF Chimera [124] or ChimeraX [125] combined with the XLink Analyzer [126]. Accordingly, the distances between the identified interacting side chains will be compared with the structures relative to the length of the cross-linker. Cross-linking positions and distance restraints can then be implemented into structural models and used for docking of subunits to complexes, modelling of protein structures or refinement of high-resolution structures [127].

1.2.3 Native MS

Native MS is a technique that enables the analysis of intact protein complexes in the gas phase. By preserving non-covalent interactions, information on the stoichiometry, topology and stability of protein complexes is provided. With this protein-protein and protein-ligand interactions as well as binding affinities can be analysed. The applicability of native MS ranges from individual small peptides and proteins up to large protein complexes and even intact macromolecular assemblies such as ribosomes or virus capsids [128–131].

Sample preparation. To preserve non-covalent interactions and to enable the analysis of protein complexes in the gas phase, a volatile buffer and an instrument modified for transmission of high masses are required [132]. Non-volatile buffer components such as salts and stabilisation reagents, e.g. detergents or glycerol, often lead to ion suppression and extensive adduct formation [132]. To prevent this, the storage buffer of the protein sample needs to be exchanged into an ESI compatible solution. A commonly used solvent is ammonium acetate solution, a volatile electrolyte ($\text{NH}_4^+\text{CH}_3\text{COO}^-$) that mimics the solvation properties of proteins under physiological conditions and stabilises low pH values, thus, preventing dramatic acidification during ionisation [133]. Buffer exchange is performed prior to the analysis often using small SEC columns, molecular cut-off filters or dialysis membranes (**Figure 8A**) [132].

Ionisation of proteins. Protein complexes are often ionised using nanoESI. Release of large globular protein assemblies into the gas phase is best explained by the ‘charged residue model’ (CRM) (Figure 8B) [134]. Nanodroplets that contain one single analyte evaporate to dryness, while the charge of the droplet is transferred to the analyte. For comparison, ionisation of disordered and partially hydrophobic analytes is often described by the ‘chain ejection model’ (CEM) (Figure 8B) [135]. In this model, unfolded chains migrate to the surface of the nanodroplet, one terminus gets expelled into the vapor phase followed by sequential ejection of the protein into the gas phase and separation from the droplet. The uptake of charges correlates with the surface accessible area of the assemblies and, therefore, provides information about the folding state of native protein structures [136–138].

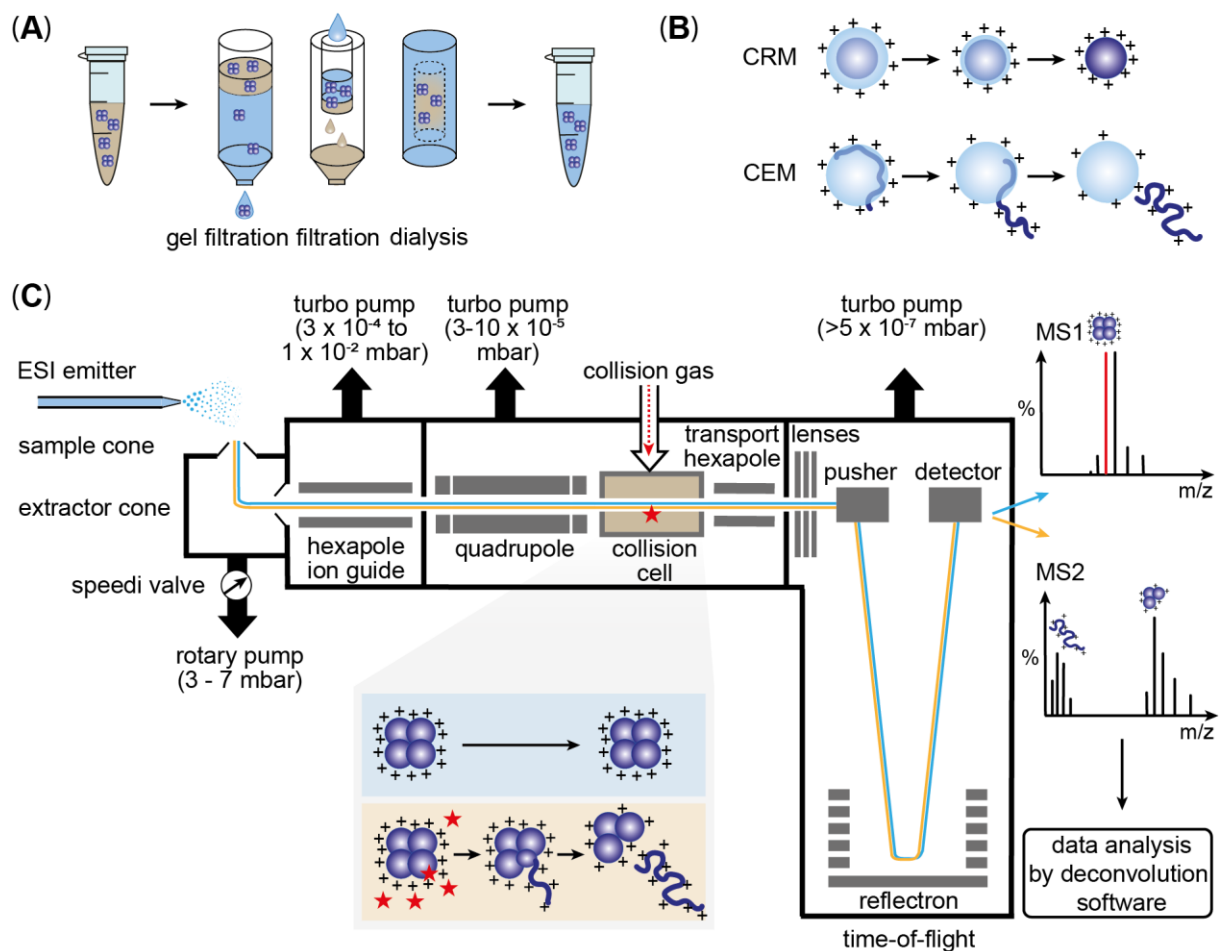


Figure 8. Native MS workflow.

(A) Sample preparation of intact protein (complexes) by buffer exchange into volatile solution. (B) Ions are generated by nanoESI following the CRM (large globular proteins) or CEM (large, disordered proteins) mechanism and are transferred into a Q-ToF Ultima mass spectrometer. (C) In MS1 mode (blue path) all ions pass through the quadrupole and the collision cell. Ions are analysed in the time-of-flight analyser and detected in the MCP detector. A charge state distribution for each protein species is acquired in an MS1 spectrum. In MS2 mode (orange path) a specific m/z is selected (red cursor) and dissociated in the collision cell. Collision of the protein with inter gas molecules (red star) leads to unfolding and dissociation of a subunit at the periphery of the protein complex. The acquired MS2 spectrum shows distributions for the dissociated subunit and the ‘stripped’ complex. Data are further processed and analysed by specific deconvolution software.

Stabilisation of non-covalent interactions. The generated ions are directly transferred into the mass spectrometer. Modified hybrid instruments are used; for instance, quadrupole-time-of-flight instruments (**Figure 8C**) [139] or quadrupole-orbitrap mass spectrometers that enable high-resolution measurements [140]. Major modifications of the instrument include an increased pressure in the transfer region between the source and the quadrupole analyser as well as a decreased radio frequency of the quadrupole [139]. Due to ‘collisional cooling’ and ‘collisional focussing’ resulting from increased pressure stages, the transmission of high m/z ions is improved [141–144]. Accordingly, ions that enter the mass spectrometer through the atmospheric pressure in the ion source are decelerated by collisions with background gas molecules, thus, losing kinetic energy and axial motion. Consequently, the ion beam is confined towards the central axis of the ion guide [141,142]. In addition, transmission of ions through the quadrupole depends on the applied radiofrequency of the alternating current, the amplitude of the ions on their trajectory through the analyser as well as the inner radius of the quadrupole rods. A decreased radiofrequency allows transmission of ions up to 32,000 m/z compared to conventional instruments [139,145].

Tandem MS of protein complexes. In a standard native MS experiment, the quadrupole operates in ‘scanning mode’ and an MS1 spectrum of all ions including the intact protein complexes as well as sub-complexes and individual proteins is acquired (**Figure 8C**). Note that, for each protein species, a Gaussian distributed charge state series is observed. If several proteins are present in the analyte, for each protein, a distribution will be detected, thus, not only providing information about the mass and the stoichiometry of assemblies, but also about the heterogeneity of the analyte. When operating the quadrupole in ‘filter mode’ (MS2), a precursor ion can be selected and dissociated by collision-induced dissociation (CID) [146], which is achieved by increasing the collisional voltage applied to the collision cell. Rather than fragmenting the backbone of the protein, peripherally bound subunits unfold due to collisions with inert gas molecules resulting in dissociation from the complex while accumulating charges on their increased surface area (**Figure 8C**) [147,148]. Dissociation of a protein complex leads to asymmetric charge partitioning and, as a consequence, yields a highly charged dissociated subunit and a so-called ‘stripped complex’ composed of the remaining subunits [148,149]. As a result, information on the subunit arrangement within the complex as well as the binding strength of subunits or ligands is determined. The annotation of the mass spectra and the calculation of the molecular weight of the proteins and complexes is performed using deconvolution software such as Massign [150] or UniDec [151].

Analysis of membrane proteins. Maintaining the natural conformation of proteins in native MS is challenging; this is particularly true for membrane proteins. Due to their amphipathic character, it is required to solubilise membrane proteins, while preserving their lipid environment that is essential for their function and stability. For this, several membrane mimetics were employed, e.g. amphipols [152], nanodiscs [153–155], styrene maleic acid lipid particles (SMAPLs) [156–159] and liposomes [160]. However, detergent micelles are the most commonly used membrane mimetics, which can be used to purify membrane proteins. In some cases, associated lipids are maintained making them accessible for the analysis. Detergent-lipid micelles can also be used to serve as vehicles to mediate lipid binding to proteins [161]. A variety of different detergents was employed for the analysis of membrane proteins [162–164]. As intact micelles produce highly heterogeneous mass spectra, detergent adducts need to be removed by collisional activation inside the mass spectrometer. Although most of the activation energy is absorbed by the detergent [164], finding the balance between sufficient energy to remove the detergent and loss of structure is still delicate. Non-ionic detergents, e.g. tetraethylene glycol monoethyl ether (C8E4), minimise ion suppression, are easy to be removed in the gas phase and are, therefore, well-suited for native MS [164]. The entire protein-lipid-detergent complexes are transferred into the gas phase and analysed as described above. The resulting mass spectra usually contain distributions corresponding to the ‘apo protein’ without lipid bound and to protein-lipid complexes, that are shifted to higher m/z values depending on the mass of the bound lipid.

1.3 Aim of the study

Exocytosis of synaptic vesicles mediated by the SNARE complex is a key step in signal transmission between neurons. Even though the general processes are understood, the detailed underlying molecular mechanisms are largely unknown. This includes formation and regulation of possible intermediates in the SNARE complex assembly. The aim of this thesis is, therefore, to unravel the stepwise analysis of the assembly of the SNARE complex and to obtain information on its regulation by Cpx1. To reach this goal, a combination of biochemical and mass spectrometric techniques will be used to explore protein-protein and protein-lipid interactions of the neuronal SNARE proteins.

To provide information on the SNARE complex assembly, individual SNARE proteins and Cpx1 will be first characterised in the absence of interaction partners, followed by incubation of the proteins forming binary or ternary complexes. Oligomerisation, complex formation, and rearrangements as well as complex stability will be monitored by native MS. Chemical cross-linking of the individual proteins using BS3 will then provide information on specific interaction sites within the proteins and their complexes.

Cpx1 is a known regulator of the SNARE-mediated membrane fusion. High-resolution structures revealed binding of Cpx1 to the SNARE complex through a groove formed by Syb2 and Stx1. However, contradictory information on inhibitory and stimulating functions based on varying mechanisms were proposed. To unravel potential regulatory functions of Cpx1 at all stages of SNARE assembly, interactions of Cpx1 with the individual SNARE proteins, binary complexes and the ternary SNARE complex will be analysed by native MS. To specifically explore the interactions of Cpx1 bound to the SNARE complex, chemical cross-linking will be used to identify interaction sites and protein arrangements including dynamic and disordered regions of all SNARE proteins as well as Cpx1.

In addition to protein interactions, lipid binding to the cytosolic domain of Syb2 as well as Cpx1 was controversially discussed in many previous studies employing different membrane mimetics as well as variants of the proteins. To investigate interactions of Syb(1-96) and Cpx1 with different phospholipids, three complementary approaches will be used. Lipid overlay assays will be performed to screen for potential interacting lipids. For this, binding of the proteins to immobilised lipids of various classes is identified by immunostaining. Using native MS, lipids will be transferred from mixed detergent-lipid micelles to the proteins, thereby, providing lipid binding affinities. To evaluate lipid binding observed in native MS measurements, liposomes simulating a curved phospholipid bilayer will be employed, and protein-lipid interactions will be elucidated by flotation of liposomes on a sucrose gradient.

In summary, this thesis will provide novel, mechanistic insights into SNARE complex assembly, including formation of intermediate complexes, interactions with the regulatory protein Cpx1 as well as protein-lipid and protein-membrane interactions of synaptic proteins.

2 Materials and methods

2.1 Materials

2.1.1 Chemicals

3-[(3-cholamidopropyl)-dimethyl ammonio]-1-propane sulphonate (CHAPS)	Carl Roth, Karlsruhe
4-(2-hydroxyethyl)-piperazine-1-ethanesulfonic acid (HEPES)	Sigma Aldrich, St. Louis, USA
Acetonitrile, LC/MS grade	Thermo Fisher Scientific, Waltham, USA
Agar-Agar	Carl Roth, Karlsruhe
Albumin fraction V of bovine serum albumin	Carl Roth, Karlsruhe
Ammonium acetate	Sigma Aldrich, St. Louis, USA
Ammonium bicarbonate	Sigma Aldrich, St. Louis, USA
Bis-(sulfosuccinimidyl) suberate (BS3)	Life Technologies, Carlsbad, USA
Calcium chloride	Sigma Aldrich, St. Louis, USA
Caesium iodide	Sigma Aldrich, St. Louis, USA
Complete™ protease inhibitor cocktail, EDTA-free	Carl Roth, Karlsruhe
Coomassie® Brilliant Blue G 250	Carl Roth, Karlsruhe
D- (+) sucrose	Carl Roth, Karlsruhe
Di-potassium hydrogen phosphate	Carl Roth, Karlsruhe
Di-sodium hydrogen phosphate	Carl Roth, Karlsruhe
Dithiothreitol	Sigma Aldrich, St. Louis, USA
Ethanol, LC/MS grade	Carl Roth, Karlsruhe
Ethylenediamine tetra acetic acid disodium dihydrate (EDTA)	Carl Roth, Karlsruhe
Formic acid, LC/MS grade	Sigma Aldrich, St. Louis, USA
Glycine	Sigma Aldrich, St. Louis, USA
Imidazole	Sigma Aldrich, St. Louis, USA
Iodoacetamide	Sigma Aldrich, St. Louis, USA
Isopropyl-β-D-thiogalactopyranoside (IPTG)	Carl Roth, Karlsruhe
Kanamycin sulphate	Carl Roth, Karlsruhe
Magnesium sulphate heptahydrate	Carl Roth, Karlsruhe
Methanol	Thermo Fisher Scientific, Waltham, USA
Milk powder	Carl Roth, Karlsruhe
n-Octyl β-D-glucopyranoside	Glycon Biochemicals, Luckenwalde

Phenylmethylsulphonyl fluoride (PMSF)	Carl Roth, Karlsruhe
Phosphate buffered saline (PBS) tablets	Carl Roth, Karlsruhe
Phosphoric acid	Carl Roth, Karlsruhe
Polyoxyethylen-20-sorbitanmonolaurat (Tween-20)	Carl Roth, Karlsruhe
Potassium-di-hydrogen phosphate	Carl Roth, Karlsruhe
RapiGest SF Surfactant	Waters Corporation, Milford, USA
Sodium acetate trihydrate	Sigma Aldrich, St. Louis, USA
Sodium chloride	Carl Roth, Karlsruhe
Tetraethylene glycol monoethyl ether (C8E4)	Glycon Biochemicals, Luckenwalde
Trifluoroacetic acid, LC/MS grade	Thermo Fisher Scientific, Waltham, USA
Tris(2-carboxyethyl) phosphine hydrochloride (TCEP)	Carl Roth, Karlsruhe
Tris(hydroxymethyl)aminomethane (Tris base)	Sigma Aldrich, St. Louis, USA
Tryptone / peptone of casein	Merck, Darmstadt
Urea	Thermo Fisher Scientific, Waltham, USA
Water, LC/MS grade	Thermo Fisher Scientific, Waltham, USA
Yeast extract	Merck, Darmstadt

2.1.2 Consumables

Acclaim™ PepMap™ 100 C18-LC column (75 µm x 500 mm, particle size 3 µm, pore size 100 Å)	Thermo Fisher Scientific, Waltham, USA
Acclaim™ PepMap™ 100 C18-LC column (300 µm x 5 mm, particle size 5 µm, pore size 100 Å)	Thermo Fisher Scientific, Waltham, USA
Amersham™ Protran® Nitrocellulose Blotting membrane (0.2 µm pore size)	GE Healthcare, Chicago, USA
Amicon® Ultra-15 Ultracel®-10K	Merck, Darmstadt
HiLoad™ 16/600 Superdex™ 75 prep grade column	GE Healthcare, Chicago, USA
HisTrap™ HP column	GE Healthcare, Chicago, USA
HiTrap™ SP HP column	GE Healthcare, Chicago, USA
HiTrap™ Q HP column	GE Healthcare, Chicago, USA
Glas capillaries GC100-T10 (1.0 OD x 0.78 x 100 L mm) without filament	HARVARD Apparatus, Holliston, USA

Membrane lipids strips P-6002	Echelon Biosciences, Salt Lake City, USA
Micro Bio-Spin™ 6 column	BioRad Laboratories, München
PD MiniTrap G25 column	GE Healthcare, Chicago, USA
Superdex™ peptide 3.2 / 300 column	GE Healthcare, Chicago, USA
Vivaspin 500-10K	Sartorius AG, Göttingen

2.1.3 Ready-to-use kits, solutions and buffers

InstantBlue™ Coomassie protein stain	Expedeon, Cambridge, UK
NuPAGE™ antioxidant	Thermo Fisher Scientific, Waltham, USA
NuPAGE™ Bis-Tris gels (4 – 12 %)	Thermo Fisher Scientific, Waltham, USA
NuPAGE™ LDS sample buffer (4x)	Thermo Fisher Scientific, Waltham, USA
NuPAGE™ MES SDS running buffer (10x)	Thermo Fisher Scientific, Waltham, USA
NuPAGE™ sample reducing agent (10x)	Thermo Fisher Scientific, Waltham, USA
Pierce® ECL western blotting detection kit	Thermo Fisher Scientific, Waltham, USA
Plasmid mini-prep kit	Thermo Fisher Scientific, Waltham, USA
SeeBlue plus 2 pre-stained protein marker	Thermo Fisher Scientific, Waltham, USA

2.1.4 Antibodies

anti-Complexin-1/2 IgG from rabbit (Cat.No. 122003)	Synaptic Systems, Göttingen
anti-SNAP25 IgG from mouse, clone 71.1 (Cat.No.110011BT)	Synaptic Systems, Göttingen
anti-Syntaxin-1A IgG from mouse, clone 78.3 (Cat.No.110111)	Synaptic Systems, Göttingen
anti-VAMP-1/2/3 IgG from mouse (Cat.No.104203)	Synaptic Systems, Göttingen
anti-mouse IgG from rabbit (Cat.No. A9044)	Merck, Darmstadt
anti-rabbit IgG from goat (Cat.No. A0545)	Merck, Darmstadt

2.1.5 Enzymes

DNase I (Cat.No. D5025-15KU)	Sigma Aldrich, St. Louis, USA
Thrombin (Cat.No. 27-0846-01)	Merck, Darmstadt
Trypsin, sequencing grade (Cat.No. 11418775001)	Merck, Darmstadt
Trypsin, sequencing grade modified (Cat.No. V5111)	Promega, Mannheim

2.1.6 Lipids

All lipids were purchased from Avanti Polar Lipids, Alabaster, USA.

1,2-dioleoyl- <i>sn</i> -glycero-3-phosphocholine	18:1/18:1 PC (DOPC)
1,2-dioleoyl- <i>sn</i> -glycero-3-phosphoethanolamine	18:1/18:1 PE (DOPE)
1,2-dioleoyl- <i>sn</i> -glycero-3-phospho-(1- <i>rac</i> -glycerol)	18:1/18:1 PG (DOPG)
1,2-dioleoyl- <i>sn</i> -glycero-3-phospho-L-serine	18:1/18:1 PS (DOPS)

2.1.7 Plasmids and proteins

Plasmids encoding SNARE proteins and Cpx1 of *Rattus norvegicus* (**Table 1**) were provided by Prof. Dr. Reinhard Jahn (Max Planck Institute for Multidisciplinary Sciences, Göttingen). Dr. Caroline Haupt (ZIK HALOmem, Halle/Saale) created the pET28a_Syntaxin-1A_1-262 and pET28a_Synaptobrevin-2_1-96 plasmids for expression of Stx1 and Syb2 without transmembrane domain using the pET28a_Syntaxin-1A and pET28a_Synaptobrevin-2 plasmids. All plasmids contain a resistance gene against kanamycin, the lactose operon for induction of the protein expression by IPTG and additional sequences encoding for an N-terminal hexa-histidine tag for purification of proteins by affinity chromatography and a thrombin cleavage site (**Supplementary Figure 1**). All proteins contain a residual of the thrombin cleavage site (GSH). Syb(49-96) was purified and provided by Dr. Caroline Haupt (ZIK HALOmem, Halle/Saale).

Table 1. Plasmids and protein variants.

Plasmid	Protein variants
pET28a_Complexin-1	Cpx1, full-length
pET28a_SNAP25-a_allCtoS	SNAP25-a, full-length, all cysteine residues mutated to serine residues (SNAP25(CtoS))
pET28a_SNAP25-a_1-83	SNAP25-a, N-terminal helix including residues 1 to 83 (SNAP25(1-83))
pET28a_Synaptobrevin-2	Syb2, full-length including transmembrane helix
pET28a_Synaptobrevin-2_49-96	Syb2, cytosolic domain including residues 49 to 96, lacking N-terminal part of SNARE motif (Syb(49-96))
pET28a_Synaptobrevin-2_1-96	Syb2, complete cytosolic domain including residues 1 to 96 (Syb(1-96))
pET28a_Syntaxin-1A_1-262	Stx1, complete cytosolic domain including residues 1 to 262 (Stx(1-262))

2.1.8 Instruments

ÄKTA™ pure chromatography system	GE Healthcare, Chicago, USA
ÄKTA™ purifier chromatography system	GE Healthcare, Chicago, USA
Avanti Mini Extruder	Avanti Polar lipids, Alabaster, USA
Cell density spectrophotometer Ultrospec 10	Amersham Biosciences, Amersham, UK
Cell disruptor	Constant Systems LTD, Northants, UK
DS-11+ spectrophotometer	DeNovix®, Wilmington, USA
Fraction collector Frac-950	GE Healthcare, Chicago, USA
Jasco J-815 circular spectropolarimeter	JASCO Deutschland, Pfungstadt
Litesizer 500 particle analyzer	Anton Paar, Graz, Austria
Luminescent image analyzer LAS-4000	Fujifilm Corporation, Tokyo, Japan
OWL HEP-1 semi-dry electroblotting system	Thermo Fisher Scientific, Waltham, USA
Q Exactive plus hybrid Quadrupole-Orbitrap mass spectrometer	Thermo Fisher Scientific, Waltham, USA
Q-ToF Ultima mass spectrometer with high mass upgrade	Waters Corporation, Milford, USA (High-mass modification by MS Vision, Almere, Nederland)
UltiMate Dionex 3000 nano-LC system	Thermo Fisher Scientific, Waltham, USA

2.1.9 Software

Croco (version 0.7.1)	J. Bender, C. Schmidt [165]
MassLynx (version 4.1)	Waters, Milford, USA
Masssign (version of 11/14/2012)	N. Morgner, C. Robinson [150]
MaxQuant (version 1.6.17)	J. Cox, M. Mann [97]
Kalliope	Anton Paar, Graz, Austria
pLink2 (version 2.3.11)	Z.L. Chen et al. [120]
PyMOL (version 5)	Schrödinger, L.L.C. [166]
Spectra Manager (version 2.0)	JASCO Deutschland
UCSF Chimera (version 1.15)	E. F. Pettersen et al. [124]
UniDec (version 6.0.1)	M. Marty et al. [151]
Xcalibur (version 4.2.47)	Thermo Fisher Scientific, Waltham, USA
Xlink Analyzer (version 1.1.4)	J. Kosinski et al. [126]
xVis	M. Grimm et al. [123]

2.2 Molecular biological methods

2.2.1 Transformation of *Escherichia coli* cells

3 µl of purified plasmid (**Table 1**) were added to 200 µl of chemically competent *Escherichia coli* BL21(DE3) cells followed by incubation on ice for 30 min. Cells were heat-shocked at 42 °C for 10 s to permeabilise the membrane and immediately incubated for 5 min on ice. Subsequently, 950 µl super optimal broth with catabolite repression (SOC) medium (**Table 2**) were added and cells were incubated at 37 °C for 60 min while gently agitating at 250 rpm. Cells were pelleted at 5000 x g and resuspended in 100 µl SOC medium. The cell suspension was dispensed on a lysogeny broth (**Table 2**) agar plate containing 30 µg/ml kanamycin for selection of transformed cells. The plates were incubated at 37 °C for approximately 16 h. For validation of the transformed plasmid by sequencing analysis, individual colonies were picked from the plates and cultivated in 5 ml lysogene broth medium containing 30 µg/ml kanamycin. Cells were harvested and plasmid DNA extracted using the plasmid mini-prep kit (Thermo Fisher Scientific) following the manufacturers protocol. For long-time storage at -80 °C, the cell suspension was mixed with 30 % (w/v) glycerol and frozen in liquid nitrogen.

2.2.2 Cell culture and protein expression

Escherichia coli BL21 (DE3) cells, transformed with the appropriate plasmid (**Table 1**), were cultured in 150 ml double-yeast tryptone medium (**Table 2**) or lysogeny broth medium (**Table 2**) in the presence of 30 µg/ml kanamycin by incubating overnight at 37 °C. Main-cultures of 500 ml double-yeast-tryptone medium or terrific broth medium (**Table 2**), each including 30 µg/ml kanamycin, were inoculated with the corresponding pre-culture to an optical density of approximately 0.05 at 590 nm. The Cell density was determined (Ultrospec 10 spectrophotometer, Amersham Biosciences). Cell cultures were grown at 37 °C until an optical density of 0.6 to 0.9 was reached. To prevent expression of chaperones, cell cultures were cooled to 22 °C prior to induction of protein expression. Expression of SNARE proteins and Cpx1 was induced with 0.4 mM and 1 mM IPTG. Cells were harvested at 4000 x g and 4 °C for 20 min, pellets were resuspended in approximately 10 ml 20 mM HEPES, pH 7.4, 500 mM NaCl, 20 mM imidazole, 0.1 mM TCEP and directly used for protein purification (**Section 2.3.1**, **Section 2.3.2**) or stored at -80 °C.

Table 2. Composition of media for bacterial cultivation.

Medium	Composition
Double-yeast tryptone	1.6 % (w/v) tryptone, 1 % (w/v) yeast extract, 0.5 % (w/v) NaCl
Lysogeny broth	1 % (w/v) tryptone, 0.5 % (w/v) yeast extract, 1 % (w/v) NaCl
SOC	2 % (w/v) peptone, 0.5 % (w/v) yeast extract, 10 mM NaCl, 2.5 mM KCl, 10 mM MgCl ₂ , 10 mM MgSO ₄ , 20 mM glucose
Terrific broth	1.2 % (w/v) tryptone, 2.4 % (w/v) yeast extract, 0.4 % (v/v) glycerol, 2.3 % (w/v) KH ₂ PO ₄ , 12.5 % (w/v) K ₂ PO ₄

2.3 Protein biochemical methods

2.3.1 Cell lysis

To the cell suspensions (**Section 2.2.2**) 5 mM magnesium sulphate heptahydrate as well as 10 µg/ml DNase I were added, and cells were mechanically lysed (cell disruptor, Constant Systems LTD). For this, a pressure of 2 kbar was repeatedly applied. After cell lysis, the lysate was immediately collected and mixed with a protease inhibitor cocktail (Roche) and 1 mM PMSF for inhibition of proteases. Cell debris was pelleted at 25,000 rpm and 4 °C for 60 min and proteins of interest were chromatographically purified (ÄKTA™ purifier, GE Healthcare) from the supernatant (**Section 2.3.2, Section 2.3.3**).

2.3.2 Protein purification of SNARE proteins

SNAP25(CtoS), Syb(1-96) and Stx(1-262) (Table 1) were isolated from cell lysate (**Section 2.3.1**) by immobilized metal affinity chromatography (IMAC) using a HisTrap™ HP column (GE Healthcare). All purification steps were performed at 4 °C in purification buffers given below (**Table 3**). The corresponding cell lysate was loaded onto the column and washed with IMAC buffer A until the baseline of the UV signal was reached. Unspecifically bound proteins were washed off the column using 50 mM to 125 mM imidazole. Proteins eluted from the column at 350 mM and 500 mM imidazole. Fractions containing the protein of interest were identified by gel electrophoresis (**Section 2.3.6**). To cleave the hexa-histidine tag, pooled fractions were dialysed overnight at 4 °C against dialysis buffer 1 containing at least 50 U thrombin. Separation of the hexa-histidine tag and the respective protein was performed by reverse IMAC following the same procedure as described above. Proteins were collected in the flow-through and fractions were pooled for dialysis overnight at 4 °C.

SNAP25(CtoS) and Stx(1-262) were further purified by anion exchange chromatography (AEC) after dialysis against dialysis buffer 2 (**Table 3**). For this, the proteins were loaded onto

a HiTrap™ Q HP column (GE Healthcare) and separated using a linear gradient of 10 mM NaCl/min using AEC buffer A and B. SNAP25(CtoS) eluted at 260 mM NaCl, while Stx(1-262) eluted at 330 mM NaCl. Syb(1-96) was dialysed against dialysis buffer 3 prior to further purification by SCX. For this, the dialysate was loaded onto a HiTrap™ SP HP column (GE Healthcare) and separated using a linear gradient of 10 mM NaCl/min using SXC buffer A and B. Syb(1-96) eluted at 200 mM NaCl. The protein content of the corresponding fractions was evaluated by gel electrophoresis (**Section 2.3.6**).

For final purification by SEC, SNAREs were concentrated using molecular weight cut-off filters of 3.5 kDa or 10 kDa (Amicon Ultra 15 Ultracell, Merck) and loaded onto a HiLoad™ 16/600 Superdex™ 75 prep grade column (GE Healthcare). Proteins were isocratically separated using SEC buffer and the fractions containing the protein of interest were concentrated. Protein concentrations of SNAP25(CtoS), Syb(1-96) and Stx(1-262) were determined by Lambert-Beer law using UV/Vis spectroscopy and the specific extinction coefficients (**Section 2.3.4**).

SNAP25(1-83) (**Table 1**) was purified according to the purification strategy of SNAP25(CtoS) with minor modifications. Since aromatic amino acid residues are absent in this construct, all purification steps were monitored at 214 nm and 235 nm detecting the absorbance of the peptide bond. Instead of purification by AEC, SNAP25(1-83) was directly purified by SEC. The protein concentration was determined using the Bradford-Assay (**Section 2.3.4**). Syb2 (**Table 1**) was purified according to the purification protocol of the soluble Syb(1-96) described above, in the presence of 1 % (w/v) CHAPS.

Table 3. Buffers for purification of SNARE proteins.

Buffers	Components
IMAC buffer A	20 mM HEPES, pH 7.4, 500 mM NaCl, 20 mM imidazole, 0.1 mM TCEP
IMAC buffer B	20 mM HEPES, pH 7.4, 500 mM NaCl, 500 mM imidazole, 0.1 mM TCEP
AEC buffer A	20 mM HEPES, pH 7.4, 50 mM NaCl, 0.1 mM TCEP
AEC buffer B	20 mM HEPES, pH 7.4, 1 M NaCl, 0.1 mM TCEP
SXC buffer A	20 mM sodium acetate, pH 5.5, 50 mM NaCl, 0.1 mM TCEP
SXC buffer B	20 mM sodium acetate, pH 5.5, 1 M NaCl, 0.1 mM TCEP
SEC buffer	20 mM HEPES, pH 7.4, 150 mM KCl, 0.1 mM TCEP, 1 mM EDTA
Dialysis buffer 1	20 mM HEPES, pH 7.4, 500 mM NaCl, 20 mM imidazole, 0.1 mM TCEP
Dialysis buffer 2	20 mM HEPES, pH 7.4, 50 mM NaCl, 0.1 mM TCEP
Dialysis buffer 3	20 mM sodium acetate, pH 5.5, 50 mM NaCl, 0.1 mM TCEP

2.3.3 Protein purification of Cpx1

Cpx1 was purified from cell lysate (**Section 2.3.1**) by IMAC using a HisTrap™ HP column (GE Healthcare). Buffers used for the purification are given below (**Table 4**) and all purification steps were performed at 4 °C. The cell lysate was loaded onto the column and the column was washed with IMAC buffer A until the baseline of the UV signal was reached again. Unspecifically bound proteins were washed off the column using 80 mM imidazole, followed by elution of Cpx1 at 300 mM imidazole. Fractions containing Cpx1 were evaluated by gel electrophoresis (**Section 2.3.6**) and combined for cleavage of the hexa-histidine tag. For this, pooled fractions were dialysed overnight at 4 °C against dialysis buffer 1 containing 200 U thrombin. The hexa-histidine tag and Cpx1 were separated by reverse IMAC following the same procedure as described above. Cpx1 was collected in the flow-through and the hexa-histidine tag eluted at 400 mM imidazole using IMAC buffer B. The flow-through was pooled and again dialysed overnight at 4 °C against dialysis buffer 2 to decrease the salt concentration for AEC. For this, the dialysate was loaded onto a HiTrap™ Q HP column (GE Healthcare) and proteins were separated with a linear gradient of 10 mM NaCl/min using AEC buffer A and B. Cpx1 eluted at 250 mM NaCl and the protein content of the corresponding fractions was evaluated by gel electrophoresis (**Section 2.3.6**). Subsequently, pooled fractions containing Cpx1 were concentrated using a molecular weight cut-off filter of 10 kDa (Amicon Ultra 15 Ultracell 10k, Merck). While concentrating Cpx1, the purification buffer was exchanged to storage buffer. The protein concentration was determined by Lambert-Beer law using UV/Vis spectroscopy and the specific extinction coefficient (**Section 2.3.4**).

Table 4. Buffers for purification of Cpx1.

Buffers	Components
IMAC buffer A	20 mM HEPES, pH 7.4, 300 mM NaCl, 0.1 mM TCEP
IMAC buffer B	20 mM HEPES, pH 7.4, 300 mM NaCl, 400 mM imidazole, 0.1 mM TCEP
AEC buffer A	20 mM HEPES, pH 7.4, 0.1 mM TCEP
AEC buffer B	20 mM HEPES, pH 7.4, 1 M NaCl, 0.1 mM TCEP
Storage buffer	20 mM HEPES, pH 7.4, 300 mM KCl, 0.1 mM TCEP, 1 mM EDTA
Dialysis buffer 1	20 mM HEPES, pH 7.4, 300 mM NaCl, 0.1 mM TCEP
Dialysis buffer 2	20 mM HEPES, pH 7.4, 50 mM NaCl, 0.1 mM TCEP

2.3.4 Determination of the protein concentration

Lambert-Beer law. For determination of the concentration of proteins containing aromatic residues, the absorbance at 280 nm was measured using a DS-11+ spectrophotometer (DeNovix®). Concentrations were then calculated according to the Lambert-Beer law using the extinction coefficient of the corresponding protein. Extinction coefficients and the molecular weights of the SNARE proteins and Cpx1 were calculated using the web-based ExPASy ProtParam tool [167] and are given below (**Table 5**).

Table 5. Protein properties of SNARE proteins and Cpx1.

Protein construct	Extinction coefficient ($M^{-1} \text{ cm}^{-1}$)	Molecular weight (g/mol)
Cpx1	4470	15403.37
SNAP25(CtoS)	6990	23553.13
SNAP25(1-83)	none	9931.01
Syb2	13980	12972.06
Syb(49-96)	12490	6039.9
Syb(1-96)	12490	10799.23
Stx(1-262)	7450	30620.21

Bradford-Assay. For SNAP25(1-83) no extinction coefficient is available, therefore, protein concentrations were determined by Bradford-Assay based on a BSA calibration curve [168]. For this, samples containing 1 μg to 10 μg BSA in 20 μl 20 mM HEPES, pH 7.4, 150 mM KCl, 0.1 mM TCEP, 1 mM EDTA were prepared. A sample omitting BSA was used as a control. Each sample was prepared in triplicates. 1 ml Bradford reagent containing 0.01 % (w/v) Coomassie Brilliant Blue G-250, 8.5 % (v/v) phosphoric acid, 4.75 % (v/v) ethanol was added to each sample, followed by incubation for 10 min at room temperature. The absorbance was determined by UV/Vis spectroscopy (DeNovix®) at 595 nm. Values were plotted and a linear regression was performed. Samples of the protein of interest were prepared as described using a dilution in the middle of the calibration curve.

2.3.5 Formation of protein complexes

Proteins were mixed in varying ratios ranging from 10 μ M to 60 μ M of the corresponding protein in 20 mM HEPES, pH 7.4, 150 mM KCl, 0.1 mM TCEP, 1 mM EDTA (**Supplementary Table 1**). For this, the stoichiometry of binary complexes mimicking the four-helical structure of the SNARE complex was considered. To promote SNARE complex formation by preventing formation of the 'dead end' complex [169], SNAP25(CtoS) and Syb(1-96) were initially mixed in 1:1 ratio, followed by equimolar addition of Stx(1-262). Interactions of Cpx1 with the SNARE proteins were analysed by equimolar addition of Cpx1 to pre-assembled SNARE complexes. Mixed proteins were incubated overnight at 4 °C, followed by chemical cross-linking (**Section 2.3.7**) and LC-MS/MS analysis (**Section 2.5.4**), or analysis by circular dichroism (CD) spectroscopy (**Section 2.4.1**) and native MS (**Section 2.5.5**). Rearrangement of pre-assembled complexes was directly followed by native MS after addition of interaction partners without further incubation.

2.3.6 Gel electrophoresis and western blotting

Proteins were electrophoretically separated on 4-12 % NuPAGE™ Bis-Tris gels in NuPAGE™ MES SDS running buffer containing 0.1 % (v/v) NuPAGE™ antioxidant (Thermo Fisher Scientific). SeeBlue Plus 2 Pre-Stained Protein Marker (Thermo Fisher Scientific) was used as molecular weight standard. Electrophoresis was performed at constant voltage of 200 V for 35 min (proteins) or 30 min (proteoliposomes). The gels were stained with InstantBlue™ Coomassie protein stain (Expedeon) or further processed for Western blotting.

(Cross-linked) proteins were transferred onto a nitrocellulose membrane (GE Healthcare) for 2 h at 50 mA using the buffers given below (**Table 6**). For this, two layer of filter papers, the 4-12 % Bis-Tris gel including the separated proteins, the nitrocellulose membrane and two additional filter papers were drained in transfer buffer and stacked on top of each other. After the transfer, the membrane was incubated in blocking buffer for 1 h at room temperature to block the membrane and inhibit unspecific antibody binding. Subsequently, the membrane was washed with PBST, followed by overnight incubation at 4 °C in primary antibody solution (**Table 6**). To remove unspecifically bound antibody, the membrane was washed again with PBST, followed by incubation for 1 h at room temperature in secondary antibody solution (**Table 6**). After washing the membrane with PBST, Pierce ECL western blotting substrate (Thermo Fisher Scientific) was added and the resulting chemiluminescence was detected using the Luminescence Image Analyzer LAS-4000 (Fujifilm).

Table 6. Buffers and solutions for western blotting

Solution	Composition
Transfer buffer	25 mM Tris Base, pH 8.3, 192 mM Glycin, 0.1 % (w/v) SDS, 10 % (v/v) methanol
PBS buffer	1.76 mM KH ₂ PO ₄ , 10 mM Na ₂ HPO ₄ , pH 7.4, 2.7 mM KCl, 137 mM NaCl
PBST buffer	PBS, 0.02 % (v/v) Tween 20
Blocking buffer	PBST, 5 % (w/v) milk powder
Primary antibody solution	PBST, 1 % (w/v) BSA containing anti-SNAP25 clone 71.1 (1:10,000), anti-Syntaxin-1A clone 78.3 (1:10,000), anti-VAMP-1/2/3 (1:10,000) or anti-Complexin-1/2 (1:1000) antibody
Secondary antibody solution	PBST, 1 % (w/v) BSA containing anti-mouse (1:10,000 for anti-SNAP25 clone 71.1 and anti-Syntaxin-1A clone 78.3) or anti-rabbit (1:10,000 for anti-Complexin-1/2 and anti-VAMP-1/2/3) antibody

2.3.7 Chemical cross-linking

For optimisation of cross-linking conditions, 10 μ M protein (complex) were cross-linked with increasing amounts of BS3 ranging from 0.1 mM up to 1.5 mM BS3, followed by incubation for 1 h at 25 °C and 350 rpm. The cross-linking reaction was quenched by addition of NuPAGE™ LDS sample buffer (Thermo Fisher Scientific). Cross-linked samples were analysed by gel electrophoresis (**Section 2.3.6**) and stained with InstantBlue™ Coomassie protein stain (Expedeon) or analysed by western blotting (**Section 2.3.6**). For identification of cross-linking sites, 10 μ M of the corresponding SNARE proteins, 40 μ M of the SNARE:Cpx1 complex and 50 μ M of Cpx1 were each cross-linked with 0.5 mM or 1.5 mM BS3 in a total volume of 100 μ l. These samples were precipitated with ethanol (**Section 2.5.1**), hydrolysed in solution (**Section 2.5.2**) and cross-linked dipeptides were enriched by SEC (**Section 2.5.3**), followed by LC-MS/MS analysis (**Section 2.5.4**).

2.3.8 Lipid overlay assay

Lipid overlay assays were performed using commercially available membrane lipids strips (Echelon Biosciences). All buffers and solutions are given below (**Table 7**). The membrane strip was blocked in blocking buffer for 1 h at room temperature prior to incubation overnight at 4 °C in PBST buffer containing 1.5 μ g/ml of the protein of interest. Subsequently, the protein solution was discarded and the membrane was washed with PBST buffer. For visualisation of protein-lipid binding, the appropriate primary antibody solution was added and the membrane was again incubated overnight at 4 °C. Following an additional washing step with PBST, the

membrane was incubated in secondary antibody solution for 1 h at room temperature. Binding of the protein to the lipids was detected using Pierce ECL western blotting substrate (Thermo Fisher Scientific) and resulting chemiluminescence was measured (Luminescence Image Analyzer LAS-4000, Fujifilm).

Table 7. Buffers and solutions for lipid overlay assay.

Solution	Composition
PBS buffer	1.76 mM KH ₂ PO ₄ , 10 mM Na ₂ HPO ₄ , pH 7.4, 2.7 mM KCl, 137 mM NaCl
PBST buffer	PBS, 0.1 % (v/v) Tween 20
Blocking buffer	PBST, 3 % (w/v) BSA
Primary antibody solution	PBST, 1 % (w/v) BSA containing anti-VAMP-1/2/3 (1:10,000) or anti-Complexin-1/2 (1:1000) antibody
Secondary antibody solution	PBST, 1 % (w/v) BSA containing anti-rabbit (1:10,000 for anti-VAMP-1/2/3 and anti-Complexin-1/2) antibody

2.3.9 Preparation of proteoliposomes and flotation assay

Preparation of proteoliposomes by association of soluble protein. Dried lipid films were dissolved in 20 mM HEPES, pH 7.4, 150 mM KCl, 0.1 mM TCEP, 1 mM EDTA by sonication and liposomes formed by hydration of the lipids for 1 h at room temperature. To obtain liposomes of defined size, liposomes were extruded by 21 strokes through a polycarbonate membrane with a pore size of 100 nm. Proteoliposomes were prepared by incubation of liposomes with soluble protein for 1 h at room temperature considering a lipid:protein ratio of 1:300 for Syb(1-96) and 1:1000 for Cpx1. Homogenic size distributions of extruded liposomes and proteoliposomes were validated by dynamic light scattering (**Section 2.4.2**). Association of soluble protein to the liposomes was verified in a flotation assay.

Flotation Assay. Proteoliposomes were separated from unbound protein on a sucrose step gradient. For this, proteoliposomes were mixed with 2.5 M sucrose to a final concentration of 1 M sucrose. This solution was overlaid with 3/4 volumes of 0.75 M sucrose, followed by 1/10 volumes of 20 mM HEPES, pH 7.4, 150 mM KCl, 0.1 mM TCEP, 1 mM EDTA. The sucrose gradient was centrifuged at 268,000 x g for 2 h at 22 °C. Due to their lower density, liposomes float on top of the sucrose gradient. To evaluate protein binding to the liposomes the top, middle and bottom fractions of the gradient were collected and analysed by gel electrophoresis (**Section 2.3.6**).

2.4 Biophysical methods

2.4.1 Circular dichroism (CD) spectroscopy

CD spectroscopy was performed using a Jasco J-815 CD spectrometer (Jasco Deutschland). For this, 30 μM to 60 μM of the individual proteins and 60 μM to 90 μM of binary complexes were used (**Section 2.3.5**). All measurements were performed in 20 mM HEPES, pH 7.4, 150 mM KCl, 0.1 mM TCEP, 1 mM EDTA. CD spectra were acquired from 195 nm to 260 nm with a step size of 0.1 nm at 10 °C. Quartz cuvettes with an optical path length of 0.01 cm or 0.001 cm were used. Baseline correction was performed by subtraction of the buffer signal of each measurement and 32 scans per measurement were averaged. To evaluate structural changes resulting from complex formation, theoretical spectra for binary complexes were calculated from the CD spectra of individual SNARE proteins and compared with the experimentally detected spectra. For this, the molar ellipticity $[\theta]$ of the individual proteins was calculated as followed:

$$[\theta] = \frac{\theta}{(10 \cdot c \cdot d)} \text{ in (deg cm}^2 \text{ dmol}^{-1}\text{)}$$

where Θ is the observed ellipticity in mdeg, c is the concentration in mol l^{-1} and d is the path length in cm. CD spectra of individual proteins were summed to obtain a theoretical molar ellipticity $[\theta]_{th}$ for binary complexes using the following equation:

$$[\theta]_{th} = [\theta]_{Protein\ 1} + [\theta]_{Protein\ 2}$$

Observed data were smoothed by the Savitzky-Golay algorithm with a smooth window of 40.

2.4.2 Dynamic light scattering (DLS)

DLS measurements were performed on a Zetasizer Pro (Malvern Panalytical Ltd, Malvern, UK) equipped with a 633 nm helium-neon laser and a detection angle of 173°. Liposomes and proteoliposomes (**Section 2.3.9**) in 20 mM HEPES, pH 7.4, 150 mM KCl, 0.1 mM TCEP, 1 mM EDTA were analysed at 25 °C using a 3 x 3 mm quartz cuvette. After an equilibration time of 60 s, each sample was measured three times using the ZS Xplorer (Version 2.3.1.4) software. To yield intensity and number-weighted particle size distributions, autocorrelation functions were automatically fitted applying the ZS Xplorer software.

2.5 Mass spectrometric methods

2.5.1 Precipitation with ethanol

Samples were diluted to a total volume of 200 μ l using water and proteins were precipitated by addition of 20 μ l 3 M sodium acetate, pH 5.3 and 600 μ l ice-cold 100 % (v/v) ethanol, followed by overnight incubation at -20 °C. The proteins were pelleted and subsequently washed with ice-cold 80 % (v/v) ethanol. Resulting protein pellets were dried in a vacuum centrifuge, hydrolysed in-solution (**Section 2.5.2**) and analysed by LC-MS/MS analysis (**Section 2.5.4**).

2.5.2 In-solution hydrolysis of (cross-linked) proteins

Protein pellets from ethanol precipitation (**Section 2.5.1**) were dissolved in 10 μ l 1 % (m/v) RapiGest (Waters Corporation) in 25 mM ammonium bicarbonate, pH 8.5. The pellet of the SNARE:Cpx1 complex was suspended in 10 μ l 8 M urea. For reduction of disulphide bonds, 10 μ l 50 mM dithiothreitol in 25 mM ammonium bicarbonate, pH 8.5, were added, followed by incubation for 1 h at 37 °C. Alkylation of free sulfhydryl groups of cysteine residues was performed by addition of 10 μ l 100 mM iodoacetamide in 25 mM ammonium bicarbonate, pH 8.5, for 1 h at 37 °C in the dark. (Cross-linked) proteins were then hydrolysed with trypsin (Promega) in a total volume of 100 μ l in 25 mM ammonium bicarbonate, pH 8.5 and at an enzyme:protein ratio of 1:20. For this, the concentration of RapiGest and urea was diluted to final concentrations of 0.1 % (m/v) and 0.8 M. The protein pellets were incubated overnight at 37 °C. RapiGest was hydrolysed by addition of 20 μ l 5 % (v/v) trifluoroacetic acid for 2 h at 37 °C, followed by centrifugation. The peptide containing supernatant was collected and dried in a vacuum centrifuge. For cross-linking analysis, cross-linked peptide pairs were enriched (**Section 2.5.3**) prior to LC-MS/MS analysis (**Section 2.5.4**).

2.5.3 Enrichment of cross-linked peptide pairs

For enrichment of low abundant cross-linked peptide pairs from linear peptides, SEC was performed using an *ÅKTA pure* chromatography system (GE Healthcare). For this, peptide pellets (**Section 2.5.2**) were dissolved in 60 μ l 30 % (v/v) acetonitrile, 0.1 % (v/v) trifluoroacetic acid and the peptides were isocratically separated on a Superdex peptide column 3.2/300 GL (GE Healthcare) at a flow rate of 50 μ l/min. Peptide elution was followed by monitoring the wavelength of 214 nm. Early fractions containing cross-linked peptide pairs were collected, dried in a vacuum centrifuge and subsequently analysed by LC-MS/MS analysis (**Section 2.5.4**).

2.5.4 LC-MS/MS analysis

(Cross-linked) peptides were analysed by reverse-phase liquid-chromatography using a DionexUltiMate 3000 RSLC nano system coupled to a Q-Exactive Plus Hybrid Quadrupol-Orbitrap mass spectrometer (Thermo Fisher Scientific). For liquid-chromatography, 0.1 % (v/v) formic acid was used as mobile phase A and 80 % (v/v) acetonitrile, 0.1 % (v/v) formic acid, was used as mobile phase B. Peptides (**Section 2.5.2**, **Section 2.5.3**) were dissolved in 2 % (v/v) acetonitrile, 0.1 % (v/v) formic acid and loaded onto a trap column (Acclaim PepMap 100 C18-LC pre-column, 300 µm I.D., particle size 5 µm, Thermo Fisher Scientific) with a flow rate of 10 µl/min. Peptide separation was performed on an analytical column (Acclaim PepMap 100 C18-LC column, 75 µm I.D., particle size 3 µm, Thermo Fisher Scientific) at a flow rate of 300 nl/min using a gradient of 4 % to 90 % mobile phase B in 69 min for protein identification and 99 min for cross-linking analysis. Considering varying hydrophobicity of cross-linked peptide pairs, the gradient was adjusted and different elution times were applied for early, middle and late fractions (**Table 8**).

Table 8. Gradients for liquid-chromatography.

Gradients were formed using 0.1 % (v/v) formic acid as mobile phase A and 80 % (v/v) acetonitrile, 0.1 % (v/v) formic acid as mobile phase B. For protein identification a 90 min gradient was used. For cross-linking analysis, 120 min gradients were adjusted depending on hydrophobicity (early fractions: highly hydrophobic; late fractions: weak hydrophobic).

Mobile phase A [%]	Mobile phase B [%]	Gradient time [min]			
		90 min	120 min (early fractions)	120 min (middle fractions)	120 min (late fractions)
96	4	0	0	0	0
92	8	3	3	3	3
85	15	-	15	-	75
75	25	60	90	90	90
50	50	64	94	94	94
10	90	65	95	95	95
10	90	69	99	99	99
96	4	70	100	100	100
96	4	90	120	120	120

Peptides eluting from the C18-LC column were directly transferred into the mass spectrometer. For data acquisition, the following parameters were applied: capillary voltage, 2.8 kV; capillary temperature, 275 °C; data dependent mode; polarity, positive. Survey full scans were acquired

in the orbitrap over a mass range of 350-1600 m/z with a resolution of 70,000 and an automatic gain control target of 3e6. The 20 most intense ions were selected and fragmented in the HCD cell at an AGC target of 1e5 and a normalized collision energy of 30 %. Precursor ions with charge states of 2+ to 8+ (for protein identification) and 3+ to 8+ (for cross-linking analysis) were selected. MS2 spectra were acquired with a resolution of 17,500 for protein identification samples and 35,000 for cross-linked dipeptide samples. Previously selected ions were dynamically excluded for 30 s. The lock mass option for internal calibration of the Orbitrap was enabled. The lock mass was set to m/z 445.120025 [170].

2.5.5 Native MS

Storage buffer of at least 20 µl protein solution was exchanged against 200 mM ammonium acetate using Micro Bio-Spin 6 gel filtration columns (BioRad) or Vivaspin 500 filtration units with a molecular weight cut-off of 10 kDa (Sartorius AG) according to the manufacturer's protocol. The protein concentration was diluted to 5 µM to 50 µM. For the analysis of protein-lipid complexes, 5 µM protein in 200 mM ammonium acetate were mixed with 5 µM, 25 µM and 50 µM lipid in 200 mM ammonium acetate, 0.5 % (v/v) C8E4. The detergent concentration was adjusted to 0.5 % (v/v) C8E4. 4 µl protein or protein-lipid sample were loaded into gold-coated glass capillaries prepared in house [132] and directly introduced into a Waters Micromass Q-ToF Ultima mass spectrometer modified for transmission of high masses [139]. For data acquisition, the following parameters were applied: capillary voltage, 1.3 kV to 1.7 kV; sample cone voltage, 35 V (protein-lipid samples) or 80 V (protein samples); RF lense voltage, 80 V; collisional voltage, 10 V to 50 V. Mass spectra were processed using MassLynx 4.1 software (Waters) and data were externally calibrated using 100 mg/ml caesium iodide solution.

2.6 Database search and data analysis

2.6.1 Identification of proteins

Protein identification was performed using MaxQuant (v.1.6.17) [97]. For this, raw data were searched against a database containing the *Escherichia coli* proteome, the amino acid sequences of the target proteins as well as defined contaminants. Following database search parameters were applied: enzyme, trypsin; missed cleavage-sites, 2; variable modifications, carbamidomethylation (cysteine), oxidation (methionine) and acetylation (N-terminus); mass accuracy, 20 ppm (precursor ions) and 4.5 ppm (fragment ions); FDR, 0.01.

2.6.2 Identification of cross-linked peptide pairs

Cross-linked peptide pairs were identified using pLink2 (v.2.3.9) [120]. For this, raw data were searched against a database including amino acid sequences of the corresponding SNARE proteins as well as Cpx1. The following search parameters were applied: enzyme, trypsin; missed cleavage sites, 3; peptide mass, 600 to 6000; peptide length, 6 to 60; precursor and fragment tolerance +/- 20 ppm; fixed modification, carbamidomethylation (cysteine); variable modification, oxidation (methionine); fragmentation, HCD; FDR, 0.05; crosslinker, BS3. BS3 cross-links primary amines of N-termini and lysine residues and to a lower extent serine, threonine and tyrosine residues. Therefore, the database search was performed twice excluding cross-links between primary amines in the second search. Mass spectra of potential cross-links were manually evaluated using the pLink2 visualization software pLabel [120]. Results tables were filtered for positively validated cross-links and summarised using CroCo software [165]. Identified cross-links were visualised using xVis software [123]. To visualise the reproducibility of cross-linking experiments, cross-links identified in three replicates were plotted in VENN diagrams.

2.6.3 Validation of identified cross-linking sites

For validation of cross-links, an available high-resolution structure of the SNARE complex (PDB ID: 1SFC) [17] including the SNARE core complex but lacking flexible structures was used. To further enable visualisation of cross-links formed towards disordered protein regions, ColabFold [171] was used to predict AlphaFold 2 structures of the individual SNARE proteins, Cpx1, the soluble SNARE complex and the SNARE:Cpx1 complex. For this, the following parameters were applied: query_sequence, protein sequences of SNAP25(CtoS), Syb(1-96), Stx(1-262) and Cpx1; template_mode, none; msa_mode, MMseqs2 (UniRef and Environmental); pair_mode, unpaired and paired; model_type, AlphaFold2-ptm and AlphaFold-multimer-v2; num_recycles, 3. Cross-links identified in at least two out of three replicates were mapped into the structures using UCSF Chimera [124] and Xlink Analyzer [126]. Cross-links with a $c_{\alpha} - c_{\alpha}$ distance of $\leq 30 \text{ \AA}$ are represented as blue lines, while cross-links with a $c_{\alpha} - c_{\alpha}$ distance of $\geq 30 \text{ \AA}$ are shown as red lines. Multimers of SNARE proteins and complexes thereof were predicted using ColabFold [171] by including the protein sequences twice during prediction to further validate intermolecular cross-links as well as parallel and antiparallel orientations of oligomers and SNARE complexes.

2.6.4 SNARE:Cpx1 model building

For visualisation of validated cross-links (**Section 2.6.3**) identified in the SNARE:Cpx1 complex, a model based on the complete SNARE complex and full-length Cpx1 structures was created using PyMOL [166]. A high resolution structure of the SNARE core complex (PDB ID: 1SFC) [17] was aligned with an incomplete structure of the SNARE:Cpx1 complex (PDB ID: KIL) [61] including the central helix of Cpx1, but lacking disordered regions as well as structures for Syb2. To this template, an AlphaFold [172] prediction of the full-length Cpx1 was aligned and a high-resolution structure of the Habc domain of Stx1 (PDB ID: 1EZ3) was added [22]. Missing structural elements of SNARE proteins such as linkers were added manually as coloured lines. Cross-linking sites are indicated as black lines.

2.6.5 Analysis of native mass spectra

Native mass spectra (**Section 2.5.5**) were analysed using MassLynx 4.1 (Waters), Massign software (version 11/14/2014) [150] and an in-house written deconvolution macro. For this, at least 100 scans per measurement were combined and smoothed twice using Savitzky Golay algorithm and a smooth window of ten. Masses were calculated from centroided spectra using MassLynx 4.1 or Massign software. For manual assignment, masses were calculated using the following equations:

$$(m/z)^* = \frac{m^{\text{Protein}} + (z+1) \cdot m^{\text{Proton}}}{z+1} \quad (m/z) = \frac{m^{\text{Protein}} + z \cdot m^{\text{Proton}}}{z}$$

with $(m/z) > (m/z)^*$ and $m^{\text{Proton}} = 1$

$$z (m/z) = \frac{(m/z)^* - 1}{(m/z) - (m/z)^*} \quad m^{\text{Protein}} = z \cdot ((m/z) - 1)$$

where m is the mass and z the charge.

2.6.6 Data availability

The mass spectrometry proteomics data have been deposited to the ProteomeXchange Consortium (<http://proteomecentral.proteomexchange.org>) via the PRIDE partner repository [173] with the dataset identifier PXD030619.

2.6.7 Statistics and Reproducibility

Purification of the proteins was confirmed by LC-MS/MS once (**Supplementary Table 2**). An FDR of 1 % was applied during all database searches (MaxQuant). All cross-linking experiments were performed three times using individual proteins or protein complexes mixed in independent experiments. An FDR of 5 % was applied during database search (pLink). Identified cross-links for each individual experiment are given (**Supplementary Table 3-6**). Native MS experiments of individual proteins, protein complexes and Syb(1-96):lipid complexes were performed at least three times. Native MS experiments of Cpx1:lipid complexes were performed once. Protein complexes and protein:lipid complexes were mixed in independent experiments. Representative mass spectra are shown. CD measurements were performed at least in duplicates for individual proteins and protein mixtures. Western blots and lipid overlay assays were performed at least three times. Representative blots are shown. Proteoliposomes were prepared in at least three independent experiments and each preparation was analysed by DLS with each sample measured three times. Flotation assays were performed at least three times and representative gels with the corresponding DLS measurement are shown.

3 Results²

3.1 Expression, purification and identification of SNARE proteins and Cpx1

To study the assembly of the SNARE complex including formation of potential intermediates and 'off pathway' complexes, soluble constructs of the SNARE proteins were used to allow rotational freedom of all compounds during complex formation. For the structural characterisation of Syb2, three protein variants were used: the full-length Syb2 including the transmembrane domain (Syb(FL)), the complete cytosolic domain including the full SNARE motif (Syb(1-96)) and a shortened cytosolic domain lacking the N-terminal half of the SNARE motif (Syb(49-96)). Stx1 was expressed without transmembrane helix (Stx(1-262)), and full-length SNAP25 was expressed with all cysteines mutated to serine residues (SNAP25(CtoS)) to prevent formation of disulfide bonds and providing additional cross-linking sites for structural analysis. In addition, the N-terminal Qb SNARE motif of SNAP25 (SNAP25(1-83)) was expressed allowing incorporation of a single SNARE motif into the complexes. To study the regulatory function of Cpx1 on SNARE complex assembly, the full-length variant was purified. All plasmids encoding these protein variants were provided by Prof. Reinhard Jahn (Max-Planck Institute for Multidisciplinary Sciences, Göttingen).

All proteins were expressed in *Escherichia coli* (**Section 2.2.2**) and isolated from cell lysate using an affinity-based purification strategy using N-terminal hexa-histidine tags (**Section 2.3.2**, **Section 2.3.3**). In the following, the purification strategy is exemplary described for Syb(1-96). After lysis of the *Escherichia coli* cells, Syb(1-96) was isolated from the cell lysate by IMAC (**Figure 9A**). Histidine-rich proteins, which unspecifically bound to the column material were eluted at 100 mM imidazole. Subsequently, Syb(1-96) eluted from the column using 350 mM to 500 mM imidazole. All fractions were then analysed by gel electrophoresis. Fractions containing an abundant protein band with an approximate molecular weight of 11 kDa corresponding to Syb(1-96) were combined (F14 to F17) and dialysed overnight while cleaving off the hexa-histidine tag by thrombin. Performing a second IMAC, the hexa-histidine tag as well as histidine-rich contaminations were removed as they associate with the column material, while Syb(1-96) was collected in the flow-through (**Figure 9B**). Syb(1-96)-containing fractions were combined (F3 to F9) and dialysed again overnight to decrease the salt concentration for subsequent purification by SCX (**Figure 9C**). Applying a linear salt gradient from 50 mM to 500 mM NaCl additional impurities differing in their overall charge from Syb(1-96) were removed. Fractions mainly containing Syb(1-96) were combined (F28 to F31) and concentrated before removing remaining contaminations by a SEC

² Parts of these results were published in J. Hesselbarth, C. Schmidt (2023) *Mass spectrometry uncovers intermediates and off-pathway complexes for SNARE complex assembly. Communications biology* 6(1):198 [174].

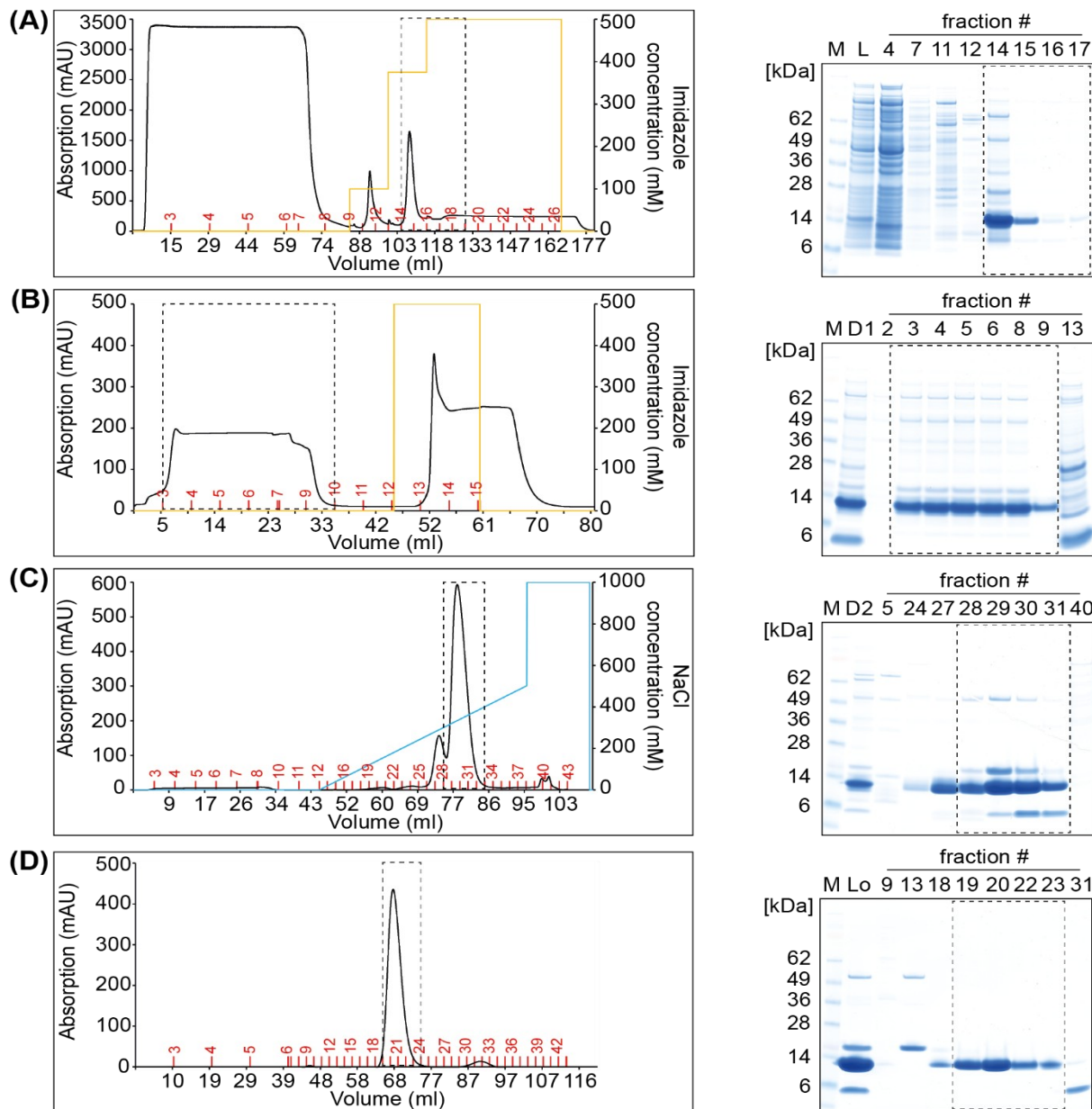


Figure 9. Purification of Syb(1-96).

Chromatograms (lhs) and gel electrophoresis of selected fractions (rhs) of the purification of Syb(1-96) by (A) IMAC (B) IMAC after thrombin cleavage (C) SCX and (D) SEC are shown. Fractions that were combined for the following purification step are indicated by dotted lines. M: marker, L: lysate, D1: dialysate after thrombin cleavage, D2: dialysate after second IMAC, Lo: concentrated fractions after SCX

(Figure 9D). Fractions containing Syb(1-96) (F19 to F23) were combined, concentrated and stored at -20°C for subsequent experiments.

Similar to the described purification protocol for Syb(1-96), the protein variants Syb(FL), Stx(1-262), SNAP25(1-83), SNAP25(CtoS) and Cpx1 were purified (**Supplementary Figures 2-6**). Note that Syb2 variants were purified by SCX, while all other proteins were purified by AEC. In addition, Syb(FL) was purified in the presence of 1 % (w/v) CHAPS to ensure solubility and integrity of the transmembrane domain. As the amino acid sequence of SNAP25(1-83) does

not include aromatic residues, the elution profiles were monitored at a wavelength of 235 nm. For Cpx1, the final SEC was omitted. Syb(49-96) was provided by Dr. Caroline Haupt (Martin Luther University Halle-Wittenberg, Halle).

Proteins used in this thesis were separated by gel electrophoresis followed by staining with Coomassie to assess purity of the purified proteins (**Figure 10A**). To confirm the protein identity by western blotting analysis, specific antibodies against the appropriate variant were used (**Figure 10B**). Low abundant degradation products and dimers were observed for Syb(FL) and Stx(FL). Low abundant impurities were observed for SNAP25(CtoS) and Stx(1-262).

Proteins and contaminations were identified by MS. For this, proteins were precipitated with ethanol, digested in solution with trypsin and analysed by LC-MS/MS (**Section 2.5**). Using the MaxQuant search engine, all proteins were verified with high sequence coverage, i.e. 100 % for SNAP25(1-83), 94.7 % for SNAP25(CtoS), 87.5 % for Stx(1-262), 80 % for Syb(1-96), 74.8 % for Syb(FL) and 88.3 % for Cpx1. A predominant contamination was DnaK (**Supplementary Table 2**), an *Escherichia coli* homologue of the human chaperone Hsp70, which is constitutively expressed during protein synthesis, presumably maintaining the integrity of the SNAREs by stabilizing their disordered structure in solution [175].

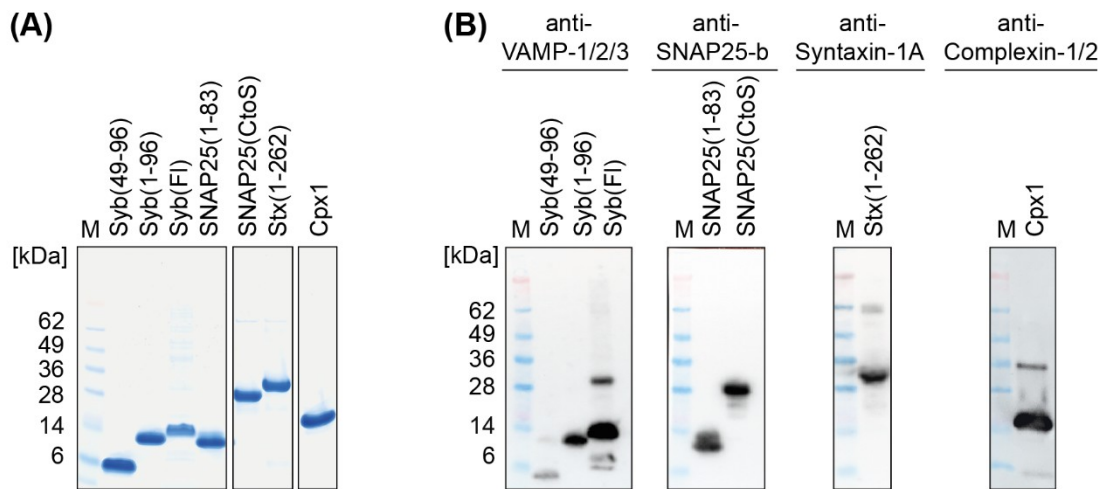


Figure 10. SDS-PAGE and Western Blot of the protein variants.

(A) 5 μ g of Syb(49-96), Syb(1-96), Syb(FL), SNAP25(1-83), SNAP25(CtoS), Stx(1-262), Stx(FL) and Cpx1 were separated by gel electrophoresis and stained with Coomassie. **(B)** Western Blots of the proteins visualised by anti-VAMP1/2/3 antibody, anti-SNAP25-b antibody, anti-Syntaxin-1A antibody and anti-Complexin-1/2 antibody. A molecular weight standard (M) was applied.

3.2 Structural characterisation of individual synaptic proteins in solution

Syb2 was previously structurally characterised in the absence of interaction partners using chemical cross-linking and native MS [176]. With decreasing structural content, increasing oligomerisation of Syb2 in solution was described. To explore whether SNAP25(CtoS), Stx(1-262) and Cpx1 exhibit the same oligomerisation behaviour in solution as discussed above for Syb2, proteins were also characterised in the absence of interaction partners. For the sake of completeness, Syb2 will also be analysed in this thesis, using the same experimental conditions for native MS and cross-linking as for SNAP25(CtoS), Stx(1-262) and Cpx1. All individual proteins were analysed by chemical cross-linking (**Section 2.3.7**), native MS (**Section 2.5.5**) and CD spectroscopy (**Section 2.4.1**).

3.2.1 Oligomerisation of different Synaptobrevin-2 variants

10 μ M Syb(49-96), Syb(1-96) and Syb(FL), were cross-linked with concentrations of 10 μ M to 3 mM BS3 cross-linker. The cross-linked proteins were separated by gel electrophoresis and visualised by Coomassie staining (**Figure 11**). For Syb(49-96) and Syb(1-96) higher oligomers were not observed, while Syb(FL) showed oligomers up to tetramers with increasing cross-linker concentration. Interestingly, Syb(1-96) and Syb(FL) showed two distinct monomeric protein bands that were not observed for Syb(49-96). These might originate from an elongated and a folded conformation involving the N-terminal peptide of Syb2, which is not included in Syb(49-96). To overcome the detection limit of Coomassie staining, oligomerisation was also analysed by western blotting. Using the anti-VAMP1/2/3 antibody for visualisation revealed low abundant oligomers up to decamers for Syb(49-96), up to octamers for Syb(1-96) and up to heptamers for Syb(FL) (**Figure 11**).

To validate oligomerisation of Syb2 without inducing covalent linkages native MS was performed. This technique preserves non-covalent interactions of proteins and protein complexes during ionisation while the proteins are transferred from the solvent into the gas phase. Depending on the surface area of a protein, different charges are acquired resulting in a Gaussian distribution of charge states [177]. Similar to the previous study [176], the oligomeric state of the Syb2 variants was analysed at increasing protein concentrations. However, to avoid formation of unspecific aggregates during ionisation, a protein concentration of maximally 50 μ M was used [178]. The native mass spectra of both, Syb(49-96) and Syb(1-96), show a single charge state distribution at 5 μ M and at 25 μ M protein concentration corresponding to monomeric Syb(49-96) (6039 Da) and Syb(1-96) (10799 Da) (**Figure 11A and 11B**). These masses agree well with the theoretically calculated masses of the variants based on the amino acid sequences, i.e. 6039.9 Da for Syb(46-96) and 10799.23 Da for Syb(1-96). At the employed concentrations, oligomer formation was not observed. However, the

mass spectra of Syb(49-96) and Syb(1-96) at a concentration of 50 μM showed several charge state distributions corresponding in mass to the dimeric (12102 Da) and trimeric (18184 Da) Syb(49-96) as well as dimeric Syb(1-96) (21598 Da) (**Figure 11A and 11B**). For the analysis of membrane proteins such as Syb(FL), detergents are required to solubilise the proteins

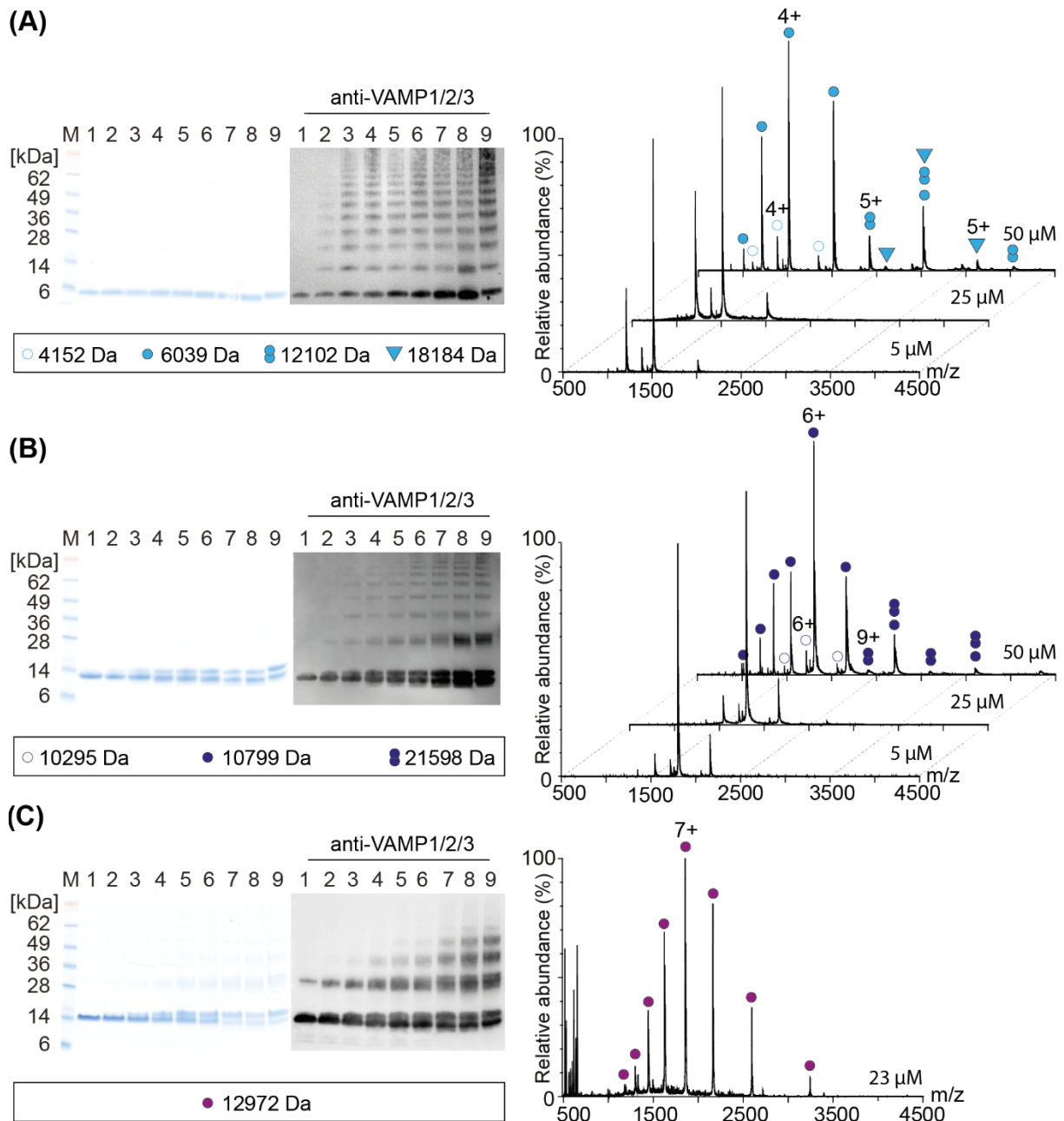


Figure 11. Oligomerisation of Syb2 variants.

10 μM of Syb2 variants were cross-linked with 0 μM (lane 1), 10 μM (lane 2), 25 μM (lane 3), 50 μM (lane 4), 75 μM (lane 5), 100 μM (lane 6), 300 μM (lane 7), 1 mM (lane 8) and 3 mM (lane 9) BS3 cross-linker. Cross-linked and non-cross-linked protein were separated by gel electrophoresis and visualised by Coomassie staining and western blotting (**lhs**). Native mass spectra of 5 μM , 25 μM and 50 μM protein are shown. Charge state distributions corresponding to monomers (circle), dimers (twin-circles) and trimers (triangle) are assigned (**rhs**). The following Syb2 variants were used: **(A)** Syb(49-96), **(B)** Syb(1-96) and **(C)** Syb(FL).

[179,162]. At the same time, detergent micelles exhibit heterogeneous sizes resulting in detergent clusters overlapping with the protein signal and impeding the analysis of proteins in the presence of detergent. To analyse the oligomeric state of membrane proteins by native MS, detergents need to be removed inside the mass spectrometer by collisional activation, releasing the intact complex [179]. Syb(FL) was purified in the zwitterionic CHAPS detergent, which is not suited for native MS. Therefore, Syb(FL) was transferred into C8E4 by SEC prior to native MS analysis. C8E4 is a non-ionic detergent requiring less activation energy and, therefore, decreasing the possibility of unintended loss of non-covalent protein-protein interactions [164]. The mass spectrum of 23 μM Syb(FL) was obtained at a collisional energy of 100 V, dissociating C8E4 clusters. One charge state distribution corresponding in mass to monomeric Syb(FL) (12972 Da) was observed (**Figure 11C**) and agrees well with the theoretically calculated mass of 12972.06 Da. Additional charge state series corresponding to oligomers, such as the dimer observed by western blotting, were not detected, presumably due to the high collisional energy applied. In conclusion, oligomerisation of Syb2 variants was observed at low protein concentrations by chemical cross-linking combined with western blotting. Using native MS formation of oligomers of the soluble Syb2 variants was also observed, however, the highest oligomeric state was a trimer of Syb(49-96). Oligomers of the Syb(FL) were not identified by native MS, presumably due to the high collisional energy applied.

To determine the secondary structure content of the Syb2 variants, CD spectroscopy was performed. For this, 0.1 $\mu\text{g}/\mu\text{l}$ of each protein variant were analysed in 7.4 mM HEPES, 50 mM KCl, 0.3 mM EDTA, 0.03 mM TCEP. In the case of Syb(FL) the buffer additionally contained 0.5 % (w/v) C8E4. The CD spectra of Syb(49-96) and Syb(1-96) both show a dominant minimum at 200 nm and a minor minimum at 225 nm revealing an intrinsically disordered structure (**Figure 12**). When compared with Syb(49-96), Syb(1-96) shows a slight increase in

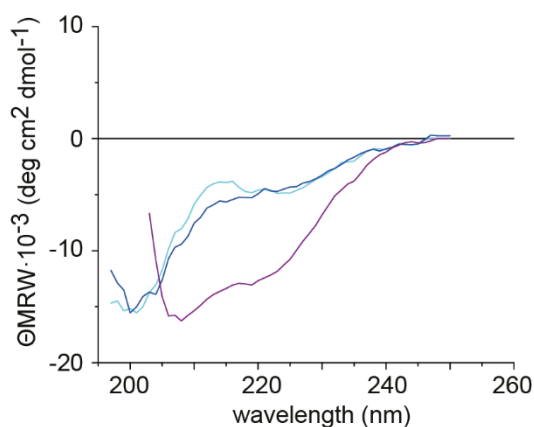


Figure 12. Secondary structure content of Syb2 variants.

CD spectra of 0.1 $\mu\text{g}/\mu\text{l}$ Syb(49-96) (light blue), Syb(1-96) (dark blue) and Syb(FL) (purple).

helicity at 205 nm, probably corresponding to a previously described helical nucleation site present at the N-terminal region of the SNARE motif that is not present in Syb(49-96) [42]. Comparison of the CD spectrum of the full-length variant with the soluble constructs reveals an increase in helicity as visualised by the shifted minimum from 200 nm to 208 nm and a second dominant minimum at 225 nm. The increased helicity likely results from the helical transmembrane domain. Consequently, the high degree of oligomerisation of the shortened Syb2 variants correlates well with a decreased helical content and an increased disorder compared to Syb(FL).

3.2.2 Structural characterisation of SNAP25(CtoS)

SNAP25(CtoS) was analysed as described above for Syb2. First, 10 μ M SNAP25(CtoS) were cross-linked with increasing amounts of BS3 cross-linker ranging from 0.5 mM up to 1.5 mM. Cross-linked SNAP25(CtoS) was then separated by gel electrophoresis, and Coomassie staining revealed oligomers up to pentamers. For evaluation of protein bands corresponding to low abundant higher molecular weight species, western blotting using a specific antibody against SNAP25-b was performed; oligomers up to heptamers were detected (**Figure 13A**). To identify specific interaction sites within SNAP25(CtoS) and oligomers thereof, 10 μ M of the protein were cross-linked with 1.5 mM BS3 cross-linker and hydrolysed in solution using trypsin. Cross-linked peptide pairs were separated from linear peptides by SEC. Fractions containing cross-linked peptide pairs were analysed by LC-MS/MS and potential cross-links were identified by database searching using the software pLink2 [120], followed by manual validation of fragment spectra.

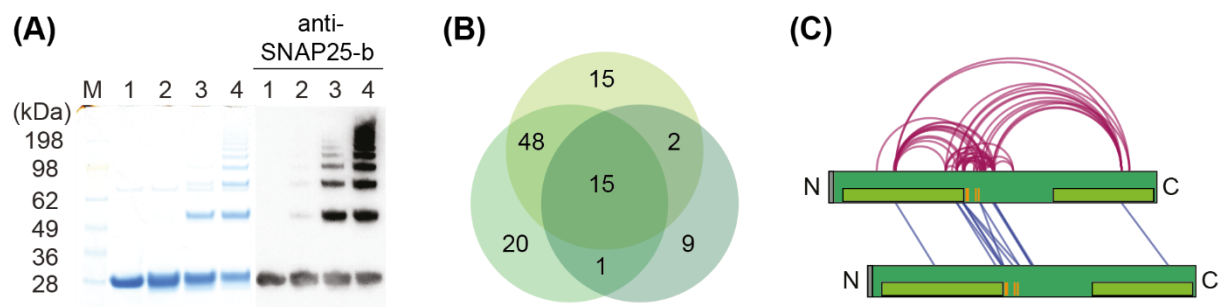


Figure 13. Cross-linking analysis of SNAP25(CtoS).

(A) 10 μ M SNAP25(CtoS) were cross-linked with 0 mM (lane 1), 0.5 mM (lane 2), 1 mM (lane 3) and 1.5 mM (lane 4) BS3 cross-linker. Cross-linked and non-cross-linked SNAP25(CtoS) were separated by gel electrophoresis and visualised by Coomassie staining and western blotting using anti-SNAP25-b antibody. **(B)** 10 μ M of SNAP25(CtoS) were cross-linked with 1.5 mM BS3 cross-linker in three replicates. The number of evaluated cross-links of each replicate is visualised in a VENN diagram. **(C)** Identified cross-links are visualised in a network plot. SNARE motifs (light green), the residual histidine tag (grey) and serine mutations (orange) are indicated. Intermolecular (blue lines) and intramolecular (purple lines) cross-links are shown. (Figure adapted from [174].)

A cross-link was positively validated if the following requirements were fulfilled: (i) both peptides show a series of at least four consecutive fragment ions, (ii) for both peptides a sufficient number of fragment ions was observed, and (iii) signals are well above the signal-to-noise ratio. A spectrum including a fragment ion that additionally contains the mass of the cross-linker and the second peptide was unambiguously identified to correspond to a cross-linked peptide pair. Cross-linked peptide pairs containing identical or overlapping peptide sequences were assigned as intermolecular cross-links, whereas different peptide sequences were considered to be intramolecular cross-links although these might also originate from different copies of the same protein. Example mass spectra of an inter- and intramolecular cross-link of SNAP25(CtoS) are shown in **Figure 14**. The intermolecular cross-link contains two identical peptides with the sequence K*AWGNNQDGVVASQPAR, which are covalently linked through their lysine side chains (K*). Both peptides were identified by series of singly charged ions ($y1^+$ to $y16^+$) fully covering the peptide sequences. Low abundant doubly charged ions ($b3^{2+}$ and $b4^{2+}$) were also observed for both peptides. These ions include the mass of the cross-linker and the second peptide, thus, verifying the position of the cross-linked residues. The example spectrum of an intramolecular cross-link of SNAP25(CtoS) includes the peptides with the sequences NLKDLGK*SSGLFISPSNK (peptide 1) and K*AWGNNQDGVVASQPAR (peptide 2) that were cross-linked through two lysine residues (K*). Peptide 1 was identified by a series of singly charged ions ($y1^+$ to $y11^+$ and $b2^+$ to $b6^+$). Peptide 2 was identified by a complete series of singly charged ions ($y1^+$ to $y14^+$) as well as the doubly charged $y15^{2+}$ -ion. The position of the cross-link was confirmed by the doubly charged $b2^{2+}$ - and $b3^{2+}$ -ions of the second peptide.

Manual validation of the fragment ion spectra revealed 53 intra- and 13 intermolecular cross-links in at least two out of three replicates (**Figure 13B**, **Supplementary Table 3**). Visualisation of the cross-links in a network plot showed that most of the cross-links are formed with the serine rich linker of SNAP25(CtoS) (**Figure 13C**). The BS3 cross-linker is not only reactive towards primary amines such as lysine side chains and the protein's N-terminus, but also towards hydroxyl groups of serine, threonine and tyrosine residues. Accordingly, the intermolecular cross-links were mainly identified between lysine and serine residues of the linkers of two copies of SNAP25(CtoS) and are mainly located C-terminal of the first SNAP25(CtoS) SNARE motif (**Figure 13C**). Intermolecular cross-links between SNARE motifs of two SNAP25(CtoS) copies were also observed indicating parallel orientation of SNAP25(CtoS) oligomers. Intramolecular cross-links were predominantly formed between the linker and the C-termini of both SNARE motifs suggesting high flexibility of the protein. Note that, these cross-links can only form if individual SNAP25(CtoS) resembles a similar conformation in solution as it adopts in the assembled SNARE complex with both SNARE

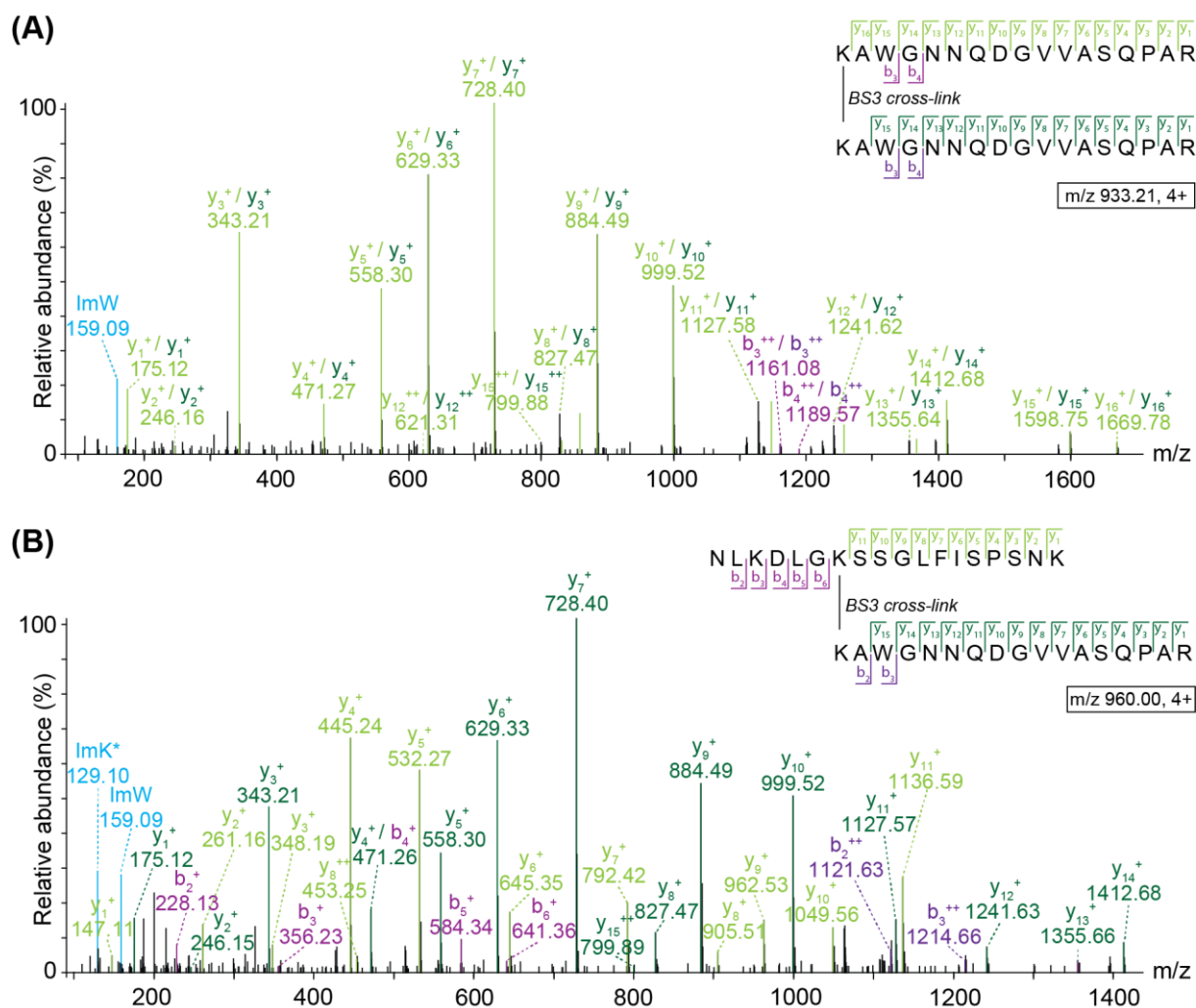


Figure 14. Example spectra of SNAP25(CtoS) cross-links.

Fragment ion spectra of **(A)** an intermolecular and **(B)** an intramolecular cross-link of SNAP25(CtoS) cross-linked with BS3. The m/z values and charges of the precursor ions are indicated (boxes). Series of y -ions (light/dark green) and b -ions (light/dark blue) as well as immonium ions and immonium related ions (Im/Im*, orange) are assigned. (Figure taken from Hesselbarth, master thesis (2019).)

motifs orientated in parallel, thus, indicating structure formation for SNAP25(CtoS) in solution **(Figure 13C)**.

The described arrangement was validated by mapping the observed cross-links onto structural models predicted by AlphaFold 2 [171,172] including disordered regions that are not available in high resolution structures **(Figure 15)**. For the visualisation of intermolecular cross-links an AlphaFold 2 prediction of dimeric SNAP25(CtoS) was used. Identified cross-links correlate well with the predicted structure and 7 out of 14 cross-links are in the expected cross-linking distance below 30 Å. However, cross-links formed between SNAP25(CtoS) linkers exceed this distance **(Figure 15A)**. Comparing the AlphaFold 2 predicted structure and a high-resolution structure of SNAP25, co-crystallized with Stx1 and Syb2, confirmed that overlength cross-links are formed by the disordered SNAP25(CtoS) linker **(Figure 15B)**. Intramolecular cross-links

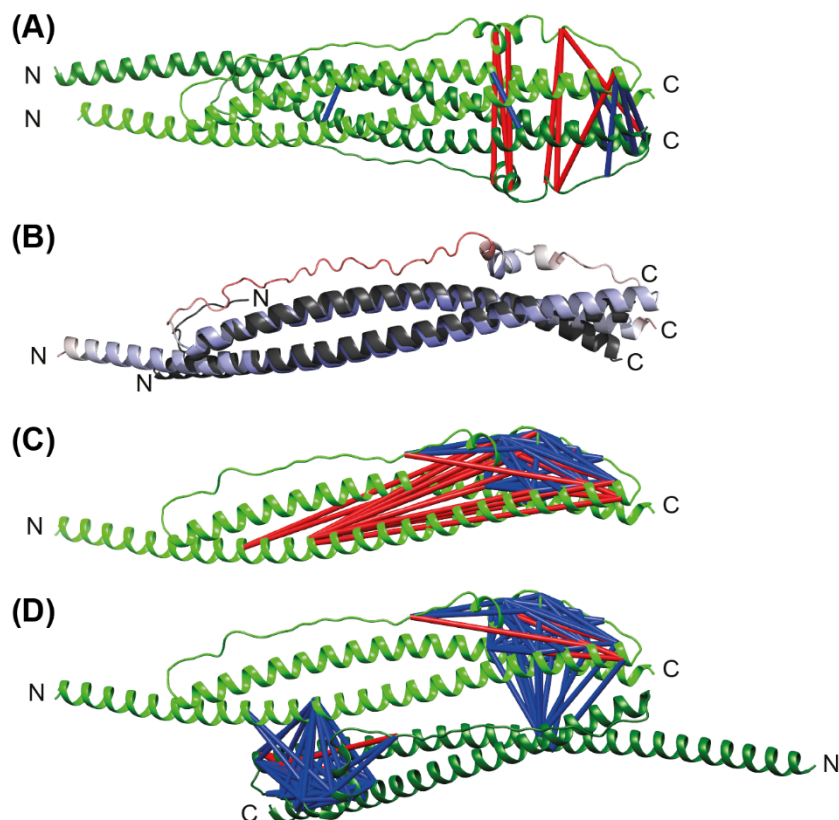


Figure 15. Validation of inter- and intramolecular interactions of SNAP25(CtoS).

AlphaFold 2 predictions of monomeric and dimeric SNAP25(CtoS) (green) are shown as cartoon representation. N- and C-termini are labelled. Cross-links identified in at least two out of three replicates are visualised and cross-linking distances corresponding to short-range (<30 Å, blue lines) and long-range (>30 Å, red lines) cross-links are highlighted. **(A)** Intermolecular cross-links are mapped onto a SNAP25(CtoS) dimer in parallel orientation. **(B)** An alignment of an AlphaFold 2 prediction of monomeric SNAP25(CtoS) (pLDDT score < 50 %, red; 50-70 %, light-red; 70-90 % light-blue; > 90 % blue) and a crystal structure of SNAP25 (black) co-crystallized with Stx1 and Syb2 [17] is shown. **(C)** Intramolecular cross-links are mapped onto a SNAP25(CtoS) monomer. **(D)** Intramolecular cross-links are mapped onto an SNAP25(CtoS) dimer in antiparallel orientation. Cross-links are shown twice.

were visualised in the structure of a SNAP25(CtoS) monomer. 34 out of 53 cross-links identified cross-links are within the expected cross-linking distance; however, 19 cross-links exceed the 30 Å threshold (**Figure 15C**). These cross-links might originate from two different copies of the protein and, therefore, represent intermolecular interactions. Including a second copy of SNAP25(CtoS) in antiparallel orientation into the arrangement resulted in positive validation of these overlength cross-links; 49 out of 53 identified cross-links are short-range cross-links (**Figure 15D**).

Oligomerisation of SNAP25(CtoS) observed by chemical cross-linking was also verified by native MS (**Figure 16A**). For this, the storage buffer of 10 µM SNAP25(CtoS) was exchanged against 200 mM ammonium acetate and the protein was directly transferred into the Ultima mass spectrometer. Several charge state distributions corresponding to monomeric

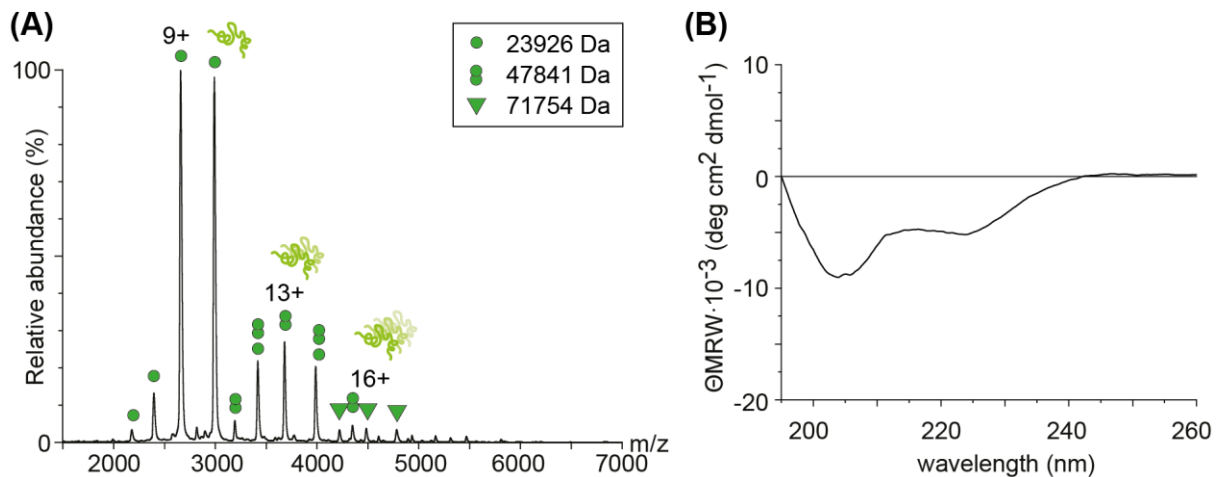


Figure 16. Native MS and CD spectroscopy of SNAP25(CtoS).

(A) Native mass spectrum of 10 μM SNAP25(CtoS). Charge state distributions corresponding to monomers (circle), dimers (twin-circles) and trimers (triangle) are assigned. (B) CD spectrum of 30 μM SNAP25(CtoS). (Figure adapted from [174].)

(23926 Da), dimeric (47841 Da) and trimeric (71754 Da) SNAP25(CtoS) were observed. Of these, the monomeric species is the main species with highest intensity, while dimeric and trimeric oligomers appear less abundant. Consequently, SNAP25(CtoS) shows a similar oligomerisation behaviour as described above for Syb2. To examine whether the observed oligomers are structured, SNAP25(CtoS) was analysed by CD spectroscopy determining the content of secondary structures (**Figure 16B**). The CD spectrum of SNAP25(CtoS) shows a dominant minimum at 205 nm and a minor minimum at 225 nm corresponding to an intrinsically disordered structure, similar to a random coil, with additional contributions from α -helices. SNAP25(CtoS) is, therefore, mostly unstructured and oligomers likely result from unspecific interactions formed between disordered regions or transiently formed structures. The helical content agrees well with a recently proposed nucleation site for SNARE complex assembly revealed by nuclear magnetic resonance spectroscopy [44]. Formation of oligomers might be an attempt to stabilise the disordered structure in the absence of other interaction partners by trying to assemble complementary SNARE motifs.

3.2.3 Characterisation of Stx(1-262) in ‘open’ and ‘closed’ conformation

Stx(1-262) was characterised in solution following the same procedure as described for SNAP25(CtoS). First, 10 μM Stx(1-262) were cross-linked with increasing amounts of BS3 cross-linker ranging from 0.5 mM up to 1.5 mM. The cross-linked protein was separated by gel electrophoresis and stained using Coomassie or analysed by western blotting using a specific antibody against Stx1. Coomassie staining revealed two distinct monomeric species formed

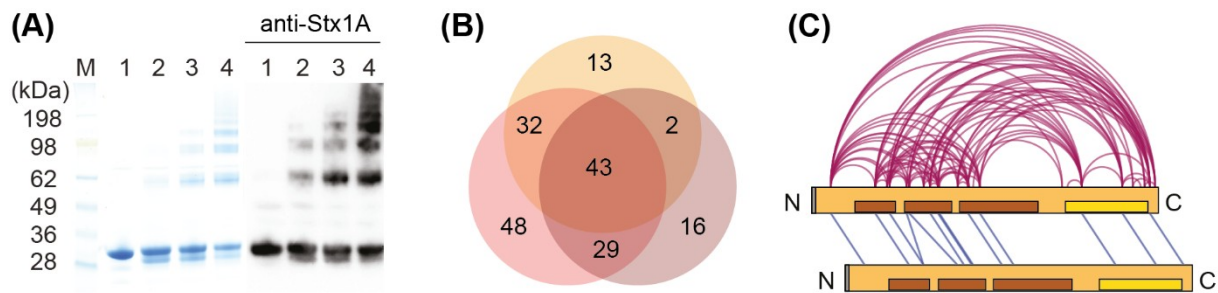


Figure 17. Cross-linking analysis of Stx(1-262).

(A) 10 μ M Stx(1-262) were cross-linked with 0 mM (lane 1), 0.5 mM (lane 2), 1 mM (lane 3) and 1.5 mM (lane 4) BS3 cross-linker. Cross-linked and non-cross-linked Stx(1-262) were separated by gel electrophoresis and visualised by Coomassie staining and western blotting using anti-Syntaxin-1A antibody. (B) 10 μ M of Stx(1-262) were cross-linked with 1.5 mM BS3 cross-linker in three independent replicates. Evaluated cross-links of each replicate are visualised in a VENN diagram. (C) Identified cross-links are visualized in a network plot. The SNARE motif (yellow), residual histidine tag (grey) and Habc domain (brown) are indicated. Intermolecular (blue lines) and intramolecular (purple lines) cross-links are shown. (Figure adapted from [174].)

by intramolecular interactions that likely correspond to the ‘open’ and ‘closed’ conformations of Stx1 [10,20,21,180]. In addition, oligomers up to tetramers were observed. Using western blotting analysis, oligomers up to pentamers were observed (**Figure 17A**).

Interaction sites within cross-linked Stx(1-262) monomers and oligomers were then determined by LC-MS/MS analysis. For this, 10 μ M Stx(1-262) were cross-linked with 1.5 mM BS3 cross-linker, the cross-linked protein was hydrolysed and cross-linked peptide pairs were enriched by SEC. LC-MS/MS analysis was performed and manual validation of the mass spectra resulted in 93 intra- and 13 intermolecular interactions identified in at least two out of three replicates (**Figure 17B**, **Supplementary Table 4**). Identified cross-links were visualised in a network plot: intramolecular cross-links are mainly located in the folded N-terminal Habc domain of Stx(1-262) or form between the Habc domain and the SNARE motif of Stx(1-262) (**Figure 17C**). These cross-links likely result from the high flexibility of the disordered SNARE motif in the absence of other SNARE proteins and the equilibrium between ‘open’ and ‘closed’ conformation. Intermolecular interactions were identified between Habc domains and SNARE motifs of two Stx(1-262) molecules indicating a parallel orientation. Note that, interactions between the SNARE motifs are only possible if these are accessible, e.g. when Stx(1-262) exhibits the ‘open’ conformation. Therefore, identified cross-links reflect an ensemble of both conformations in the absence of other SNARE proteins or regulatory proteins such as Munc18. To validate the cross-linking sites, intermolecular cross-links were mapped onto an AlphaFold 2 prediction of dimeric Stx(1-262), showing a parallel orientation of two Stx(1-262) molecules in ‘open’ conformation (**Figure 18A**). All identified cross-links that formed between Habc domains as well as the SNARE motifs of two Stx(1-262) molecules are in the expected

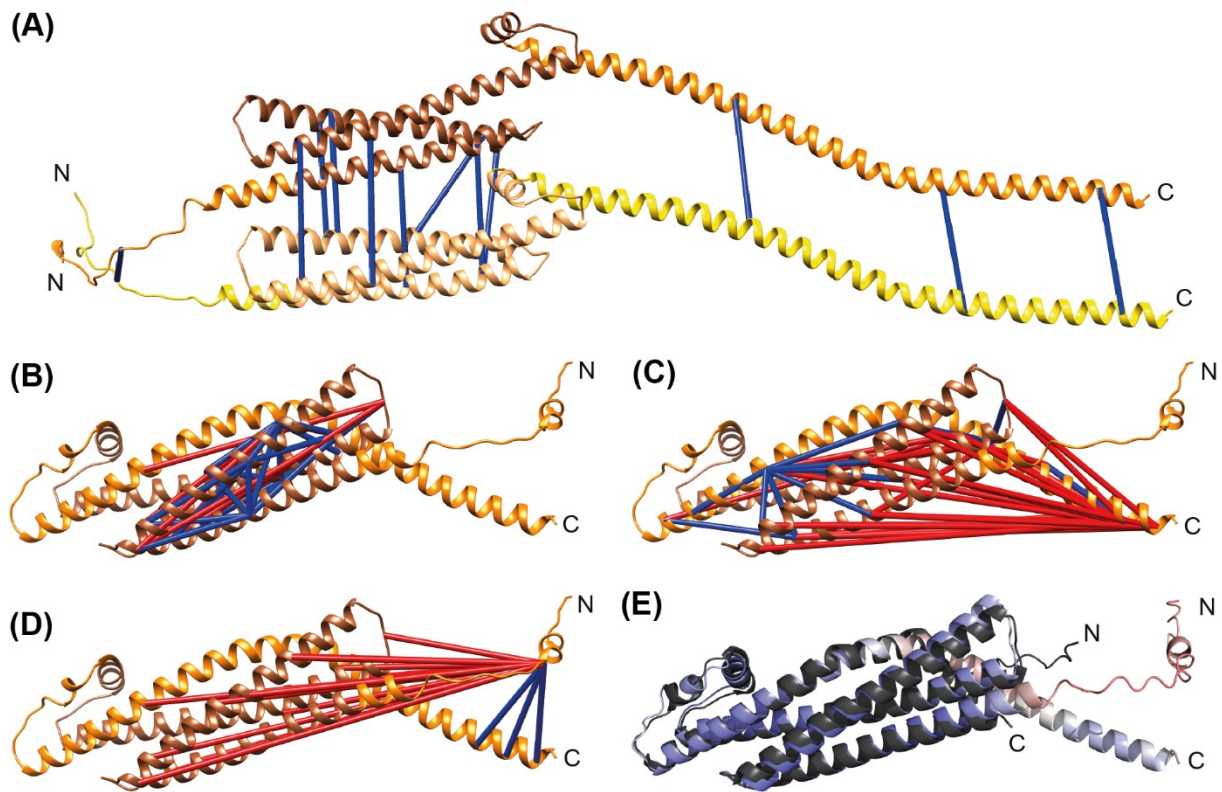


Figure 18. Validation of inter- and intramolecular interactions of Stx(1-262).

AlphaFold 2 predictions of monomeric and dimeric Stx(1-262) (yellow, orange) including disordered structures and the Habc domain (dark and light brown) are shown as cartoon representation. N- and C-termini are labelled. Cross-links identified in at least two out of three replicates are visualised and cross-linking distances corresponding to short-range (<30 Å, blue lines) and long-range (>30 Å, red lines) cross-links are highlighted. **(A)** Intermolecular cross-links are mapped onto a Stx(1-262) dimer in 'open' conformation with parallel orientation. Intramolecular cross-links were mapped into a Stx(1-262) monomer in 'closed' conformation. Cross-links that formed **(B)** within the Habc domain, **(C)** towards the SNARE motif and **(D)** towards the N-terminal peptide of Stx(1-262) are shown. **(E)** Alignment of an AlphaFold prediction of Stx(1-262) in 'closed' conformation (pLDDT score < 50%, red; 50-70%, light-red; 70-90% light-blue; >90% blue) and a crystal structure of Stx1 co-crystallized with Munc18 (black) are shown (PDB ID: 7XSJ [179]).

distance range, thus, validating a parallel assembly of Stx(1-262) molecules in 'open' conformation. Intramolecular interactions were also plotted into an AlphaFold 2 prediction of Stx(1-262) corresponding to Stx1 in complex with Munc18 and representing its 'closed' conformation [180]. 24 out of 31 cross-links formed within the folded Habc domain are within the expected distance range of 30 Å (**Figure 18B**). 15 out of 43 cross-links between the Habc domain and the N-terminal region of the SNARE motif are within the expected cross-linking distance and are, therefore, in agreement with the 'closed' conformation (**Figure 18C**). The remaining 28 cross-links formed with the C-terminal region of the SNARE motif of Stx(1-262) exceed the 30 Å distance threshold (**Figure 18C**). From the cross-links formed with the N-terminal peptide of Stx(1-262) 14 out of 18 cross-links are long-range cross-links (**Figure 18D**). Aligning the AlphaFold 2 prediction and an available high-resolution crystal structure of Stx1 co-crystallized with Munc18 [180] confirmed that the N-terminal peptide and

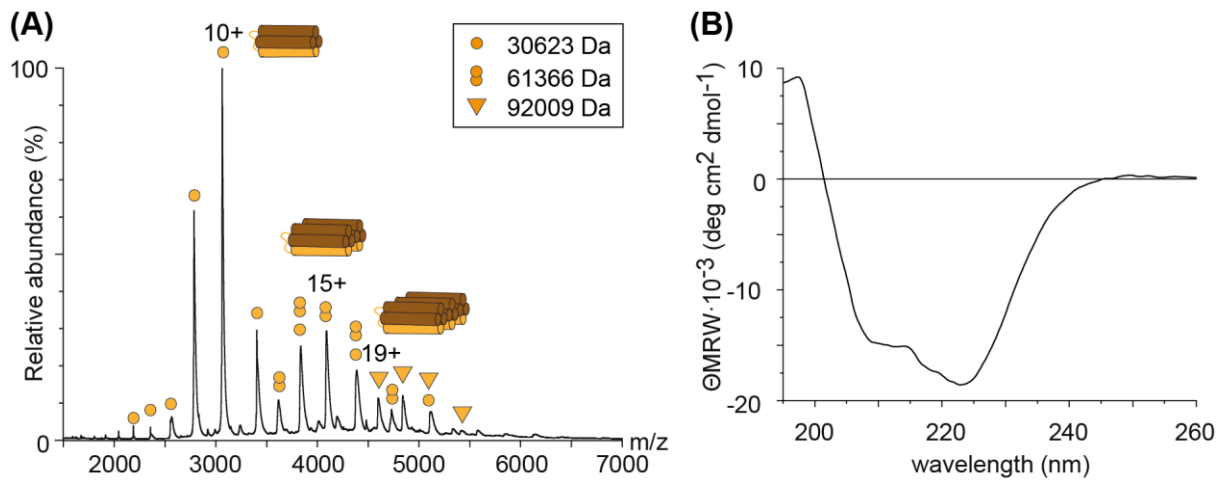


Figure 19. Native MS and CD spectroscopy of Stx(1-262).

(A) Native mass spectrum of 10 μ M Stx(1-262). Charge state distributions corresponding to monomers (circle), dimers (twin-circles) and trimers (triangle) are assigned. **(B)** CD spectrum of 30 μ M Stx(1-262). (Figure adapted from [174].)

the C-terminal half of the SNARE motif are highly flexible, thereby, explaining the observed overlength cross-links (**Figure 18E**).

To analyse oligomer formation of Stx(1-262) without introduction of covalent linkages by BS3 cross-linker, native MS was performed. Again, the storage buffer of Stx(1-262) was exchanged against 200 mM ammonium acetate and a mass spectrum was acquired using the Q-ToF Ultima mass spectrometer. Charge state distributions corresponding to monomers (30623 Da) that agree well with the theoretical mass of 30620.21 Da, as well as dimers (61366 Da) and trimers (92009 Da) were observed (**Figure 19A**). Again, the monomer of Stx(1-262) showed the highest intensity. Dimers and trimers of Stx(1-262) were observed at lower intensity.

For the analysis of the structural content of Stx(1-262), CD spectroscopy was employed. The CD spectrum shows two dominant minima at 210 nm and 225 nm revealing a helical structure for Stx(1-262) (**Figure 19B**). In the 'closed' conformation, the disordered SNARE motif intercalates into the folded Habc domain, leading to an almost completely folded Stx(1-262) molecule as shown previously by protein crystallography of Stx1 in complex with Munc18 [180] (**Figure 18E**). Due to the large and structured Habc domain, the contribution of the unstructured SNARE motif in 'open' conformation is negligible and most of the secondary structure is attributed to the Habc domain. The observed oligomerisation might, therefore, result from unspecific interactions of helical arrangements. The stabilisation of the disordered SNARE motif, as described for SNAP25(CtoS) above, might be another explanation. However, for this, Stx(1-262) is required to adopt the 'open' conformation.

3.2.4 Oligomerisation of the SNARE regulator Cpx1

Cpx1 was characterised following the same procedure as described for the SNARE proteins. Using increasing amounts of BS3 cross-linker, 10 μ M Cpx1 were cross-linked, separated by gel electrophoresis and visualised by Coomassie staining. Comparison of cross-linked and non-cross-linked Cpx1 revealed mainly monomeric Cpx1 and a low abundant dimeric species. Performing western blotting analysis using a specific antibody against Cpx1 uncovered additional low-abundant multimers up to heptamers (**Figure 20A**).

For identification of specific interaction sites, 50 μ M Cpx1 were cross-linked with a 10-fold molar excess of BS3, the cross-linked protein was hydrolysed and analysed by LC-MS/MS analysis. Manual validation of cross-linked spectra yielded 31 intra- and 3 intermolecular cross-links in two out of three replicates (**Figure 20B**, **Supplementary Table 5**). Visualising the protein interactions of Cpx1 in a network plot showed that many interactions were formed between the NTD and AH of Cpx1 as well as the CTD and CH (**Figure 20C**).

Further validation by mapping intermolecular interactions onto an AlphaFold 2 prediction of dimeric Cpx1 revealed oligomer formation through parallel interactions; a minor number of cross-links was identified, however, two out of three are in the expected distance range smaller 30 Å (**Figure 21A**). The majority of the identified intramolecular cross-links are formed towards the flexible termini of Cpx1 and 21 out of 31 cross-links exceed the expected 30 Å distance threshold (**Figure 21B**). Considering the high degree of disorder of Cpx1 and the predicted structure representing an ensemble of conformations, overlength cross-links were expected to be identified. This observation highlights the conformational diversity of Cpx1 in the absence of interaction partners. However, some of the cross-links might form between peptides

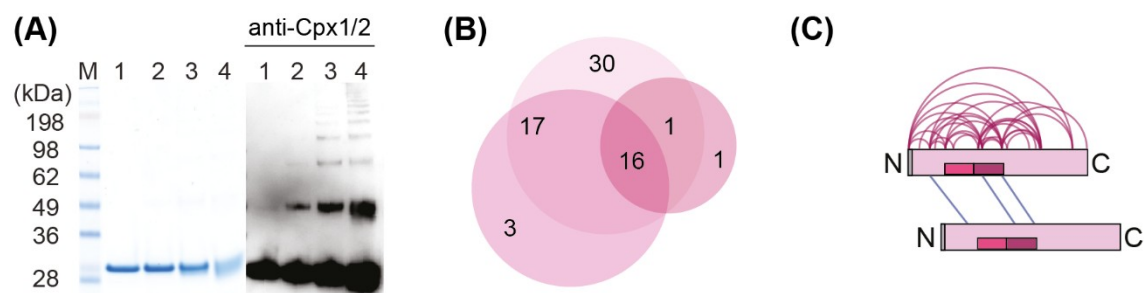


Figure 20. Cross-linking analysis of Cpx1.

(A) 10 μ M Cpx1 (light pink) were cross-linked with 0 mM (lane 1), 0.01 mM (lane 2), 0.1 mM (lane 3) and 1 mM (lane 4) BS3 cross-linker. Cross-linked and non-cross-linked Cpx1 were separated by gel electrophoresis and visualised by Coomassie staining and western blotting using anti-Complexin-1/2 antibody. (B) 50 μ M of Cpx1 were cross-linked with 0.5 mM BS3 cross-linker in three individual experiments. Evaluated cross-links of each replicate are visualised as VENN diagram. (C) Identified cross-links are visualised in a network plot. The AH (magenta), the CH (purple) and the residual histidine tag (grey) are indicated. Intermolecular (blue lines) and intramolecular (purple lines) cross-links are shown. (Figure adapted from [174].)

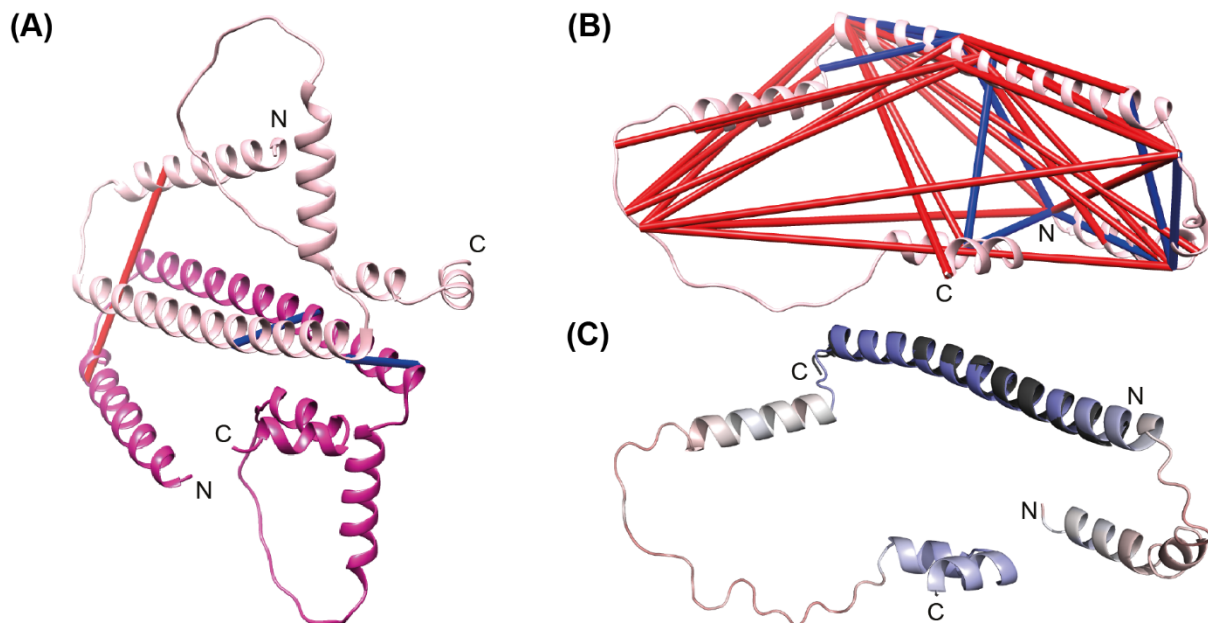


Figure 21. Validation of inter- and intramolecular interactions of Cpx1.

AlphaFold 2 predictions of monomeric and dimeric Cpx1 (light and dark pink) including disordered structures are shown as cartoon representation with labelled N- and C-termini. Cross-links identified in at least two of three replicates are visualised and cross-linking distances corresponding to short-range (< 30 Å, blue lines) and long-range (> 30 Å, red lines) cross-links are highlighted. **(A)** Intermolecular cross-links are mapped onto a Cpx1 dimer in parallel orientation. **(B)** Intramolecular cross-links are mapped onto a Cpx1 monomer. **(C)** An alignment of an AlphaFold prediction (pLDDT score < 50%, red; 50-70%, light-red; 70-90% light-blue; >90% blue) of monomeric Cpx1 and a crystal structure (black) of Cpx1 co-crystallized with the SNARE complex (PDB ID: 1KIL [61]) is shown.

originating from several Cpx1 molecules and, therefore, represent intermolecular interactions. Consequently, antiparallel orientations of Cpx1 molecules are also conceivable.

Analysing Cpx1 by native MS in the absence of covalent linkages revealed three charge state distributions corresponding to a highly abundant monomer (15403 Da) and low abundant dimers (30807 Da) and trimers (46284 Da) revealing the same oligomerisation behaviour as observed for the SNARE proteins (**Figure 22A**). The determined mass for the monomeric species agrees well with the theoretical mass of 15403.37 Da.

The structural content of Cpx1 was again analysed by CD spectroscopy. Although Cpx1 contains two highly disordered terminal domains represented by missing structural information in the high-resolution crystal structure (**Figure 21C**), helical structures as confirmed by two distinct minima at 210 nm and 225 nm in the CD spectrum were determined (**Figure 22B**). The helical content is likely attributed to the CH of Cpx1. Oligomerisation of Cpx1 suggests that stabilisation of the protein in the absence of interaction partners occurs in a similar manner as observed above for the SNARE proteins. In summary, even though Cpx1 is not considered a SNARE protein, it shows a comparable structural behaviour.

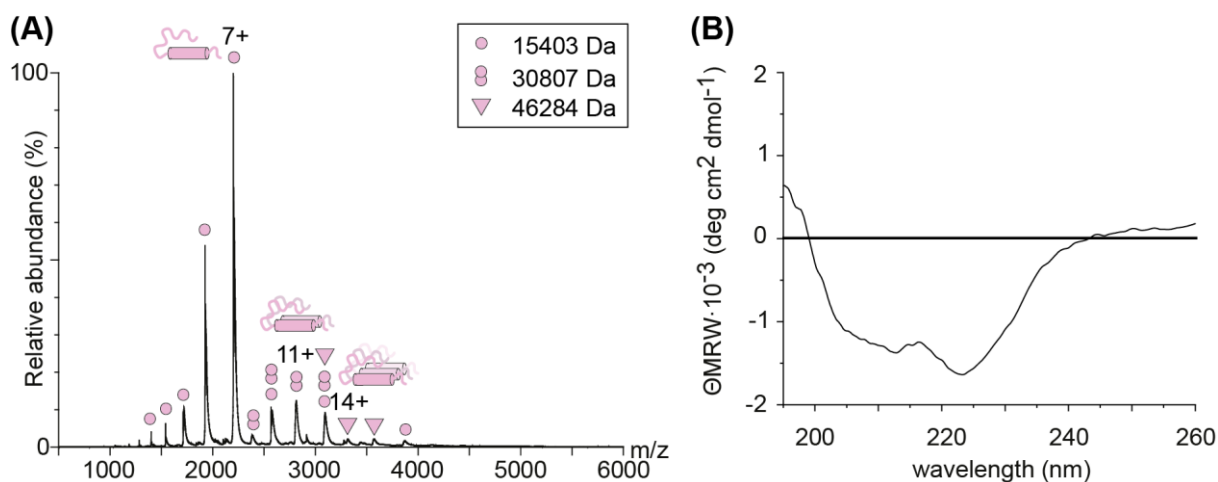


Figure 22. Native MS and CD spectroscopy of Cpx1.

(A) Native mass spectrum of 10 μM Cpx1. Charge state distributions corresponding to monomers (circle), dimers (twin-circles) and trimers (triangle) are assigned. (B) CD spectrum of 30 μM Cpx1 showing two dominant minima at 210 nm and 225 nm. (Figure adapted from [174].)

3.3 Assembly of the SNARE complex and its regulation by Cpx1

3.3.1 Formation of binary complexes and reorganisation into the SNARE complex

SNAP25 and Stx1, both located at the pre-synaptic membrane, were shown to form a 1:1 ‘acceptor’ complex providing an interaction surface for Syb2, thus, promoting the assembly of the full SNARE complex [181]. Although this assembly sequence is widely accepted, alternative pathways including formation of different intermediate complexes, e.g. composed of SNAP25 and Syb2 [182–184] or Stx1, Syb2 and Munc18 [33–36], are controversially discussed. Therefore, the SNARE complex assembly was analysed by native MS (Section 2.5.5), and the formation of binary intermediates and ‘off-pathway’ complexes as well as the reorganisation of binary complexes and formation of the ternary SNARE complex was explored.

3.3.1.1 Formation of the ‘dead end’ complex by SNAP25(CtoS) and Stx(1-262)

SNAP25(CtoS) and Stx(1-262) were mixed in a 1:1 ratio and assembled complexes were analysed by native MS (Figure 23A). The mass spectrum showed several charge state distributions corresponding to monomers of SNAP25(CtoS) (23840 Da) and Stx(1-262) (30622 Da) as well as complexes thereof. The following SNAP25(CtoS):Stx(1-262) complexes with the given stoichiometry were observed: 1:1 (54464 Da), 2:1 (78465 Da), 1:2 (85091 Da), 2:2 (109132 Da) and 2:4 (170278 Da). The species with the highest intensity corresponds to the 1:2 SNAP25(CtoS):Stx(1-262) complex, in which the binding site for Syb2 is occupied by an additional copy of Stx(1-262) as previously described [16], thereby resembling the

stoichiometry of the four-helical SNARE complex (Qaabc). In addition, a charge state distribution with decreased intensity corresponding to a 2:1 SNAP25(CtoS):Stx(1-262) complex was observed; in this complex, SNAP25(CtoS) contributes four SNARE motifs to the assembly, while Stx(1-262) contributes one SNARE motif. Considering a structural assembly similar to the ternary SNARE complex, one SNARE motif of SNAP25(CtoS) is likely located outside the four-helical bundle (Qabbc*). In both assemblies, the central layer of the complex is formed by four glutamine residues (4Q:0R). A low abundant species corresponding to a 1:1 SNAP25(CtoS):Stx(1-262) complex represents the previously reported 'acceptor' complex providing the binding site for Syb2 [181]. The complexes with a stoichiometry of 2:2 and 2:4

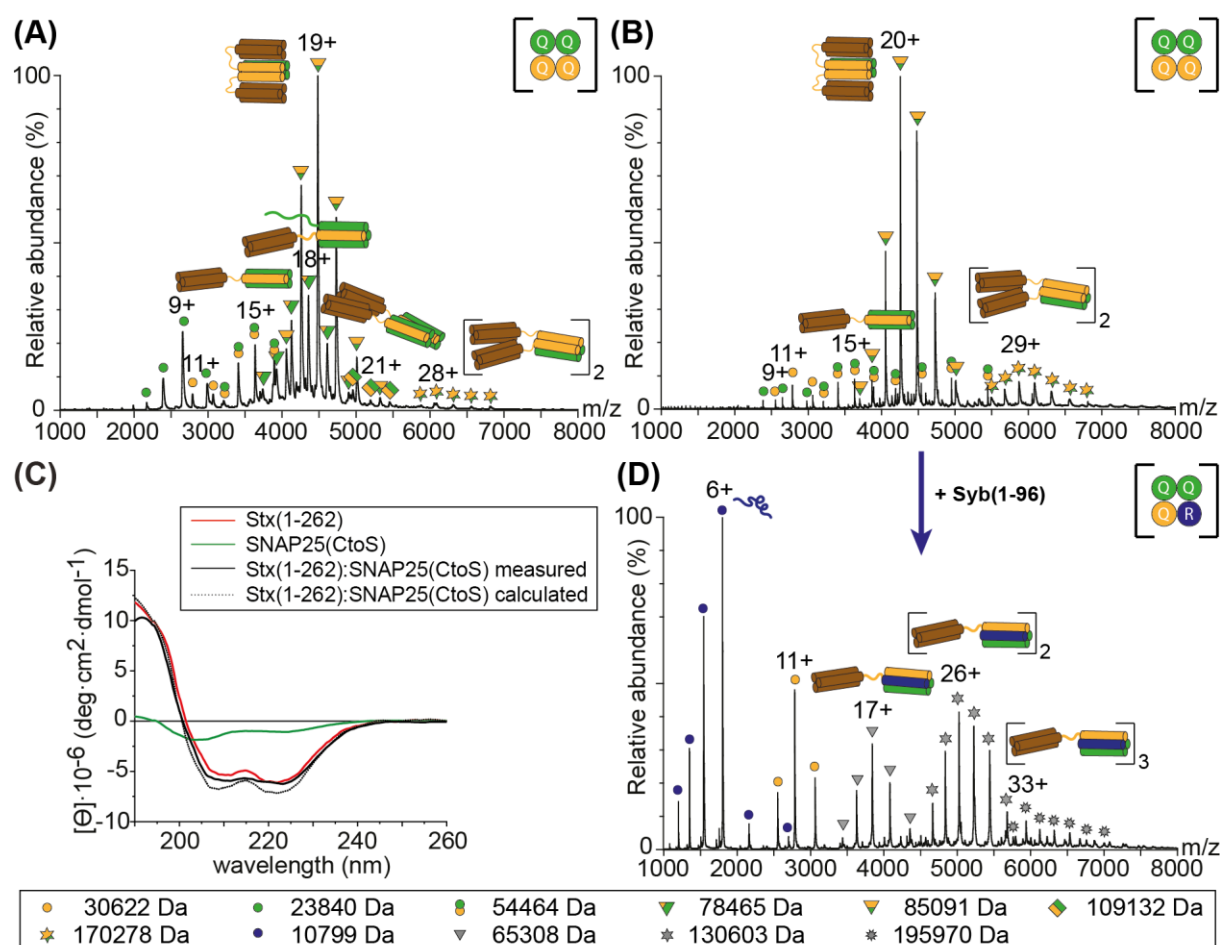


Figure 23. Formation and reorganisation of SNAP25(CtoS):Stx(1-262) complexes.

SNAP25(CtoS) and Stx(1-262) were mixed in (A) 1:1 and (B) 1:2 ratio and analysed by native MS. Charge state distributions of monomeric SNAP25(CtoS) (green circles) and Stx(1-262) (yellow circles) as well as SNAP25(CtoS):Stx(1-262) complexes with 1:1 (green-yellow twin-circles), 2:1 (green triangle with yellow left corner), 1:2 (yellow triangle with green bottom corner), 2:2 (yellow/green squares) and 2:4 (yellow stars with green corner) stoichiometry were observed. (C) CD spectra of monomeric SNAP25(CtoS) and Stx(1-262) as well as a theoretically calculated and a measured CD spectrum of the 1:2 Stx(1-262):SNAP25(CtoS) mixture. (D) Addition of Syb(1-96) at a 1.2 molar excess to the pre-assembled SNAP25(CtoS):Stx(1-262) complexes results in formation of the SNARE complex. Monomeric Syb(1-96) (blue circles) and Stx(1-262) (orange circles) as well as monomeric (grey triangles), dimeric (grey hexagonal stars) and trimeric (grey nonagonal stars) SNARE complexes are assigned. (Figure adapted from [174].)

are dimers of the 1:1 and 1:2 SNAP25(CtoS):Stx(1-262) complexes revealing oligomerisation of complexes at low protein concentration. Low abundant monomers of individual SNAP25(CtoS) and Stx(1-262) and the absence of the previously observed oligomers indicate a preference for complex formation over oligomerisation when physiological interaction partners are available. The predominant 1:2 SNAP25(CtoS):Stx(1-262) complex was previously observed in a liposome fusion assay revealing that the complex is kinetically trapped; consequently, the complex was termed the 'dead end' complex [169]. To assess the formation of this complex, SNAP25(CtoS) and Stx(1-262) were incubated at a 1:2 molar ratio promoting formation of this complex (**Figure 23B**). Indeed, the complex with the highest intensity observed at this mixing ratio is the 1:2 complex suggesting that this stoichiometry is preferred and likely most stable in the absence of Syb2. SNAP25(CtoS):Stx(1-262) complexes with 2:1 and 2:2 stoichiometry were not detected in this experiment indicating that these complexes are less stable and that the equilibrium shifted towards the formation of the preferred 1:2 SNAP25(CtoS):Stx(1-262) complex. The presence of the 1:1 SNAP25(CtoS):Stx(1-262) complex suggest that this complex is a stable intermediate to form the 'dead end' complex by providing a binding surface for Stx(1-262).

Next, the structural content of the mixture of SNAP25(CtoS) and Stx(1-262) was analysed to interrogate if the complexes formed are indeed structured and comparable to the helical structure of the assembled SNARE complex. For this, CD spectroscopy was performed (**Figure 23C**). While individual SNAP25(CtoS) exhibited a random coil structure with some helical content, characteristic for a disordered protein, a fully helical structure was determined for Stx(1-262). A theoretical spectrum, in which the proteins do not interact with each other and which is based on the CD spectra of the individual proteins, was calculated for the binary complexes. Comparison of this spectrum with the experimentally obtained spectrum of the SNAP25(CtoS):Stx(1-262) mixture revealed only minor changes in the helicity. According to the high-resolution crystal structures of Stx(1-262) in its 'closed' conformation (interacting with Munc18) and in 'open' conformation (interacting with the SNAREs), the helical content of Stx(1-262) is comparable [17,22,180]. For SNAP25(CtoS) only the Qb SNARE motif was described to be partially structured in solution [44]. Marginal changes in the CD spectrum of the protein mixture might, therefore, mostly originate from a disorder-to-order transition of the second SNARE motif of SNAP25(CtoS).

To explore whether the observed 1:2 SNAP25(CtoS):Stx(1-262) complex is indeed kinetically trapped, a 1.2 molar excess of Syb(1-96) was added to the pre-assembled complexes (**Figure 23D**). Surprisingly, none of the previously detected SNAP25(CtoS):Stx(1-262) complexes were observed. Instead, charge state distributions corresponding to monomers (65308 Da), dimers (130603 Da) and trimers (195970 Da) of the fully assembled SNARE complex (3Q:1R, QabcR) were detected. These results indicate a higher binding affinity for

Syb(1-96) compared to Stx(1-262). Unexpectedly, only monomeric Syb(1-96) and Stx(1-262) were observed indicating a rearrangement of the 1:2 SNAP25(CtoS):Stx(1-262) complex rather than a complete disassembly of the 'dead end' complex and reassembly into the SNARE complex. In this case, the R-SNARE Syb(1-96) substitutes the Q-SNARE Stx(1-262), while the 'acceptor' complex remains intact; consequently, individual SNAP25(CtoS) is not detected. However, binding of Syb(1-96) to the 'acceptor' complex and thereby shifting the equilibrium between the 1:1 and 1:2 SNAP25(CtoS):Stx(1-262) complexes is also conceivable.

To validate the stoichiometry of the monomeric and dimeric SNARE complex, the 16+ and 25+ charge states, respectively, were selected for collision induced dissociation (**Figure 24**). To dissociate complexes in native MS the collisional energy is increased, resulting in dissociation of the peripheral subunit that requires the least activation energy for unfolding. As a result, an unfolded and, therefore, highly charged monomer and a so-called 'stripped' complex composed of the remaining protein subunits are observed [148,185]. Syb(1-96) dissociates from the monomeric as well as from the dimeric SNARE complexes yielding the highly charged monomeric protein (**Figure 24**). In the case of the monomeric SNARE complex, the 'stripped' complex corresponds to the 1:1 SNAP25(CtoS):Stx(1-262) 'acceptor' complex (54471 Da) (**Figure 24A**). For the dimeric SNARE complex, two consecutive dissociation events occurred yielding the 2:2:1 SNAP25(Ctos):Stx(1-262):Syb(1-96) complex (119750 Da) and a 2:2 SNAP25(CtoS):Stx(1-262) second generation dissociation product (108950 Da) omitting both Syb(1-96) molecules (**Figure 24B**). Ready dissociation of Syb(1-96) indicates that this subunit is least stably incorporated into the SNARE complex, and that the 'acceptor' complex composed of SNAP25(CtoS) and Stx(1-262) is stably formed providing a solid interaction surface for Syb(1-96) to assemble.

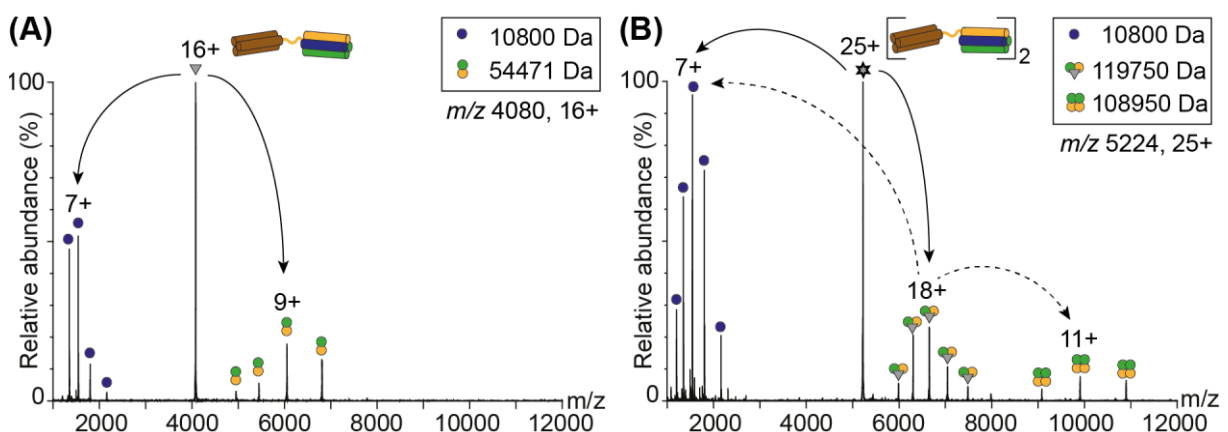


Figure 24. Collision induced dissociation of the ternary SNARE complex.

(A) The 16+ charge state of the monomeric SNARE complex (grey triangle) and (B) the 25+ charge state of the dimeric SNARE complex (grey hexagonal star) were selected for collisional induced dissociation. Charge state distributions corresponding to the dissociated subunit Syb(1-96) (blue circle) as well as first and second generation 'stripped' complexes of 1:1 SNAP25(CtoS):Stx(1-262) (green-yellow twin-circles), 2:2 (two green and two yellow circles), 1:2:2 Syb(1-96):SNAP25(CtoS):Stx(1-262) (green-yellow twin-circles grey triangle) stoichiometry were observed. (Figure adapted from [174].)

3.3.1.2 SNARE complex stoichiometry mimicked by SNAP25(CtoS) and Syb(1-96)

To analyse complex formation between SNAP25(CtoS) and Syb(1-96) by native MS, the SNAREs were incubated at a 1:2 ratio providing an excess of Syb(1-96) to promote formation of a four-helical bundle (**Figure 25A**). The native mass spectrum showed charge state distributions corresponding to monomeric SNAP25(CtoS) (23096 Da), monomeric Syb(1-96) (10800 Da) and dimeric SNAP25(CtoS) (47694 Da). Interestingly, binary complexes composed of SNAP25(CtoS) and Syb(1-96) with a stoichiometry of 2:1 (58513 Da) and a dimer thereof with a stoichiometry of 4:2 (117040 Da) were also observed. Similar to the previously observed 2:1 SNAP25(CtoS):Stx(1-262) complex, the SNAP25(CtoS):Syb(1-96) complex

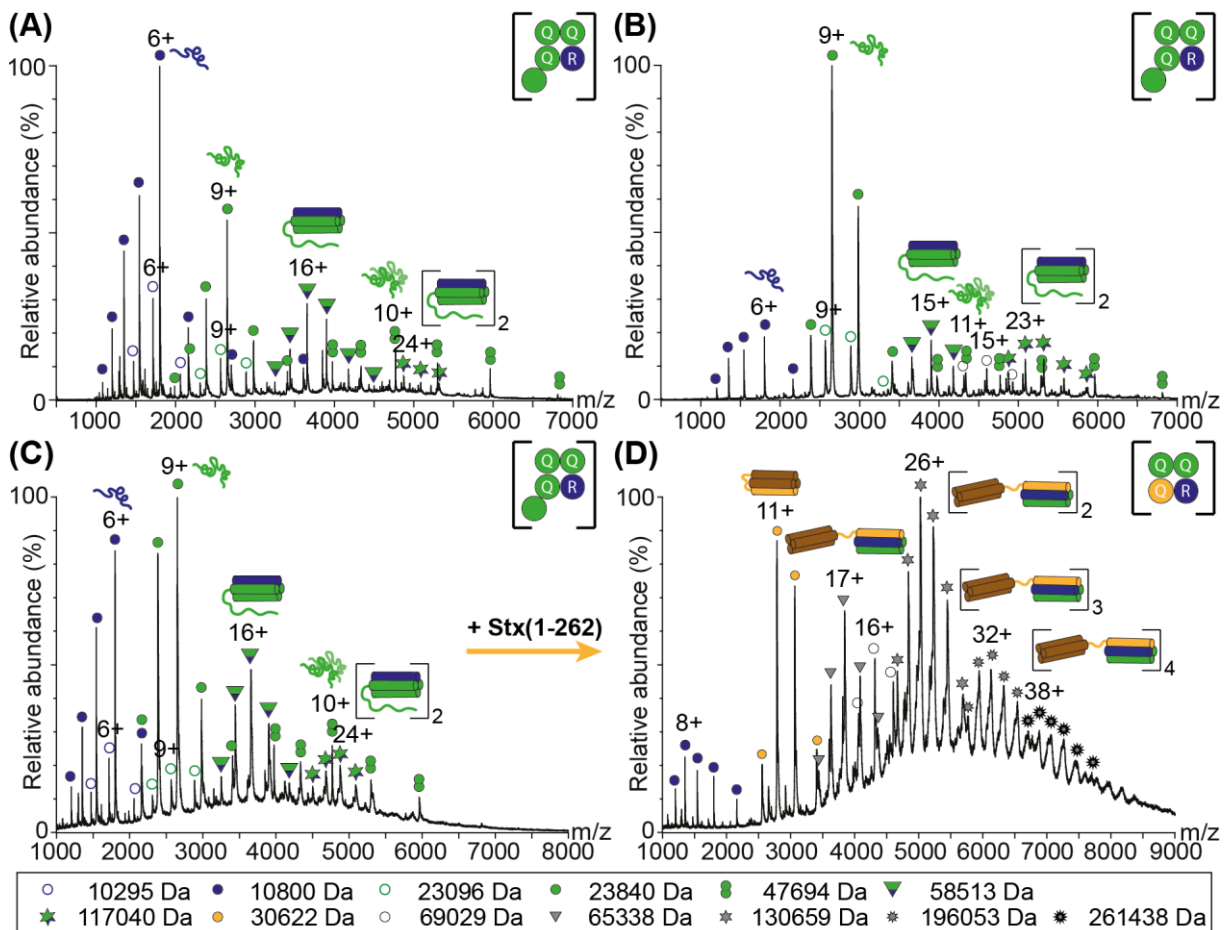


Figure 25. Formation and reorganisation of SNAP25(CtoS):Syb(1-96) complexes.

SNAP25(CtoS) and Syb(1-96) were mixed in (A) 1:2 (B) 2:1 and (C) 1:1 ratio and analysed by native MS. Charge state distributions corresponding to monomeric SNAP25(CtoS) (green circles), monomeric Syb(1-96) (blue circles), dimeric SNAP25(CtoS) (green-twin-circles) as well as binary SNAP25(CtoS):Syb(1-96) complexes with a stoichiometry of 2:1 (green-blue triangle) and 4:2 (green-blue hexagonal stars) were observed. Degradation products of SNAP25(CtoS) and Syb(1-96) (open circles) are also assigned. (D) Equimolar addition of Stx(1-262) to the pre-assembled SNAP25(CtoS):Syb(1-96) complexes results in formation of monomeric (grey triangles), dimeric (grey hexagonal stars), trimeric (grey nonagonal stars) and tetrameric (grey dodecagonal stars) SNARE complexes. Monomeric Syb(1-96) (blue circles) and Stx(1-262) (orange circles) were also observed. (Figure adapted from [174].)

contains four SNAP25(CtoS) SNARE motifs and one Syb(1-96) motif. However, considering formation of a four-helical bundle, only three SNAP25(CtoS) SNARE motifs contribute to the complex, while one motif is located outside the four-helical bundle (Qbbcc**R*) as already described above for the 2:1 SNAP25(CtoS):Stx(1-262) complex (Qabbcc**R*). In such an arrangement, the central layer of the complex is in agreement with the four-helical bundle of the SNARE complex (3Q:1R). Although an excess of Syb(1-96) was employed, only one copy of the R-SNARE was incorporated into the complex. Two copies of Syb(1-96), each molecule providing an arginine residues in the central layer, might prevent complex formation due to electrostatic repulsion. Therefore, the binding site of Stx(1-262) was occupied by one helix of the available Q-SNARE SNAP25(CtoS). While oligomers were not observed for Syb(1-96), indicating a preference to form complexes in the presence of physiological interaction partners, a dimer of SNAP25(CtoS) was detected (**Figure 25A**). Note, that the charge state distribution of this SNAP25(CtoS) dimer appears at higher *m/z* values compared to the 2:1 SNAP25(CtoS):Syb(1-96) complex. As complexes with higher molecular weight provide an increased surface area, more charges will be acquired during ionisation resulting in higher *m/z* values. Consequently, the observed SNAP25(CtoS) dimer is likely a gas phase dissociation product of the 2:1 SNAP25(CtoS):Syb(1-96) complex, rather than an oligomer formed in solution. This assumption is supported by the higher charged dimer observed for individual SNAP25(CtoS) (**see Figure 16A**). To validate formation of the expected dissociation products, collisional induced dissociation of the 2:1 SNAP25(CtoS):Syb(1-96) complex was performed confirming the SNAP25(CtoS) dimer to be the ‘stripped’ complex and revealing Syb(1-96) less stably incorporated into the complex (**Figure 26A**). This is also true for the

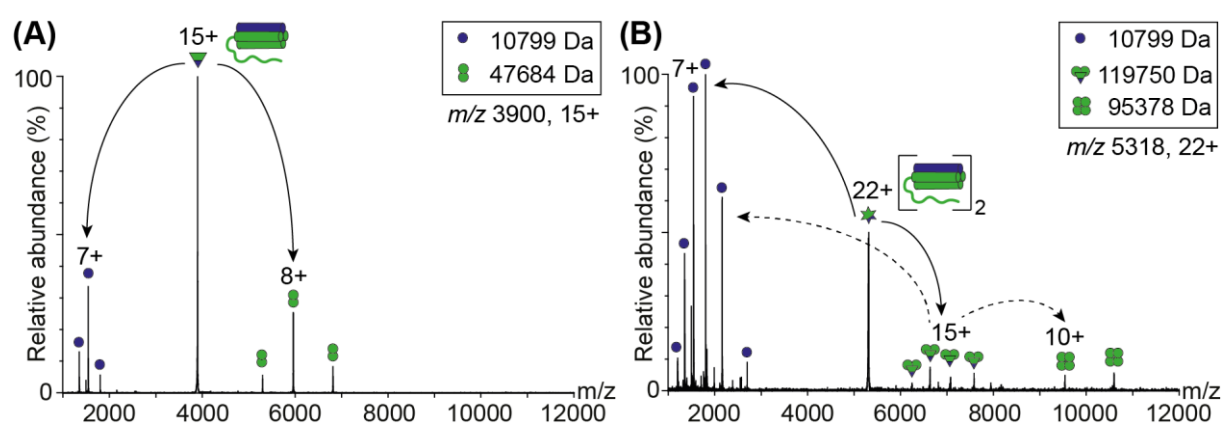


Figure 26. Collision induced dissociation of SNAP25(CtoS):Syb(1-96) complexes.

(A) The 15+ charge state of the monomeric 2:1 SNAP25(CtoS):Syb(1-96) complex (green-blue triangle) and **(B)** the 22+ charge state of the 4:2 SNAP25(CtoS):Syb(1-96) complex (green-blue triangle) were selected for collisional induced dissociation. Charge state distributions corresponding to the dissociated subunit Syb(1-96) (blue circle) as well as first and second generation ‘stripped’ complexes were observed namely, a dimer of SNAP25(CtoS) (green twin-circles) and complexes of SNAP25(CtoS):Syb(1-96) with a stoichiometry of 4:1 (green-blue triangle and green twin-circles) and 2:2 (four green circles). (Figure adapted from [174].)

4:2 SNAP25(CtoS):Syb(1-96) complex, which dissociates in a similar manner as the dimeric SNARE complex described above (**Figure 26B**). For both protein mixtures, SNAP25(CtoS) and Stx(1-262) as well as SNAP25(CtoS) and Syb(1-96), the same collisional energy of 10 V was applied. Although the 3Q:1R conformation of the 2:1 SNAP25(CtoS):Syb(1-96) complex is expected to be more stable compared to the 1:2 SNAP25(CtoS):Stx(1-262) complex (4Q:0R), dissociation was only observed for the 2:1 SNAP25(CtoS):Syb(1-96) complex indicating that stable complex formation requires an ‘acceptor’ complex containing Stx(1-262). Note, that a 1:1 SNAP25(CtoS):Syb(1-96) complex was not observed, suggesting that stable association of Syb(1-96) requires an interaction surface formed by three interacting SNARE motifs. In order to shift the equilibrium of SNAP25(CtoS) and Syb(1-96) promoting formation of the 2:1 complex, the incubation ratios were varied. However, when incubating SNAP25(CtoS) and Syb(1-96) at a 2:1 and 1:1 ratio, the same 2:1 SNAP25(CtoS):Syb(1-96) complex and a dimer thereof were observed (**Figure 25B and 25C**). As a result, formation of the 3Q:1R stoichiometry resembling the four-helical structure of the SNARE complex is indeed preferred.

Again, CD spectroscopy was performed to evaluate the structural content of the SNAP25(CtoS):Syb(1-96) protein mixture. While individual SNAP25(CtoS) and Syb(1-96) were both found to be disordered with only minor helical structures (**Figure 27**), comparison of the theoretically calculated spectrum of both proteins, that do not interact with each other, and the experimentally determined spectrum revealed meaningful structural rearrangements. A signal shift from 203 nm to 208 nm and an increase in ellipticity at 220 nm verifies formation of alpha-helical SNAP25(CtoS):Syb(1-96) complexes structurally similar to the four-helical ternary SNARE complex. However, the structure of the SNARE motif of SNAP25(CtoS) that is presumably not involved in the formation of the four-helical bundle remains unknown.

To elucidate, if the pre-assembled binary complexes rearrange into the SNARE complex, Stx(1-262) was added in equimolar amounts to the protein mixture (**Figure 25D**). Immediately

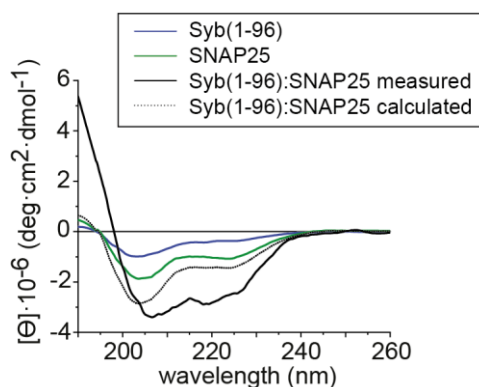


Figure 27. CD spectra of SNAP25(CtoS), Syb(1-96) and binary SNARE complexes.

CD spectra of monomeric SNAP25(CtoS) and Syb(1-96) as well as calculated and measured CD spectra of the 2:1 Syb(1-96):SNAP25(CtoS) mixture are shown. (Figure adapted from [174].)

after addition of Stx(1-262), charge state distributions corresponding to monomeric (65029 Da), dimeric (130659 Da), trimeric (196053 Da) and even tetrameric (261438 Da) SNARE complexes were observed. Accordingly, the second copy of SNAP25(CtoS) was replaced and the preferred SNARE complex (3Q:1R) was formed. While the exact mechanism remains unclear, prompt dissociation of Syb(1-96) as well as the high stability for the SNAP25(CtoS) dimer suggest dissociation of Syb(1-96) at first. This assumption is strengthened by the presence of monomeric Syb(1-96) in the mass spectrum (**Figure 25D**).

To specifically assess, which SNARE motif of SNAP25(CtoS) is replacing Stx(1-262) in the 2:1 SNAP25(CtoS):Syb(1-96) complex, the assembly of the complex was interrogated using SNAP25(1-83), i.e. the Qb SNARE motif of SNAP25(CtoS). Analysing SNAP25(1-83) in the absence of interaction partners revealed several charge state distributions corresponding to monomers (9931 Da) as well as low abundant dimers (19862 Da) and trimers (29840 Da) of SNAP25(1-83) (**Figure 28A**). Formation of these SNAP25(1-83) oligomers suggest that the oligomerisation observed for the SNARE proteins is driven by interacting SNARE motifs rather than unspecific interactions. When incubating SNAP25(1-83) and Syb(1-96), one additional charge state series corresponding to monomeric Syb(1-96) (10799 Da) was detected (**Figure 28B**). Interestingly, a dimer of SNAP25(1-83) including two SNARE motifs such as in SNAP25(CtoS) was also observed. However, formation of a binary complex was not observed suggesting that either the linker of SNAP25(CtoS) or the amino acid sequence of the Qc SNARE motif are crucial for stable complex formation. After equimolar incubation of Syb(1-96), SNAP25(CtoS) and SNAP25(1-83) charge state series corresponding in mass to monomers of Syb(1-96) (10799 Da), SNAP25(CtoS) (23844 Da) and SNAP25(1-83) (9931 Da) were observed (**Figure 28C**). In addition, a complex composed of Syb(1-96), SNAP25(CtoS) and SNAP25(1-83) with a stoichiometry of 1:1:1 (44577 Da) was identified. This observation reveals substitution of Stx(1-262) by the N-terminal Qb SNARE motif of SNAP25(CtoS) resulting in a ternary complex mimicking the stoichiometry of the SNARE complex (QbbcR). A dimer of this complex (89198 Da) was also detected (**Figure 28C**).

Interestingly, a heterodimer formed by SNAP25(CtoS) and SNAP25(1-83) with higher m/z ratio when compared with the ternary complex could also be assigned. Collision induced dissociation of the ternary complex confirmed that the SNAP25(CtoS):SNAP25(1-83) complex is a gas phase product resulting from prompt dissociation of Syb(1-96) (**Figure 28D**). Surprisingly, Syb(1-96) is dissociating from the complex, although SNAP25(1-83) is the smaller subunit and it is replacing Stx(1-262) in the assembly, suggesting that an intermediate 'acceptor' complex is indeed formed by SNAP25 and Stx1 rather than a complex involving Syb2. A complex including a second copy of the full-length SNAP25(CtoS) molecule was not observed, indicating that incorporation of a single SNARE motif is sterically preferred.

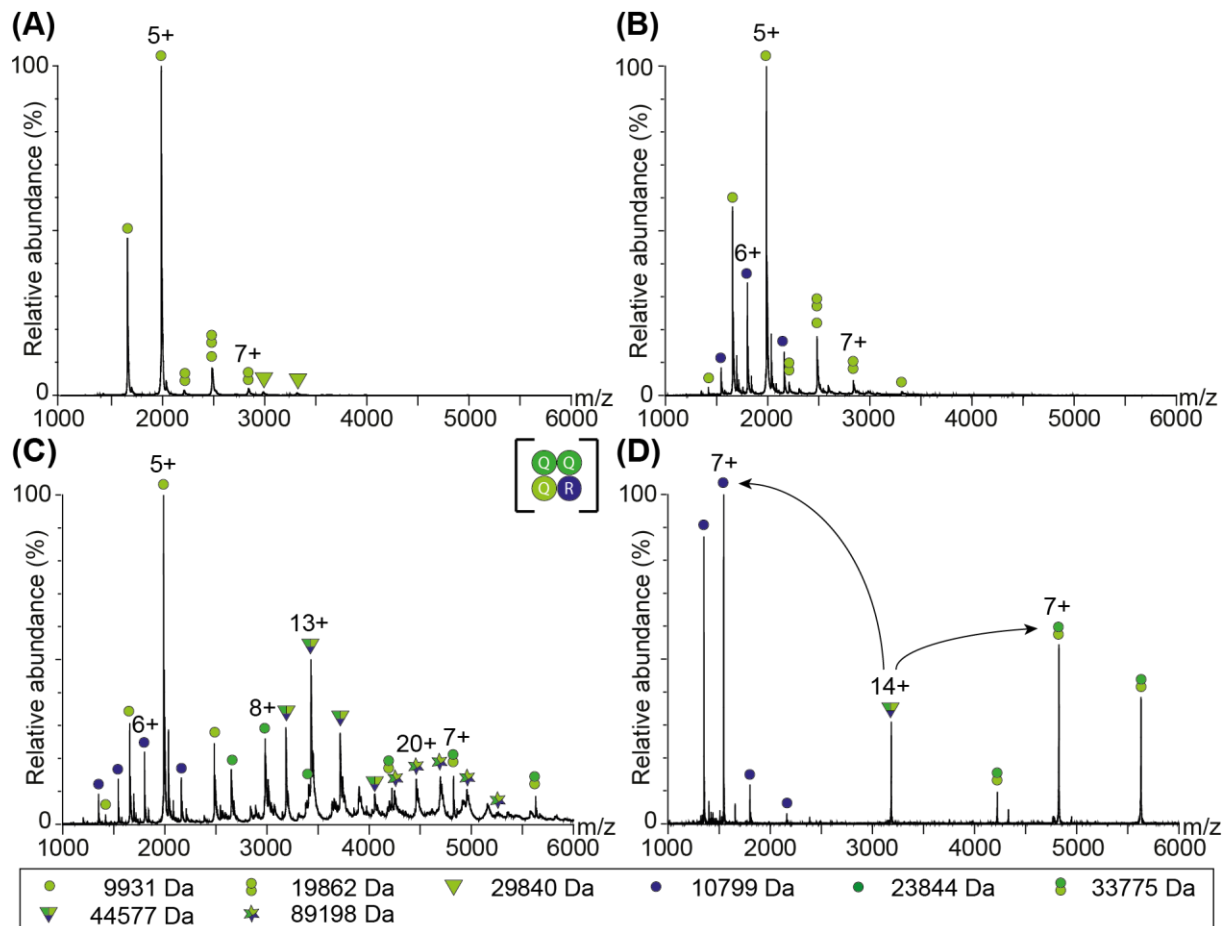


Figure 28. Complex formation involving SNAP25(1-83).

Native mass spectra of SNAP25(1-83) **(A)** in the absence of interaction partners, **(B)** equimolarly incubated with Syb(1-96) and **(C)** equimolarly incubated with Syb(1-96) and SNAP25(CtoS). Charge state distributions corresponding to monomeric SNAP25(CtoS) (green circles), dimeric SNAP25(CtoS) (green-twin-circles), monomeric Syb(1-96) (blue circles) as well as a 1:1 SNAP25(CtoS):SNAP25(1-83) complex and 1:1:1 (green-blue triangle) and 2:2:2 SNAP25(CtoS):SNAP25(1-83):Syb(1-96) complexes (green-blue hexagonal star) are assigned. **(D)** The 14+ charge state of the 1:1:1 SNAP25(CtoS):SNAP25(1-83):Syb(1-96) complex was selected for collisional induced dissociation. Charge state distributions corresponding to the dissociated subunit Syb(1-96) (blue circle) and the 'stripped' complex of 1:1 SNAP25(CtoS):SNAP25(1-83) (green-twin-circles) were detected.

In summary, for stable complex formation, an 'acceptor' complex is required, which is formed by three SNARE motifs and not only contains the N-terminal, but also the C-terminal SNARE motif of SNAP25(CtoS). This assumption is supported by the absence of the 1:1 SNAP25(CtoS):Syb(1-96) (QbcR) as well as 1:1, 2:1 and 3:1 SNAP25(1-83):Syb(1-96) complexes (QbR, QbbR, QbbbR). However, it is also conceivable that the linker of SNAP25(CtoS) is crucial to guide both SNARE motifs into the correct parallel orientation and thereby enabling binding of the third SNARE motif.

3.3.1.3 Stabilisation of Syb(1-96) and Stx(1-262) interactions by Cpx1

For investigation of the complex formation between Syb(1-96) and Stx(1-262), both SNARE proteins were incubated at a 1:1 ratio and analysed by native MS. Charge state distributions corresponding to high abundant monomers of Syb(1-96) (10800 Da) and Stx(1-262) (30622 Da) were observed (**Figure 29A**). Distributions corresponding to complexes formed between Syb(1-96) and Stx(1-262) were, surprisingly, not detected. Interestingly, the oligomerisation observed for the individual proteins in the absence of an interaction partner (see **Figures 11 and 19**) seems to be impeded as only a low abundant dimer of Stx(1-262)

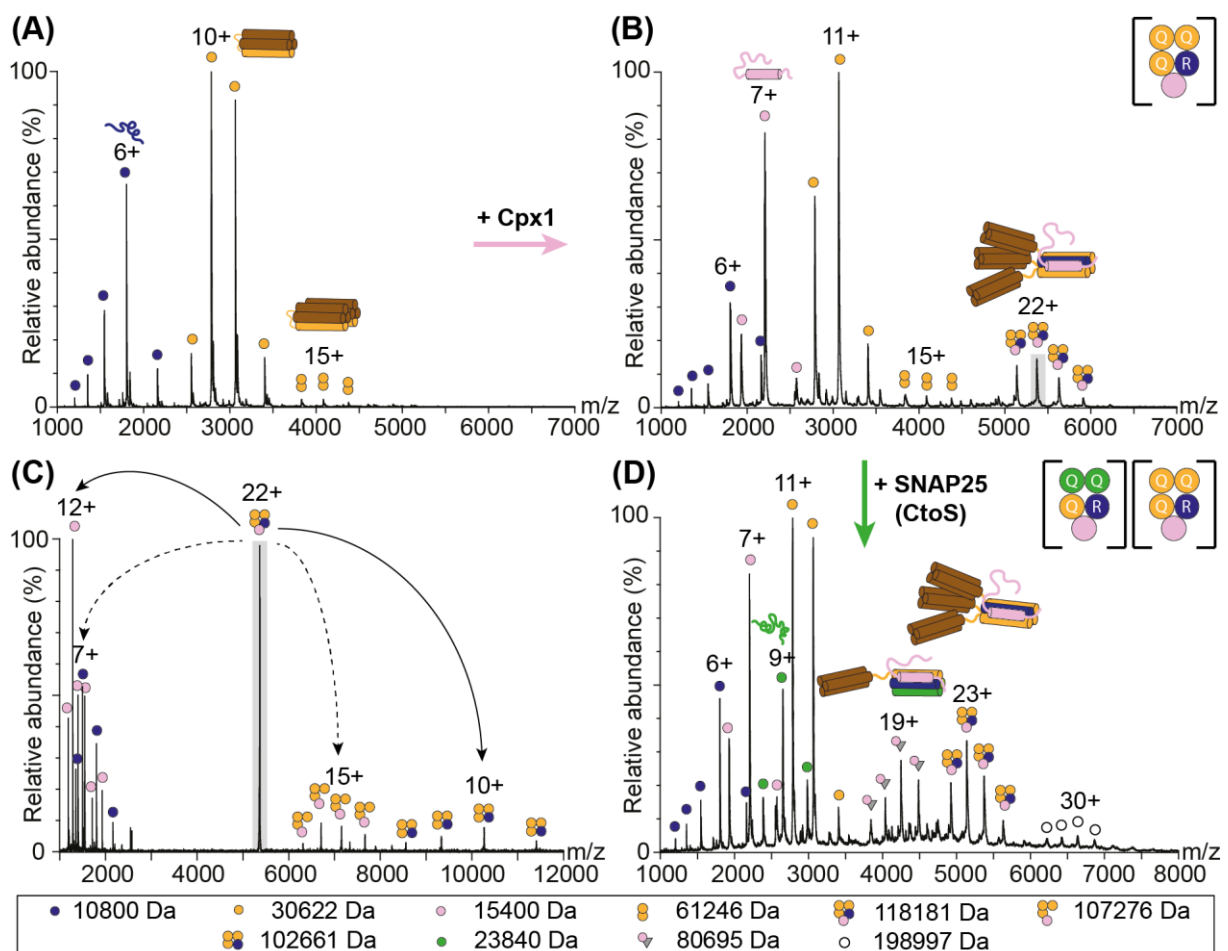


Figure 29. Stabilisation of the binary Syb(1-96):Stx(1-262) complex by Cpx1.

(A) Syb(1-96) and Stx(1-262) were mixed at a 1:1 ratio and analysed by native MS. Charge state distributions corresponding to monomeric Syb(1-96) (blue circles), monomeric Stx(1-262) (orange circles) and dimeric Stx(1-262) (orange twin-circles) were observed. (B) Equimolar addition of Cpx1 (pink circles) to the Syb(1-96):Stx(1-262) protein mixture results in formation of a 1:3:1 Syb(1-96):Stx(1-262):Cpx1 complex (orange-blue-pink circles). (C) The 22+ charge state of the 1:3:1 Syb(1-96):Stx(1-262):Cpx1 complex was selected for collision induced dissociation. Dissociation of the subunits Syb(1-96) (blue circle) and Cpx1 (pink circle) from the selected complex yielded the two 'stripped' 3:1 Stx(1-262):Cpx1 (orange-pink circles) and 3:1 Stx(1-262):Syb(1-96) (orange-blue circles) complexes. (D) Upon equimolar addition of SNAP25(CtoS) (green circle) to the pre-assembled 1:3:1 Syb(1-96):Stx(1-262):Cpx1 complex (orange-blue-pink circles), the 1:1:1:1 Syb(1-96):Stx(1-262):SNAP25(CtoS):Cpx1 complex (grey triangle-pink circle) formed. (Figure adapted from [174].)

was detected. This leads to the assumption that both SNAREs transiently interact with each other, however, do not form a stable complex that could be preserved during transfer into the gas phase.

To analyse if Syb(1-96) and Stx(1-262) undergo structural rearrangements, CD spectroscopy was performed. For this, a calculated spectrum was again compared with the experimentally recorded CD spectrum of the SNARE mixture showing a decrease in alpha-helicity (**Figure 30**). The presence of Syb(1-96) likely shifted the equilibrium of both Stx(1-262) conformations towards the 'open' form. Consequently, dissociation of the SNARE motif of Stx(1-262) from its Habc domain made it available for interactions with the SNARE motif of Syb(1-96) leading to lower helical content. The absence of a stable binary complex highlights the role of SNAP25 as an interaction partner as well as a general necessity for regulatory proteins to stabilise interactions between Syb(1-96) and Stx(1-262).

Cpx1 is a well-known regulator of the SNARE assembly [40]. High resolution crystal structures and a site-directed mutagenesis study revealed Cpx1 to be a physiological interaction partner of Syb2 and Stx1 that binds the interface provided by both SNAREs in the SNARE complex in an antiparallel orientation [60,61,186]. Assuming that Cpx1 interacts with Syb(1-96) and Stx(1-262) and possibly stabilises a transiently formed binary complex, it was added in equimolar amounts to the pre-incubated proteins. Immediately upon addition of Cpx1, formation of a Syb(1-96):Stx(1-262):Cpx1 complex with a stoichiometry of 1:3:1 was observed (**Figure 29B**). In this arrangement, Syb(1-96) provides the R-SNARE motif, while two additional Stx(1-262) molecules substitute the two alpha helices of SNAP25(CtoS) providing in total three Q-SNARE motifs, thereby, resembling the stoichiometry of the SNARE complex (3Q:1R, QaaaR). Assuming a similar arrangement of the binary complex as in the SNARE complex, Cpx1 likely binds to Syb(1-96) and Stx(1-262) peripherally rather than supplementing one of the SNARE helices.

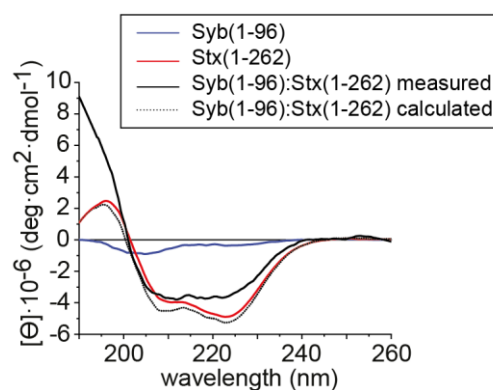


Figure 30. CD spectra of Stx(1-262), Syb(1-96) and binary SNARE complexes.

CD spectra of monomeric Stx(1-262) and Syb(1-96) as well as calculated and measured CD spectra of the 1:1 Syb(1-96):Stx(1-262) mixture are shown. (Figure adapted from [174].)

Therefore, collision induced dissociation was performed to target the topology of the 1:3:1 Syb(1-96):Stx(1-262):Cpx1 complex (**Figure 29C**). For this, the 22+ charge state of the distribution of this ternary complex was selected and dissociated by increasing the collisional energy. Surprisingly, dissociation of the 1:3:1 Syb(1-96):Stx(1-262):Cpx1 complex yielded two highly charged monomeric subunits and two lower charged 'stripped' complexes indicating selection of a complex with the same mass, but different topology. Dissociation of Cpx1 yielded the 1:3 Syb(1-96):Stx(1-262) complex (102661 Da) confirming indeed the expected peripheral position of Cpx1 (**Figure 29C**). In a second dissociation event, Syb(1-96) disassembled yielding a 3:1 Stx(1-262):Cpx1 complex (107276 Da) indicating least stable incorporation into the selected complex as observed above for other binary complexes (**Figure 29C**). However, binding of Cpx1 to an interface formed by Syb(1-96) and Stx(1-262) should prevent dissociation of Syb(1-96), suggesting that Cpx1 might also bind other interfaces of the complex, for instance an interface formed by two Stx(1-262) molecules, which would enable dissociation of Syb(1-96). Replacement of Syb(1-96) by Cpx1 forming a helical bundle with the three Stx(1-262) molecules and thereby providing a binding interface for Syb(1-96) seems unlikely because of the missing SNARE motif. The presence of Cpx1 stabilises the Stx(1-262):Syb(1-96) interface, therefore, enabling the detection of a complex mimicking the stoichiometry of the SNARE complex and indicating that the binding interface of the 3:1 Stx(1-262):Syb(1-96) complex is comparable to the interface present in the SNARE complex.

To test whether the third SNARE reorganises the pre-assembled 1:3:1 Syb(1-96):Stx(1-262):Cpx1 complex causing disassembly of two Stx(1-262) molecules, SNAP25(CtoS) was added in equimolar amounts (**Figure 29D**). Indeed, an additional charge state distribution corresponding in mass to the 1:1:1:1 SNAP25(CtoS):Syb(1-96):Stx(1-262):Cpx1 complex (80695 Da) was observed. Interestingly, following complex formation over time revealed that immediately after addition of SNAP25(CtoS) only the previously identified 1:3:1 complex was present (**Supplementary Figure 7**). After several minutes of incubation, the intensity of the 1:3:1 complex decreased, while an additional distribution corresponding to the SNARE complex binding one copy of Cpx1 appeared. The intensity of this complex increased over time, and after approximately 10 min, the SNARE:Cpx1 complex was the only complex observed (**Supplementary Figure 7**). Although Cpx1 stably bound to the complex, replacement of two Stx(1-262) molecules by SNAP25(CtoS), reassembling into the SNARE complex, is possible. However, this process takes several minutes suggesting that blocking one interface decelerates either the disassembly of the Stx(1-262) copies for rearrangement of the complex or the disassembly of the full complex assuming that the exchange of individual helices is not possible. Nonetheless, both scenarios impede new complex formation.

3.3.2 Characterising interactions of Cpx1 with the SNARE proteins

Cpx1 is a well-known regulator of the SNARE assembly; it is proposed to exhibit both stimulating and inhibitory functions during SNARE mediated membrane fusion [56,187]. High-resolution crystal structures visualise antiparallel binding of Cpx1 to the SNARE complex, through interactions of the central helix with an interface formed by Syb2 and Stx1 [61,77,186]. This arrangement suggests that Cpx1 adopts its regulatory function in the late steps of the SNARE assembly. However, it is still unclear whether Cpx1 binds the individual SNAREs or other intermediate complexes and possibly has a role at the early stages of the SNARE assembly. For this reason, interactions of Cpx1 with individual SNARE proteins and pre-assembled binary complexes providing varying interaction interfaces as well as interactions of Cpx1 with the fully assembled SNARE complex were characterised by native MS (Section 2.5.5). In addition, chemical cross-linking (Section 2.3.7) combined with LC-MS/MS analysis (Section 2.5.4) was used to shed light on the specific interactions formed between the SNARE complex and Cpx1, including flexible regions of Cpx1 that are not included in the available high-resolution structures.

3.3.2.1 Identification of binding interfaces for Cpx1

Cpx1 was incubated at equimolar ratios with each individual SNARE protein and analysed by native MS (Figure 31). In the mass spectra, charge state series corresponding to monomers of SNAP25(CtoS) (23842 Da), Stx(1-262) (30620 Da), Syb(1-96) (10800 Da) and Cpx1 (15402 Da) were assigned. Complex formation involving Cpx1 was, however, not observed.

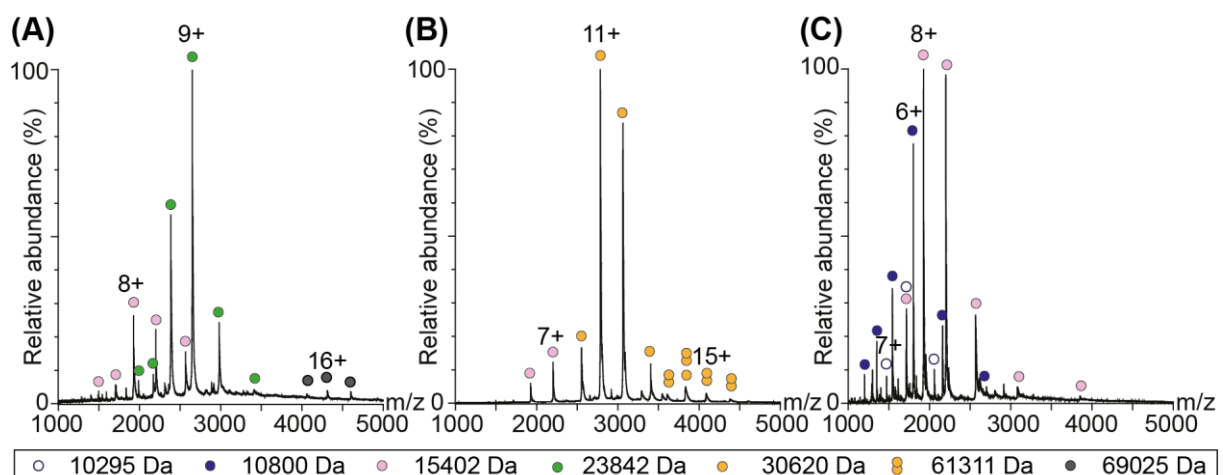


Figure 31. Individual SNARE proteins do not interact with Cpx1.

The SNARE proteins were incubated with Cpx1 (pink circles) in a 1:1 molar ratio and analysed by native MS. Charge state distributions corresponding to monomers of the SNARE proteins and Cpx1 as well as low abundant dimers of Stx(1-262) were observed. (A) SNAP25(CtoS) (green circles) (B) Stx(1-262) (orange circles) (C) Syb(1-96) (blue circles). (Figure adapted from [174].)

Although collision induced dissociation of the 1:3:1 Syb(1-96):Stx(1-262):Cpx1 complex resulted in formation of a 3:1 Stx(1-262):Cpx1 complex (see **Figure 29C**), this arrangement was not observed when incubating Stx(1-262) and Cpx1. With the exception of a low abundant Stx(1-262) dimer, oligomerisation of SNARE proteins and Cpx1 as observed for the individually analysed proteins (see **Figure 16, 19 and 22**) was not monitored. The absence of both, oligomers of each protein and complexes formed between the SNARE proteins and Cpx1, indicates transient interactions between the proteins that do not lead to formation of stable complexes which cannot be preserved by native MS. Although Stx(1-262) and Syb(1-96) are known to interact with Cpx1, the individual proteins are not sufficient for formation of a stable complex suggesting that a binding interface such as the one present in the 1:3:1 Syb(1-96):Stx(1-262):Cpx1 complex is required for the assembly (see **Figure 29**).

To test whether Cpx1 binds complexes that provide an interface containing either Stx(1-262) or Syb(1-69), SNAP25(CtoS) and Stx(1-262) as well as SNAP25(CtoS) and Syb(1-96) were mixed at a 1:2 ratio to pre-assemble binary complexes. Subsequently, equimolar amounts of Cpx1 were added (**Figure 32**). Compared to the native mass spectra of the binary complexes omitting Cpx1 (see **Figure 23 and 25**), only one additional charge state series corresponding to monomeric Cpx1 (15399 Da) was observed. The absence of complexes including Cpx1 reveals that binding of Cpx1 to interfaces formed by SNAP25(CtoS) and Stx(1-262) or

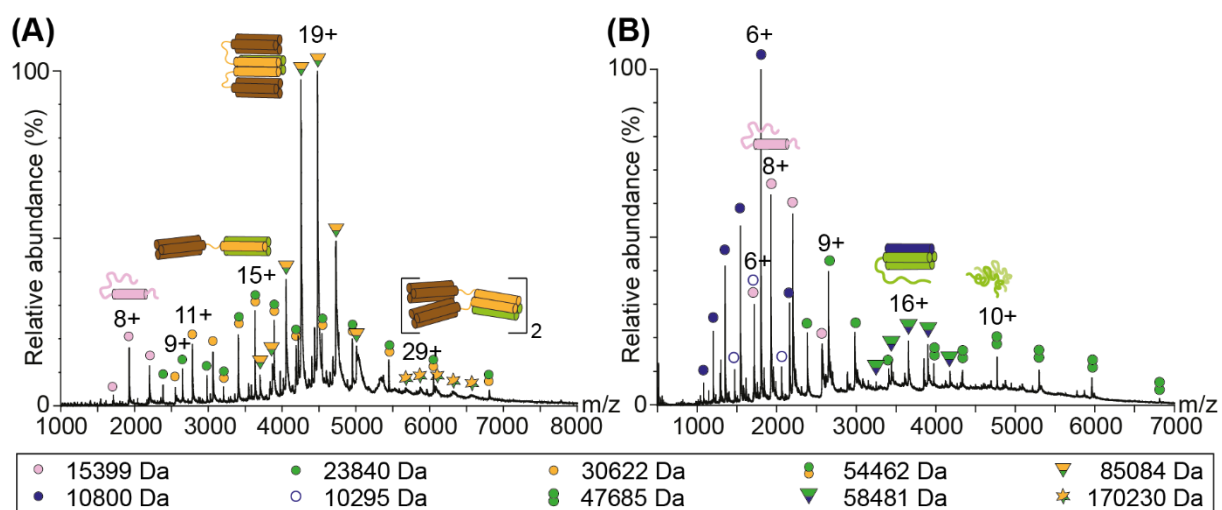


Figure 32. Binary complexes do not interact with Cpx1.

SNARE proteins were incubated to form binary complexes, followed by equimolarly addition of Cpx1 and analysis by native MS. **(A)** SNAP25(CtoS) and Stx(1-262) were incubated in 1:2 molar ratio and charge state distributions corresponding to monomeric Cpx1 (pink circle), SNAP25(CtoS) (green circle) and Stx(1-262) (orange circle) as well as binary complexes composed of SNAP25(CtoS) and Stx(1-262) in a 1:1 (green-orange twin-circles), 1:2 (orange-green triangles) and 2:4 (orange-green stars) stoichiometry were observed. **(B)** SNAP25(CtoS) and Syb(1-96) were incubated in 1:2 molar ratio. Charge state distributions corresponding to monomeric Cpx1 (pink circle), Syb(1-96) (blue circle) and SNAP25(CtoS) (green circle), dimeric SNAP25(CtoS) (green twin-circles) as well as binary complexes composed of SNAP25(CtoS) and Syb(1-96) with a stoichiometry of 2:1 (green-blue triangle) were observed. (Figure adapted from [174].)

SNAP25(CtoS) and Syb(1-96) does not occur. Consequently, the presence of Stx(1-262) or Syb(1-96) is not sufficient for stable binding of Cpx1. Furthermore, binding of Cpx1 was not observed to interfaces formed by two copies of Stx(1-262) or SNAP25(CtoS) as well as both proteins such as provided by the ‘acceptor’ complex suggesting that indeed an interaction site containing both Stx(1-262) and Syb(1-96) is required for stable binding.

3.3.2.2 Disassembly of SNARE complex oligomers by Cpx1

To assemble the ternary SNARE complex (3Q:1R, QabcR), SNAP25(CtoS), Stx(1-262) and Syb(1-96) were mixed in equimolar amounts and incubated overnight. Analysis by native MS showed charge state distributions corresponding in mass to monomeric (65306 Da), dimeric (130632 Da) and trimeric SNARE complexes (195970 Da) (**Figure 33A**). SNARE complex multimers were already observed after rearrangement of binary complexes into the SNARE complex (see **Figures 23, 25 and 29**). Note that the monomer and dimer of the SNARE complex are highly abundant and show similar intensities indicating stable oligomer formation. The trimeric SNARE complex on the contrary, is less abundant. Assuming that Cpx1 binds in a similar fashion to the fully assembled SNARE complex, providing the natural Syb(1-96):Stx(1-262) binding interface as observed for the interface in the 1:3:1 Syb(1-96):Stx(1-262):Cpx1 complex (**Figure 29**), Cpx1 was added to the pre-assembled SNARE oligomers.

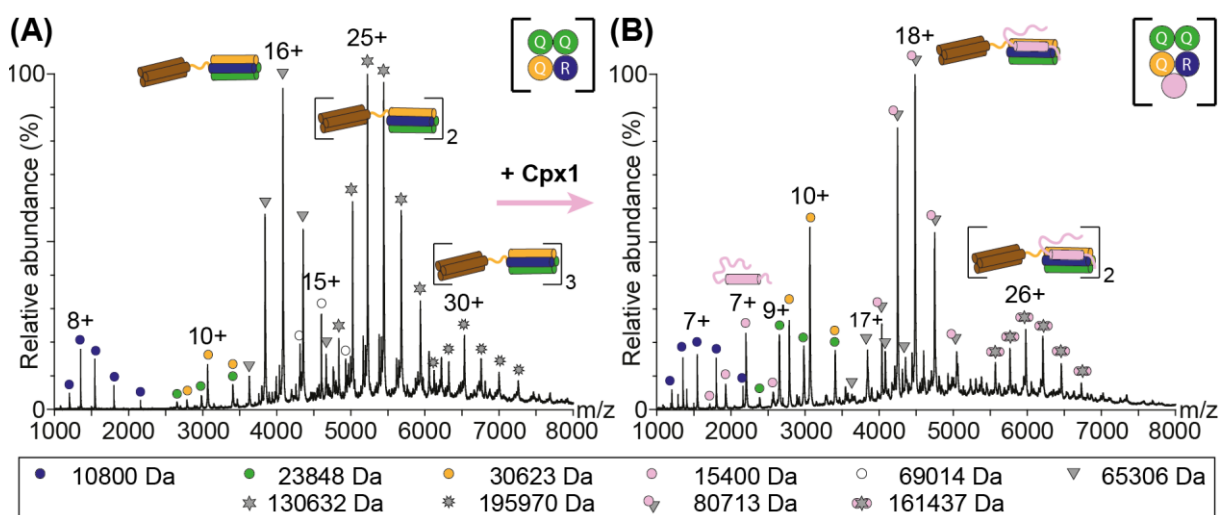


Figure 33. Disassembly of SNARE complex oligomers by Cpx1.

(A) Syb(1-96) (blue), SNAP25(CtoS) (green) and Stx(1-262) (orange) were mixed at a 1:1:1 ratio and analysed by native MS. Charge state distributions corresponding to monomers of the SNARE proteins (coloured circles) as well as monomeric (grey triangles), dimeric (grey hexagonal stars) and trimeric (grey nonagonal stars) SNARE complexes are assigned. (B) Addition of Cpx1 (pink circle) reduced SNARE complex oligomerisation. Series of charge states corresponding to monomers (grey triangle-pink circle) and dimers (grey hexagonal star-pink circle) of the SNARE:Cpx1 complex were observed. (Figure adapted from [174].)

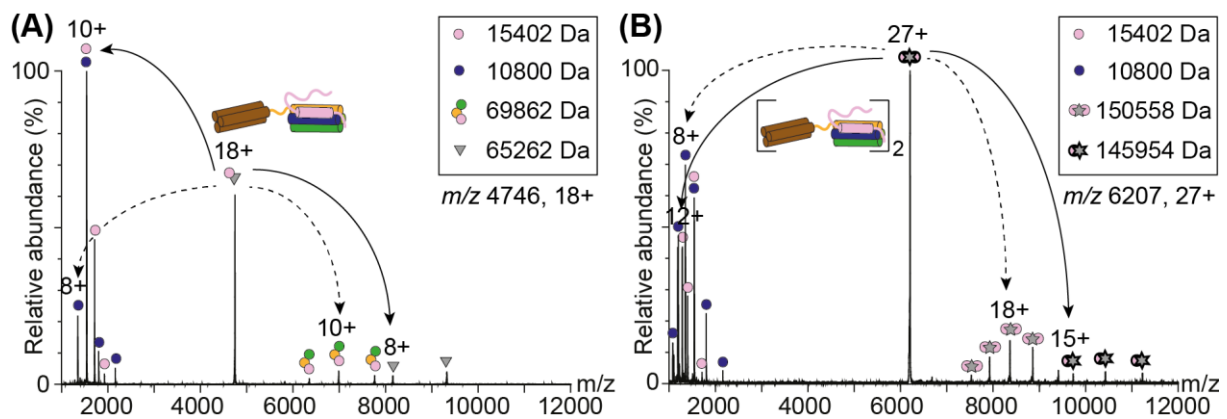


Figure 34. Collision induced dissociation of the SNARE:Cpx1 complex.

(A) The 18+ charge state of the monomeric SNARE:Cpx1 complex (grey triangle pink circle) and (B) the 27+ charge state of the dimeric SNARE:Cpx1 complex (grey hexagonal star-pink circle) were selected for collisional induced dissociation. Charge state distributions corresponding to the dissociated subunits Syb(1-96) (blue circle) and Cpx1 (pink circle) as well as 'stripped' complexes with a stoichiometry of 1:1:1 SNAP25(CtoS):Stx(1-262):Cpx1 (green-yellow-pink circle), 1:1:1 Syb(1-96):SNAP25(CtoS):Stx(1-262) (grey triangle) as well as 1:2:2:2 (grey pentagonal star pink twin-circles) and 2:2:2:1 Syb(1-96):SNAP25(CtoS):Stx(1-262):Cpx1 (grey hexagonal star-pinkcircle) were observed. (Figure adapted from [174].)

Immediately after addition of Cpx1, binding to the SNARE complex was observed resulting in two charge state distributions corresponding to the SNARE:Cpx1 complex and a dimer thereof (Figure 33B). Importantly, the monomeric complex is high abundant, while the dimeric species shows remarkably reduced intensity. SNARE complex oligomers without Cpx1 were not detected and only a low abundant SNARE complex monomer was observed. Cpx1 appears to impede SNARE complex oligomerisation by binding to the complex and presumably blocking the interaction surface formed by two SNARE complexes. Validating the stoichiometry of the observed complexes by collision induced dissociation reveals a similar dissociation pattern as monitored for the 1:3:1 Syb(1-96):Stx(1-262):Cpx1 complex (see Figure 29). For the monomeric SNARE:Cpx1 complex dissociation of Cpx1 yielded a 'stripped' SNARE complex, while dissociation of Syb(1-96) led to formation of the 1:1:1 SNAP25(CtoS):Stx(1-262):Cpx1 complex with unknown structural arrangement (Figure 34A). Disassembly of the dimeric SNARE:Cpx1 complex resulted in formation of 'stripped' complexes omitting either Syb(1-96) or Cpx1 (Figure 34B). Although dissociation of Syb(1-96) should be sterically hindered due to binding of Cpx1, its dissociation still confirms least stable incorporation into the complexes. Disassembly of Cpx1 on the contrary was, however, expected and confirmed binding at the periphery of the complexes.

To identify the interactions formed between the SNARE proteins and Cpx1 that lead to dissociation of SNARE complex oligomers, chemical cross-linking was performed. The SNARE:Cpx1 complex was pre-assembled, cross-linked using increasing concentrations of BS3 cross-linker and separated by gel electrophoresis followed by Coomassie staining to

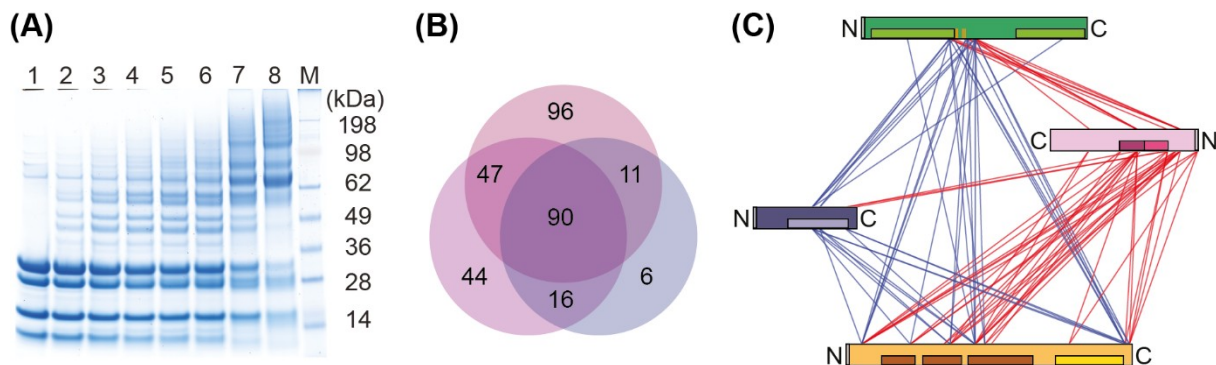


Figure 35. Cross-linking analysis of the SNARE:Cpx1 complex.

(A) 40 μ M pre-assembled SNARE:Cpx1 complex were cross-linked with 0 mM (lane 1), 0.01 mM (lane 2), 0.03 mM (lane 3), 0.05 mM (lane 4), 0.075 mM (lane 5), 0.1 mM (lane 6), 0.3 mM (lane 7) and 1 mM (lane 8) BS3 cross-linker. Cross-linked and non-cross-linked complex were separated by gel electrophoresis and visualised by Coomassie staining. (B) 40 μ M SNARE:Cpx1 complex were cross-linked with 1 mM BS3 cross-linker in three individual replicates. Evaluated cross-links of each replicate are visualised in a VENN diagram. (C) Identified cross-links are visualized in a network plot. SNAP25(CtoS) (green), Syb(1-96) (blue), Stx(1-262) (orange) and Cpx1 (pink) are shown as coloured bars. SNARE motifs (light green or blue and yellow), helices of the Habc domain of Stx(1-262) (brown) as well as the central helix (pink) and accessory helix (purple) of Cpx1 are highlighted. Intermolecular cross-links between SNARE proteins (blue lines) and towards Cpx1 (red lines) are shown. (Figure adapted from [174].)

identify a suitable cross-linker concentration capturing the whole complex (**Figure 35A**). For identification of cross-linking sites, the complex was then cross-linked with 1 mM BS3 and subsequently unfolded using urea. Trypsin digestion in solution resulted in cross-linked dipeptides that were enriched by SEC. LC-MS/MS analysis and a database search led to the identification of 154 intramolecular and 162 intermolecular cross-links as well as 21 cross-links that were formed between homooligomers of the individual proteins (**Supplementary Table 6**). Of these, 100 intramolecular and 82 intermolecular cross-links were identified in at least two out of three experiments (**Figure 35B**). Visualising intermolecular cross-links in a network plot showed that most of the interactions between the SNAREs were formed between the linker of SNAP25(CtoS), the SNARE motif of Syb(1-96) and the C-terminus of Stx(1-262) (**Figure 35C**). These interactions indicate a parallel orientation of the SNARE proteins as previously described for the fully assembled SNARE complex [17,18]. In addition, many cross-links are formed with the Habc domain of Stx(1-262) presumably resulting from its high flexibility. Cross-links formed between the N-terminus as well as the CH of Cpx1 and the SNAREs are mainly located in the linker region of SNAP25(CtoS) adjacent to its Qb SNARE motif and the C-termini of Syb(1-96) and Stx(1-262) and, therefore, reveal antiparallel binding of Cpx1 to the SNARE complex.

Validation of the observed cross-links was achieved by mapping of the cross-links into available high-resolution structures, however, flexible protein regions that contain cross-linking sites are not present in these structures. To enable visualisation of all identified cross-

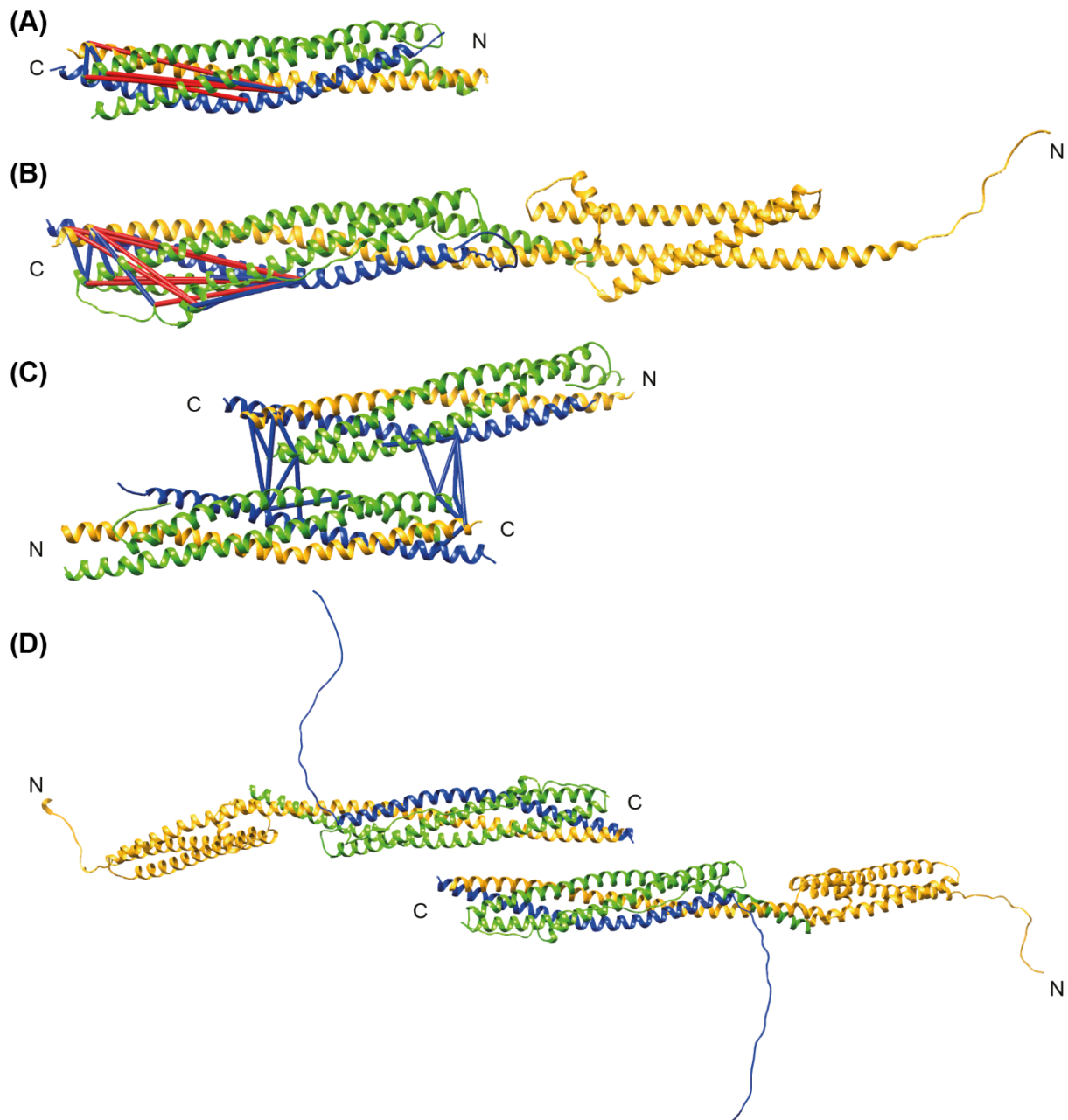


Figure 36. Validation of intermolecular interactions between SNARE proteins.

SNAP25 (green); Syb2 (blue) and Stx1 (orange) are shown in cartoon representation. Short-range (< 30 Å, blue lines) and long-range (> 30 Å, red lines) cross-links, identified in at least two out of three replicates, are visualised. Cross-links are shown in **(A)** a high-resolution structure of the SNARE complex (PDB ID: 1SFC [17]) lacking disordered regions, **(B)** an AlphaFold 2-multimer prediction of the monomeric SNARE complex including flexible regions and **(C)** two high-resolution SNARE complexes in antiparallel orientation. Note that cross-links are shown twice in this model. **(D)** An AlphaFold 2-multimer prediction of a dimer of the SNARE complex in antiparallel orientation is shown. (Figure adapted from [174])

links, AlphaFold 2 predictions of monomeric and dimeric complexes were additionally used **(Figure 36)**. Of 16 identified intermolecular cross-links formed between the SNARE proteins within the SNARE:Cpx1 complex, eight cross-links were visualised in the high-resolution crystal structure of the SNARE core complex, which lacks the flexible linker of SNAP25 as well

as the Habc domain of Stx1 [17] (**Figure 36A**). Four of these cross-links are within the expected distance range $< 30 \text{ \AA}$ and formed between the C-termini of the SNAREs. However, four cross-links exceed the distance threshold and are formed between the C-termini and lysine residues close to the central arginine of Syb(1-96). Using the AlphaFold 2 multimer model, which provides a structure based on the complete sequence of the SNARE complex, allowed mapping of all 16 cross-links (**Figure 36B**). Of these, seven cross-links exceed the distance range, while nine short range cross-links $< 30 \text{ \AA}$ correlate well with the predicted structure. Most overlength cross-links result from interactions involving the flexible linker of SNAP25(CtoS). Considering multimerisation of the SNARE:Cpx1 complex as observed by native MS (**see Figure 33**), cross-links formed towards the centre of the SNARE core might originate from a second copy of the SNARE complex. Including a second high-resolution SNARE complex into the validation and docking the complexes in antiparallel orientation using UCSF chimera and Xlink Analyzer [124,126], all eight cross-links present in the SNARE core satisfy the distance restraints and are, therefore, positively validated (**Figure 36C**). To verify the suggested arrangement, a dimer of the SNARE complex was predicted using AlphaFold 2, which indeed confirms antiparallel orientation of the SNARE complexes (**Figure 36D**). Since available high resolution structures only include the CH of Cpx1, while the disordered termini containing the cross-linking sites remain unresolved [61,77], visualisation of the cross-links formed with Cpx1 within the SNARE:Cpx1 complex was achieved by mapping the cross-links into an AlphaFold 2 prediction of the monomeric complex (**Figure 37**). In this prediction, Cpx1

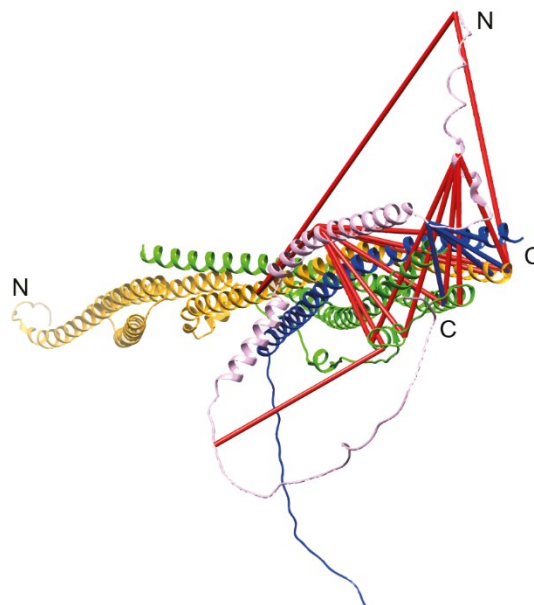


Figure 37. Validation of intermolecular interactions of Cpx1 within the SNARE:Cpx1 complex. SNAP25(CtoS) (green), Syb(1-96) (blue), Stx(1-262) (orange) and Cpx1 (pink) are shown in cartoon representation. Short-range ($< 30 \text{ \AA}$, blue lines) and long-range ($> 30 \text{ \AA}$, red lines) cross-links identified in at least two out of three replicates are visualised. Cross-links are shown in an AlphaFold 2 multimer prediction of the monomeric SNARE:Cpx1 complex. (Figure adapted from [174].)

indeed binds in an antiparallel orientation to the SNARE complex. The N- and C-terminal domains of Cpx1 are visualised including additional helical segments and are randomly oriented; an interaction of these with the complex was, however, not predicted. In addition, the linker of Stx(1-262) connecting its Qa SNARE motif and the Habc domain is predicted as an helical elongation of the SNARE motif, thus, the Habc domain of Stx(1-262) is directed away from the SNARE core. For the sake of clarity, only 21 out of 37 intermolecular cross-links formed between Cpx1 and the four-helical bundle are visualised in the prediction (**Figure 37**). Of these, 16 long-range cross-links $> 30 \text{ \AA}$ were formed with flexible regions of SNAP25(CtoS) and Cpx1 as well as the central lysine K54 of Cpx1. These might also result from interactions formed with a second copy of the SNARE:Cpx1 complex as described above for the interactions of the SNARE proteins. However, five short-range cross-links were observed between the NTD of Cpx1 and the C-terminal SNARE complex. Note that all disordered regions are captured in one conformation rather than multiple possible conformations and, therefore, only represent a 'snapshot' of possible structures. Consequently, most interactions are displayed as overlength cross-links (**Figure 37**).

Attempting to visualise and validate all identified cross-links including the ones formed with the Habc domain of Stx(1-262) as well as those that might originate from a second copy of the SNARE:Cpx1 complex, a structural model was created. For this, a high-resolution structure of the partially resolved SNARE:Cpx1 complex was aligned with a full-length AlphaFold prediction of Cpx1 containing its disordered N- and C-terminal domains (**Figure 38A**). Note that the N-terminal domain of Cpx1 was manually repositioned to visualise a conformation in which interactions with the core SNARE complex are possible. In addition, a high-resolution structure of the Habc domain of Stx1 was added twice to the arrangement visualising varying interactions sites with the SNARE core complex resulting from the flexible linker of Stx1 (**Figure 38A**). Regions that are not present in the crystal structure, such as the linker of SNAP25 as well as the linker and the C-terminus of Stx(1-262) were indicated by coloured lines. Cross-links identified in 2 out of 3 experiments are shown as dotted lines, while cross-links identified in all replicates are shown as solid lines. For the sake of clarity, cross-links formed between Cpx1 and the Habc domain of Stx(1-262) (**Figure 38A**) as well as cross-links formed towards the SNARE core complex (**Figure 38B**) are visualised separately. The Habc domain of Stx(1-262) interacts via the residues K12, K57, K88, K94, K117, K126 and S132 with either the CH of Cpx1 involving the lysine residues K26, K51, K54 and K96 or with the NTD of Cpx1 including the N-terminus (G-2) as well as the lysine residues K14 and K18 (**Figure 38B**). In this model, the CH and the NTD of Cpx1 are located at opposite sides of the SNARE complex. For formation of these cross-links, high flexibility of the Habc domain is required and likely results from the flexible linker that connects it to the Qa SNARE motif of Stx(1-262). Interactions formed between Cpx1 and the SNARE proteins involve G-2, K14 and

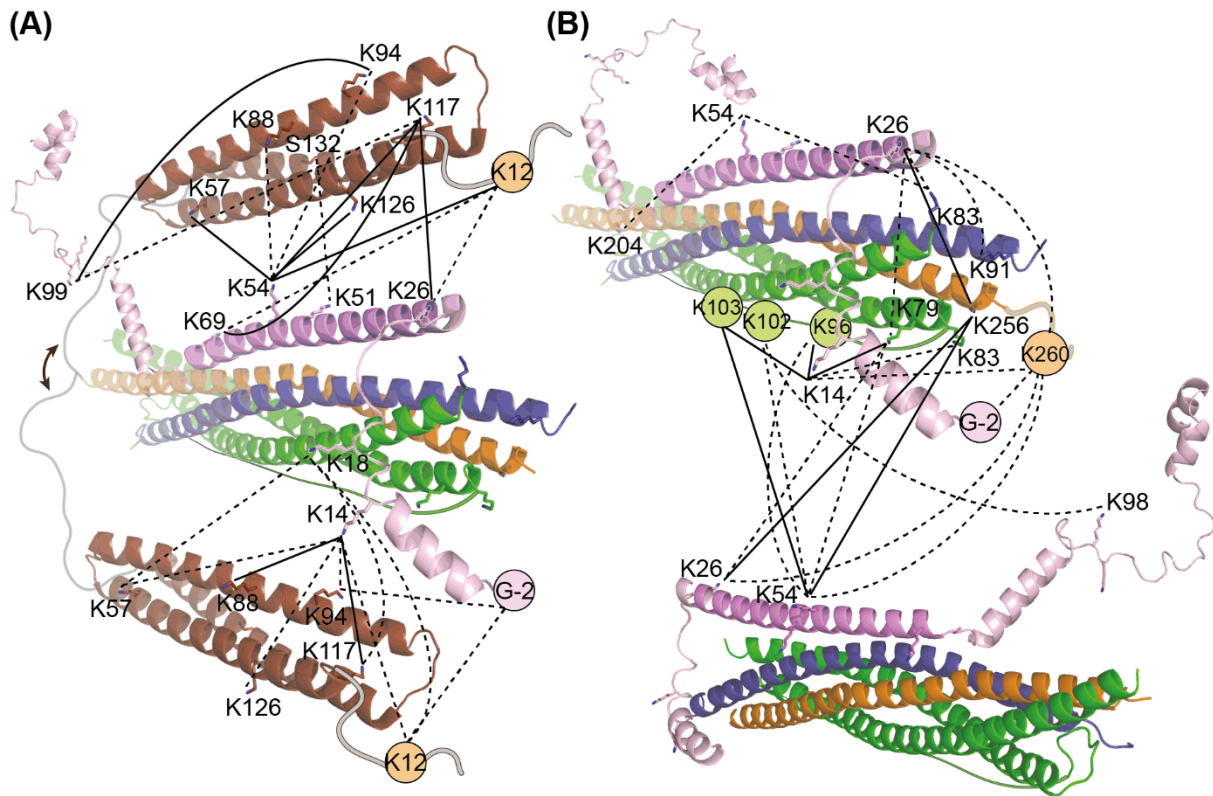


Figure 38. Model of the SNARE:Cpx1 complex.

Cpx1 (pink), Syb(1-96) (blue), the SNARE motif (orange) and the Habc domain of Stx(1-262) (brown) as well as SNAP25(CtoS) (green) are shown. Disordered structures of SNAREs are shown as coloured lines. Cross-linked residues are labelled. Cross-links identified in 2 out of 3 replicates (dotted lines) or 3 out of 3 replicates (solid lines) are shown. Interactions between Cpx1 and **(A)** the Habc domain of Stx(1-262) and **(B)** the SNARE complex are visualised. Two copies of the Habc domain and the SNARE complex are shown. (Figure adapted from [174].)

K26 of the N-terminal domain of Cpx1 as well as K83 and K91 of Syb(1-96), K256 and K260 of Stx(1-262) and K79 and K83 of SNAP25(CtoS) (**Figure 38B**). All of these residues are located at the C-terminus of the SNARE complex. The NTD of Cpx1 appears to overlap with the C-termini of the SNAREs, thus, clamping the SNARE complex and likely blocking the interaction surface of SNARE oligomers. As a consequence, Cpx1 might sterically hinder SNARE complex multimerisation resulting in a decreased intensity as observed by native MS (**see Figure 33**). In addition, cross-links formed between K26, K54 and K98 of Cpx1 and K79, K96, K102 and K103 of SNAP25(CtoS) as well as K256 and K260 of Stx(1-262) are unlikely to be formed within one SNARE:Cpx1 complex, since the involved residues are located at opposite sides of the complex (**Figure 38B**). Adding a second copy of the SNARE:Cpx1 complex into the model in an antiparallel orientation, as also validated above (**see Figure 36**), indeed satisfies all cross-links.

3.4 Structural characterisation of Syb(1-96) and Cpx1 in a lipid environment

While the protein machinery of SNARE-mediated membrane fusion was extensively investigated, less is known about the role of lipids. Depending on the membrane mimetic used, contrary structural content of the cytosolic domain of Syb2 was reported; for instance, a helical nucleation site observed in micelles that was absent in liposomes and nanodiscs [42,45,48]. A patch of positively charged residues was proposed to be critical for lipid binding of the juxtamembrane domain and insertion of aromatic residues into the membrane was described to promote membrane fusion by bending of the membrane [48,51]. However, the negatively charged residues of the R-SNARE motif were described to induce electrostatic repulsion between Syb2 and the membrane, keeping its SNARE motif available for interactions with other SNARE proteins [51]. Cpx1, on the other hand, is well known to interact with membranes and was shown to promote and inhibit the SNARE assembly, although the underlying mechanism is still enigmatic. Cpx1 contains a C-terminal lipid binding motif composed of two consecutive amphipathic helices. These helices undergo a disorder-to-order transition upon binding to membranes, which occurs in a curvature-dependent manner [68,75,76]. The N-terminal amphipathic helix was also described to bind lipid membranes and is sensitive towards membrane curvature, although the membrane binding affinity mostly results from the C-terminus of Cpx1 [188,189]. While lipid binding of Cpx1 appears to be independent on the lipid class, a preference for PI(4,5)P₂ membranes was proposed [190,189]. To specifically assess the interactions of the cytosolic domain of Syb2 (Syb(1-96)) as well as Cpx1 with individual lipids, interactions of both proteins with immobilized lipids on membrane strips (**Section 2.3.8**), solubilised lipids (**Section 2.5.5**) and lipids forming a phospholipid bilayer (**Section 2.3.9**) were investigated.

3.4.1 Interactions of Syb(1-96) with lipids

To interrogate lipid binding of Syb(1-96), a lipid overlay assay was performed. For this, commercially available membrane lipid strips with immobilised lipids of different classes were incubated with Syb(1-96). Binding of the protein to the lipids was then analysed using the specific anti-VAMP-1/2/3 antibody as well as a secondary antibody. The emitted chemiluminescence revealed binding of Syb(1-96) to lipids that provide negative charges such as phosphatidic acid (PA), cardiolipin (CL) as well as phosphatidylinositol phosphate (PI(4)P), phosphatidylinositol bisphosphate (PI(4,5)P₂) and phosphatidylinositol trisphosphate (PI(3,4,5)P₃) (**Figure 39**). In addition to cholesterol, the main components of the synaptic vesicle membrane are phosphatidylserine (PS), phosphatidylethanolamine (PE) and phosphatidylcholine (PC) [3,191,192]. While Syb(1-96) binds negatively charged PS, binding

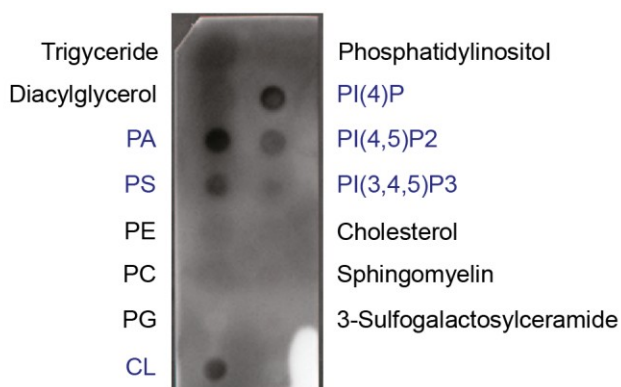


Figure 39. Lipid overlay assay of Syb(1-96).

Commercially available membrane strips with spotted lipids of different classes were incubated with Syb(1-96). Binding of Syb(1-96) to the lipids was detected using the anti-VAMP-1/2/3 antibody.

to cholesterol as well as zwitterionic PE and PC was not observed (**Figure 39**). Interestingly, Syb(1-96) binds lipids containing one or two negative charges that are not in vicinity, e.g. PA, PS and PI(4)P, stronger than lipids containing several negative charges in proximity, e.g. CL, PI(4,5)P₂ and PI(3,4,5)P₃. Although phosphatidylglycerol (PG), phosphatidylinositol (PI) and sphingomyelin also provide a negative charge, binding was not observed. Binding to additional lipid classes such as triglycerides, diacylglycerol and 3-Sulfogalactosylceramide was also not observed (**Figure 39**).

To gain further insights into the binding of Syb(1-96) to individual lipids, a native MS approach based on the transfer of lipids from detergent-lipid micelles was used [161]. Based on the lipid composition of the synaptic vesicle membrane, the standard lipids DOPS, DOPE and DOPC were assessed. Since Syb(1-96) preferentially binds negatively charged lipids, DOPG was also employed to include a negatively charged lipid that is physiologically not relevant in the synapse. To perform lipid transfer, detergent-lipid micelles were assembled by mixing the lipid of interest with the non-ionic detergent C8E4, which was previously described to be well-suited to analyse lipid interactions with soluble proteins [193], in 200 mM ammonium acetate. These micelles were subsequently mixed with Syb(1-96) to form protein-lipid complexes presumably during ionisation, although the mechanism is still enigmatic [161,193]. Protein-lipid complexes show the same charge state distribution as the apo-protein and consequently appear as additional peak series shifted to higher m/z values depending on the number of lipids bound. Syb(1-96) was analysed without lipids and with increasing concentrations of each lipid, and lipid binding to Syb(1-96) increased for all lipids in a concentration-dependent manner (**Supplementary Figure 8 and 9**). A detailed analysis of the native MS spectra, acquired when a ten-fold excess of lipid over Syb(1-96) was used, shows binding of two or three lipids with comparable intensity indicating that binding of individual lipids was not specific (**Figure 40**).

For DOPS and DOPC, a higher number of associated lipids was observed for lower charge states. Due to faster acceleration in the electric fields of the mass spectrometer, higher charge states experience higher collisional energy presumably leading to dissociation of bound lipids. Singly-charged gas phase clusters of C8E4 and lipids were also observed (**Figure 40**). Interestingly, a Gaussian distribution of charge series of Syb(1-96) in the presence of DOPS

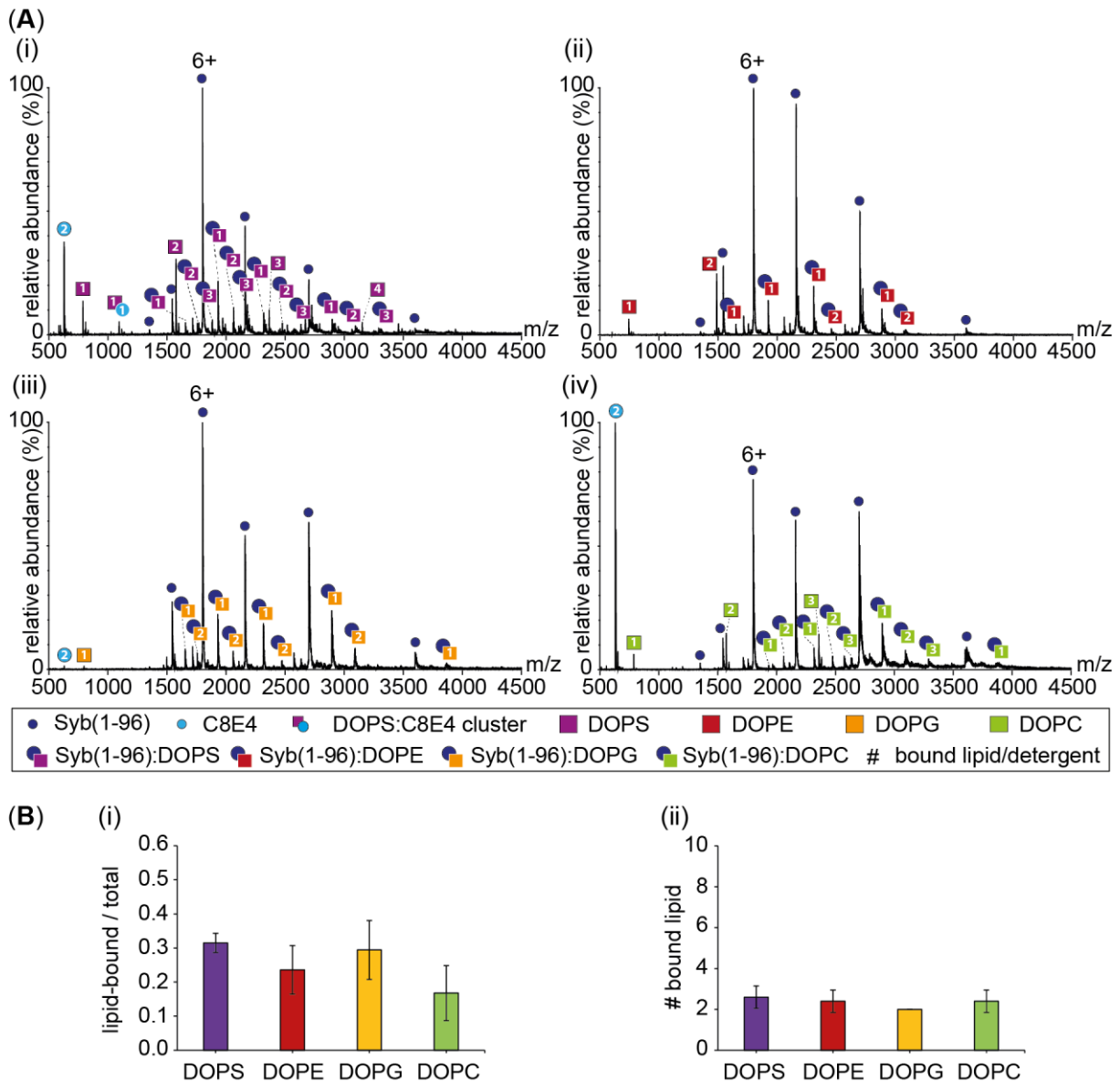


Figure 40. Native MS of Syb(1-96) interacting with lipids of different classes.

5 μM Syb(1-96) were mixed with 50 μM of each lipid in 0.5 % C8E4 and analysed by native MS. **(A)** Charge state distributions corresponding in mass to monomeric Syb(96) (blue circle), dimeric C8E4 (light blue circle), lipid clusters (coloured squares with number of lipids), C8E4:DOPS clusters (light blue circle purple square) and Syb(1-96):lipid complexes with up to three (i) DOPS (blue circle purple square), (ii) DOPE (blue circle red square), (iii) DOPG (blue circle orange square) and (iv) DOPC (blue circle green square) lipids are assigned. **(B)** The mass spectra were deconvolved and signal intensities extracted. (i) The relative abundance of Syb(1-96):lipid complexes and (ii) the total number of lipids bound to Syb(1-96) in five (DOPS/DOPE/DOPC) and three (DOPG) replicates are shown. Error bars represent standard deviations.

and DOPE, but not in the presence of DOPG and DOPC, was observed suggesting that different conformations are present that might result from structural rearrangements. The acquired mass spectra were deconvolved followed by extraction of the peak intensities of the lipid-free and lipid-bound states of Syb(1-96) using UniDec [151] (**Figure 40B (i)**). Normalising the intensity of Syb(1-96):lipid complexes to the total signal intensity of all species detected, revealed indeed similar lipid binding for the different lipid classes; although, binding of negatively charged DOPS and DOPG was slightly higher compared to the zwitterionic DOPE and DOPC. However, when analysing the total number of bound lipids, a significant difference was not observed. Accordingly, binding of two or three DOPS, DOPE and DOPC as well as a maximum of two DOPG molecules was observed (**Figure 40B (ii)**).

In the next step, binding of Syb(1-96) to phospholipid bilayers, composed of each lipid used above and resembling a more physiological environment, was explored. For this, dried lipid films of the individual lipids were dissolved in aqueous buffer and extruded through a polycarbonate membrane forming membrane vesicles of defined size. These liposomes were then incubated with Syb(1-96) at a protein:lipid ratio of 1:300 [48], tested for a homogenous size of 100 nm and subsequently overlaid with a sucrose gradient (**Figure 41**). Following centrifugation, liposomes, due to their lower density, float on top of the gradient. Proteins that are stably interacting with the liposomes will co-migrate and are, therefore, identified in the top fractions of the sucrose gradient. If the protein is not binding to the liposomes, it remains as 'free' protein in the bottom fraction. Top, middle and bottom fractions of the sucrose gradient were, therefore, collected and analysed by gel electrophoresis (**Figure 41A**). In contrast to the

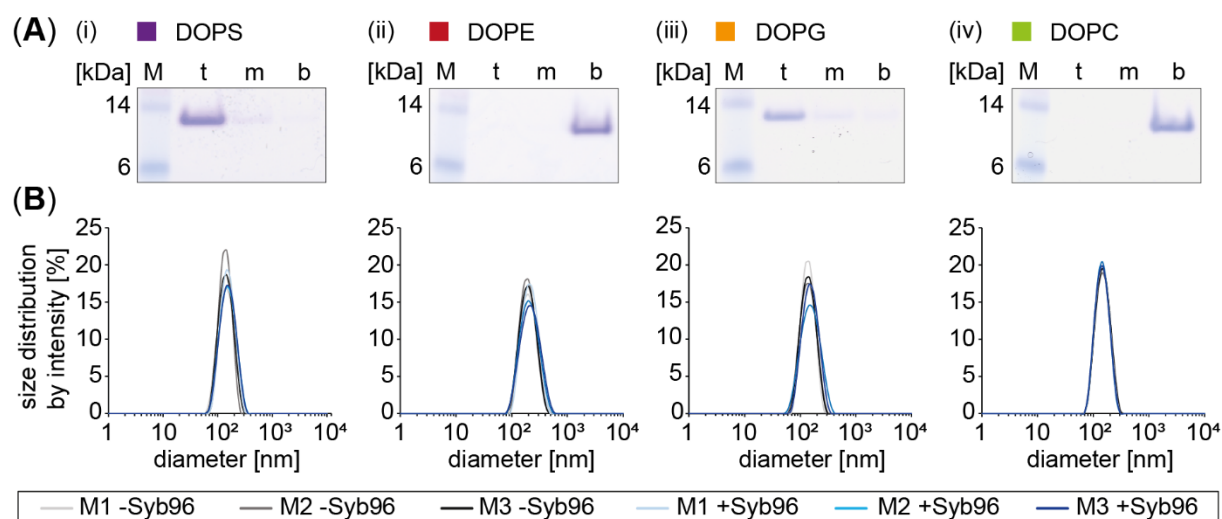


Figure 41. Binding of Syb(1-96) to liposomes.

(A) Binding of Syb(1-96) to (i) DOPS, (ii) DOPE, (iii) DOPG and (iv) DOPC liposomes was analysed by flotation on a sucrose gradient. Top (t), middle (m) and bottom (b) fractions of the gradient were analysed by gel electrophoresis. **(B)** The homogenous size distribution of liposomes was validated by DLS. Intensity-weighted size distributions before (grey, black) and after addition of Syb(1-96) (blue) are shown.

native MS measurements that showed lipid binding independent of the lipid class, Syb(1-96) bound only to liposomes composed of the negatively charged DOPS and DOPG (**Figure 41A (i, iii)**). Association to liposomes composed of zwitterionic DOPE or DOPC was not observed (**Figure 41A (ii, iv)**). In summary, Syb(1-96) shows a preference for negatively charged lipids in solution. Interactions with these lipids might be formed with the patch of positively charged residues of the juxtamembrane domain as previously reported [48,51]. Binding to zwitterionic lipids, however, might be prevented due to electrostatic repulsion occurring from the positive charges of the ethanolamine and choline head groups.

3.4.2 Interactions of Cpx1 with lipids

Following the same procedure as described above for Syb(1-96), interactions between Cpx1 and varying lipid classes were screened in a lipid overlay assay using the specific anti-Complexin-1/2 antibody as well as a secondary antibody. Although Cpx1 contains amphipathic helices at both termini, binding was only observed to the negatively charged lipids PA, PS, CL, PI, PI(4)P, PI(4,5)P₂ and PI(3,4,5)P₃ (**Figure 42**). Note that the highest intensity was observed for DOPS and that, with increasing degree of phosphorylation of the inositol headgroup, the signal intensity decreased. This is in contrast to the previously announced specificity of Cpx1 for PI(4,5)P₂ [189]. Binding to cholesterol, PE, PC or sphingomyelin as well as triglyceride, diacylglycerol and 3-Sulfogalactosylceramide was not observed.

To explore interactions of Cpx1 with solubilised lipids, Cpx1 was mixed with increasing concentration of five up to 50 μ M of DOPS, DOPE, DOPG or DOPC and subsequently analysed by native MS (**Supplementary Figure 10 and 11**). In the absence of lipids, Cpx1:C8E4 complexes were formed; however, these complexes disassembled with increasing lipid concentration favouring the formation of Cpx1:lipid complexes. Interestingly, for DOPS

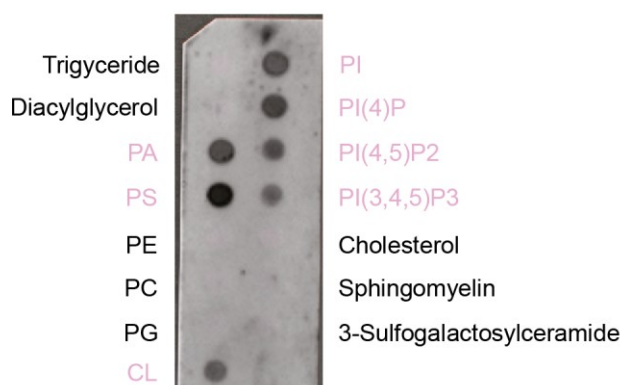


Figure 42. Lipid overlay assay of Cpx1.

Commercially available membrane strips with spotted lipids of different classes were incubated with Cpx1. Binding of Cpx1 to the lipids was detected using anti-Complexin-1/2 antibody.

and DOPC, low abundant Cpx1:C8E4 complexes remained at higher lipid concentration. Again, lipid binding was observed for each lipid and with increasing lipid concentration a higher intensity of lipid adducts was observed (**Supplementary Figure 10 and 11**). Comparing the native mass spectra acquired at 50 μ M lipid revealed binding of the lipids with different capacity. While Cpx1 binds up to three DOPS and up to four DOPE molecules (**Figure 43A (i, ii)**), complexes involving DOPG or DOPC showed binding of up to eight lipid molecules

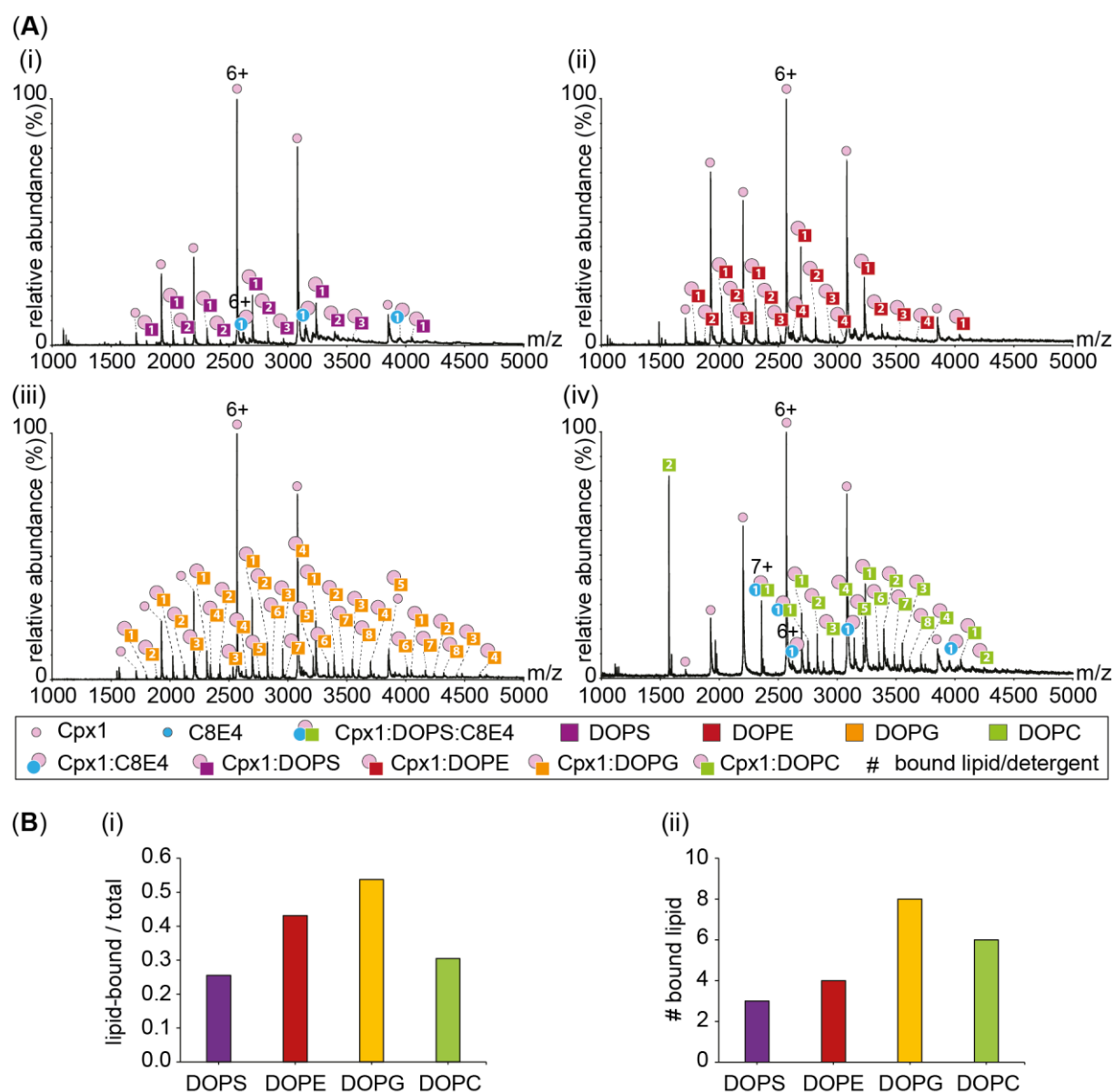


Figure 43. Native MS of Cpx1 interacting with lipids of different classes.

5 μ M Cpx1 were mixed with 50 μ M of each lipid in 0.5 % C8E4 and analysed by native MS. **(A)** Charge state distributions corresponding in mass to monomeric Cpx1 (light pink circle), lipid clusters (coloured squares with number of lipids), C8E4:lipid clusters (light blue circle coloured square) and Cpx1:lipid complexes with up to three **(i)** DOPS (light pink circle purple square), **(ii)** DOPE (light pink circle red square), **(iii)** DOPG (light pink circle orange square) and **(iv)** DOPC (light pink circle green square) lipids are assigned. **(B)** The mass spectra were deconvoluted and signal intensities extracted. **(i)** The relative abundance of Cpx1:lipid complexes and **(ii)** the total number of lipids bound to Cpx1 in one experiment are shown.

(**Figure 43A (iii, iv)**). This is in contrast to the lipid overlay assay showing the strongest binding to DOPS, while binding to DOPE, DOPC or DOPG was not observed. Singly-charged clusters of DOPE and DOPC were also observed. Dissociation of DOPC molecules from higher charge states indicates less stable interactions with Cpx1 than with other lipids (**Figure 43A (iv)**). For DOPS, DOPG and DOPC, Gaussian distributions of charge state series of Cpx1 were detected, while an equal distribution was not observed for DOPE. To determine binding preferences of Cpx1 for the varying lipids, mass spectra were deconvolved and the intensities of Cpx1 and Cpx1:lipid complexes were extracted and normalised to the total signal intensity of all species detected (**Figure 43B (i)**). With the exception of DOPC, the relative abundance of the Cpx1:lipid complexes correlates well with the total number of bound lipids (**Figure 43B (ii)**). The specificity for negatively charged lipids as observed in the lipid overlay assay could not be confirmed. Instead, the relative abundance of Cpx1:lipid complexes containing the zwitterionic DOPE and the negatively charged DOPG was comparably higher than obtained for complexes containing the zwitterionic DOPC or the negatively charged DOPS. Surprisingly, Cpx1:DOPG complexes show the highest relative abundance, in contrast to Cpx1:DOPS complexes, which show the lowest relative abundance. Note that native MS was performed only once and additional replicates are required to confirm these results.

To interrogate binding of Cpx1 to phospholipid membranes composed of DOPS, DOPE, DOPG or DOPC, liposomes of 100 nm size were prepared as described above and incubated with Cpx1 using a protein:lipid ratio of 1:1000. The size distribution of the liposomes before and after addition of Cpx1 was monitored by DLS and the protein:lipid mixtures were separated by centrifugation using a sucrose gradient (**Figure 44A and B**). Flotation analysis revealed binding of Cpx1 to DOPS, DOPG and DOPC liposomes; interactions with DOPE membranes were not observed (**Figure 44A**). While binding of Cpx1 to DOPC membranes seems to be less stable as indicated by a higher amount of 'free' protein in the bottom fraction, for DOPS and DOPG liposomes small amounts of unbound Cpx1 were observed. The size distribution of the liposomes without Cpx1 was homogenous; however, immediately after addition of the protein to the liposomes composed of DOPS and DOPG the protein:lipid mixtures became turbid. Determining the intensity weighted size distribution of these proteoliposomes revealed formation of particles with increased size (**Figure 44B (i, iii)**). Cpx1 contains amphipathic helices on both termini, which were shown to interact with membranes [68,75,76,188,189]. Accordingly, Cpx1 presumably bridges several liposomes by interacting through both termini, leading to formation of 'liposome aggregates'. However, individual large particles appear with a disproportionately higher signal intensity in the intensity-weighted size distribution as they evoke increased light scattering. Therefore, the size distribution weighted by number was

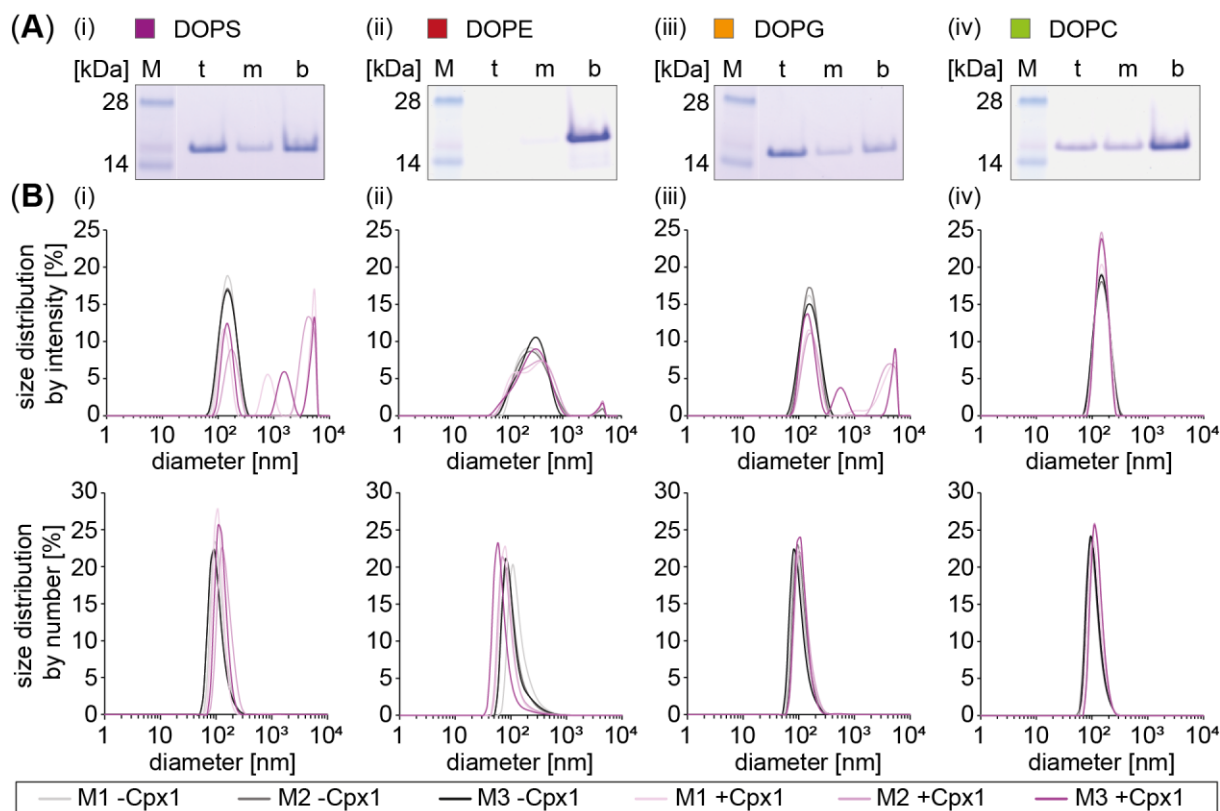


Figure 44. Binding of Cpx1 to liposomes.

(A) Binding of Cpx1 to (i) DOPS, (ii) DOPE, (iii) DOPG and (iv) DOPC liposomes was analysed by flotation on a sucrose gradient and top (t), middle (m) and bottom (b) fractions of the gradient were analysed by gel electrophoresis. **(B)** The homogenous size distribution of liposomes was analysed by DLS weighted by intensity (top) and number (bottom) before (grey, black) and after addition of Cpx1 (pink).

taken into account for comparison (**Figure 44B**). A negligible increase in size upon addition of Cpx1 without additional distributions was observed, thus, validating the previously observed intensity-weighted distributions as a result of individual particles.

In summary, the lipid overlay assay revealed a preference of Cpx1 for negatively charged lipids, which could not be confirmed by native MS and flotation analysis. Instead, binding to both negatively charged and zwitterionic lipids was observed, presumably due to hydrophobic interactions formed between the amphipathic helices and the fatty acyl chains of the lipids. The latter are available in detergent:lipid micelles and might also be available during insertion of the lipid binding domains into the membrane.

4 Discussion and outlook

4.1 Methodological aspects

In this thesis, native MS and chemical cross-linking combined with MS were used to characterise individual synaptic proteins as well as their complexes to provide structural information on the SNARE complex assembly and its regulation.

Native MS. Native MS is a powerful technique for determining the stoichiometry of proteins and their assemblies. By preserving non-covalent interactions in the gas phase, it enables the analysis of proteins in their near-native conformation. Accordingly, the topology and subunit arrangement of complexes as well as ligand binding and complex stability can be assessed. With respect to the experiments performed in this thesis, native MS was particularly useful as it enables the analysis of heterogeneous protein mixtures containing several populations of protein complexes of varying intensities. Furthermore, native MS allows real-time monitoring of dynamic processes such as the assembly or disassembly of the complexes, which is not possible when using the classical structural biology techniques such as Cryo-EM or X-ray crystallography.

To perform native MS, two pre-requisites have to be fulfilled: (i) A specific instrument modified for transmission of high masses is required, and (ii) the purification buffer of the protein needs to be replaced by a volatile solution [132]. Importantly, the decreasing pH in the ESI droplet, applied heat during evaporation and the loss of the hydration shell as well as changing the buffer and transferring the proteins from solution into the gas phase might affect the stability of the proteins [194–196]. The gas phase and solution structures might, therefore, not be comparable. While the overall structure of globular proteins was shown to remain in the gas phase [197,198], in some cases unfolding and refolding was observed [199,200]. For disordered proteins, structural rearrangements such as collapsed structures and kinetically trapped gas phase conformations were described [201]. The loss of the hydration shell was further hypothesised to enhance intramolecular electrostatic interactions, thereby, increasing the number of conformations during transfer from solution into the gas phase [202]. In a combined model of the CRM and CEM, partially folded local regions were described to be trapped in the droplet while flexible regions are ejected due to charge equilibration. Consequently, the probability that structured motifs are formed is higher during solvent evaporation and, as a result, the number of trapped structures increases, leading to different solution conformations entering a kinetically trapped gas phase state [203]. The charge state distribution of proteins, therefore, already provides information on their folding state. Folded proteins are represented by a Gaussian-shaped charge state series, whereas proteins lacking

a structure result in overlapping or tailed charge state distributions shifted to higher m/z values [204].

Importantly, all complexes observed in this thesis show a normal distributed series of charge states and, therefore, likely represent folded structures. Surprisingly, in some cases, individual SNARE proteins that are disordered in solution show a normal distribution of charge states indicating that a collapsed gas phase state or an ordered conformation formed. However, under optimised experimental conditions, maintaining solution-like structures is possible [205]. Note that the observed masses are, in some cases, slightly higher than the theoretical masses of individual proteins and their complexes, which is attributed to buffer and solvent adducts resulting from low activation energies during the analysis to prevent disruption of non-covalent interactions [206]. Nonetheless, even assuming differences between solution and gas phase structures, the sole goal of this study was the identification of sub-complexes or 'off-pathway' complexes during SNARE assembly. To answer this question, correct folding of the proteins in the gas phase is not required.

An additional aspect that needs to be considered is the protein concentration employed during the measurement. Due to solvent evaporation during ionisation, protein concentrations $\geq 50 \mu\text{M}$ increase the probability to trap more than one molecule in one ESI droplet, thereby, generating non-specific oligomers [178]. Considering this limitation, protein concentrations up $\leq 50 \mu\text{M}$ were used. The formation of non-specific aggregates during ESI can, therefore, be excluded. In addition, the proteins and their complexes were also analysed by using complementary biochemical techniques, such as SDS PAGE and Western Blotting of cross-linked complexes. Using these approaches, the assemblies observed by native MS were also identified in solution and are consequently not considered to be gas phase products. Nonetheless, the main advantage of native MS over other structural techniques is that it allows to unravel a heterogeneous mixture of complexes in the same measurement. As the complexes observed in the mass spectra are sufficiently resolved, complexes of different composition and even stoichiometry can be distinguished. Assuming a similar ionisation efficiency of the complexes of similar molecular weight and surface area, even a semi-quantitative comparison is possible.

In addition to soluble protein complexes, native MS is also well-suited to characterise membrane proteins and their lipid interactions. However, the analysis of membrane proteins is challenging as it requires solubilisation of the proteins and the lipids. For this, detergent micelles are commonly used, which is often accompanied by peak broadening and ion suppression, an effect resulting from the different ionisation efficiency of proteins, lipids and detergents [207,208]. To overcome these limitations, associated detergent molecules are removed from the protein by increasing the collisional energy resulting in release of the protein from the detergent micelle [179,209]. Although most of the collisional energy is likely absorbed

by the micelle [179], conformational changes of the protein and, as a consequence, the loss of protein-protein or protein-lipid interactions are often observed. On the other hand, this effect can be used to assess the stability of membrane proteins in the presence of various lipids and provide information about the lipid binding strength [210]. Dissociation of bound detergent molecules from membrane proteins was further described to preserve the native-like conformation of the protein in the gas phase [211].

Importantly, detergent micelles cannot only be used to stabilise integral membrane proteins [209,211,212], they further allow the transfer of lipids from detergent-lipid micelles to proteins providing information about lipid binding affinities [161,210]. Although the mechanisms of the lipid transfer is still elusive, it proved to be useful to analyse lipid interactions of membrane associated proteins and peptides [213,214]. Note that, only few detergents are suited for native MS analysis: non-ionic and zwitterionic detergents are recommended as these require less activation energy [163,164,215]. C8E4 is a non-ionic detergent, which was previously shown to stabilise soluble proteins, while enabling lipid transfer to membrane associated proteins [193]. This approach is well-suited to analyse protein-lipid interactions and was, therefore, also used in this thesis. While the obtained results were comparable to those obtained in solution when using liposome flotation assays, additional questions arose. Most importantly, the number of associated lipids observed in the mass spectra cannot be explained and needs to be addressed in future studies. Elucidating the mechanism of lipid transfer from mixed detergent-lipid micelles to the proteins will be a first step for interpretation of the observations.

Chemical cross-linking. This technique preserves protein-protein interactions by covalently linking pairs of functional groups in proximity. Depending on the used cross-linking reagent, different distance constrains are obtained, providing information about the three-dimensional orientation of the proteins. The identified constrains can then be implemented into structural modelling approaches. As the identification of interacting side chains is performed at the level of peptides, this technique is theoretically not limited in the protein size and can further be applied to dynamic proteins and heterogenous protein mixtures. As this thesis focusses on the formation of protein complexes and their regulation, chemical cross-linking is a well-suited approach to complement the data observed by native MS.

The analysis of proteins by chemical cross-linking depends on the primary structure of the involved proteins and the cross-linking conditions have to be optimised with respect to the used cross-linker reagent and its concentration as well as the enzymatic digestion. A wide variety of cross-linking reagents of different chemistry is available [216]. In this study, the homobifunctional cross-linker BS3 was used, which mainly interacts with primary amines of lysine residues and the protein's N-terminus as well as to a lower extent with hydroxyl groups of serine, threonine and tyrosine residues [107]. Lysine residues are solvent accessible and

equally distributed in most proteins including the SNARE proteins and Cpx1 and are, therefore, a suitable cross-linking target. As cross-linking traps protein structures, it can in principle lead to structural artefacts. These might arise from capturing a rare conformation inducing further cross-linking events, thus, impairing the effect and forming irrelevant conformations. On the other hand, if protein molecules are in proximity due to high protein concentrations, a protein-protein interaction that is not reflecting a functional interaction might be captured [217]. In order to prevent formation of artefacts, both the cross-linker and the protein concentration have to be optimised [217,218]. Taking this into account, the BS3 cross-linker was titrated to identify an appropriate concentration and low protein concentrations of 10 μ M were used for the cross-linking experiments. Nevertheless, disordered proteins are structurally diverse and, consequently, the identified cross-links likely represent an ensemble of conformations. While this is not problematic for the identification of protein interactions, as requested in this thesis, a quantitative comparison of different conformations should be avoided and was therefore not intended.

When lysine residues are targeted during the cross-linking reaction, enzymatic digestion using trypsin might result in a reduced hydrolysis efficiency as modified residues would not be recognised by the enzyme resulting in larger peptides [218]. Note that, in this thesis, a complete sequence coverage of the cross-linked proteins was observed and limitations due to limited hydrolysis can be excluded. However, the generally low abundance of cross-linked peptide pairs compared to linear peptides often requires the enrichment of the cross-links. Therefore, cross-linked peptides pairs were separated from linear peptides by SEC prior to the LC-MS/MS analysis and instrument parameters were optimised, e.g. by excluding doubly-charged ions from fragmentation to increase the identification rate.

When analysing homodimers, differentiation between inter- and intramolecular interactions is particularly difficult by cross-linking, due to identical sequences of the monomeric subunits. Intermolecular interactions will therefore only be identified if a cross-linked dipeptide contained overlapping or identical peptide sequences. As the SNARE proteins and Cpx1 do not contain repeating sequences, identical sequences must originate from two copies of the same protein. Different peptide sequences, on the other hand, were in this study considered to be intramolecular cross-links although these might also originate from different copies of the same protein. This problem could be circumvented by labelling the protein with heavy isotopes, e.g. ^{15}N , during protein expression and equally mixing it with unlabelled protein (^{14}N) directly before the cross-linking reaction [219,220]. However, this approach requires a specialised data analysis workflow and analysis software [221–223], and was, therefore, not followed in this thesis. Considering this limitation, an alternative approach using visualisation of the identified cross-links in monomeric and dimeric high-resolution structures as well as predicted structural models was used, thus, identifying cross-links violating spatial restraints and determining the

relative orientation of subunits within the protein assemblies [126]. The visualised cross-links are mapped at C α -C α distances to allow for varying side-chain conformations. Cross-links are visualised as satisfied to an upper distance limit of 30 Å, which includes the cross-linker spacer length, the maximum length of the appropriate side-chain rotamers and a small additional tolerance to account for molecular motions [127]. Note that, computational predictions using AlphaFold2 depend on existing high-resolution structures such as provided by the protein data bank [224]. Although AlphaFold 2 is capable of identifying and visualising disordered structures it is limited to reflect dynamic and multiple protein conformations [224]. Recently AlphaFold2 was shown to preferably predict disordered proteins with high confidence in their conditionally folded state, which they adopt, for instance, when binding to an interaction partner [225].

In Summary, native MS mainly provides information on the quaternary structure of protein arrangements, while chemical cross-linking MS provides details on the protein interactions that form. The strength of this thesis is, therefore, that the two techniques provide complementary information that is not achievable with the individual methods alone. As an example, the identification of protein interactions in the SNARE complex using cross-linking does not include information on the stoichiometry of the assembly and the oligomerisation of the complex, as observed in this thesis by native MS. *Vice versa*, the formation of antiparallel oligomers of the SNARE complex is not amenable by native MS and requires insights from chemical cross-linking. As indicated by this example, the combination of the two techniques is particularly powerful for the research question of this thesis. In many cases, sub-complexes of different stoichiometry were identified, which otherwise would have been undetected. Without this knowledge, false assumptions during the interpretation of cross-linking results are likely. Finally, considering limitations of other structural techniques, the two approaches have additional advantages: the demand for sample amounts is low, labelling of the proteins is not required and sample impurities can be excluded during the analysis.

4.2 Structural characterisation of individual synaptic proteins

The SNARE proteins spontaneously assemble into the SNARE complex [16]. The assembly, however, proceeds slowly, taking minutes to hours for completion, *in vitro* when employing the soluble domains of the proteins or when incorporating full-length proteins into liposomes [226,227]. The tendency of the SNARE proteins to reversibly form homo- and heterooligomeric complexes varying in their stoichiometry and composition might be an explanation for the decelerated assembly. In this thesis, SNARE proteins as well as the regulator Cpx1 were first structurally characterised in the absence of interaction partners to analyse their oligomerisation behaviour including specific interaction sites formed within the assemblies. Native MS and chemical cross-linking revealed an 'aggregation-like' oligomerisation; instead of a defined

stoichiometry, all proteins form oligomers with increasing number of units. This behaviour was previously described for different Syb2 variants [176] and was also observed in this thesis (**Figure 11**). Formation of higher oligomers was shown to originate from interactions of the cytosolic domain of Syb2, rather than its transmembrane domain as earlier suggested, and correlates with an increasing degree of disorder [176]. The observed interactions were, therefore, described to be unspecific. In this thesis, a similar oligomerisation behaviour was also observed for SNAP25(CtoS), Stx(1-262) and Cpx1 (**Figure 16, 19 and 22**); accordingly a high number of cross-links was identified (**Figure 13, 17 and 20**).

SNAP25(CtoS) is natively disordered. Mapping the identified cross-links into predicted monomers and dimers of SNAP25(CtoS) revealed parallel and antiparallel orientations in the oligomeric arrangement (**Figure 15**). In the presynaptic membrane, SNAP25 is organised in clusters surrounding clusters of Stx1, presumably serving as a reserve pool to fast isolate monomers for formation of the 'acceptor' complex [228,229]. From that point of view, formation of parallel oligomers might be of physiological relevance, while antiparallel orientations might result from the lack of the membrane anchor. Whether SNAP25(CtoS) adopts a fully helical structure or only forms partially helical structures is unclear. SNARE motifs have been described to be extremely versatile in their conformations, and structural changes between random coils and helical conformations, in which parts of the domains are alpha-helical while other parts remain unstructured, were described [15,183]. Note that proper integration of flexible and disordered protein regions cannot be reflected by the predicted structures as discussed above. In addition, AlphaFold2 predictions of SNAP25 represent its conditionally folded state, as part of the SNARE complex, explaining the four-helical parallel dimer of SNAP25 [225]. Nevertheless, AlphaFold 2 predictions enable the visualisation of cross-links and, thereby, positively validate intermolecular cross-links in the SNAP25(CtoS) dimer, indicating that SNAP25(CtoS) adopts a similar structure as in the SNARE complex (**Figure 15**). Cross-links formed towards the flexible linker exceeded the distance threshold, which is attributed to the disorder of the linker and the fact that only one possible conformation is visualised (**Figure 15**). Addition of a second copy of SNAP25(CtoS) into the arrangement, indeed allowed validation of some cross-links to be intermolecular cross-links that formed with a second SNAP25(CtoS) copy. As a result, most cross-links were positively validated. SNAP25 was shown to be primarily disordered in solution containing some backbone order towards the N-terminus [15,25,44,230], which was also confirmed by CD spectroscopy (**Figure 16**). Fully helical arrangements could not be confirmed. However, it was shown, that the helicity of SNAP25 increases upon increasing amounts of NaCl and SNAP25 even forms oligomers at high concentrations [15]. The Qb SNARE motif of SNAP25(CtoS) was previously described to form parallel oriented dimers without interaction partners [230] and both SNAP25-SNARE motifs were found to preferentially align in parallel [183]. All of these findings are in agreement

with the intra- and intermolecular cross-links observed in this thesis. In addition, SNAP25 interactions are responsible for antiparallel dimerisation of SNARE complexes [231], which was also observed here (**Figure 36**) and agrees with the cross-links in antiparallel orientation (**Figure 15**). Consequently, oligomerisation of SNAP25(CtoS) is likely driven by transient interactions through complementary SNARE motifs, attempting to stabilise their structure. Identified cross-links, therefore, likely reflect an ensemble of different partially folded SNAP25(CtoS) molecules that dynamically assemble in parallel and antiparallel orientation without forming fully helical structures.

Stx1 is also highly dynamic in the absence of regulatory proteins, such as Munc18. It adopts an 'open' or 'closed' conformation, which influence the ability to bind to other SNARE proteins [10–12]. In the 'open' conformation, Stx1-SNARE motif Qa does not interact with the Habc domain and is consequently available for interactions with other SNARE motifs. In addition, Stx1 forms well-structured dimeric and tetrameric Qa bundles in solution [22,23], trimers when incorporated into liposomes [231] and higher ordered clusters in native membranes [24,228]. Identified intermolecular cross-links, mapped onto a dimer of Stx(1-262), agree well with Stx(1-262) adopting an 'open' conformation with both Stx(1-262) copies oriented in parallel (**Figure 18**). As Stx(1-262) is not restricted by a transmembrane anchor allowing rotational freedom of the protein, parallel and antiparallel orientations are conceivable. However, the identified cross-links do not support an antiparallel orientation, as described for a Stx1 tetramer formed by antiparallel oriented dimers [23,230]. Antiparallel orientations could, therefore, not be confirmed in this thesis. In the 'closed' conformation, the Qa SNARE motif is partially intercalated into the Habc domain agreeing well with identified cross-links formed between the N-terminal part of Qa SNARE motif and the Habc domain (**Figure 18**). This intercalation, however, requires the SNARE motif to be highly flexible and CD spectroscopy previously revealed a concentration dependent increase in helicity of the Qa SNARE motif probably resulting from its self-assembly [25]. A previous electron paramagnetic resonance (EPR) study further described an equilibrium of Qa between an ordered and a disordered conformation that is only rearranged upon binding of Munc18 [232]. Considering the protein concentrations used in the cross-linking experiment and the absence of regulatory proteins such as Munc18, the Qa SNARE motif is disordered. Consequently, the cross-links observed in this study reflect both 'open' and 'closed' conformations of Stx(1-262), which are likely present in a dynamic equilibrium as suggested earlier [12,232].

Cpx1 is a highly disordered protein in solution and was to-date mainly structurally characterised in the presence of the SNARE complex [60,61]. Oligomerisation of Cpx1 in the absence of interaction partners as revealed in this thesis was so far not described (**Figure 22**). Low-abundant dimers of Cpx1 were only observed in a cross-linking study, when Cpx1 was bound to the SNARE complex [78]. Considering the available binding site of Cpx1 provided by the

SNARE complex, oligomerisation might not be physiologically required for its regulatory function in the final steps of the SNARE assembly. Consequently, the oligomerisation might result from the high degree of disorder of Cpx1 and the attempt to stabilise the structure as previously discussed for the SNAREs. This is supported by the cross-linking analysis; most of the intramolecular interactions are represented by overlength cross-links correlating with the high flexibility of the NTD and CTD of Cpx1 in the absence of interaction partners (**Figure 21**). The cross-links, therefore, represent an ensemble of conformations reflecting the conformational diversity of Cpx1. On the other hand, Cpx1 was shown to phase separate driven by its NTD [233] and to be recruited and enriched by synaptic vesicle associated proteins, such as α -Synuclein, Syt1 and Synapsin 1 [234–236]. Based on these observations, it is conceivable that the observed oligomerisation represents a nucleation site for higher ordered assemblies. Increasing the local concentration might facilitate formation of transient interactions, thereby, influencing adjacent binding events [237].

4.3 Analysis of the SNARE complex assembly

For the SNARE complex assembly two pathways are commonly proposed: (i) SNAP25 and Stx1 form an ‘acceptor’ complex providing a binding site for Syb2 and (ii) Stx1 and Syb2 are chaperoned by Munc18 forming a ‘template’ complex for association of SNAP25. To identify intermediate and ‘off-pathway’ complexes in the SNARE complex assembly and to obtain mechanistic insights into this process, SNARE proteins were mixed and complex formation was monitored.

Formation of binary and ternary complexes mimicking the stoichiometry of the SNARE complex. In the presence of an interaction partner, SNARE proteins preferably interact with each other forming sub-complexes rather than oligomers indicating a higher affinity for complementary SNARE motifs. While individual SNAREs are unable to form tetrameric structures similar to the four-helical SNARE complex, the binary complexes observed in this thesis adopt a defined stoichiometry. The first complex that was analysed was the sub-complex formed between SNAP25(CtoS) and Stx(1-262). Considering that both proteins are located at the presynaptic membrane, formation of the 1:1 ‘acceptor’ complex as a starting point of the assembly appears logical. However, in the absence of the R-SNARE Syb2, the position of the fourth SNARE motif is occupied by an available Q-SNARE leading to formation of a 4Q:0R stoichiometry, namely the 1:2 SNAP25(CtoS):Stx(1-262) complex (Qaabc, **Figure 23A and B**). This observation is in agreement with previous studies, which also identified formation of this so-called ‘dead end’ complex in the absence of Syb2 [16,25,26]. Most studies addressing SNARE complex assembly make different attempts to circumvent formation of this complex; for instance, by using an excess of SNAP25 to bind all available Stx1 molecules

[169,238]. It is assumed that formation of the 1:1 'acceptor' complex is favoured under these conditions. In this thesis, when varying the incubation ratios, the stoichiometry of the 'dead end' complex could not be challenged, suggesting that the proteins adopt a preferred stoichiometry. The sequence of SNARE complex assembly is still elusive and although it is commonly accepted that it proceeds through the intermediate 'acceptor' complex [169,181], an alternative pathway was suggested [230]. In this pathway, the 'dead end' complex was proposed to be an essential intermediate for SNARE complex formation in the absence of regulatory proteins. Using kinetic measurements and EPR spectroscopy, the authors showed that binding to SNAP25 requires dimerisation of Stx1 as an initial step. They further claimed that there is no evidence for formation of an 1:1 intermediate complex [230]. However, in this thesis, dimers of Stx(1-262) were not detected after addition of SNAP25(CtoS) and formation of the 1:1 'acceptor' complex (Qabc) was observed at low abundance (**Figure 23A and B**). Consequently, the data presented here are more in line with formation of the 'dead end' complex by binding of a second Stx(1-262) molecule to the 'acceptor' complex. A previous fluorescent anisotropy study revealed a significantly reduced binding rate of Syb2 to the 'acceptor' complex in the presence of an excess of SNAP25 [239]. The authors reasoned that the inhibition of the complex formation by SNAP25 results from formation of a 1:2 Stx1:SNAP25 complex [239]. Interestingly, a complex composed of two SNAP25(CtoS) and one Stx(1-262) molecules was also observed in this thesis (**Figure 23A**). Following the 4Q:0R composition of the 'zero layer' (see above), one of the SNARE motifs of SNAP25(CtoS) would be located exterior of the core bundle (Qabbc*). The individual Qb SNARE motif of SNAP25 was previously described to associate with Stx1 alone forming a complex of 2:2 stoichiometry (Qaabb) [240]. In combination with Syb2 stable complex formation was only observed, when the binding site of the Qc SNARE motif was occupied by an additional Qb motif (QabbR) or Stx1 molecule (QaabR) [230]. Interactions between Stx1 and the Qc SNARE motif, on the other hand, were shown to be weak resulting in formation of an unstable complex (QaacR) [230]. These observations support the suggestion that the Qb motif of SNAP25(CtoS) binds to the 'acceptor' complex, while the Qc motif of the second SNAP25(CtoS) molecule remains exterior of the SNARE helical bundle. However, future studies addressing complex formation using the individual Qb and Qc SNARE motifs of SNAP25 are required to answer this question.

When R- and Q SNAREs are available, the 3Q:1R stoichiometry resembling the four-helical structure of the SNARE complex is imitated. Incubating SNAP25(CtoS) and Syb(1-96), a complex with a stoichiometry of 2:1 was observed (**Figure 25**); in this complex an additional SNAP25(CtoS) molecule is integrated (Qbbcc*R), similar to the 2:1 SNAP25(CtoS):Stx(1-262) complex. Again, the stoichiometry of this complex could not be challenged by varying protein mixing ratios indicating a stable conformation. To address the assumption that the Qb SNARE

motif of the second SNAP25(CtoS) copy is incorporated in the arrangement, complex formation was followed using SNAP25(1-83). The Qb motif of SNAP25(CtoS) is readily associating to the binding site of Stx(1-262) forming a complex in which SNAP25(CtoS), Syb(1-96) and SNAP25(1-83) each contribute one molecule (QbbcR, **Figure 28C**). Consequently, the Qb motif of SNAP25(CtoS) is indeed integrating into the complex as suggested earlier validating the 3Q:1R stoichiometry. Importantly, although full-length SNAP25(CtoS) is present, the complex involving SNAP25(1-83) is exclusively formed. Binding of the individual Qb motif appears to be favoured, presumably due to less sterical hindrance caused by the additional Qc motif of full-length SNAP25(CtoS). The observed SNAP25(CtoS) dimer (**Figure 25A to C**) and 1:1 SNAP25(CtoS):SNAP25(1-83) complex (**Figure 28C**), both composed of at least three SNARE motifs, indicate that for association of Syb(1-96) a complex providing a binding site similar to the 'acceptor' complex is required. It is conceivable that the 1:2 Syb(1-96):SNAP25(CtoS) complex formed due to association of a second SNAP25(CtoS) to the 1:1 Syb(1-96):SNAP25(CtoS) complex (QbcR). In PC12 cells this 1:1 complex was previously proposed, providing a high affinity binding site for Stx1 [182]; this complex was, however, not observed in this thesis. The absence of this complex is further supporting the assumption that three SNARE motifs are required for subsequent binding of Syb2. Note that stable complex formation is only observed if Qb and Qc SNARE motifs are available; Syb(1-96) is not forming complexes if the Qb SNARE motif is exclusively present (**Figure 28B**).

In the case of Stx(1-262) and Syb(1-96), complex formation was not observed (**Figure 29A**). However, upon addition of Cpx1 a complex composed of three Stx(1-262) molecules and one Syb(1-96) molecule was stabilised (QaaaR, **Figure 29B**). This complex resembles a complex with 3Q:1R stoichiometry. The observation that the presence of both SNAREs decreased their tendency to self-assemble, led to the suggestions that transient interactions were formed. Interactions between both proteins were previously described to be weak [241,242]. An early NMR spectroscopy study analysed the interactions between Syb2 and Stx1 employing either the complete cytosolic domain of Stx1 or the isolated Qa SNARE motif [243]. The authors showed that the R-SNARE motif of Syb2 entirely interacts with the isolated Qa-SNARE motif, whereas only few residues bind to the cytosolic domain containing the Habc domain [243]. Based on these results, stable complex formation without Cpx1 was presumably not observed, because of competing interactions of the Qa SNARE motif with the Habc domain and the R SNARE motif of Syb2. In the presence of Cpx1, the equilibrium of both Stx1 conformations is likely shifted towards the 'open' state, thereby, facilitating complex formation by ensuring accessibility of the Qa SNARE motif.

Interestingly, all observed complexes contain only one R SNARE suggesting that two arginine residues in the central layer prevent complex formation. A previous study performing a mutational analysis of the central 'zero' layer examined the role of the glutamine and arginine

residues [244]. Based on this study, two arginine residues in the central layer led to electrostatic and sterical hindrance and, therefore, prevent complex formation. Four glutamine residues, on the other hand, allow complex formation and membrane fusion, although the formed complexes are less stable compared to the SNARE complex [244]. These observations are in agreement with the 4Q:0R and 3Q:1R stoichiometry observed in this thesis.

Although several studies showed that the SNARE assembly occurs zipper-like from the N- to the C-terminus, the mechanism guiding the SNARE motifs during the assembly is still elusive. The Q SNARE motifs are exchangeable and easily occupy available binding sites in parallel and antiparallel orientation [22,27,245]. Complex formation might, therefore, not result from specific interacting residues but originate from the overall structure of the SNAREs. This assumption is supported by stable non-cognate complexes obtained when using other members of the SNARE protein family [246,247]. The recurring hydrophobic residues of the SNARE motifs might guide complex formation as these are less prone to be solvent accessible and tend to form the hydrophobic layers of the four-helix bundle. However, these assumptions do not explain why the individual SNARE proteins do not form stable tetramers and preferably assemble into complexes that are all in agreement with the 4Q:0R and 3Q:1R stoichiometry (Qaabc, Qabbcc*, Qbbcc*R, QbbcR, QaaaR). Results obtained in this thesis suggest that the affinity of a SNARE motif for a complementary motif is higher than for the same SNARE motif. In addition, stable complex formation requires at least three complementary SNARE motifs or a regulatory protein for stabilisation. It further appears that the amount of available interaction partners does not define formation of the complexes, but rather specific interaction partners are responsible for stability of the complexes. These properties are likely encoded in the sequence of the different SNARE motifs.

Rearrangements of binary complexes and formation of the SNARE complex. Addressing the question if the observed binary complexes represent trapped 'off-pathway' complexes, their rearrangements after addition of the third SNARE protein were analysed. As soon as the protein was added to the pre-assembled binary complexes, rearrangements of the complexes into the ternary SNARE complex (QabcR) were observed (**Figure 23D, 25D and 29D**). Therefore, the ternary SNARE complex represents the preferred and most stable conformation. From a physiological point of view, this is reasonable as fusion of synaptic vesicles with the presynaptic membrane is only achieved when Syb2 associates with Stx1 and SNAP25. The rearrangements of the complexes were, however, found to proceed at different time scales; while the 'dead end' complex immediately reorganised, binary complexes composed of SNAP25(CtoS) and Syb(1-96) or Stx(1-262) and Syb(1-96) showed extended time scales.

The 'dead end' complex was previously described to be kinetically trapped [169]. While the previously described complex assembled from membrane-anchored variants, in this thesis, soluble variants of the SNARE proteins were employed. Consequently, the variants are not restricted by the membranes allowing disassembly and reassembly in parallel and antiparallel orientations. Although an excess of Stx(1-262) favouring formation of the 'dead end' complex was used, immediate and exclusive formation of the SNARE complex was observed. As a result, Stx(1-262) and Syb(1-96) do not compete for the binding site on the 'acceptor' complex. Binding of Syb(1-96) prevails, presumably due to its higher affinity for the 'acceptor' complex interface compared to Stx1; this observation is in agreement with a previous isothermal titration calorimetry study [248]. An equilibrium between the 'dead end' complex and the 'acceptor' complex, both identified in this thesis, might accelerate rearrangements into the SNARE complex. A similar assumption was made in a study addressing the organisation of the plasma membrane in PC12 cells [249]. Accordingly, Stx1 forms tight clusters that interact at their periphery with surrounding diffuse clusters of SNAP25. SNAP25 is recruited to the Stx1 clusters through alpha-helical interactions of its Qb SNARE motif forming complexes at the interfaces of the clusters [249]. The high abundance of SNAP25 prevents formation of the 'dead end' complex, thereby, supporting formation of the 'acceptor' complex [249]. Note that individual SNAP25(CtoS) was not observed when adding Syb(1-96) to the 'dead end' complex suggesting a rearrangement through dissociation of Stx(1-262) followed by association of Syb(1-96) rather than a complete disassembly of the 'dead end' complex.

On the contrary, complete incorporation of Stx(1-262) into the pre-assembled 2:1 SNAP25:Syb(1-96) complex required overnight incubation. As this complex contains two SNAP25(CtoS) molecules, of which one Qc SNARE motif is presumably unfolded and not involved in the core complex as discussed above, this unstructured loop might cause sterical hindrance. As the used soluble variants possess full rotational freedom, antiparallel arrangements of the SNARE motifs might also explain the decelerated reassembly. Antiparallel configurations were previously reported as low-energy states that do not interconvert at an hour time scale [27,28]. The mechanism of the rearrangement is, however, unclear. A stable 1:1 SNAP25(CtoS):Syb(1-96) complex was not observed, accordingly, dissociation of one SNAP25(CtoS) molecule followed by association of Stx(1-262) is not reflected in the obtained data. Complete disassembly of the binary complex and formation of the SNARE complex through the 'acceptor' complex by association of Syb(1-96) would, however, explain extended time scales.

Incorporation of SNAP25(CtoS) into the 1:3:1 Syb(1-96):Stx(1-262):Cpx1 complex also proceeds comparatively slow. Stable oligomer formation of Stx1 in parallel and antiparallel orientations, as described above, might hamper subunit exchange [23,25,250]. Considering that the disassembly of two Stx(1-262) molecules is required to enable binding of one

SNAP25(CtoS) molecule and the observation that Stx1 trimers are comparably stable [231], explains the slow replacement of the subunits. On the other hand, antiparallel binding of Cpx1 to Stx(1-262) and Syb(1-96), which was shown to stabilise the interaction, might lock the interface of both proteins within the complex. Consequently, structural rearrangements would be impeded. Assuming a similar conformation of Cpx1 within the 1:3:1 Syb(1-96):Stx(1-262):Cpx1 complex, as described in the SNARE:Cpx1 model provided in this thesis (**Figure 38**), the N-terminus of Cpx1 clamps the C-termini of the SNAREs, thereby, inhibiting dissociation of Stx(1-262). The rearrangement, therefore, likely occurs through dissociation of a Stx(1-262) dimer or sequential dissociation of monomers of Stx(1-262), while the Syb(1-96):Stx(1-262) interface is still preserved by Cpx1.

Stability of binary and ternary complexes. SNAP25(CtoS) and Syb(1-96) were found to weakly interact. Moderate collisional energies during MS analysis readily caused dissociation of the complexes resulting in 'stripped' complexes composed of two SNAP25(CtoS) or one SNAP25(CtoS) and one SNAP25(1-83) molecules (**Figure 25 and 28**). In comparison, the 'dead end' complex, the 'acceptor' complex, the SNARE complex and the 1:3:1 Syb(1-96):Stx(1-262):Cpx1 complex were found to be very stable; dissociation was only observed during tandem MS analysis (**Figure 24, 26, 28D, 29C and 34**). In general, Syb(1-96) was shown to readily dissociate from all binary and ternary complexes upon increasing collisional energy, suggesting least stable incorporation into the complexes. Considering the rapid rearrangement of the 'dead end' complex into the SNARE complex as well as formation of the 'acceptor' complex, which was previously characterised as being highly stable [183] and also observed during tandem MS analysis, SNAP25 and Stx1 likely form the platform for rapid assembly of Syb2. This is further supported by their co-localisation on the presynaptic membrane [228,249]. From a functional point of view, rapid formation of the SNARE complex is required for fast membrane fusion and binding to an available 'acceptor' complex is, therefore, kinetically preferred. Least stable incorporation of Syb2 into the SNARE complex might also facilitate its disassembly during recycling of the SNARE proteins by the NSF/ α -SNAP machinery after membrane fusion [251]. On the other hand, the proposed 'acceptor' complex might only be relevant in the minimal fusion machinery studied *in vitro* omitting regulatory proteins.

Consideration of the 'template' model. An alternative SNARE assembly pathway describes the alignment of Syb2 and Stx1 mediated by Munc18 to form a 'template' complex for recruitment of SNAP25 [36,37]. This hypothesised pathway does not include formation of an 'acceptor' complex composed of Stx1 and SNAP25. While Munc18 binds Stx1 with high affinity in solution, keeping it in its 'closed' conformation [29], interactions with Syb2 were described

to be weak [35,252]. However, a cryo-EM structure showed both, Syb2 and Stx1, bound to Munc18 [34]. Note that, to obtain the high-resolution structure as well as the optical tweezer experiments supporting the model, N-terminal cross-linking of Syb2 and Stx1 was required [34–36,252]. Accordingly, interactions between both proteins are presumably transient and require additional stabilisation. This assumption is supported in this thesis; complex formation between Syb(1-96) and Stx(1-262) was only observed upon addition of Cpx1. Although Munc18 was not included in these experiments, the observed complex reveals that interactions between Syb2 and Stx1 in the absence of SNAP25 are possible albeit require a third protein. Nevertheless, considering that cross-linking was required to obtain the high-resolution structure, information on the sequence of the assembly is not provided as restricting the proteins hinders potential interactions. It is further worth mentioning that Munc18 was described to have a lower affinity for Stx1 in native membranes containing SNAP25 [253], and that it is less abundant in neurons compared to the SNARE proteins [254]. Most of the SNAREs are, therefore, free and available to form ‘acceptor’ and ‘dead end’ complexes. The role of Munc18 needs to be determined in future studies, especially considering that previous studies provide evidence for Munc18 to promote formation and binding to the ‘acceptor’ complex [31,32,255].

Multimerisation of binary and ternary complexes. SNARE proteins mediate fusion of synaptic vesicles with the plasma membrane and, thereby, formation of the fusion pore. The mechanism to form the pore as well as its structure remains elusive. A variety of studies discuss the number of SNARE complexes contributing to this process. Some *in vitro* fusion experiments showed that, in principle, one SNARE complex is sufficient for membrane fusion [256,257]; representing the minimal fusion machinery. However, others proposed that up to ten SNARE complexes are required for membrane fusion [258,259], which is in line with *in vivo* studies finding the number to range between three and fifteen [260–262]. In this thesis, multimerisation of the SNARE complex up to tetramers was observed (**Figure 25 and 33**). Using native MS, the observed multimers showed high intensities indicating that multimerisation is prevalent in solution. The cross-linking analysis performed in this thesis further revealed SNARE complexes to interact through their C-termini, but not their N-termini, adopting an antiparallel orientation. Visualisation of the identified cross-linking sites using high-resolution structures and structural predictions further evaluated the binding site to be formed by SNAP25(CtoS). Interestingly, dimerisation was also observed for binary complexes containing SNAP25(CtoS); the stabilised complex composed of Stx(1-262) and Syb(1-96), however, did not dimerise (**Figure 25, 28 and 29**). This observation further supports previous findings that interactions between SNARE complexes occur through an interaction site provided by SNAP25(CtoS); binary complexes, therefore, likely resemble the structure of the

SNARE complex. Although several SNARE complexes were proposed to be involved in membrane fusion, they do not necessarily directly interact with each other. Note that soluble variants of the SNARE proteins were employed in this study, therefore, allowing rotational freedom of the complexes. As SNARE proteins are restricted in their orientation when anchored to membranes, formation of oligomers in antiparallel orientation is likely impeded. Tight contacts between the membranes and interactions with bulky, regulatory proteins such as Syt1 or Munc18, presumably impose steric hindrance. Accordingly, oligomerisation through the cytosolic domain of the SNARE complex might result from the approach performed in this study, rather than being physiologically relevant.

4.4 Interactions of Cpx1 with SNARE proteins.

It is well established that fusion of synaptic vesicles with the presynaptic membrane is regulated by Syt1 and Cpx1. However, a variety of contradictory models for the regulation was proposed and the underlying mechanisms are highly debated. High-resolution structures of Cpx1 co-crystallised with the SNARE complex revealed binding of Cpx1 to a groove formed by Syb2 and Stx1 within the SNARE complex [61,77]. Consequently, binding of Cpx1 after initialisation of the assembly was suggested; accordingly, Cpx1 is involved in regulation of the late steps of membrane fusion. In this thesis, binding of Cpx1 to the Syb2:Stx1 interface was confirmed and specific interaction sites with the SNARE complex were identified leading to a structural model that agrees well with the proposed 'clamping' model.

Cpx1 preferentially binds the surface provided by Syb2 and Stx1. To address the specificity of Cpx1 for the Syb2:Stx1 interface, binding to the individual proteins as well as complexes providing alternative interaction interfaces, such as SNAP25(CtoS):SNAP25(CtoS), Stx(1-262):Stx(1-262), SNAP25(CtoS):Stx(1-262) or SNAP25(CtoS):Syb(1-96), was investigated (**Figure 32**). In this thesis, Cpx1 exclusively formed complexes when both, Syb(1-96) and Stx(1-262), were present; binding to the individual proteins was not monitored (**Figure 31**). This observation supports the necessity for an interaction surface provided by Syb(1-96) and Stx(1-262) confirming its regulatory function in the late steps of membrane fusion after initialisation of the assembly. Complex formation between Syb(1-96) and Stx(1-262) in the absence of SNAP25(CtoS) was, interestingly, only observed upon addition of Cpx1 (see above). Consequently, Cpx1 not only binds to both proteins but furthermore stabilises their interactions. This observation is in agreement with a previous study that used magnetic tweezers, revealing an enhanced mechanical stability of the SNARE complex when Cpx1 is bound [84]. The authors suggested that the increased stability originates from a conformational change induced by the NTD of Cpx1, when clamping the SNARE complex in a so-called 'linker-open' conformation [84]. Stabilisation of the trans-

SNARE complex by Cpx1 was further suggested to support zippering by overcoming the repulsive force between both membranes [61]. Considering that Cpx1 bound to the 1:3 Syb(1-96):Stx(1-262) complex and the SNARE complex (**Figure 29 and 33**) led to the assumption that both complexes are similarly structured and the structure of the binary complex indeed resembles the SNARE complex.

Considerations of the inhibition models. A variety of inhibitory pathways was described for Cpx1. Several studies suggested that blocking the binding site of Syb2 by the AH of Cpx1 interferes with the further assembly of the SNARE complex, thereby, inhibiting membrane fusion. One study suggested that the AH of Cpx1 replaces parts of Syb2 in the SNARE complex [79]. Other studies proposed simultaneous binding of Cpx1 to a partially assembled SNARE complex via its CH and to a second SNARE complex through its AH, thereby, bridging two SNARE complexes resulting in a 'zigzag' array [74,77]. Bridging of the complexes was even proposed to form ring-like structures to support formation of the fusion pore [263]. Note that for these studies variants of Cpx1, e.g. mutated 'superclamp' variants including replacement of charged residues of the AH to hydrophobic residues, were used. In addition, C-terminally truncated Syb2 variants were applied to maintain the Stx1:SNAP25 binding site available for association of the AH [74,77]. For the experiments performed in this thesis, the wild-type Cpx1 was used and binding to the 'acceptor' complex providing the required binding site for Syb2 was not observed (**Figure 32**). This observation is supported by an earlier NMR study, which did not detect interactions between wildtype or 'superclamp' Cpx1 with C-terminally truncated SNARE complexes [80]. Furthermore, considering the hydrophobicity of the binding pocket formed by Stx(1-262) and SNAP25(CtoS), it is hard to imagine that the charged AH of Cpx1 inserts into the complex. Nevertheless, when a partially zippered SNARE complex would be available, binding might be observed. Previous studies, using binding-deficient Cpx1 variants that include point mutations or deletions of the CH, revealed a loss of function of Cpx1 [59,264]. Based on these studies, binding of Cpx1 to the SNARE complex through the CH is mandatory for its activity. As the 'acceptor' complex, observed in this thesis, is not providing the Syb2:Stx1 binding interface, association of Cpx1 through the CH is presumably not possible and the required orientation of the AH relative to a second SNARE complex might not be achieved. In addition, soluble variants of the proteins were used in this thesis and bridging of complexes in membrane environment, when complexes are in proximity, cannot be excluded. However, in contrast to the above hypothesised multimerisation of SNARE complexes, disassembly of SNARE complex multimers upon addition of Cpx1 was clearly observed in this thesis (**Figure 33**). Nevertheless, a low abundant dimer of the SNARE:Cpx1 complex was detected and tandem MS revealed dissociation of either Cpx1 or Syb2 resulting in 'stripped' complexes omitting the respective protein (**Figure 34**). Based on

this observation, Syb(1-96) and the AH of Cpx1 might compete for the binding site and the dimers could potentially represent bridged complexes.

Cpx1 clamps the SNARE complex. The structural model provided in this thesis (**Figure 38**) confirmed the antiparallel binding of Cpx1 to the SNARE complex as earlier observed by X-ray crystallography [61]. Furthermore, it provides information on the interactions of the AH and NTD of Cpx1, when bound to the SNARE complex. Accordingly, it was shown that the AH interacts with the C-termini of Syb(1-96), SNAP25(CtoS) and Stx(1-262). This observation is in agreement with a recent study revealing interactions formed within the SNARE:Cpx1 complex reconstituted into liposomes [78]. Photo-cross-linking captured the complex and showed that the AH of Cpx1 binds the membrane-proximal part of Syb2 and SNAP25. The authors suggested that the SNARE complex is captured in an inactive state, suppressing final zippering of the SNARE proteins by restraining Syb2 and SNAP25 [78]. A recent molecular dynamic simulation study also observed interactions of the AH with C-terminal residues of the SNARE motifs of Syb2 and SNAP25 [265]. The authors further showed that the AH of Cpx1 is oriented towards the vesicle membrane and distorts due to sterical hindrance if a continuous straight helix is formed. They suggested that an energy barrier might be established that deaccelerates SNARE zippering [265]. The model proposed in this thesis confirms interactions between the AH and NTD of Cpx1 with the C-terminal SNARE complex. Furthermore, it extends previous models by identifying specific interaction sites, including interactions involving the disordered NTD of Cpx1. The flexible loop of the NTD was further shown to interact with the C-terminal part of the Qb SNARE motif and the linker of SNAP25, thereby, overlaying the SNARE complex. The results observed here are, therefore, in line with the proposed 'clamping' model. Note that Cpx1 was added to the pre-incubated SNARE proteins. Due to missing regulatory proteins and restriction by membranes, it is likely that the proteins are fully zippered, possibly throughout the linker region. Although Cpx1 is proposed to bind partially zippered SNARE complexes to prevent progression of the zippering [59,64,72,79,266] and, thereby, the assembly of the linkers of Syb2 and Stx1 [78,84], binding and clamping of the fully assembled SNAREs was observed in this thesis.

In summary, Cpx1 exclusively binds to complexes providing the Syb2:Stx1 interface, thereby, stabilising these complexes. It further clamps the C-termini of the SNARE complex, which prevents formation of SNARE complex multimers and presumably inhibits proceeding of the SNARE zippering. In additional experiments, the SNARE assembly remains to be analysed in the presence of Cpx1 and membranes. By incorporating the SNARE proteins into membrane mimetics, the partially assembled trans-SNARE complex could be captured. This system

should further be extended by including additional regulatory proteins, such as Syt1, Munc18 and Munc13.

4.5 Structural characterisation of synaptic proteins in lipid environment

Syb2 and Cpx1, are part of the membrane fusion machinery and interactions with lipids are, therefore, suggested to influence the SNARE complex assembly and its regulation. To analyse lipid binding affinities of Syb(1-96) and Cpx1, a multidisciplinary approach was used. For this, binding of the proteins to immobilised lipids, solubilised lipids and to membranes was analysed.

Screening for lipid classes by binding to immobilised lipids. First, lipid overlay assays were performed to screen for binding of Syb(1-96) and Cpx1 to different lipid classes. Both proteins preferentially bound to negatively charged lipids (**Figure 39 and 42**). The observed binding to PA, PS, PI(4)P, PI(4,5)P₂ and PI(3,4,5)P₃ is in agreement with the cellular location of the lipids, as these are part of the synaptic vesicle or plasma membrane [267,268]. Note that binding to PE, PC and cholesterol, which are also part of the vesicular membrane [3], was not observed. Surprisingly, both proteins bound to CL, which is specific to the inner mitochondrial membrane [269] and, therefore, biologically not relevant for synaptic proteins. This observation indicates that the interactions of Syb(1-96) and Cpx1 with the lipids are mainly driven by electrostatic attraction to the negatively charged headgroups. On the contrary, PG is negatively charged, however, binding of Cpx1 and Syb(1-96) was not observed. Considering the chemistry of the lipids, binding was only monitored to lipids that contain easily accessible phosphate groups and, therefore, negative charges. In the case of PG, the negative charge might be shielded by the glycerol group. Surprisingly, although increasing phosphorylation of the inositol ring provides additional negative charges, Syb(1-96) and Cpx1 show less binding to multiple phosphorylated PI. Syb(1-96) contains one patch of positively charged amino acids in the JMD. As the rest of the SNARE is mainly negatively charged, an increasing number of phosphate groups might result in electrostatic repulsion. Cpx1 was previously described to have a high affinity for PI(4,5)P₂ [189], which could not be confirmed in this thesis. However, as it is unclear how the lipids are immobilised and oriented on the membrane lipid strips, it is conceivable that the lipids are not properly accessible for the proteins during the assay.

Interactions with solubilised lipids. Using native MS, the binding affinities of Syb(1-96) and Cpx1 for DOPS, DOPE, DOPC as well as DOPG were assessed (**Figure 40 and 43**). For both proteins, binding to all lipids employed in this thesis was observed. Although the lipid overlay assays revealed a preference for negatively charged lipids, interactions including the zwitterionic lipids DOPE and DOPC were also observed. Protein-lipid interactions formed in solution were shown to be stabilised in the gas phase [214]. As hydrophobic interactions

cannot be preserved during the transfer into the gas phase, observed protein-lipid complexes are mainly attributed to electrostatic interactions formed towards the headgroups of the lipids [214]. Consequently, binding of DOPE and DOPC might occur through negatively charged residues, such as the SNARE motif of Syb(1-96). However, Syb(1-96) showed slightly higher affinity for DOPS and DOPG, which agrees with the previous observed preference for negatively charged lipids (**Figure 40**). Surprisingly, this specificity cannot be confirmed for Cpx1. Instead, the binding affinity of Cpx1 for the negatively charged DOPG and zwitterionic DOPE was higher than for the zwitterionic DOPC or the negatively charged DOPS (**Figure 43**). A previous study addressed binding of Cpx1 to membranes of varying composition and revealed the highest affinity for negatively charged membranes containing high amounts of PI(4,5)P₂ [189]. When comparing cholesterol:POPC membranes that additionally contain POPE or POPS, the authors observed a higher affinity for membranes containing POPE [189]. This is in line with a high affinity observed for the negatively charged DOPG followed by DOPE and DOPC in this thesis. The lowest affinity for DOPS might be attributed to the chemistry of the lipid. The serine group of DOPS might sterically hinder binding of Cpx1 to the phosphate group. Interestingly, the lipid binding capacity of Cpx1 of up to eight lipids is comparably higher than that for Syb(1-96) as well as for previous performed lipid binding studies [213,214]. This observation might result from the charged patches and the available amphipathic motifs of Cpx1. However, it needs to be considered that the measurements for Cpx1 were performed only once and replicates are required for comprehensive results. Furthermore, the mechanism of the lipid transfer is unknown and the influence of the available contact sites as well as the properties of the proteins, therefore, require further investigations.

Interactions with membranes. Finally, interactions of Syb(1-96) and Cpx1 with phospholipid bilayers were investigated. Binding of Syb(1-96) to DOPS and DOPG liposomes was observed and correlates well with the results from previous experiments (**Figure 41**). This observation agrees with former studies suggesting that PS plays an essential role in the interactions of Syb(1-96) with the vesicular membrane [47,48]. Binding to DOPG, which is not a component of the membrane of synaptic vesicles, leads to the assumption that the observed interactions in general rely on electrostatic attraction rather than lipid specificity. These interactions presumably originate from the negatively charged headgroups of the lipids and the positively charged JMD of Syb(1-96) as mentioned before [48–51].

For Cpx1, contradictory results compared to the previous experiments were obtained. Native MS revealed a low binding affinity for DOPS and a high affinity for DOPC. On the contrary, Cpx1 clearly interacts with negatively charged DOPS liposomes, while binding to zwitterionic DOPC was observed at lower affinity (**Figure 44**). The affinities observed by native MS are, therefore, not reflecting solution interactions and the results should be cautiously interpreted.

However, binding of Cpx1 to DOPG liposomes is in line with the high binding affinity observed by native MS. As Cpx1 contains amphipathic helices, the interactions with membranes are not restricted to electrostatic attraction and are, therefore, less specific as the helices are capable of intercalating into the membrane. Surprisingly, binding to DOPE liposomes was not observed, although the binding affinity observed by native MS was even higher compared to DOPS. This observation is likely attributed to the experimental approach; liposomes solely composed of DOPE are difficult to form due to their low solubility and instability in aqueous solution. Consequently, the applied amount of lipid in the experiment might differ from the theoretically calculated lipid concentration. Interestingly, immediately upon addition of Cpx1 to DOPS and DOPG, a turbidity of the solution was observed and formation of aggregates was confirmed by DLS analysis (**Figure 44**). As Cpx1 contains amphipathic motifs on both termini, this effect might result from Cpx1 bridging liposomes, thereby, forming a pool of vesicles. Although the membrane affinity of Cpx1 was shown to mainly arise from its CTD, a higher amount of negative charges of the membrane can also mediate binding of the NTD [189]. Consequently, as DOPS and DOPG liposomes are highly negatively charged, clustering of vesicles by Cpx1 is conceivable. On the other hand, the C-terminal 21 residues of Cpx1 were described to have the same pore-forming probability as the antimicrobial peptide melittin [270]. Using a pore-formation assay and cryo-EM, the authors revealed remodelling and perforation of giant unilamellar vesicles by the CTD of Cpx1 [270]. The increased heterogeneity of liposomes observed in this thesis could, therefore, also originate from membrane remodelling and pore formation.

In summary, for both proteins a preference for negatively charged lipids with easily-accessible phosphate groups was observed. Comparative lipid binding studies using lipid mixtures resembling the vesicular and plasma membrane including phosphatidyl inositol phosphates remain to be performed in future studies.

5 References

- [1] J. Hesselbarth, C. Schmidt, Disorder-to-order transition of Synaptobrevin-2: Tracing the conformational diversity of a synaptic SNARE protein, *Journal of structural biology* 214 (2022) 107824.
- [2] T.C. Südhof, The molecular machinery of neurotransmitter release (Nobel lecture), *Angewandte Chemie (International ed. in English)* 53 (2014) 12696–12717.
- [3] S. Takamori, M. Holt, K. Stenius, E.A. Lemke, M. Grønborg, D. Riedel, H. Urlaub, S. Schenck, B. Brügger, P. Ringler, S.A. Müller, B. Rammner, F. Gräter, J.S. Hub, B.L. de Groot, G. Mieskes, Y. Moriyama, J. Klingauf, H. Grubmüller, J. Heuser, F. Wieland, R. Jahn, Molecular anatomy of a trafficking organelle, *Cell* 127 (2006) 831–846.
- [4] W.A. Catterall, A.P. Few, Calcium channel regulation and presynaptic plasticity, *Neuron* 59 (2008) 882–901.
- [5] T. Söllner, M.K. Bennett, S.W. Whiteheart, R.H. Scheller, J.E. Rothman, A protein assembly-disassembly pathway in vitro that may correspond to sequential steps of synaptic vesicle docking, activation, and fusion, *Cell* 75 (1993) 409–418.
- [6] J.J.E. Chua, S. Kindler, J. Boyken, R. Jahn, The architecture of an excitatory synapse, *Journal of cell science* 123 (2010) 819–823.
- [7] R. Jahn, R.H. Scheller, SNAREs—engines for membrane fusion, *Nature reviews. Molecular cell biology* 7 (2006) 631–643.
- [8] T. Söllner, S.W. Whiteheart, M. Brunner, H. Erdjument-Bromage, S. Geromanos, P. Tempst, J.E. Rothman, SNAP receptors implicated in vesicle targeting and fusion, *Nature* 362 (1993) 318–324.
- [9] I. Fernandez, J. Ubach, I. Dulubova, X. Zhang, T.C. Südhof, J. Rizo, Three-dimensional structure of an evolutionarily conserved N-terminal domain of syntaxin 1A, *Cell* 94 (1998) 841–849.
- [10] I. Dulubova, S. Sugita, S. Hill, M. Hosaka, I. Fernandez, T.C. Südhof, J. Rizo, A conformational switch in syntaxin during exocytosis: role of munc18, *The EMBO journal* 18 (1999) 4372–4382.
- [11] S.H. Gerber, J.-C. Rah, S.-W. Min, X. Liu, H. de Wit, I. Dulubova, A.C. Meyer, J. Rizo, M. Arancillo, R.E. Hammer, M. Verhage, C. Rosenmund, T.C. Südhof, Conformational switch of syntaxin-1 controls synaptic vesicle fusion, *Science (New York, N.Y.)* 321 (2008) 1507–1510.
- [12] M. Margittai, J. Widengren, E. Schweinberger, G.F. Schröder, S. Felekyan, E. Haustein, M. König, D. Fasshauer, H. Grubmüller, R. Jahn, C.A.M. Seidel, Single-molecule fluorescence resonance energy transfer reveals a dynamic equilibrium between closed and open conformations of syntaxin 1, *Proceedings of the National Academy of Sciences of the United States of America* 100 (2003) 15516–15521.
- [13] Y. Gao, S. Zorman, G. Gundersen, Z. Xi, L. Ma, G. Sirinakis, J.E. Rothman, Y. Zhang, Single reconstituted neuronal SNARE complexes zipper in three distinct stages, *Science (New York, N.Y.)* 337 (2012) 1340–1343.
- [14] D. Min, K. Kim, C. Hyeon, Y.H. Cho, Y.K. Shin, T.Y. Yoon, Mechanical unzipping and re-zipping of a single SNARE complex reveals hysteresis as a force-generating mechanism, *Nat Commun* 4 (2013) 1705.
- [15] D. Fasshauer, D. Bruns, B. Shen, R. Jahn, A.T. Brünger, A structural change occurs upon binding of syntaxin to SNAP-25, *Journal of Biological Chemistry* 272 (1997) 4582–4590.

- [16] D. Fasshauer, H. Otto, W.K. Eliason, R. Jahn, A.T. Brünger, Structural changes are associated with soluble N-ethylmaleimide-sensitive fusion protein attachment protein receptor complex formation, *The Journal of biological chemistry* 272 (1997) 28036–28041.
- [17] R.B. Sutton, D. Fasshauer, R. Jahn, A.T. Brunger, Crystal structure of a SNARE complex involved in synaptic exocytosis at 2.4 Å resolution, *Nature* 395 (1998) 347–353.
- [18] A. Stein, G. Weber, M.C. Wahl, R. Jahn, HELICAL EXTENSION OF THE NEURONAL SNARE COMPLEX INTO THE MEMBRANE, spacegroup C 1 2 1, 2009.
- [19] D. Fasshauer, R.B. Sutton, A.T. Brunger, R. Jahn, Conserved structural features of the synaptic fusion complex: SNARE proteins reclassified as Q- and R-SNAREs, *Proceedings of the National Academy of Sciences of the United States of America* 95 (1998) 15781–15786.
- [20] C. Ma, W. Li, Y. Xu, J. Rizo, Munc13 mediates the transition from the closed syntaxin-Munc18 complex to the SNARE complex, *Nature structural & molecular biology* 18 (2011) 542–549.
- [21] X. Yang, S. Wang, Y. Sheng, M. Zhang, W. Zou, L. Wu, L. Kang, J. Rizo, R. Zhang, T. Xu, C. Ma, Syntaxin opening by the MUN domain underlies the function of Munc13 in synaptic-vesicle priming, *Nature structural & molecular biology* 22 (2015) 547–554.
- [22] J.C. Lerman, J. Robblee, R. Fairman, F.M. Hughson, Structural analysis of the neuronal SNARE protein syntaxin-1A, *Biochemistry* 39 (2000) 8470–8479.
- [23] K.M. Misura, R.H. Scheller, W.I. Weis, Self-association of the H3 region of syntaxin 1A. Implications for intermediates in SNARE complex assembly, *The Journal of biological chemistry* 276 (2001) 13273–13282.
- [24] J.J. Sieber, K.I. Willig, C. Kutzner, C. Gerding-Reimers, B. Harke, G. Donnert, B. Rammner, C. Eggeling, S.W. Hell, H. Grubmüller, T. Lang, Anatomy and dynamics of a supramolecular membrane protein cluster, *Science (New York, N.Y.)* 317 (2007) 1072–1076.
- [25] M. Margittai, D. Fasshauer, S. Pabst, R. Jahn, R. Langen, Homo- and heterooligomeric SNARE complexes studied by site-directed spin labeling, *The Journal of biological chemistry* 276 (2001) 13169–13177.
- [26] W. Xiao, M.A. Poirier, M.K. Bennett, Y.K. Shin, The neuronal t-SNARE complex is a parallel four-helix bundle, *Nature structural biology* 8 (2001) 308–311.
- [27] K. Weninger, M.E. Bowen, S. Chu, A.T. Brunger, Single-molecule studies of SNARE complex assembly reveal parallel and antiparallel configurations, *Proceedings of the National Academy of Sciences of the United States of America* 100 (2003) 14800–14805.
- [28] W. Liu, R.F. Stout, V. Pappas, Ternary SNARE complexes in parallel versus antiparallel orientation: examination of their disassembly using single-molecule force spectroscopy, *Cell calcium* 52 (2012) 241–249.
- [29] P. Burkhardt, D.A. Hattendorf, W.I. Weis, D. Fasshauer, Munc18a controls SNARE assembly through its interaction with the syntaxin N-peptide, *The EMBO journal* 27 (2008) 923–933.
- [30] S. Wang, U.B. Choi, J. Gong, X. Yang, Y. Li, A.L. Wang, X. Yang, A.T. Brunger, C. Ma, Conformational change of syntaxin linker region induced by Munc13s initiates SNARE complex formation in synaptic exocytosis, *The EMBO journal* 36 (2017) 816–829.
- [31] D. Dawidowski, D.S. Cafiso, Munc18-1 and the Syntaxin-1 N Terminus Regulate Open-Closed States in a t-SNARE Complex, *Structure (London, England: 1993)* 24 (2016) 392–400.

- [32] S. Jakhanwal, C.-T. Lee, H. Urlaub, R. Jahn, An activated Q-SNARE/SM protein complex as a possible intermediate in SNARE assembly, *The EMBO journal* 36 (2017) 1788–1802.
- [33] T. André, J. Classen, P. Brenner, M.J. Betts, B. Dörr, S. Kreye, B. Zuidinga, M. Meijer, R.B. Russell, M. Verhage, T.H. Söllner, The Interaction of Munc18-1 Helix 11 and 12 with the Central Region of the VAMP2 SNARE Motif Is Essential for SNARE Templating and Synaptic Transmission, *eNeuro* 7 (2020).
- [34] K.P. Stepien, J. Xu, X. Zhang, X.-C. Bai, J. Rizo, SNARE assembly enlightened by cryo-EM structures of a synaptobrevin-Munc18-1-syntaxin-1 complex, *Science advances* 8 (2022) eabo5272.
- [35] Y. Xu, L. Su, J. Rizo, Binding of Munc18-1 to synaptobrevin and to the SNARE four-helix bundle, *Biochemistry* 49 (2010) 1568–1576.
- [36] J. Jiao, M. He, S.A. Port, R.W. Baker, Y. Xu, H. Qu, Y. Xiong, Y. Wang, H. Jin, T.J. Eisemann, F.M. Hughson, Y. Zhang, Munc18-1 catalyzes neuronal SNARE assembly by templating SNARE association, *eLife* 7 (2018).
- [37] Y. Zhang, F.M. Hughson, Chaperoning SNARE Folding and Assembly, *Annual review of biochemistry* 90 (2021) 581–603.
- [38] S. Wang, Y. Li, J. Gong, S. Ye, X. Yang, R. Zhang, C. Ma, Munc18 and Munc13 serve as a functional template to orchestrate neuronal SNARE complex assembly, *Nat Commun* 10 (2019) 69.
- [39] Y. Park, J.K. Ryu, Models of synaptotagmin-1 to trigger Ca²⁺-dependent vesicle fusion, *FEBS letters* 592 (2018).
- [40] H.T. McMahon, M. Missler, C. Li, T.C. Südhof, Complexins: cytosolic proteins that regulate SNAP receptor function, *Cell* 83 (1995).
- [41] R. Mohrmann, M. Dhara, D. Bruns, Complexins: small but capable, *Cellular and Molecular Life Sciences* 72 (2015) 4221–4235.
- [42] J.F. Ellena, B. Liang, M. Wiktor, A. Stein, D.S. Cafiso, R. Jahn, L.K. Tamm, Dynamic structure of lipid-bound synaptobrevin suggests a nucleation-propagation mechanism for trans-SNARE complex formation, *Proceedings of the National Academy of Sciences of the United States of America* 106 (2009) 20306–20311.
- [43] B. Liang, V. Kiessling, L.K. Tamm, Prefusion structure of syntaxin-1A suggests pathway for folding into neuronal trans-SNARE complex fusion intermediate, *Proceedings of the National Academy of Sciences of the United States of America* 110 (2013) 19384–19389.
- [44] T. Stief, L. Gremer, S. Pribicevic, D.F. Espinueva, K. Vormann, R. Biehl, R. Jahn, Á. Pérez-Lara, N.-A. Lakomek, Intrinsic Disorder of the Neuronal SNARE Protein SNAP25a in its Pre-fusion Conformation, *Journal of molecular biology* 435 (2023) 168069.
- [45] K.D. Brewer, W. Li, B.E. Horne, J. Rizo, Reluctance to membrane binding enables accessibility of the synaptobrevin SNARE motif for SNARE complex formation, *Proceedings of the National Academy of Sciences of the United States of America* 108 (2011) 12723–12728.
- [46] M. Bowen, A.T. Brunger, Conformation of the synaptobrevin transmembrane domain, *Proceedings of the National Academy of Sciences of the United States of America* 103 (2006) 8378–8383.
- [47] B. Liang, D. Dawidowski, J.F. Ellena, L.K. Tamm, D.S. Cafiso, The SNARE motif of synaptobrevin exhibits an aqueous-interfacial partitioning that is modulated by membrane curvature, *Biochemistry* 53 (2014) 1485–1494.

- [48] N.-A. Lakomek, H. Yavuz, R. Jahn, Á. Pérez-Lara, Structural dynamics and transient lipid binding of synaptobrevin-2 tune SNARE assembly and membrane fusion, *Proceedings of the National Academy of Sciences of the United States of America* 116 (2019) 8699–8708.
- [49] D.H. Murray, L.K. Tamm, Clustering of syntaxin-1A in model membranes is modulated by phosphatidylinositol 4,5-bisphosphate and cholesterol, *Biochemistry* 48 (2009) 4617–4625.
- [50] G. van den Bogaart, K. Meyenberg, H.J. Risselada, H. Amin, K.I. Willig, B.E. Hubrich, M. Dier, S.W. Hell, H. Grubmüller, U. Diederichsen, R. Jahn, Membrane protein sequestering by ionic protein–lipid interactions, *Nature* 479 (2011) 552–555.
- [51] D. Williams, J. Vicôgne, I. Zaitseva, S. McLaughlin, J.E. Pessin, Evidence that electrostatic interactions between vesicle-associated membrane protein 2 and acidic phospholipids may modulate the fusion of transport vesicles with the plasma membrane, *Molecular biology of the cell* 20 (2009) 4910–4919.
- [52] D.-H. Kweon, C.S. Kim, Y.-K. Shin, Regulation of neuronal SNARE assembly by the membrane, *Nat Struct Mol Biol* 10 (2003) 440–447.
- [53] D.-H. Kweon, C.S. Kim, Y.-K. Shin, Insertion of the Membrane-proximal Region of the Neuronal SNARE Coiled Coil into the Membrane, *Journal of Biological Chemistry* 278 (2003) 12367–12373.
- [54] J. Han, K. Pluhackova, D. Bruns, R.A. Böckmann, Synaptobrevin transmembrane domain determines the structure and dynamics of the SNARE motif and the linker region, *Biochimica et biophysica acta* 1858 (2016) 855–865.
- [55] S.S. Rathore, Y. Liu, H. Yu, C. Wan, M. Lee, Q. Yin, M.H.B. Stowell, J. Shen, Intracellular Vesicle Fusion Requires a Membrane-Destabilizing Peptide Located at the Juxtamembrane Region of the v-SNARE, *Cell reports* 29 (2019) 4583–4592.e3.
- [56] T. Trimbuch, C. Rosenmund, Should I stop or should I go? The role of complexin in neurotransmitter release, *Nat Rev Neurosci* 17 (2016) 118–125.
- [57] J. Rizo, Mechanism of neurotransmitter release coming into focus, *Protein science: a publication of the Protein Society* 27 (2018) 1364–1391.
- [58] M. Xue, Y.Q. Lin, H. Pan, K. Reim, H. Deng, H.J. Bellen, C. Rosenmund, Tilting the balance between facilitatory and inhibitory functions of mammalian and *Drosophila* Complexins orchestrates synaptic vesicle exocytosis, *Neuron* 64 (2009) 367–380.
- [59] M. Xue, K. Reim, X. Chen, H.-T. Chao, H. Deng, J. Rizo, N. Brose, C. Rosenmund, Distinct domains of complexin I differentially regulate neurotransmitter release, *Nat Struct Mol Biol* 14 (2007) 949–958.
- [60] S. Pabst, J.W. Hazzard, W. Antonin, T.C. Südhof, R. Jahn, J. Rizo, D. Fasshauer, Selective interaction of complexin with the neuronal SNARE complex. Determination of the binding regions, *The Journal of biological chemistry* 275 (2000).
- [61] X. Chen, D.R. Tomchick, E. Kovrigin, D. Araç, M. Machius, T.C. Südhof, J. Rizo, Three-dimensional structure of the complexin/SNARE complex, *Neuron* 33 (2002) 397–409.
- [62] Y. Lai, J. Diao, D.J. Cipriano, Y. Zhang, R.A. Pfuetzner, M.S. Padolina, A.T. Brunger, Complexin inhibits spontaneous release and synchronizes Ca²⁺-triggered synaptic vesicle fusion by distinct mechanisms, *eLife Sciences Publications, Ltd* (2014).
- [63] E.A. Prinslow, K.P. Stepien, Y.-Z. Pan, J. Xu, J. Rizo, Multiple factors maintain assembled trans-SNARE complexes in the presence of NSF and α SNAP, *eLife* 8 (2019).

- [64] A. Maximov, J. Tang, X. Yang, Z.P. Pang, T.C. Südhof, Complexin controls the force transfer from SNARE complexes to membranes in fusion, *Science (New York, N.Y.)* 323 (2009).
- [65] M. Xue, T.K. Craig, J. Xu, H.-T. Chao, J. Rizo, C. Rosenmund, Binding of the complexin N terminus to the SNARE complex potentiates synaptic-vesicle fusogenicity, *Nat Struct Mol Biol* 17 (2010) 568–575.
- [66] Y. Lai, U.B. Choi, Y. Zhang, M. Zhao, R.A. Pfuetzner, A.L. Wang, J. Diao, A.T. Brunger, N-terminal domain of complexin independently activates calcium-triggered fusion, *Proceedings of the National Academy of Sciences of the United States of America* 113 (2016) E4698-707.
- [67] D. Snead, A.L. Lai, R.T. Wragg, D.A. Parisotto, T.F. Ramlall, J.S. Dittman, J.H. Freed, D. Eliezer, Unique Structural Features of Membrane-Bound C-Terminal Domain Motifs Modulate Complexin Inhibitory Function, *Frontiers in molecular neuroscience* 10 (2017).
- [68] D. Snead, R.T. Wragg, J.S. Dittman, D. Eliezer, Membrane curvature sensing by the C-terminal domain of complexin, *Nature communications* 5 (2014) 4955.
- [69] Y.J. Kaeser-Woo, X. Yang, T.C. Südhof, C-terminal complexin sequence is selectively required for clamping and priming but not for Ca²⁺ triggering of synaptic exocytosis, *The Journal of neuroscience: the official journal of the Society for Neuroscience* 32 (2012) 2877–2885.
- [70] R.T. Wragg, D. Snead, Y. Dong, T.F. Ramlall, I. Menon, J. Bai, D. Eliezer, J.S. Dittman, Synaptic vesicles position complexin to block spontaneous fusion, *Neuron* 77 (2013) 323–334.
- [71] J. Malsam, F. Seiler, Y. Schollmeier, P. Rusu, J.M. Krause, T.H. Söllner, The carboxy-terminal domain of complexin I stimulates liposome fusion, *Proceedings of the National Academy of Sciences of the United States of America* 106 (2009) 2001–2006.
- [72] J. Tang, A. Maximov, O.-H. Shin, H. Dai, J. Rizo, T.C. Südhof, A complexin/synaptotagmin 1 switch controls fast synaptic vesicle exocytosis, *Cell* 126 (2006) 1175–1187.
- [73] K.D. Brewer, T. Bacaj, A. Cavalli, C. Camilloni, J.D. Swarbrick, J. Liu, A. Zhou, P. Zhou, N. Barlow, J. Xu, A.B. Seven, E.A. Prinslow, R. Voleti, D. Häussinger, A.M.J.J. Bonvin, D.R. Tomchick, M. Vendruscolo, B. Graham, T.C. Südhof, J. Rizo, Dynamic binding mode of a Synaptotagmin-1-SNARE complex in solution, *Nat Struct Mol Biol* 22 (2015) 555–564.
- [74] U.B. Choi, M. Zhao, Y. Zhang, Y. Lai, A.T. Brunger, Complexin induces a conformational change at the membrane-proximal C-terminal end of the SNARE complex, *eLife* 5 (2016).
- [75] F. Seiler, J. Malsam, J.M. Krause, T.H. Söllner, A role of complexin-lipid interactions in membrane fusion, *FEBS letters* 583 (2009) 2343–2348.
- [76] J. Gong, Y. Lai, X. Li, M. Wang, J. Leitz, Y. Hu, Y. Zhang, U.B. Choi, D. Cipriano, R.A. Pfuetzner, T.C. Südhof, X. Yang, A.T. Brunger, J. Diao, C-terminal domain of mammalian complexin-1 localizes to highly curved membranes, *Proceedings of the National Academy of Sciences of the United States of America* 113 (2016) E7590-E7599.
- [77] D. Kümmel, S.S. Krishnakumar, D.T. Radoff, F. Li, C.G. Giraud, F. Pincet, J.E. Rothman, K.M. Reinisch, Complexin cross-links prefusion SNAREs into a zigzag array, *Nature structural & molecular biology* 18 (2011).

- [78] J. Malsam, S. Bärfuss, T. Trimbuch, F. Zarebidaki, A.F. Sonnen, K. Wild, A. Scheutzow, L. Rohland, M.P. Mayer, I. Sinning, J.A. Briggs, C. Rosenmund, T.H. Söllner, Complexin Suppresses Spontaneous Exocytosis by Capturing the Membrane-Proximal Regions of VAMP2 and SNAP25, *Cell reports* 32 (2020).
- [79] C.G. Giraudo, A. Garcia-Diaz, W.S. Eng, Y. Chen, W.A. Hendrickson, T.J. Melia, J.E. Rothman, Alternative zippering as an on-off switch for SNARE-mediated fusion, *Science (New York, N.Y.)* 323 (2009) 512–516.
- [80] T. Trimbuch, J. Xu, D. Flaherty, D.R. Tomchick, J. Rizo, C. Rosenmund, Re-examining how complexin inhibits neurotransmitter release, *eLife* 3 (2014) e02391.
- [81] D.T. Radoff, Y. Dong, D. Snead, J. Bai, D. Eliezer, J.S. Dittman, The accessory helix of complexin functions by stabilizing central helix secondary structure, *eLife* 3 (2014).
- [82] F. Li, F. Pincet, E. Perez, C.G. Giraudo, D. Tareste, J.E. Rothman, Complexin activates and clamps SNAREpins by a common mechanism involving an intermediate energetic state, *Nat Struct Mol Biol* 18 (2011) 941–946.
- [83] L. Yin, J. Kim, Y.-K. Shin, Complexin splits the membrane-proximal region of a single SNAREpin, *The Biochemical journal* 473 (2016) 2219–2224.
- [84] M.J. Shon, H. Kim, T.-Y. Yoon, Focused clamping of a single neuronal SNARE complex by complexin under high mechanical tension, *Nat Commun* 9 (2018) 3639.
- [85] M. Yamashita, J.B. Fenn, Electrospray ion source. Another variation on the free-jet theme, *J. Phys. Chem.* 88 (1984) 4451–4459.
- [86] G.I. Taylor, Disintegration of water drops in an electric field, *Proc. R. Soc. Lond. A* 280 (1964) 383–397.
- [87] J.V. Iribarne, B.A. Thomson, On the evaporation of small ions from charged droplets, *The Journal of Chemical Physics* 64 (1976) 2287–2294.
- [88] M. Wilm, M. Mann, Analytical properties of the nanoelectrospray ion source, *Analytical chemistry* 68 (1996) 1–8.
- [89] A. Michalski, E. Damoc, J.-P. Hauschild, O. Lange, A. Wieghaus, A. Makarov, N. Nagaraj, J. Cox, M. Mann, S. Horning, Mass spectrometry-based proteomics using Q Exactive, a high-performance benchtop quadrupole Orbitrap mass spectrometer, *Molecular & cellular proteomics: MCP* 10 (2011) M111.011015.
- [90] I.V. Chernushevich, A.V. Loboda, B.A. Thomson, An introduction to quadrupole-time-of-flight mass spectrometry, *Journal of mass spectrometry: JMS* 36 (2001) 849–865.
- [91] W. Paul, H. Steinwedel, Notizen: Ein neues Massenspektrometer ohne Magnetfeld, *Zeitschrift für Naturforschung A* 8 (1953) 448–450.
- [92] W.C. Wiley, I.H. McLaren, Time-of-Flight Mass Spectrometer with Improved Resolution, *Review of Scientific Instruments* 26 (1955) 1150–1157.
- [93] A. Makarov, Electrostatic axially harmonic orbital trapping: a high-performance technique of mass analysis, *Analytical chemistry* 72 (2000) 1156–1162.
- [94] A.S. Tremsin, J.B. McPhate, A. Steuer, W. Kockelmann, A. M Paradowska, J.F. Kelleher, J.V. Vallerga, O.H.W. Siegmund, W.B. Feller, High-Resolution Strain Mapping Through Time-of-Flight Neutron Transmission Diffraction with a Microchannel Plate Neutron Counting Detector, *Strain* 48 (2012) 296–305.
- [95] J. Ladislav Wiza, Microchannel plate detectors, *Nuclear Instruments and Methods* 162 (1979) 587–601.
- [96] J.V. Olsen, B. Macek, O. Lange, A. Makarov, S. Horning, M. Mann, Higher-energy C-trap dissociation for peptide modification analysis, *Nature methods* 4 (2007) 709–712.

- [97] J. Cox, M. Mann, MaxQuant enables high peptide identification rates, individualized p.p.b.-range mass accuracies and proteome-wide protein quantification, *Nature biotechnology* 26 (2008) 1367–1372.
- [98] S. Aggarwal, A.K. Yadav, False Discovery Rate Estimation in Proteomics, *Methods in molecular biology* (Clifton, N.J.) 1362 (2016) 119–128.
- [99] S.J. Kim, J. Fernandez-Martinez, I. Nudelman, Y. Shi, W. Zhang, B. Raveh, T. Herricks, B.D. Slaughter, J.A. Hogan, P. Upla, I.E. Chemmama, R. Pellarin, I. Echeverria, M. Shivaraju, A.S. Chaudhury, J. Wang, R. Williams, J.R. Unruh, C.H. Greenberg, E.Y. Jacobs, Z. Yu, M.J. de La Cruz, R. Mironska, D.L. Stokes, J.D. Aitchison, M.F. Jarrold, J.L. Gerton, S.J. Ludtke, C.W. Akey, B.T. Chait, A. Sali, M.P. Rout, Integrative structure and functional anatomy of a nuclear pore complex, *Nature* 555 (2018) 475–482.
- [100] A. Linden, M. Deckers, I. Parfentev, R. Pflanz, B. Homberg, P. Neumann, R. Ficner, P. Rehling, H. Urlaub, A Cross-linking Mass Spectrometry Approach Defines Protein Interactions in Yeast Mitochondria, *Molecular & cellular proteomics: MCP* 19 (2020) 1161–1178.
- [101] F.J. O'Reilly, L. Xue, A. Graziadei, L. Sinn, S. Lenz, D. Tegunov, C. Blötz, N. Singh, W.J.H. Hagen, P. Cramer, J. Stülke, J. Mahamid, J. Rappsilber, In-cell architecture of an actively transcribing-translating expressome, *Science (New York, N.Y.)* 369 (2020) 554–557.
- [102] J.D. Chavez, C.F. Lee, A. Caudal, A. Keller, R. Tian, J.E. Bruce, Chemical Crosslinking Mass Spectrometry Analysis of Protein Conformations and Supercomplexes in Heart Tissue, *Cell systems* 6 (2018) 136-141.e5.
- [103] C. Iacobucci, A. Sinz, To Be or Not to Be? Five Guidelines to Avoid Misassignments in Cross-Linking/Mass Spectrometry, *Analytical chemistry* 89 (2017) 7832–7835.
- [104] M.L. Mendes, L. Fischer, Z.A. Chen, M. Barbon, F.J. O'Reilly, S.H. Giese, M. Bohlke-Schneider, A. Belsom, T. Dau, C.W. Combe, M. Graham, M.R. Eisele, W. Baumeister, C. Speck, J. Rappsilber, An integrated workflow for crosslinking mass spectrometry, *Molecular systems biology* 15 (2019) e8994.
- [105] A. Leitner, R. Reischl, T. Walzthoeni, F. Herzog, S. Bohn, F. Förster, R. Aebersold, Expanding the chemical cross-linking toolbox by the use of multiple proteases and enrichment by size exclusion chromatography, *Molecular & cellular proteomics: MCP* 11 (2012) M111.014126.
- [106] J.V. Staros, N-hydroxysulfosuccinimide active esters: bis(N-hydroxysulfosuccinimide) esters of two dicarboxylic acids are hydrophilic, membrane-impermeant, protein cross-linkers, *Biochemistry* 21 (1982) 3950–3955.
- [107] S. Kalkhof, A. Sinz, Chances and pitfalls of chemical cross-linking with amine-reactive N-hydroxysuccinimide esters, *Anal Bioanal Chem* 392 (2008) 305–312.
- [108] Z. Grabarek, J. Gergely, Zero-length crosslinking procedure with the use of active esters, *Analytical biochemistry* 185 (1990) 131–135.
- [109] R. Fritzsche, C.H. Ihling, M. Götze, A. Sinz, Optimizing the enrichment of cross-linked products for mass spectrometric protein analysis, *Rapid communications in mass spectrometry: RCM* 26 (2012) 653–658.
- [110] M.S. Ritorto, K. Cook, K. Tyagi, P.G.A. Pedrioli, M. Trost, Hydrophilic strong anion exchange (hSAX) chromatography for highly orthogonal peptide separation of complex proteomes, *Journal of proteome research* 12 (2013) 2449–2457.
- [111] B. Steigenberger, R.J. Pieters, A.J.R. Heck, R.A. Scheltema, PhoX: An IMAC-Enrichable Cross-Linking Reagent, *ACS central science* 5 (2019) 1514–1522.

- [112] D. Tan, Q. Li, M.-J. Zhang, C. Liu, C. Ma, P. Zhang, Y.-H. Ding, S.-B. Fan, L. Tao, B. Yang, X. Li, S. Ma, J. Liu, B. Feng, X. Liu, H.-W. Wang, S.-M. He, N. Gao, K. Ye, M.-Q. Dong, X. Lei, Trifunctional cross-linker for mapping protein-protein interaction networks and comparing protein conformational states, *eLife* 5 (2016).
- [113] A. Kao, C. Chiu, D. Vellucci, Y. Yang, V.R. Patel, S. Guan, A. Randall, P. Baldi, S.D. Rychnovsky, L. Huang, Development of a novel cross-linking strategy for fast and accurate identification of cross-linked peptides of protein complexes, *Molecular & cellular proteomics: MCP* 10 (2011) M110.002212.
- [114] C.B. Gutierrez, C. Yu, E.J. Novitsky, A.S. Huszagh, S.D. Rychnovsky, L. Huang, Developing an Acidic Residue Reactive and Sulfoxide-Containing MS-Cleavable Homobifunctional Cross-Linker for Probing Protein-Protein Interactions, *Analytical chemistry* 88 (2016) 8315–8322.
- [115] L. Fischer, Z.A. Chen, J. Rappsilber, Quantitative cross-linking/mass spectrometry using isotope-labelled cross-linkers, *Journal of proteomics* 88 (2013) 120–128.
- [116] C. Schmidt, C.V. Robinson, A comparative cross-linking strategy to probe conformational changes in protein complexes, *Nature protocols* 9 (2014) 2224–2236.
- [117] L. Kolbowski, M.L. Mendes, J. Rappsilber, Optimizing the Parameters Governing the Fragmentation of Cross-Linked Peptides in a Tribrid Mass Spectrometer, *Analytical chemistry* 89 (2017) 5311–5318.
- [118] L. Schnirch, M. Nadler-Holly, S.-W. Siao, C.K. Frese, R. Viner, F. Liu, Expanding the Depth and Sensitivity of Cross-Link Identification by Differential Ion Mobility Using High-Field Asymmetric Waveform Ion Mobility Spectrometry, *Analytical chemistry* 92 (2020) 10495–10503.
- [119] O. Rinner, J. Seebacher, T. Walzthoeni, L.N. Mueller, M. Beck, A. Schmidt, M. Mueller, R. Aebersold, Identification of cross-linked peptides from large sequence databases, *Nature methods* 5 (2008) 315–318.
- [120] Z.-L. Chen, J.-M. Meng, Y. Cao, J.-L. Yin, R.-Q. Fang, S.-B. Fan, C. Liu, W.-F. Zeng, Y.-H. Ding, D. Tan, L. Wu, W.-J. Zhou, H. Chi, R.-X. Sun, M.-Q. Dong, S.-M. He, A high-speed search engine pLink 2 with systematic evaluation for proteome-scale identification of cross-linked peptides, *Nature communications* 10 (2019) 3404.
- [121] M. Götze, J. Pettelkau, S. Schaks, K. Bosse, C.H. Ihling, F. Krauth, R. Fritzsche, U. Kühn, A. Sinz, StavroX—a software for analyzing crosslinked products in protein interaction studies, *J. Am. Soc. Mass Spectrom.* 23 (2012) 76–87.
- [122] M. Götze, J. Pettelkau, R. Fritzsche, C.H. Ihling, M. Schäfer, A. Sinz, Automated assignment of MS/MS cleavable cross-links in protein 3D-structure analysis, *J. Am. Soc. Mass Spectrom.* 26 (2015) 83–97.
- [123] M. Grimm, T. Zimniak, A. Kahraman, F. Herzog, xVis: a web server for the schematic visualization and interpretation of crosslink-derived spatial restraints, *Nucleic acids research* 43 (2015) W362-9.
- [124] E.F. Pettersen, T.D. Goddard, C.C. Huang, G.S. Couch, D.M. Greenblatt, E.C. Meng, T.E. Ferrin, UCSF Chimera—a visualization system for exploratory research and analysis, *Journal of computational chemistry* 25 (2004) 1605–1612.
- [125] E.C. Meng, T.D. Goddard, E.F. Pettersen, G.S. Couch, Z.J. Pearson, J.H. Morris, T.E. Ferrin, UCSF ChimeraX: Tools for structure building and analysis, *Protein science: a publication of the Protein Society* 32 (2023) e4792.
- [126] J. Kosinski, A. von Appen, A. Ori, K. Karius, C.W. Müller, M. Beck, Xlink Analyzer: software for analysis and visualization of cross-linking data in the context of three-dimensional structures, *Journal of structural biology* 189 (2015) 177–183.

- [127] A. Graziadei, J. Rappsilber, Leveraging crosslinking mass spectrometry in structural and cell biology, *Structure* (London, England: 1993) 30 (2022) 37–54.
- [128] C. Schmidt, M. Zhou, H. Marriott, N. Morgner, A. Politis, C.V. Robinson, Comparative cross-linking and mass spectrometry of an intact F-type ATPase suggest a role for phosphorylation, *Nat Commun* 4 (2013) 1985.
- [129] M. Frick, C. Schwieger, C. Schmidt, Liposomes as Carriers of Membrane-Associated Proteins and Peptides for Mass Spectrometric Analysis, *Angewandte Chemie* (International ed. in English) 60 (2021) 11523–11530.
- [130] C. Uetrecht, C. Versluis, N.R. Watts, W.H. Roos, G.J.L. Wuite, P.T. Wingfield, A.C. Steven, A.J.R. Heck, High-resolution mass spectrometry of viral assemblies: molecular composition and stability of dimorphic hepatitis B virus capsids, *Proceedings of the National Academy of Sciences of the United States of America* 105 (2008) 9216–9220.
- [131] D.R. Benjamin, C.V. Robinson, J.P. Hendrick, F.U. Hartl, C.M. Dobson, Mass spectrometry of ribosomes and ribosomal subunits, *Proceedings of the National Academy of Sciences of the United States of America* 95 (1998) 7391–7395.
- [132] H. Hernández, C.V. Robinson, Determining the stoichiometry and interactions of macromolecular assemblies from mass spectrometry, *Nature protocols* 2 (2007) 715–726.
- [133] L. Konermann, Addressing a Common Misconception: Ammonium Acetate as Neutral pH “Buffer” for Native Electrospray Mass Spectrometry, *J. Am. Soc. Mass Spectrom.* 28 (2017) 1827–1835.
- [134] M. Dole, L.L. Mack, R.L. Hines, R.C. Mobley, L.D. Ferguson, M.B. Alice, Molecular Beams of Macroions, *The Journal of Chemical Physics* 49 (1968) 2240–2249.
- [135] L. Konermann, A.D. Rodriguez, J. Liu, On the formation of highly charged gaseous ions from unfolded proteins by electrospray ionization, *Analytical chemistry* 84 (2012) 6798–6804.
- [136] I.A. Kaltashov, A. Mohimen, Estimates of protein surface areas in solution by electrospray ionization mass spectrometry, *Analytical chemistry* 77 (2005) 5370–5379.
- [137] I.A. Kaltashov, R.R. Abzalimov, Do ionic charges in ESI MS provide useful information on macromolecular structure?, *J. Am. Soc. Mass Spectrom.* 19 (2008) 1239–1246.
- [138] C. Santambrogio, A. Natalello, S. Brocca, E. Ponzini, R. Grandori, Conformational Characterization and Classification of Intrinsically Disordered Proteins by Native Mass Spectrometry and Charge-State Distribution Analysis, *Proteomics* 19 (2019) e1800060.
- [139] F. Sobott, H. Hernández, M.G. McCammon, M.A. Tito, C.V. Robinson, A tandem mass spectrometer for improved transmission and analysis of large macromolecular assemblies, *Analytical chemistry* 74 (2002) 1402–1407.
- [140] S. Tamara, M.A. den Boer, A.J.R. Heck, High-Resolution Native Mass Spectrometry, *Chemical reviews* 122 (2022) 7269–7326.
- [141] I.V. Chernushevich, B.A. Thomson, Collisional cooling of large ions in electrospray mass spectrometry, *Analytical chemistry* 76 (2004) 1754–1760.
- [142] D.J. Douglas, J.B. French, Collisional focusing effects in radio frequency quadrupoles, *J. Am. Soc. Mass Spectrom.* 3 (1992) 398–408.
- [143] N. Tahallah, M. Pinkse, C.S. Maier, A.J. Heck, The effect of the source pressure on the abundance of ions of noncovalent protein assemblies in an electrospray ionization orthogonal time-of-flight instrument, *Rapid communications in mass spectrometry: RCM* 15 (2001) 596–601.

- [144] A.N. Krutchinsky, I.V. Chernushevich, V.L. Spicer, W. Ens, K.G. Standing, Collisional damping interface for an electrospray ionization time-of-flight mass spectrometer, *J. Am. Soc. Mass Spectrom.* 9 (1998) 569–579.
- [145] H.R. Morris, T. Paxton, A. Dell, J. Langhorne, M. Berg, R.S. Bordoli, J. Hoyes, R.H. Bateman, High sensitivity collisionally-activated decomposition tandem mass spectrometry on a novel quadrupole/orthogonal-acceleration time-of-flight mass spectrometer, *Rapid communications in mass spectrometry: RCM* 10 (1996) 889–896.
- [146] K.R. Jennings, Collision-induced decompositions of aromatic molecular ions, *International Journal of Mass Spectrometry and Ion Physics* 1 (1968) 227–235.
- [147] L. Konermann, E. Ahadi, A.D. Rodriguez, S. Vahidi, Unraveling the mechanism of electrospray ionization, *Analytical chemistry* 85 (2013) 2–9.
- [148] J.L. Benesch, J.A. Aquilina, B.T. Ruotolo, F. Sobott, C.V. Robinson, Tandem mass spectrometry reveals the quaternary organization of macromolecular assemblies, *Chemistry & biology* 13 (2006).
- [149] K. Pagel, S.-J. Hyung, B.T. Ruotolo, C.V. Robinson, Alternate dissociation pathways identified in charge-reduced protein complex ions, *Analytical chemistry* 82 (2010) 5363–5372.
- [150] N. Morgner, C.V. Robinson, Massign: an assignment strategy for maximizing information from the mass spectra of heterogeneous protein assemblies, *Analytical chemistry* 84 (2012) 2939–2948.
- [151] M.T. Marty, A.J. Baldwin, E.G. Marklund, G.K.A. Hochberg, J.L.P. Benesch, C.V. Robinson, Bayesian deconvolution of mass and ion mobility spectra: from binary interactions to polydisperse ensembles, *Analytical chemistry* 87 (2015) 4370–4376.
- [152] T.G. Watkinson, A.N. Calabrese, F. Giusti, M. Zoonens, S.E. Radford, A.E. Ashcroft, Systematic analysis of the use of amphipathic polymers for studies of outer membrane proteins using mass spectrometry, *International Journal of Mass Spectrometry* 391 (2015) 54–61.
- [153] T.H. Bayburt, S.G. Sligar, Self-assembly of single integral membrane proteins into soluble nanoscale phospholipid bilayers, *Protein science: a publication of the Protein Society* 12 (2003) 2476–2481.
- [154] I.G. Denisov, Y.V. Grinkova, A.A. Lazarides, S.G. Sligar, Directed self-assembly of monodisperse phospholipid bilayer Nanodiscs with controlled size, *Journal of the American Chemical Society* 126 (2004) 3477–3487.
- [155] M.T. Marty, K.K. Hoi, J. Gault, C.V. Robinson, Probing the Lipid Annular Belt by Gas-Phase Dissociation of Membrane Proteins in Nanodiscs, *Angewandte Chemie (International ed. in English)* 55 (2016) 550–554.
- [156] T. Ravula, N.Z. Hardin, A. Ramamoorthy, Polymer nanodiscs: Advantages and limitations, *Chemistry and physics of lipids* 219 (2019) 45–49.
- [157] N. Hellwig, O. Peetz, Z. Ahdash, I. Tascón, P.J. Booth, V. Mikusevic, M. Diskowski, A. Politis, Y. Hellmich, I. Hänel, E. Reading, N. Morgner, Native mass spectrometry goes more native: investigation of membrane protein complexes directly from SMALPs, *Chemical communications (Cambridge, England)* 54 (2018) 13702–13705.
- [158] K.K. Hoi, J.F. Bada Juarez, P.J. Judge, H.-Y. Yen, Di Wu, J. Vinals, G.F. Taylor, A. Watts, C.V. Robinson, Detergent-free Lipodisc Nanoparticles Facilitate High-Resolution Mass Spectrometry of Folded Integral Membrane Proteins, *Nano letters* 21 (2021) 2824–2831.
- [159] E. Henrich, O. Peetz, C. Hein, A. Laguerre, B. Hoffmann, J. Hoffmann, V. Dötsch, F. Bernhard, N. Morgner, Analyzing native membrane protein assembly in nanodiscs by combined non-covalent mass spectrometry and synthetic biology, *eLife* 6 (2017).

- [160] D.S. Chorev, H. Tang, S.L. Rouse, J.R. Bolla, A. von Kügelgen, L.A. Baker, Di Wu, J. Gault, K. Grünewald, T.A.M. Bharat, S.J. Matthews, C.V. Robinson, The use of sonicated lipid vesicles for mass spectrometry of membrane protein complexes, *Nature protocols* 15 (2020) 1690–1706.
- [161] M. Landreh, J. Costeira-Paulo, J. Gault, E.G. Marklund, C.V. Robinson, Effects of Detergent Micelles on Lipid Binding to Proteins in Electrospray Ionization Mass Spectrometry, *Analytical chemistry* 89 (2017) 7425–7430.
- [162] A. Laganowsky, E. Reading, J.T.S. Hopper, C.V. Robinson, Mass spectrometry of intact membrane protein complexes, *Nature protocols* 8 (2013) 639–651.
- [163] L.H. Urner, I. Liko, H.-Y. Yen, K.-K. Hoi, J.R. Bolla, J. Gault, F.G. Almeida, M.-P. Schweder, D. Shutin, S. Ehrmann, R. Haag, C.V. Robinson, K. Pagel, Modular detergents tailor the purification and structural analysis of membrane proteins including G-protein coupled receptors, *Nat Commun* 11 (2020) 564.
- [164] E. Reading, I. Liko, T.M. Allison, J.L.P. Benesch, A. Laganowsky, C.V. Robinson, The role of the detergent micelle in preserving the structure of membrane proteins in the gas phase, *Angewandte Chemie (International ed. in English)* 54 (2015) 4577–4581.
- [165] J. Bender, C. Schmidt, The CroCo cross-link converter: a user-centred tool to convert results from cross-linking mass spectrometry experiments, *Bioinformatics (Oxford, England)* 36 (2020) 1296–1297.
- [166] L. Schrödinger, *The PyMOL Molecular Graphics System* (2010).
- [167] Gasteiger E., Hoogland C., Gattiker A., Duvaud S., Wilkins M.R., Appel R.D., Bairoch A., Protein Identification and Analysis Tools on the ExPASy Server, in: J.M. Walker (Ed.) *The Proteomics Protocols Handbook*, Humana Press, 2005.
- [168] M.M. Bradford, A rapid and sensitive method for the quantitation of microgram quantities of protein utilizing the principle of protein-dye binding, *Analytical biochemistry* 72 (1976) 248–254.
- [169] A.V. Pobbati, A. Stein, D. Fasshauer, N- to C-terminal SNARE complex assembly promotes rapid membrane fusion, *Science (New York, N.Y.)* 313 (2006) 673–676.
- [170] J.V. Olsen, L.M.F. de Godoy, G. Li, B. Macek, P. Mortensen, R. Pesch, A. Makarov, O. Lange, S. Horning, M. Mann, Parts per million mass accuracy on an Orbitrap mass spectrometer via lock mass injection into a C-trap, *Molecular & cellular proteomics: MCP* 4 (2005) 2010–2021.
- [171] M. Mirdita, K. Schütze, Y. Moriwaki, L. Heo, S. Ovchinnikov, M. Steinegger, ColabFold: making protein folding accessible to all, *Nature methods* 19 (2022) 679–682.
- [172] J. Jumper, R. Evans, A. Pritzel, T. Green, M. Figurnov, O. Ronneberger, K. Tunyasuvunakool, R. Bates, A. Židek, A. Potapenko, A. Bridgland, C. Meyer, S.A.A. Kohl, A.J. Ballard, A. Cowie, B. Romera-Paredes, S. Nikolov, R. Jain, J. Adler, T. Back, S. Petersen, D. Reiman, E. Clancy, M. Zielinski, M. Steinegger, M. Pacholska, T. Berghammer, S. Bodenstein, D. Silver, O. Vinyals, A.W. Senior, K. Kavukcuoglu, P. Kohli, D. Hassabis, Highly accurate protein structure prediction with AlphaFold, *Nature* 596 (2021) 583–589.
- [173] Y. Perez-Riverol, J. Bai, C. Bandla, D. García-Seisdedos, S. Hewapathirana, S. Kamatchinathan, D.J. Kundu, A. Prakash, A. Frericks-Zipper, M. Eisenacher, M. Walzer, S. Wang, A. Brazma, J.A. Vizcaíno, The PRIDE database resources in 2022: a hub for mass spectrometry-based proteomics evidences, *Nucleic acids research* 50 (2022) D543-D552.
- [174] J. Hesselbarth, C. Schmidt, Mass spectrometry uncovers intermediates and off-pathway complexes for SNARE complex assembly, *Communications biology* 6 (2023) 198.

- [175] K. Bhasne, E.M. Clerico, A. Bogoiian-Mullen, L.M. Gierasch, Elucidating the role of the Hsc70 chaperone in SNARE complex assembly, *Biophysical Journal* 122 (2023) 152a.
- [176] S. Wittig, C. Haupt, W. Hoffmann, S. Kostmann, K. Pagel, C. Schmidt, Oligomerisation of Synaptobrevin-2 Studied by Native Mass Spectrometry and Chemical Cross-Linking, *Journal of the American Society for Mass Spectrometry* 30 (2019) 149–160.
- [177] M. Barth, C. Schmidt, Native mass spectrometry-A valuable tool in structural biology, *Journal of mass spectrometry: JMS* 55 (2020) e4578.
- [178] J.L.P. Benesch, B.T. Ruotolo, D.A. Simmons, C.V. Robinson, Protein complexes in the gas phase: technology for structural genomics and proteomics, *Chemical reviews* 107 (2007) 3544–3567.
- [179] N.P. Barrera, N. Di Bartolo, P.J. Booth, C.V. Robinson, Micelles protect membrane complexes from solution to vacuum, *Science (New York, N.Y.)* 321 (2008) 243–246.
- [180] W. Li, Y. Xing, Y. Wang, T. Xu, E. Song, W. Feng, A non-canonical target-binding site in Munc18-1 domain 3b for assembling the Mint1-Munc18-1-syntaxin-1 complex, *Structure (London, England: 1993)* 31 (2023) 68-77.e5.
- [181] D. Fasshauer, M. Margittai, A transient N-terminal interaction of SNAP-25 and syntaxin nucleates SNARE assembly, *The Journal of biological chemistry* 279 (2004) 7613–7621.
- [182] Y.A. Chen, S.J. Scales, R.H. Scheller, Sequential SNARE assembly underlies priming and triggering of exocytosis, *Neuron* 30 (2001) 161–170.
- [183] K. Weninger, M.E. Bowen, U.B. Choi, S. Chu, A.T. Brunger, Accessory proteins stabilize the acceptor complex for synaptobrevin, the 1:1 syntaxin/SNAP-25 complex, *Structure (London, England: 1993)* 16 (2008).
- [184] E.R. Chapman, S. An, N. Barton, R. Jahn, SNAP-25, a t-SNARE which binds to both syntaxin and synaptobrevin via domains that may form coiled coils, *Journal of Biological Chemistry* 269 (1994) 27427–27432.
- [185] B.L. Schwartz, K.J. Light-Wahl, R.D. Smith, Observation of noncovalent complexes to the avidin tetramer by electrospray ionization mass spectrometry, *Journal of the American Society for Mass Spectrometry* 5 (1994).
- [186] Q. Zhou, P. Zhou, A.L. Wang, D. Wu, M. Zhao, T.C. Südhof, A.T. Brunger, The primed SNARE-complexin-synaptotagmin complex for neuronal exocytosis, *Nature* 548 (2017) 420–425.
- [187] D. Snead, D. Eliezer, Intrinsically disordered proteins in synaptic vesicle trafficking and release, *Journal of Biological Chemistry* 294 (2019) 3325–3342.
- [188] R. Zdanowicz, A. Kreutzberger, B. Liang, V. Kiessling, L.K. Tamm, D.S. Cafiso, Complexin Binding to Membranes and Acceptor t-SNAREs Explains Its Clamping Effect on Fusion, *Biophysical Journal* 113 (2017) 1235–1250.
- [189] Q. Liang, A.P. Ofosuhene, V. Kiessling, B. Liang, A.J.B. Kreutzberger, L.K. Tamm, D.S. Cafiso, Complexin-1 and synaptotagmin-1 compete for binding sites on membranes containing PtdInsP2, *Biophysical Journal* 121 (2022) 3370–3380.
- [190] E.M. Grasso, M.S. Terakawa, A.L. Lai, Y. Xue Xie, T.F. Ramlall, J.H. Freed, D. Eliezer, Membrane Binding Induces Distinct Structural Signatures in the Mouse Complexin-1C-Terminal Domain, *Journal of molecular biology* 435 (2023) 167710.
- [191] A. Nagy, R.R. Baker, S.J. Morris, V.P. Whittaker, The preparation and characterization of synaptic vesicles of high purity, *Brain research* 109 (1976) 285–309.
- [192] J.W. Deutsch, R.B. Kelly, Lipids of synaptic vesicles: relevance to the mechanism of membrane fusion, *Biochemistry* 20 (1981) 378–385.

- [193] T. Kundlacz, J. Bender, C. Schmidt, Effects of non-ionic and zwitterionic detergents on soluble proteins during native mass spectrometry experiments, *International Journal of Mass Spectrometry* 468 (2021) 116652.
- [194] C.L. Gatlin, F. Turecek, Acidity Determination in Droplets Formed by Electrospraying Methanol-Water Solutions, *Anal. Chem.* 66 (1994) 712–718.
- [195] U.A. Mirza, B.T. Chait, Do proteins denature during droplet evolution in electrospray ionization?, *International Journal of Mass Spectrometry and Ion Processes* 162 (1997) 173–181.
- [196] P.G. Wolynes, Biomolecular folding in vacuo!!!(?), *Proceedings of the National Academy of Sciences of the United States of America* 92 (1995) 2426–2427.
- [197] M. Bakhtiari, L. Konermann, Protein Ions Generated by Native Electrospray Ionization: Comparison of Gas Phase, Solution, and Crystal Structures, *The journal of physical chemistry. B* 123 (2019) 1784–1796.
- [198] M.Z. Steinberg, R. Elber, F.W. McLafferty, R.B. Gerber, K. Breuker, Early structural evolution of native cytochrome c after solvent removal, *Chembiochem: a European journal of chemical biology* 9 (2008) 2417–2423.
- [199] K.B. Shelimov, M.F. Jarrold, Conformations, Unfolding, and Refolding of Apomyoglobin in Vacuum: An Activation Barrier for Gas-Phase Protein Folding, *Journal of the American Chemical Society* 119 (1997) 2987–2994.
- [200] E.R. Badman, S. Myung, D.E. Clemmer, Evidence for unfolding and refolding of gas-phase cytochrome C ions in a Paul trap, *J. Am. Soc. Mass Spectrom.* 16 (2005) 1493–1497.
- [201] J.Y. Han, T.S. Choi, C.E. Heo, M.K. Son, H.I. Kim, Gas-phase conformations of intrinsically disordered proteins and their complexes with ligands: Kinetically trapped states during transfer from solution to the gas phase, *Mass spectrometry reviews* 38 (2019) 483–500.
- [202] A.J. Borysik, D. Kovacs, M. Guharoy, P. Tompa, Ensemble Methods Enable a New Definition for the Solution to Gas-Phase Transfer of Intrinsically Disordered Proteins, *Journal of the American Chemical Society* 137 (2015) 13807–13817.
- [203] R. Beveridge, A.S. Phillips, L. Denbigh, H.M. Saleem, C.E. MacPhee, P.E. Barran, Relating gas phase to solution conformations: Lessons from disordered proteins, *Proteomics* 15 (2015) 2872–2883.
- [204] R. Grandori, C. Santambrogio, S. Brocca, G. Invernizzi, M. Lotti, Electrospray-ionization mass spectrometry as a tool for fast screening of protein structural properties, *Biotechnology journal* 4 (2009) 73–87.
- [205] K. Breuker, F.W. McLafferty, Stepwise evolution of protein native structure with electrospray into the gas phase, 10(-12) to 10(2) s, *Proceedings of the National Academy of Sciences of the United States of America* 105 (2008) 18145–18152.
- [206] F. Sobott, C.V. Robinson, Characterising electrosprayed biomolecules using tandem-MS—the noncovalent GroEL chaperonin assembly, *International Journal of Mass Spectrometry* 236 (2004) 25–32.
- [207] K.L. Rundlett, D.W. Armstrong, Mechanism of signal suppression by anionic surfactants in capillary electrophoresis-electrospray ionization mass spectrometry, *Anal. Chem.* 68 (1996) 3493–3497.
- [208] L.L. Ilag, I. Ubarretxena-Belandia, C.G. Tate, C.V. Robinson, Drug binding revealed by tandem mass spectrometry of a protein-micelle complex, *Journal of the American Chemical Society* 126 (2004) 14362–14363.

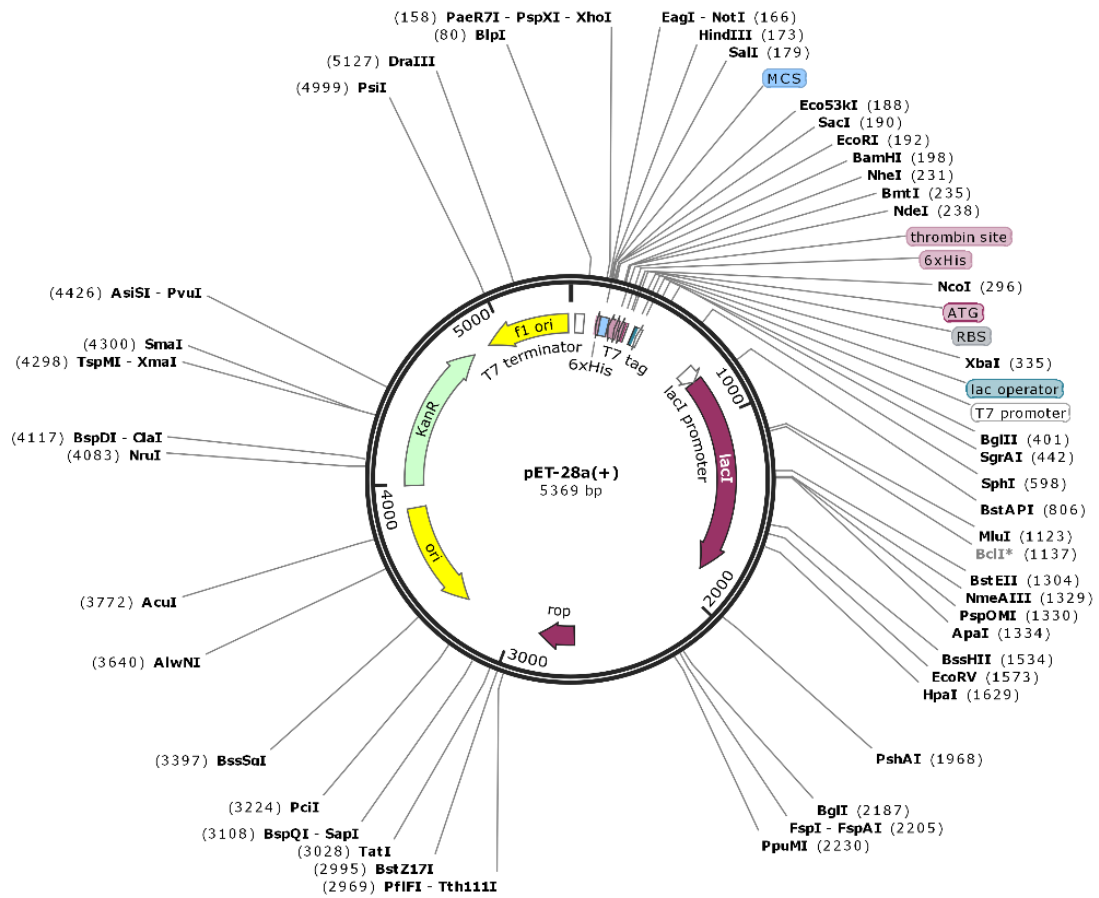
- [209] N.P. Barrera, S.C. Isaacson, M. Zhou, V.N. Bavro, A. Welch, T.A. Schaedler, M.A. Seeger, R.N. Miguel, V.M. Korkhov, H.W. van Veen, H. Venter, A.R. Walmsley, C.G. Tate, C.V. Robinson, Mass spectrometry of membrane transporters reveals subunit stoichiometry and interactions, *Nature methods* 6 (2009) 585–587.
- [210] A. Laganowsky, E. Reading, T.M. Allison, M.B. Ulmschneider, M.T. Degiacomi, A.J. Baldwin, C.V. Robinson, Membrane proteins bind lipids selectively to modulate their structure and function, *Nature* 510 (2014) 172–175.
- [211] A.J. Borysik, D.J. Hewitt, C.V. Robinson, Detergent release prolongs the lifetime of native-like membrane protein conformations in the gas-phase, *Journal of the American Chemical Society* 135 (2013) 6078–6083.
- [212] E. Reading, T.A. Walton, I. Liko, M.T. Marty, A. Laganowsky, D.C. Rees, C.V. Robinson, The Effect of Detergent, Temperature, and Lipid on the Oligomeric State of MscL Constructs: Insights from Mass Spectrometry, *Chemistry & biology* 22 (2015) 593–603.
- [213] J. Bender, T. Kundlacz, L.S.P. Rudden, M. Frick, J. Bieber, M.T. Degiacomi, C. Schmidt, Ca²⁺-dependent lipid preferences shape synaptotagmin-1 C2A and C2B dynamics: Insights from experiments and simulations, *Structure (London, England: 1993)* 32 (2024) 1691-1704.e5.
- [214] T. Kundlacz, C. Schmidt, Deciphering Solution and Gas-Phase Interactions between Peptides and Lipids by Native Mass Spectrometry, *Anal. Chem.* 95 (2023) 17292–17299.
- [215] J.-S. Behnke, L.H. Urner, Emergence of mass spectrometry detergents for membrane proteomics, *Anal Bioanal Chem* 415 (2023) 3897–3909.
- [216] L. Piersimoni, P.L. Kastritis, C. Arlt, A. Sinz, Cross-Linking Mass Spectrometry for Investigating Protein Conformations and Protein-Protein Interactions—A Method for All Seasons, *Chemical reviews* 122 (2022) 7500–7531.
- [217] J. Rappsilber, The beginning of a beautiful friendship: cross-linking/mass spectrometry and modelling of proteins and multi-protein complexes, *Journal of structural biology* 173 (2011) 530–540.
- [218] A. Sinz, C. Arlt, D. Chorev, M. Sharon, Chemical cross-linking and native mass spectrometry: A fruitful combination for structural biology, *Protein science: a publication of the Protein Society* 24 (2015) 1193–1209.
- [219] T. Taverner, N.E. Hall, R.A.J. O’Hair, R.J. Simpson, Characterization of an antagonist interleukin-6 dimer by stable isotope labeling, cross-linking, and mass spectrometry, *Journal of Biological Chemistry* 277 (2002) 46487–46492.
- [220] D.B. Lima, J.T. Melchior, J. Morris, V.C. Barbosa, J. Chamot-Rooke, M. Fioramonte, T.A.C.B. Souza, J.S.G. Fischer, F.C. Gozzo, P.C. Carvalho, W.S. Davidson, Characterization of homodimer interfaces with cross-linking mass spectrometry and isotopically labeled proteins, *Nature protocols* 13 (2018) 431–458.
- [221] E.V. Petrotchenko, J.J. Serpa, K.A.T. Makepeace, N.I. Brodie, C.H. Borchers, (14)N(15)N DXMSMS Match program for the automated analysis of LC/ESI-MS/MS crosslinking data from experiments using (15)N metabolically labeled proteins, *Journal of proteomics* 109 (2014) 104–110.
- [222] Z. Kukačka, M. Rosůlek, J. Jelínek, L. Slavata, D. Kavan, P. Novák, LinX: A Software Tool for Uncommon Cross-Linking Chemistry, *Journal of proteome research* 20 (2021) 2021–2027.
- [223] A. Gaber, G. Gunčar, M. Pavšič, Proper evaluation of chemical cross-linking-based spatial restraints improves the precision of modeling homo-oligomeric protein complexes, *BMC bioinformatics* 20 (2019) 464.

- [224] L. Wang, Z. Wen, S.-W. Liu, L. Zhang, C. Finley, H.-J. Lee, H.-J.S. Fan, Overview of AlphaFold2 and breakthroughs in overcoming its limitations, *Computers in biology and medicine* 176 (2024) 108620.
- [225] T.R. Alderson, I. Pritišanac, Đ. Kolarić, A.M. Moses, J.D. Forman-Kay, Systematic identification of conditionally folded intrinsically disordered regions by AlphaFold2, *Proceedings of the National Academy of Sciences of the United States of America* 120 (2023) e2304302120.
- [226] K.L. Nicholson, M. Munson, R.B. Miller, T.J. Filip, R. Fairman, F.M. Hughson, Regulation of SNARE complex assembly by an N-terminal domain of the t-SNARE Sso1p, *Nature structural biology* 5 (1998) 793–802.
- [227] T. Weber, B.V. Zemelman, J.A. McNew, B. Westermann, M. Gmachl, F. Parlati, T.H. Söllner, J.E. Rothman, SNAREpins: minimal machinery for membrane fusion, *Cell* 92 (1998) 759–772.
- [228] D. Bar-On, S. Wolter, S. van de Linde, M. Heilemann, G. Nudelman, E. Nachliel, M. Gutman, M. Sauer, U. Ashery, Super-resolution imaging reveals the internal architecture of nano-sized syntaxin clusters, *Journal of Biological Chemistry* 287 (2012) 27158–27167.
- [229] C. Rickman, C.N. Medine, A.R. Dun, D.J. Moulton, O. Mandula, N.D. Halemani, S.O. Rizzoli, L.H. Chamberlain, R.R. Duncan, t-SNARE protein conformations patterned by the lipid microenvironment, *Journal of Biological Chemistry* 285 (2010) 13535–13541.
- [230] S. Pribicevic, A.C. Graham, D.S. Cafiso, A. Perez-Lara, R. Jahn, Intermediate steps in the formation of neuronal SNARE complexes, *The Journal of biological chemistry* (2024) 107591.
- [231] M.A. Poirier, J.C. Hao, P.N. Malkus, C. Chan, M.F. Moore, D.S. King, M.K. Bennett, Protease resistance of syntaxin.SNAP-25.VAMP complexes. Implications for assembly and structure, *The Journal of biological chemistry* 273 (1998) 11370–11377.
- [232] D. Dawidowski, D.S. Cafiso, Allosteric control of syntaxin 1a by Munc18-1: characterization of the open and closed conformations of syntaxin, *Biophysical Journal* 104 (2013) 1585–1594.
- [233] M. Hardenberg, A. Horvath, V. Ambrus, M. Fuxreiter, M. Vendruscolo, Widespread occurrence of the droplet state of proteins in the human proteome, *Proceedings of the National Academy of Sciences of the United States of America* 117 (2020) 33254–33262.
- [234] A. Agarwal, A. Chandran, F. Raza, I.-M. Ungureanu, C. Hilcenko, K. Stott, N.A. Bright, N. Morone, A.J. Warren, J. Lautenschläger, VAMP2 regulates phase separation of α -synuclein, *Nature cell biology* 26 (2024) 1296–1308.
- [235] M. Zhu, H. Xu, Y. Jin, X. Kong, B. Xu, Y. Liu, H. Yu, Synaptotagmin-1 undergoes phase separation to regulate its calcium-sensitive oligomerization, *The Journal of Cell Biology* 223 (2024).
- [236] T. Yoshida, K.-I. Takenaka, H. Sakamoto, Y. Kojima, T. Sakano, K. Shibayama, K. Nakamura, K. Hanawa-Suetsugu, Y. Mori, Y. Hirabayashi, K. Hirose, S. Takamori, Compartmentalization of soluble endocytic proteins in synaptic vesicle clusters by phase separation, *iScience* 26 (2023) 106826.
- [237] H. Wu, M. Fuxreiter, The Structure and Dynamics of Higher-Order Assemblies: Amyloids, Signalosomes, and Granules, *Cell* 165 (2016) 1055–1066.
- [238] Y.J. Wang, F. Li, N. Rodriguez, X. Lafosse, C. Gourier, E. Perez, F. Pincet, Snapshot of sequential SNARE assembling states between membranes shows that N-terminal transient assembly initializes fusion, *Proceedings of the National Academy of Sciences of the United States of America* 113 (2016) 3533–3538.

- [239] F. Li, N. Tiwari, J.E. Rothman, F. Pincet, Kinetic barriers to SNAREpin assembly in the regulation of membrane docking/priming and fusion, *Proceedings of the National Academy of Sciences of the United States of America* 113 (2016) 10536–10541.
- [240] K.M. Misura, L.C. Gonzalez, A.P. May, R.H. Scheller, W.I. Weis, Crystal structure and biophysical properties of a complex between the N-terminal SNARE region of SNAP25 and syntaxin 1a, *The Journal of biological chemistry* 276 (2001) 41301–41309.
- [241] N. Calakos, M.K. Bennett, K.E. Peterson, R.H. Scheller, Protein-protein interactions contributing to the specificity of intracellular vesicular trafficking, *Science (New York, N.Y.)* 263 (1994) 1146–1149.
- [242] J. Pevsner, S.C. Hsu, J.E. Braun, N. Calakos, A.E. Ting, M.K. Bennett, R.H. Scheller, Specificity and regulation of a synaptic vesicle docking complex, *Neuron* 13 (1994) 353–361.
- [243] J. Hazzard, T.C. Südhof, J. Rizo, NMR analysis of the structure of synaptobrevin and of its interaction with syntaxin, *Journal of biomolecular NMR* 14 (1999) 203–207.
- [244] R. Ossig, H.D. Schmitt, G.B. de, D. Riedel, S. Keränen, H. Ronne, H. Grubmüller, R. Jahn, Exocytosis requires asymmetry in the central layer of the SNARE complex, *The EMBO journal* 19 (2000).
- [245] Y. Lai, U.B. Choi, J. Leitz, H.J. Rhee, C. Lee, B. Altas, M. Zhao, R.A. Pfuetzner, A.L. Wang, N. Brose, J. Rhee, A.T. Brunger, Molecular Mechanisms of Synaptic Vesicle Priming by Munc13 and Munc18, *Neuron* 95 (2017) 591-607.e10.
- [246] D. Fasshauer, W. Antonin, M. Margittai, S. Pabst, R. Jahn, Mixed and non-cognate SNARE complexes. Characterization of assembly and biophysical properties, *Journal of Biological Chemistry* 274 (1999) 15440–15446.
- [247] B. Yang, L. Gonzalez, R. Prekeris, M. Steegmaier, R.J. Advani, R.H. Scheller, SNARE interactions are not selective. Implications for membrane fusion specificity, *Journal of Biological Chemistry* 274 (1999) 5649–5653.
- [248] K. Wiederhold, D. Fasshauer, Is assembly of the SNARE complex enough to fuel membrane fusion?, *Journal of Biological Chemistry* 284 (2009) 13143–13152.
- [249] J. Mertins, J. Finke, R. Sies, K.M. Rink, J. Hasenauer, T. Lang, The mesoscale organization of syntaxin 1A and SNAP25 is determined by SNARE-SNARE interactions, *eLife* 10 (2021).
- [250] P. Zhong, Y.A. Chen, D. Tam, D. Chung, R.H. Scheller, G.P. Miljanich, An alpha-helical minimal binding domain within the H3 domain of syntaxin is required for SNAP-25 binding, *Biochemistry* 36 (1997).
- [251] X. Huang, S. Sun, X. Wang, F. Fan, Q. Zhou, S. Lu, Y. Cao, Q.-W. Wang, M.-Q. Dong, J. Yao, S.-F. Sui, Mechanistic insights into the SNARE complex disassembly, *Science advances* 5 (2019) eaau8164.
- [252] D. Parisotto, M. Pfau, A. Scheutzw, K. Wild, M.P. Mayer, J. Malsam, I. Sinning, T.H. Söllner, An extended helical conformation in domain 3a of Munc18-1 provides a template for SNARE (soluble N-ethylmaleimide-sensitive factor attachment protein receptor) complex assembly, *Journal of Biological Chemistry* 289 (2014) 9639–9650.
- [253] D. Schütz, F. Zilly, T. Lang, R. Jahn, D. Bruns, A dual function for Munc-18 in exocytosis of PC12 cells, *The European journal of neuroscience* 21 (2005) 2419–2432.
- [254] B.G. Wilhelm, S. Mandad, S. Truckenbrodt, K. Kröhnert, C. Schäfer, B. Rammner, S.J. Koo, G.A. Claßen, M. Krauss, V. Haucke, H. Urlaub, S.O. Rizzoli, Composition of isolated synaptic boutons reveals the amounts of vesicle trafficking proteins, *Science (New York, N.Y.)* 344 (2014) 1023–1028.

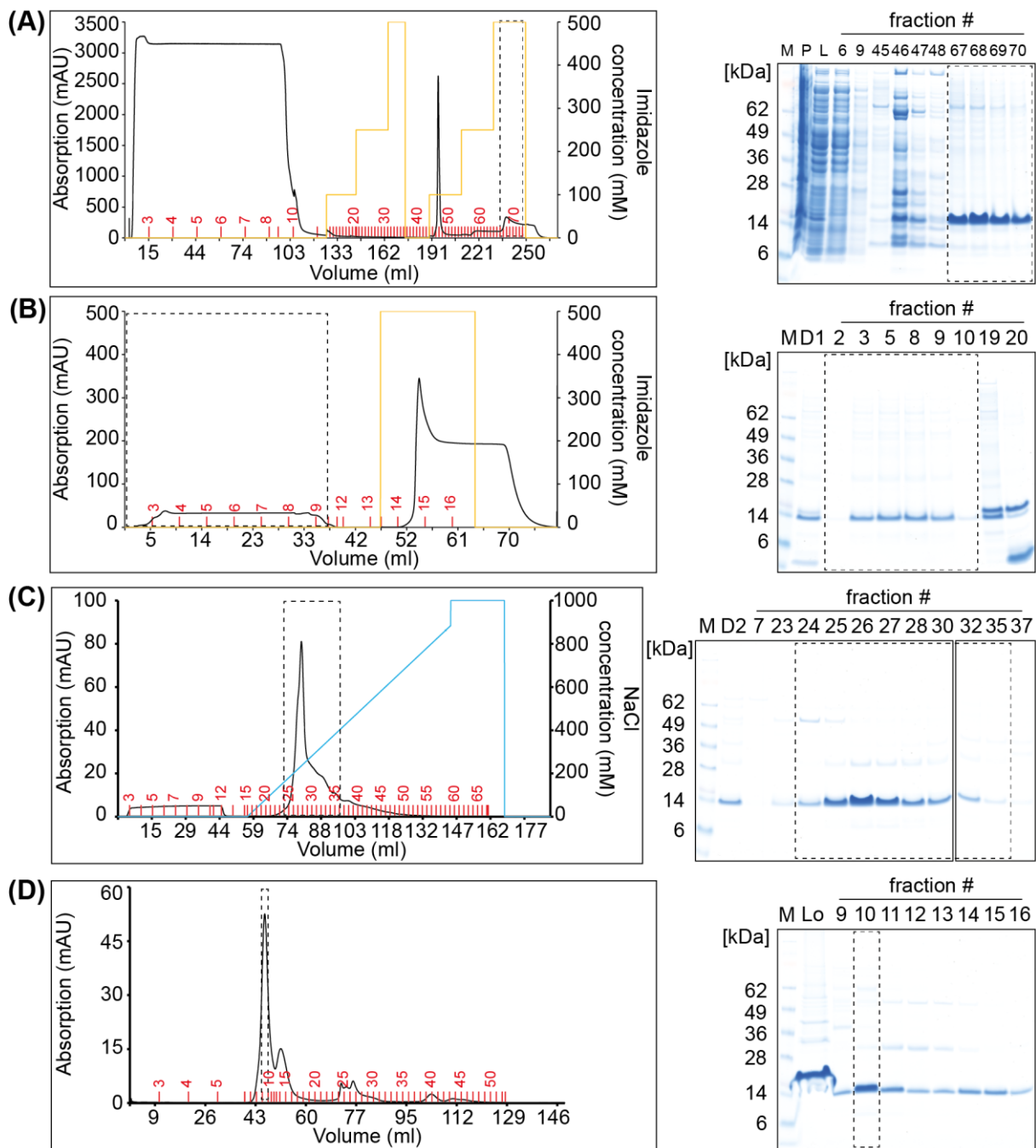
- [255] F.E. Zilly, J.B. Sørensen, R. Jahn, T. Lang, Munc18-bound syntaxin readily forms SNARE complexes with synaptobrevin in native plasma membranes, *PLoS biology* 4 (2006) e330.
- [256] M.E. Bowen, K. Weninger, A.T. Brunger, S. Chu, Single molecule observation of liposome-bilayer fusion thermally induced by soluble N-ethyl maleimide sensitive-factor attachment protein receptors (SNAREs), *Biophysical Journal* 87 (2004) 3569–3584.
- [257] G. van den Bogaart, M.G. Holt, G. Bunt, D. Riedel, F.S. Wouters, R. Jahn, One SNARE complex is sufficient for membrane fusion, *Nature structural & molecular biology* 17 (2010) 358–364.
- [258] E. Karatekin, J. Di Giovanni, C. Iborra, J. Coleman, B. O’Shaughnessy, M. Seagar, J.E. Rothman, A fast, single-vesicle fusion assay mimics physiological SNARE requirements, *Proceedings of the National Academy of Sciences of the United States of America* 107 (2010) 3517–3521.
- [259] M.K. Domanska, V. Kiessling, A. Stein, D. Fasshauer, L.K. Tamm, Single vesicle millisecond fusion kinetics reveals number of SNARE complexes optimal for fast SNARE-mediated membrane fusion, *Journal of Biological Chemistry* 284 (2009) 32158–32166.
- [260] Y. Hua, R.H. Scheller, Three SNARE complexes cooperate to mediate membrane fusion, *Proceedings of the National Academy of Sciences of the United States of America* 98 (2001) 8065–8070.
- [261] J.E. Keller, F. Cai, E.A. Neale, Uptake of botulinum neurotoxin into cultured neurons, *Biochemistry* 43 (2004) 526–532.
- [262] R. Mohrmann, H. de Wit, M. Verhage, E. Neher, J.B. Sørensen, Fast vesicle fusion in living cells requires at least three SNARE complexes, *Science (New York, N.Y.)* 330 (2010) 502–505.
- [263] M. Bera, S. Ramakrishnan, J. Coleman, S.S. Krishnakumar, J.E. Rothman, Molecular determinants of complexin clamping and activation function, *eLife* 11 (2022).
- [264] J.A. Martin, Z. Hu, K.M. Fenz, J. Fernandez, J.S. Dittman, Complexin has opposite effects on two modes of synaptic vesicle fusion, *Current biology: CB* 21 (2011) 97–105.
- [265] J. Rizo, L. Sari, Y. Qi, W. Im, M.M. Lin, All-atom molecular dynamics simulations of Synaptotagmin-SNARE-complexin complexes bridging a vesicle and a flat lipid bilayer, *eLife* 11 (2022).
- [266] F. Li, D. Kümmel, J. Coleman, K.M. Reinisch, J.E. Rothman, F. Pincet, A half-zippered SNARE complex represents a functional intermediate in membrane fusion, *Journal of the American Chemical Society* 136 (2014) 3456–3464.
- [267] M.R. Wenk, P. de Camilli, Protein-lipid interactions and phosphoinositide metabolism in membrane traffic: insights from vesicle recycling in nerve terminals, *Proceedings of the National Academy of Sciences of the United States of America* 101 (2004) 8262–8269.
- [268] Y.J. Kim, M.-L. Guzman-Hernandez, E. Wisniewski, T. Balla, Phosphatidylinositol-Phosphatidic Acid Exchange by Nir2 at ER-PM Contact Sites Maintains Phosphoinositide Signaling Competence, *Developmental cell* 33 (2015) 549–561.
- [269] G. Paradies, V. Paradies, F.M. Ruggiero, G. Petrosillo, Role of Cardiolipin in Mitochondrial Function and Dynamics in Health and Disease: Molecular and Pharmacological Aspects, *Cells* 8 (2019).
- [270] K.C. Courtney, L. Wu, T. Mandal, M. Swift, Z. Zhang, M. Alaghemandi, Z. Wu, M.M. Bradberry, C. Deo, L.D. Lavis, N. Volkmann, D. Hanein, Q. Cui, H. Bao, E.R. Chapman, The complexin C-terminal amphipathic helix stabilizes the fusion pore open state by sculpting membranes, *Nat Struct Mol Biol* 29 (2022) 97–107.

6 Supplement



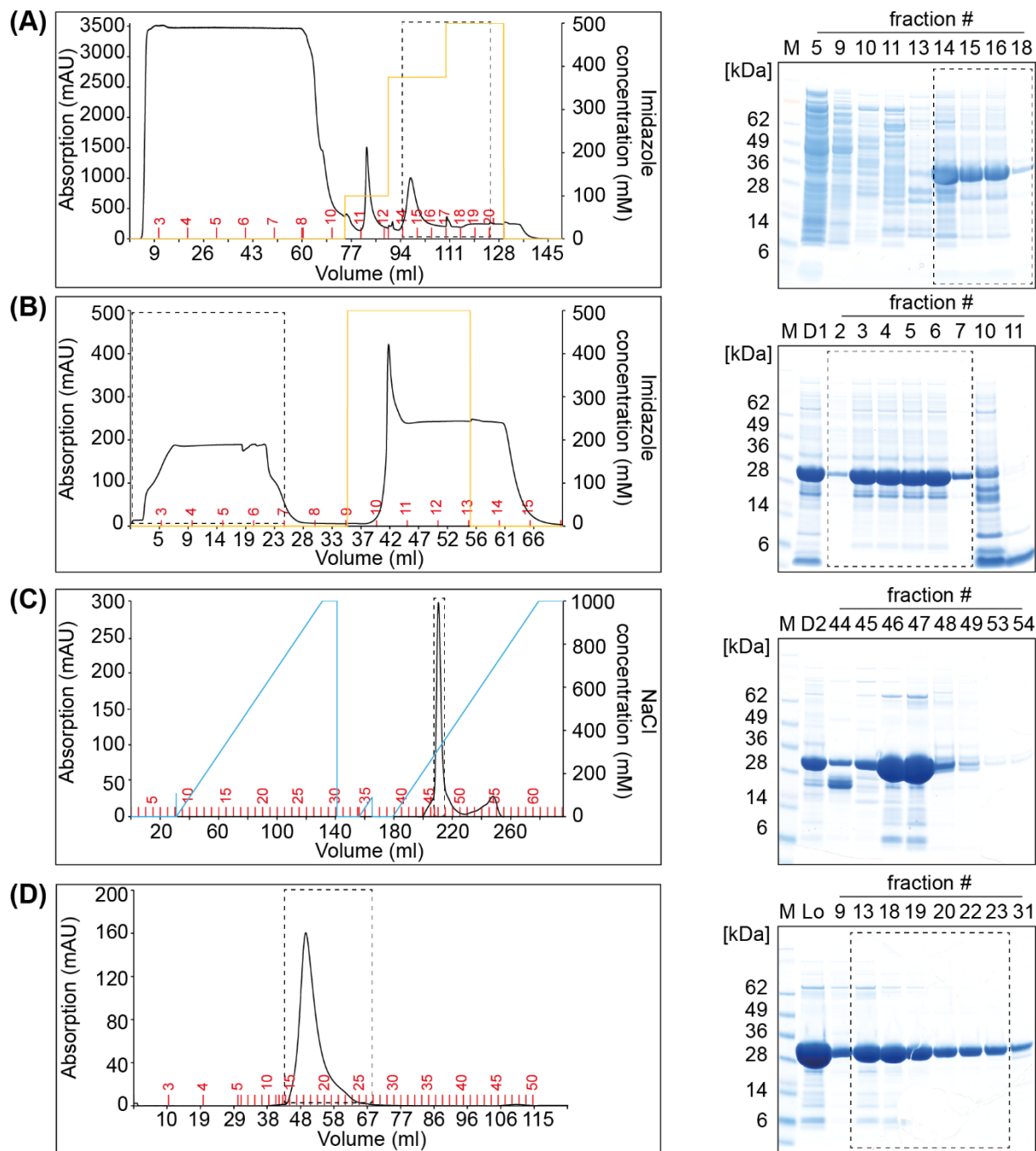
Supplementary Figure 1. Plasmid map of pET28a.

Cleavage sites of restriction enzymes with the respective name of the enzyme, multiple cloning site (MCS), thrombin cleavage site, N-terminal hexa-histidine tag (6xHis), kanamycin resistance (KanR) and lactose operon (lacI) are encoded and labelled. Encoded sequences are shown as arrows. All proteins were expressed using the same plasmid architecture. (created by SnapGene)



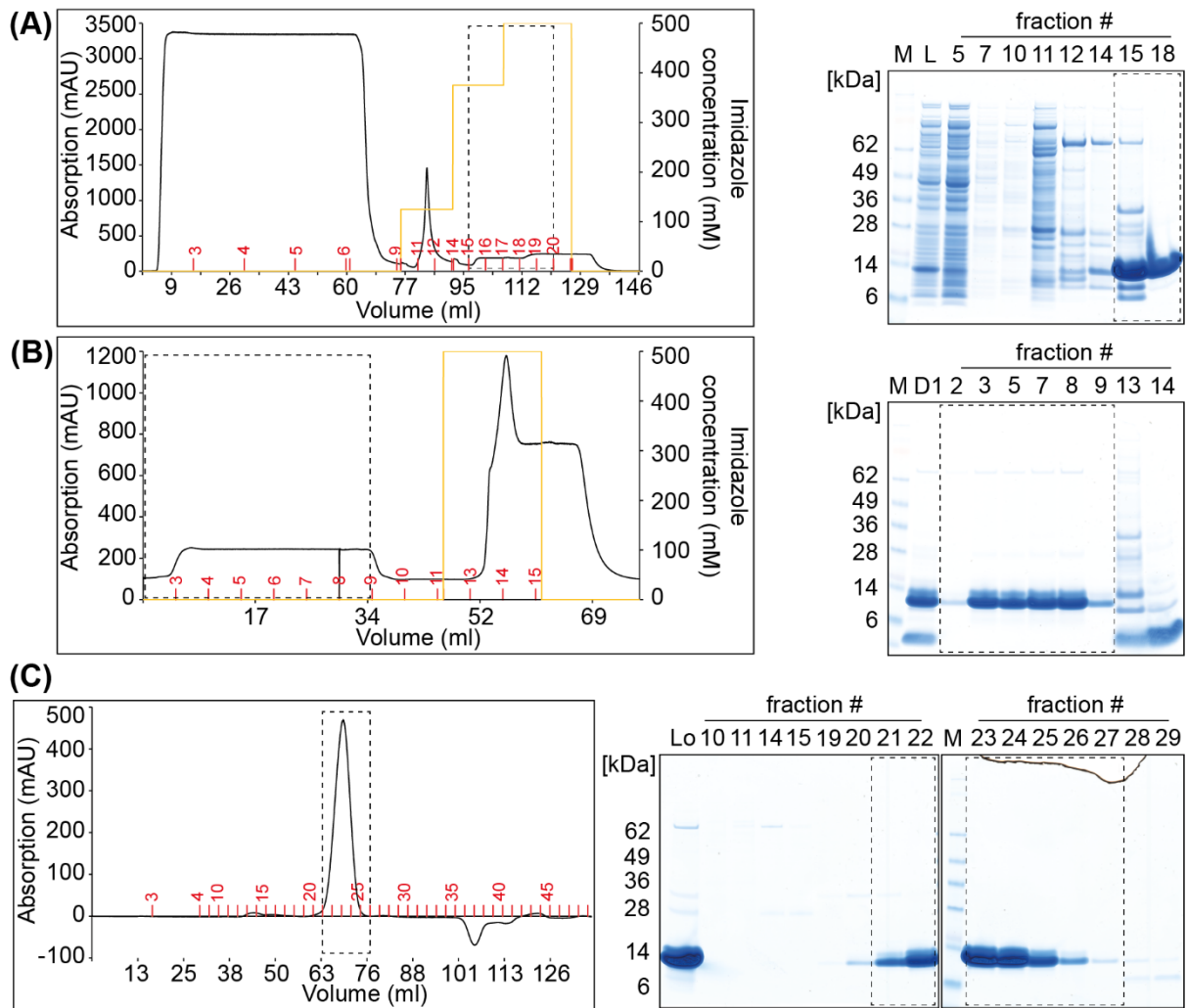
Supplementary Figure 2. Purification of Syb(FL).

Chromatograms (lhs) and gel electrophoresis of selected fractions (rhs) of the purification of Syb(FL) by (A) IMAC (B) IMAC after thrombin cleavage (C) SCX and (D) SEC are shown. Fractions that were combined for the following purification step are indicated by dotted lines. M: marker, P: pellet, L: lysate, D1: dialysate after thrombin cleavage reaction, D2: dialysate after second IMAC, Lo: concentrated fractions after SCX



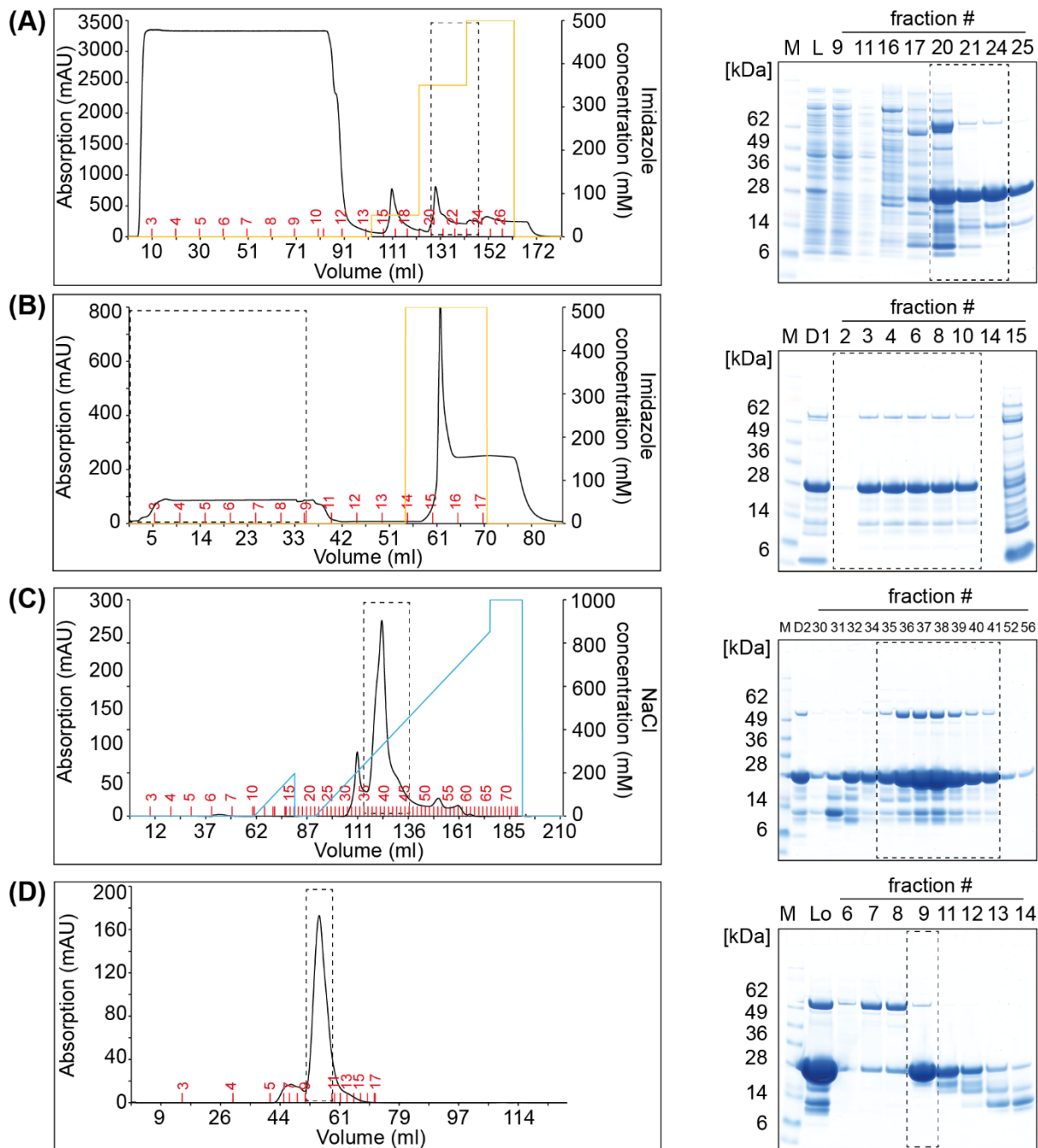
Supplementary Figure 3. Purification of Stx(1-262).

Chromatograms (lhs) and gel electrophoresis of selected fractions (rhs) of the purification of Stx(1-262) by **(A)** IMAC **(B)** IMAC after thrombin cleavage **(C)** AEC and **(D)** SEC are shown. Fractions that were combined for the following purification step are indicated by dotted lines. M: marker, L: lysate, D1: dialysate after thrombin cleavage reaction, D2: dialysate after second IMAC, Lo: concentrated fractions after AEC



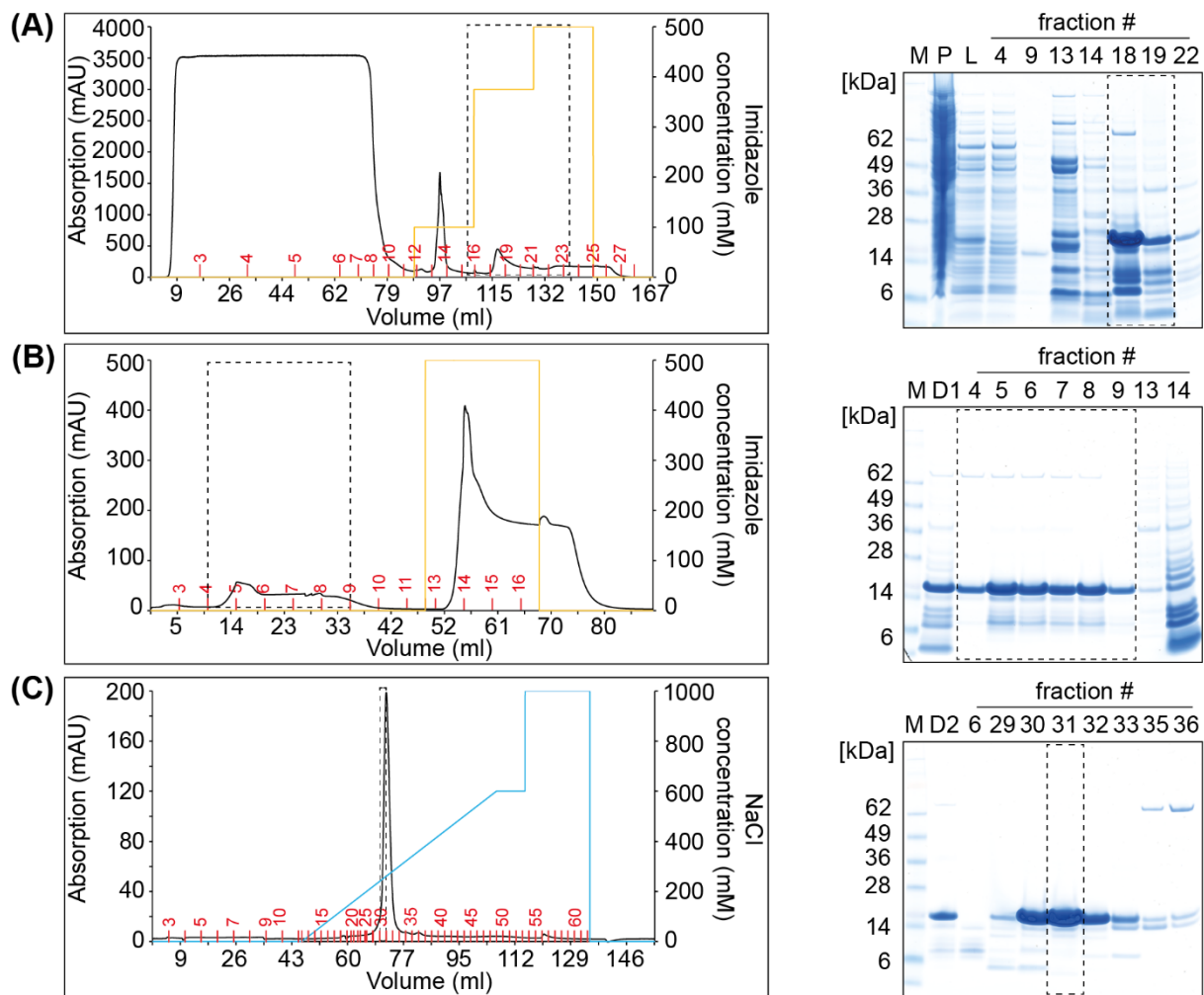
Supplementary Figure 4. Purification of SNAP25(1-83).

Chromatograms (lhs) and gel electrophoresis of selected fractions (rhs) of the purification of SNAP25(1-83) by (A) IMAC (B) IMAC after thrombin cleavage and (D) SEC are shown. Fractions that were combined for the following purification step are indicated by dotted lines. M: marker, L: lysate, D1: dialysate after thrombin cleavage reaction, Lo: concentrated fractions after AEC



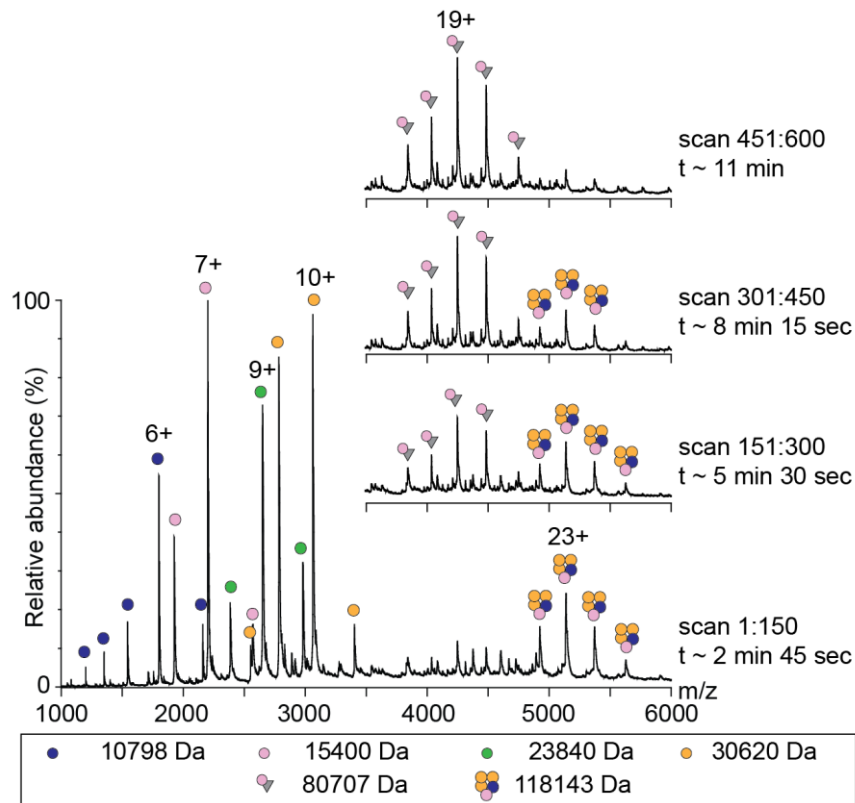
Supplementary Figure 5. Purification of SNAP25(CtoS).

Chromatograms (lhs) and gel electrophoresis of selected fractions (rhs) of the purification of SNAP25(CtoS) by (A) IMAC (B) IMAC after thrombin cleavage (C) AEC and (D) SEC are shown. Fractions that were combined for the following purification step are indicated by dotted lines. M: marker, L: lysate, D1: dialysate after thrombin cleavage reaction, D2: dialysate after second IMAC, Lo: concentrated fractions after AEC



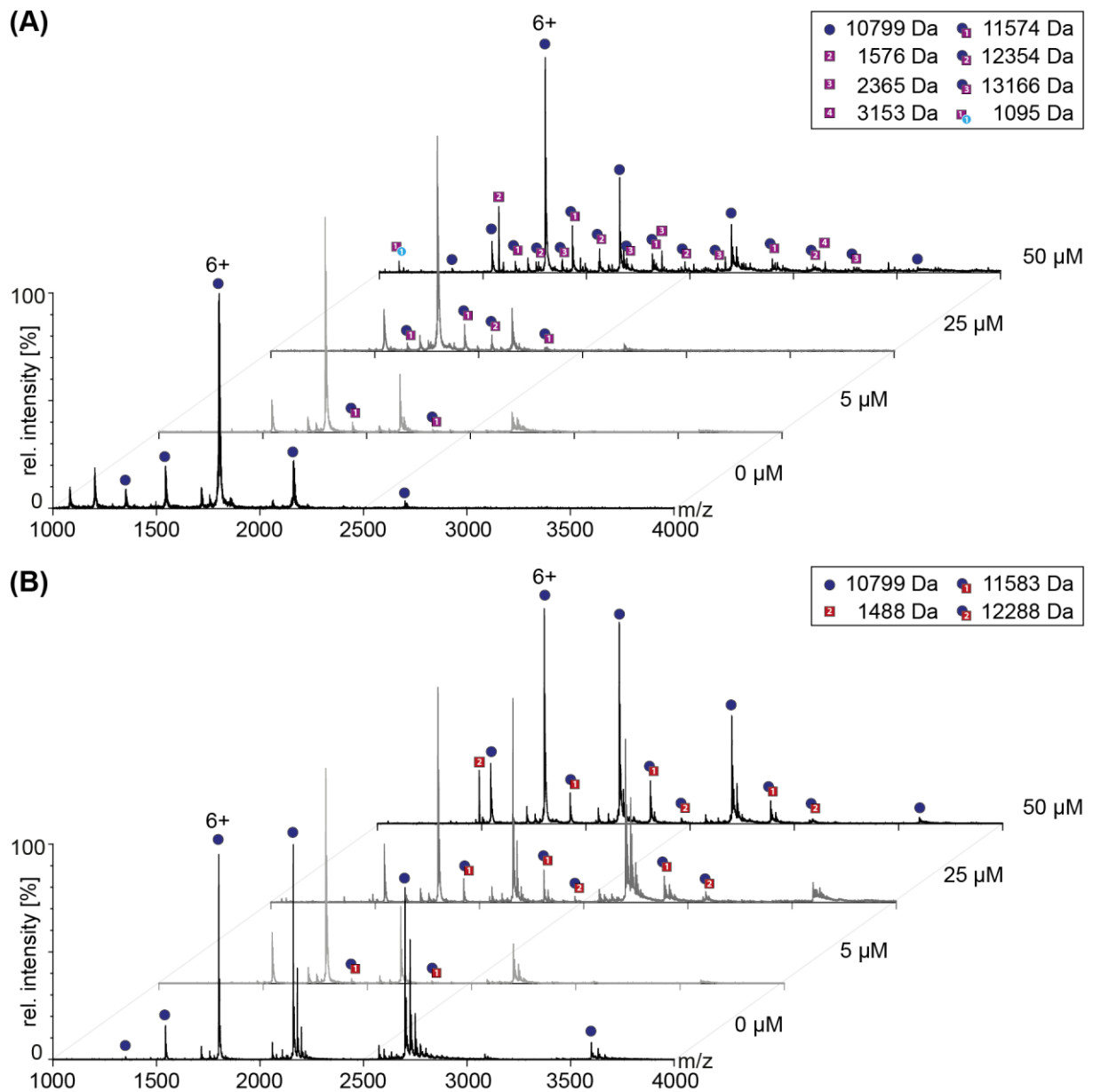
Supplementary Figure 6. Purification of Cpx1.

Chromatograms (lhs) and gel electrophoresis of selected fractions (rhs) of the purification of Cpx1 by (A) IMAC (B) IMAC after thrombin cleavage (C) AEC are shown. Fractions that were combined for the following purification step are indicated by dotted lines. M: marker, P: pellet, L: lysate, D1: dialysate after thrombin cleavage reaction, D2: dialysate after second IMAC



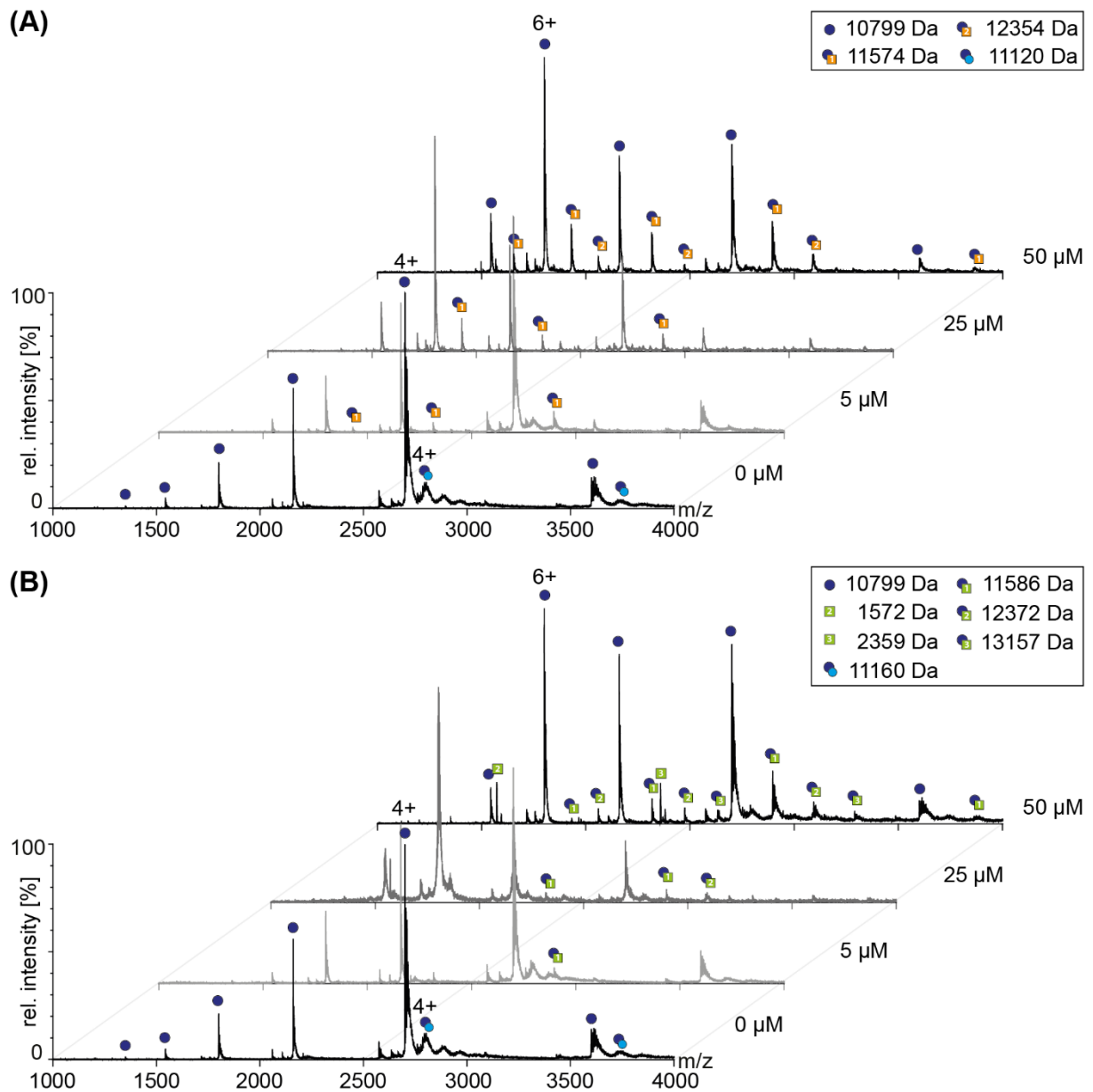
Supplementary Figure 7. Rearrangement of the ternary Syb(1-96):Stx(1-262):Cpx1 complex.

Syb(1-96), Stx(1-262) and Cpx1 were pre-incubated forming the ternary 1:3:1 complex (main panel, yellow-blue-pink circles). Upon addition of SNAP25(CtoS), the ternary SNARE complex binding one Cpx1 molecule is formed (grey triangle-pink circle). Rearrangements of the pre-assembled complex occur over several minutes (scan time 1s, inter scan time 0.1 s); at incubation times above 11 minutes, the SNARE:Cpx1 complex is exclusively observed.



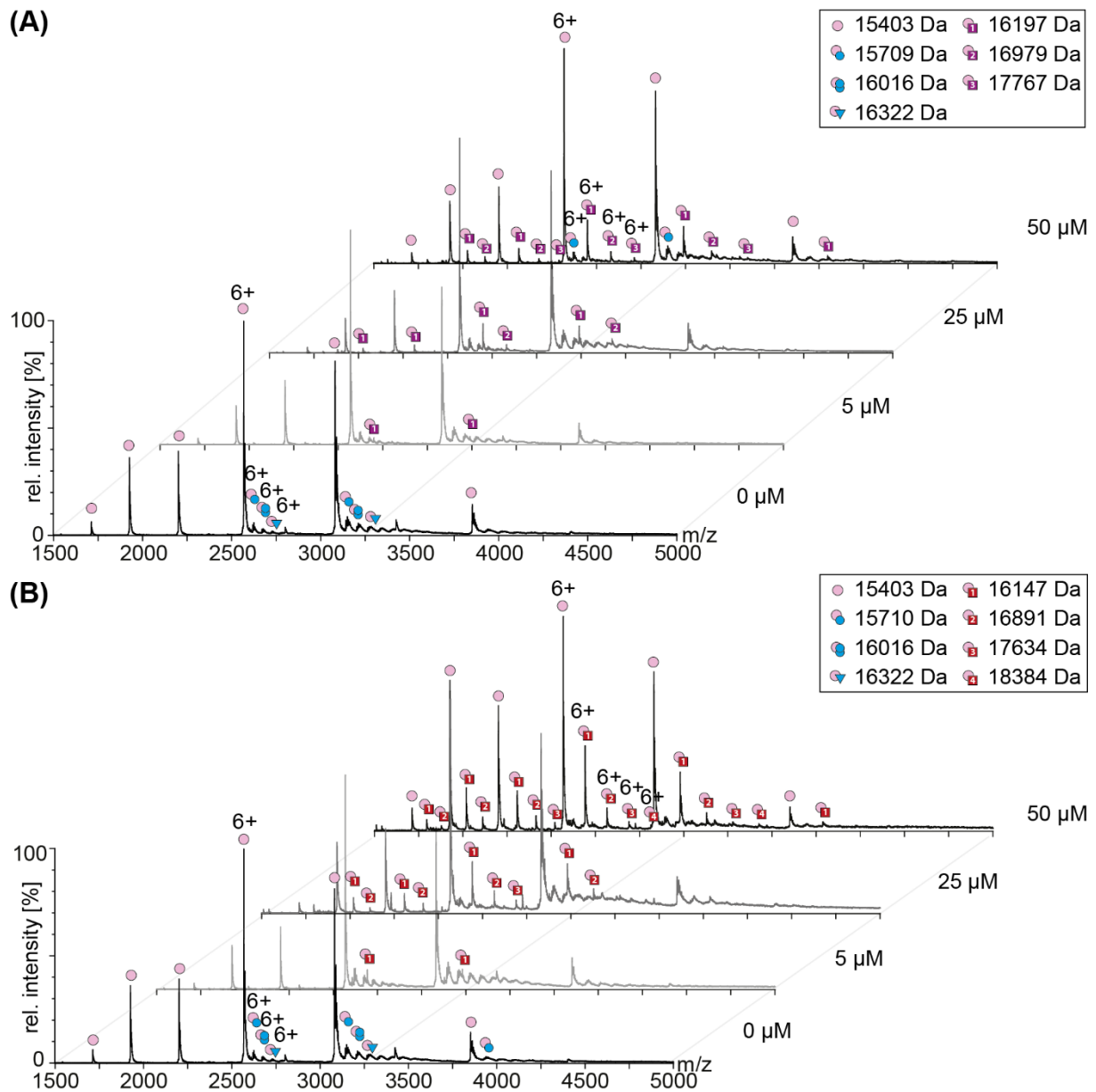
Supplementary Figure 8. DOPS and DOPE binding of Syb(1-96) analysed by native MS.

5 μM Syb(1-96) were mixed with increasing lipid concentration in 0.5 % C8E4. Lipid binding was analysed by native MS. Charge state distributions corresponding in mass to monomeric Syb(1-96) (blue circle), lipid clusters (coloured squares with number of lipids), DOPS:C8E4 clusters (light blue circle purple square) and Syb(1-96):lipid complexes with (A) DOPS (blue circle purple square) and (B) DOPE (blue circle red square) lipids are assigned.



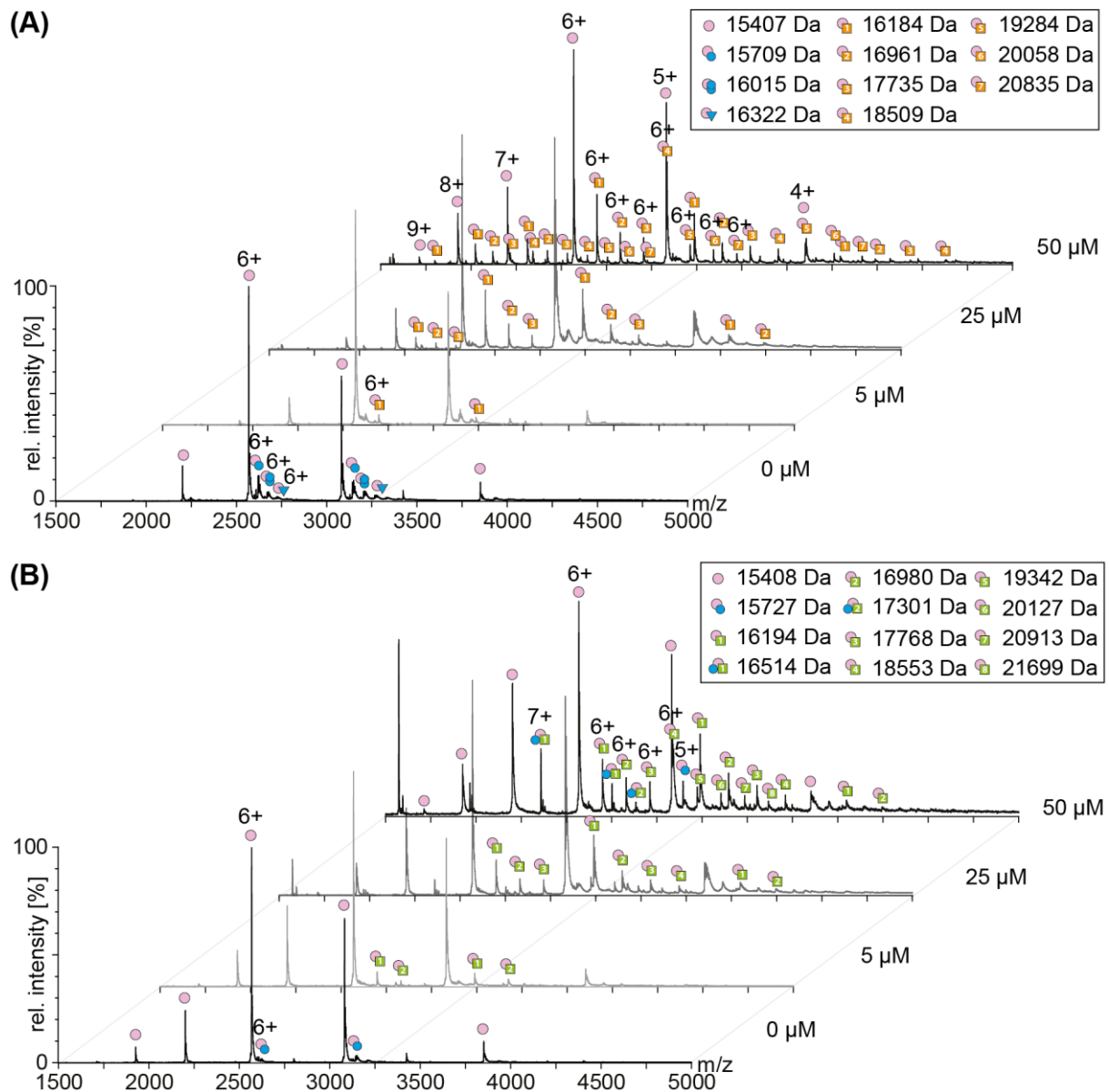
Supplementary Figure 9. DOPG and DOPC binding of Syb(1-96) analysed by native MS.

5 μM Syb(1-96) were mixed with increasing lipid concentration in 0.5 % C8E4. Lipid binding was analysed by native MS. Charge state distributions corresponding in mass to monomeric Syb(1-96) (blue circle), lipid clusters (coloured squares with number of lipids), Syb(1-96):C8E4 complexes (blue and light blue circles) and Syb(1-96):lipid complexes with (A) DOPG (blue circle orange square) and (B) DOPC (blue circle green square) lipids are assigned.



Supplementary Figure 10. DOPS and DOPE binding of Cpx1 analysed by native MS.

5 μM Cpx1 were mixed with increasing lipid concentration in 0.5 % C8E4. Lipid binding was analysed by native MS. Charge state distributions corresponding in mass to monomeric Cpx1 (light pink circle), Cpx1:C8E4 complexes (light pink and light blue circle and triangle) and Cpx1:lipid complexes with **(A)** DOPS (light pink circle purple square) and **(B)** DOPE (light pink circle red square) lipids are assigned.



Supplementary Figure 11. DOPG and DOPC binding of Cpx1 analysed by native MS.

5 μM Cpx1 were mixed with increasing lipid concentration in 0.5 % C8E4. Lipid binding was analysed by native MS. Charge state distributions corresponding in mass to monomeric Cpx1 (light pink circle), Cpx1:C8E4 coplexes (light pink and light blue circle and triangle), Cpx1:C8E4:lipid complexes (light pink and light blue circles green square) and Cpx1:lipid complexes with **(A)** DOPG (light pink circle orange square) and **(B)** DOPC (light pink circle green square) lipids are assigned.

Supplementary Table 1. Incubation ratios of SNARE proteins and Cpx1.

SNAP25(CtoS)	SNAP25(1-83)	Stx(1-262)	Syb(1-96)	Cpx1
1		1		
1		2		
1			1	
1			2	
2			1	
	1		1	
1	1		1	
		1	1	
1		1	1	
1				1
		1		1
			1	1
1		2		1
		1	1	1
1			2	1
1		1	1	1

Supplementary Table 2. Protein identification. The hit number, the protein name (and database accession number of contaminating *Escherichia coli* proteins), the number of identified peptide sequences, the observed sequence coverage and the MaxQuant (MQ) protein score are given for each protein in the different samples.

Protein sample	Hit	Protein	Peptide sequences	Sequence coverage [%]	MQ Score
Cpx1	1	Cpx1	19	88.3	323.31
	2	Serine hydroxymethyltransferase (A0A140N8X9)	6	19.9	86.90
	3	Histidine triad (HIT) protein (A0A140ND09)	7	96.6	83.33
	4	Dihydrolipoyl dehydrogenase (A0A140NBS3)	6	15.0	44.00
	5	ATP synthase subunit alpha (A0A140ND72)	4	9.6	30.45
SNAP25(CtoS)	1	SNAP25(CtoS)	38	94.7	323.31
	2	Chaperone protein DnaK (A0A140NFV3)	46	74.5	323.31
	3	Elongation factor Tu (A0A140NCI6; A0A140N6W0)	15	52.8	130.83
	4	ATP synthase subunit beta (A0A140NHS0)	13	38.0	107.06
	5	Dihydrolipoyl dehydrogenase (A0A140NBS3)	12	34.2	106.18
SNAP25(1-83)	1	SNAP25(1-83) (P0A9A9)	20	100.0	323.31
	2	Ferric uptake regulation protein (P0ABA6)	6	66.9	105.27
	3	ATP synthase gamma chain (P37655)	1	4.9	6.70
	4	Putative cellulose biosynthesis protein BcsQ (P0AEX9)	1	5.8	6.60
	5	Maltose-binding periplasmic protein (P0AE18)	6	21.0	45.83
Stx(1-262)	1	Stx(1-262)	33	83.8	323.31
	2	Chaperone protein DnaK (A0A140NFV3)	32	57.8	267.96
	3	SNAP25(CtoS)	18	70.8	224.46
	4	ATP synthase subunit beta (A0A140NHS0)	10	29.3	74.34
	5	30S ribosomal protein S1 (A0A140NBA5)	8	18.5	54.46
Syb(1-96)	1	Syb(1-96)	16	94.9	323.31
	2	Ferric uptake regulation protein (A0A140NE13)	8	65.5	117.29

Protein sample	Hit	Protein	Peptide sequences	Sequence coverage [%]	MQ Score
Syb(1-96)	3	PTS system, mannose/fructose/sorbose family, IIA subunit (A0A140NBF2)	6	24.5	49.61
	4	SNAP25 (CtoS)	4	26.3	37.39
	5	Outer membrane chaperone Skp (OmpH) (A0A140NFE9)	2	14.9	31.55
Syb(FL)	1	Syb(FL)	17	74.8	323.31
	2	ATP synthase subunit alpha (P0ABB0)	31	72.1	323.31
	3	ATP synthase subunit beta (P0ABB4)	31	88.3	323.31
	4	Aspartate carbamoyltransferase regulatory chain (P0A7F3)	12	83.7	283.36
	5	Elongation factor Tu 2 (P0CE48)	25	83.5	323.31

Supplementary Table 3. Cross-links identified in SNAP25(CtoS). The protein names, the peptide sequences of the cross-linked peptides and the cross-linked residues are given. Cross-linked residues are highlighted (bold) in the peptide sequences. The pLink score and the number of acquired tandem mass spectra are given for each cross-link in each replicate.

protein 1	protein 2	sequence 1	sequence 2	residue 1	residue 2	replicate 1		replicate 2		replicate 3	
						score	# spectra	score	# spectra	score	# spectra
homomultimeric cross-links											
SN25(CtoS)	SN25(CtoS)	MLQLVEESKDAGIR	MLQLVEES K DAGIR	43	43	4,15E-06	14			1,12E-19	61
SN25(CtoS)	SN25(CtoS)	VEEGMNHINQDMKEAEK	VEEGMNHINQDMKEAEK	75	75	5,46E-04	13				
SN25(CtoS)	SN25(CtoS)	VEEGMNHINQDMKEAEK	EAEK N LK	75	79			1,99E-03	18		
SN25(CtoS)	SN25(CtoS)	EAEK N LK	N L KDLGK	79	82			1,06E-03	13		
SN25(CtoS)	SN25(CtoS)	N L KDLGK	N L KDLGK	82	82	3,81E-12	58	1,51E-10	31		
SN25(CtoS)	SN25(CtoS)	N L KDLGKSSGLFISPSNK	N L KDLGKSSGLFISPSNK	82	86	2,78E-07	82	4,98E-05	47		
SN25(CtoS)	SN25(CtoS)	DLG K SSGLFISPSNK	DLG K SSGLFISPSNK	86	86	6,32E-06	23	3,01E-06	11		
SN25(CtoS)	SN25(CtoS)	DLG K SSGLFISPSNK	S SGLFISPSNK	86	87	3,08E-04	4	9,01E-03	10		
SN25(CtoS)	SN25(CtoS)	DLG K SSGLFISPSNK	S SGLFISPSNK	86	93	2,37E-05	26	1,50E-03	12		
SN25(CtoS)	SN25(CtoS)	DLG K SSGLFISPSNK	S SGLFISPSNK	86	95	3,78E-04	11				
SN25(CtoS)	SN25(CtoS)	DLG K SSGLFISPSNK	S SGLFISPSN K LK	86	97	3,10E-06	44	8,20E-04	34		
SN25(CtoS)	SN25(CtoS)	S SGLFISPSNK	S SGLFISPSNK	87	87			6,03E-04	7		
SN25(CtoS)	SN25(CtoS)	S SGLFISPSNK	S SGLFISPSNK	93	87	1,33E-08	49				
SN25(CtoS)	SN25(CtoS)	S SGLFISPSNK	S SGLFISPSNK	93	93	2,41E-05	11				
SN25(CtoS)	SN25(CtoS)	S SGLFISPSN K LK	S SGLFISPSNK	97	87	2,22E-05	5	5,31E-06	5		
SN25(CtoS)	SN25(CtoS)	S SGLFISPSN K LK	S SGLFISPSNK	97	93			1,66E-01	3		
SN25(CtoS)	SN25(CtoS)	S SGLFISPSN K LK	S SGLFISPSN K LK	97	97	1,36E-05	34	3,23E-05	50		
SN25(CtoS)	SN25(CtoS)	S SGLFISPSN K LK	L K SSDAYK	97	99	9,19E-08	58	2,78E-07	26		
SN25(CtoS)	SN25(CtoS)	L K SSDAY K K	L K SSDAYK	99	99	2,12E-07	32				
SN25(CtoS)	SN25(CtoS)	SSDAY K K	S SSDAYK	105	100			7,85E-11	25		
SN25(CtoS)	SN25(CtoS)	SSDAY K K	SSDAY K K	105	105	2,01E-16	38	4,69E-11	35		
SN25(CtoS)	SN25(CtoS)	K AWGNNQDGVVASQPAR	SSDAY K K	106	105	3,15E-07	50	5,89E-07	31		
SN25(CtoS)	SN25(CtoS)	K AWGNNQDGVVASQPAR	K AWGNNQDGVVASQPAR	106	106	1,59E-08	71	2,55E-11	38	9,18E-17	2
SN25(CtoS)	SN25(CtoS)	IME K ADSNK	IME K ADSNK	187	187			5,95E-08	39		
SN25(CtoS)	SN25(CtoS)	IME K ADSNK	ADSN K TR	187	192	7,31E-06	32	3,44E-09	27		
intramolecular cross-links											
SN25(CtoS)	SN25(CtoS)	ADQLADES L ESTR	L K SSDAYK	31	99	1,05E-06	8	4,88E-06	8		

protein 1	protein 2	sequence 1	sequence 2	residue 1	residue 2	replicate 1		replicate 2		replicate 3	
						score	# spectra	score	# spectra	score	# spectra
SN25(CtoS)	SN25(CtoS)	ADQLADESLESTR	SSDAYK	31	105			2,01E-04	3		
SN25(CtoS)	SN25(CtoS)	MLQLVEESKDAGIR	ADQLADESLESTR	42	28					1,09E-06	5
SN25(CtoS)	SN25(CtoS)	MLQLVEESKDAGIR	SSGLFISPSNK	42	87	5,28E-06	12	5,26E-05	5		
SN25(CtoS)	SN25(CtoS)	MLQLVEESKDAGIR	SSGLFISPSNK	42	93	3,05E-07	44				
SN25(CtoS)	SN25(CtoS)	MLQLVEESKDAGIR	SSGLFISPSNK	42	95	3,25E-07	11	3,37E-04	11		
SN25(CtoS)	SN25(CtoS)	MLQLVEESKDAGIR	SSDAYK	42	100	1,47E-07	13	6,38E-07	5		
SN25(CtoS)	SN25(CtoS)	MLQLVEESKDAGIR	ADQLADESLESTR	43	28					1,68E-06	2
SN25(CtoS)	SN25(CtoS)	MLQLVEESKDAGIR	EAEKNLK	43	79	5,05E-04	39				
SN25(CtoS)	SN25(CtoS)	MLQLVEESKDAGIR	NLKDLGK	43	82	1,13E-06	105	1,76E-05	96	2,11E-09	14
SN25(CtoS)	SN25(CtoS)	MLQLVEESKDAGIR	DLGKSSGLFISPSNK	43	86	4,94E-08	23	9,68E-05	25	6,53E-26	12
SN25(CtoS)	SN25(CtoS)	MLQLVEESKDAGIR	SSGLFISPSNKLK	43	97	3,53E-11	56	2,15E-05	81	3,47E-19	11
SN25(CtoS)	SN25(CtoS)	MLQLVEESKDAGIR	LKSSDAYK	43	99	1,33E-08	67	2,72E-14	70	1,26E-18	5
SN25(CtoS)	SN25(CtoS)	MLQLVEESKDAGIR	SSDAYK	43	100	2,78E-09	25	4,44E-06	9		
SN25(CtoS)	SN25(CtoS)	MLQLVEESKDAGIR	SSDAYK	43	105	2,28E-06	73	1,89E-06	54		
SN25(CtoS)	SN25(CtoS)	MLQLVEESKDAGIR	IMEKADSNK	43	187	6,93E-05	63	5,17E-06	148	7,69E-10	13
SN25(CtoS)	SN25(CtoS)	MLQLVEESKDAGIR	ADSNKTR	43	192	1,26E-03	22	4,62E-03	17		
SN25(CtoS)	SN25(CtoS)	TLVMLDEQGEQLDR	MLQLVEESKDAGIR	49	42					3,77E-12	14
SN25(CtoS)	SN25(CtoS)	TLVMLDEQGEQLDR	MLQLVEESKDAGIR	49	43					4,74E-06	1
SN25(CtoS)	SN25(CtoS)	VEEGMNHINQDMKEAEK	MLQLVEESKDAGIR	75	43	3,18E-06	32			1,75E-14	33
SN25(CtoS)	SN25(CtoS)	VEEGMNHINQDMKEAEK	TLVMLDEQGEQLDR	75	49					2,38E-12	5
SN25(CtoS)	SN25(CtoS)	VEEGMNHINQDMKEAEK	NLKDLGK	75	82	3,28E-04	98	5,31E-05	172	4,01E-09	21
SN25(CtoS)	SN25(CtoS)	VEEGMNHINQDMKEAEK	SSGLFISPSNKLK	75	97	2,01E-06	22				
SN25(CtoS)	SN25(CtoS)	VEEGMNHINQDMKEAEK	LKSSDAYK	75	99	2,30E-04	32	5,40E-07	64		
SN25(CtoS)	SN25(CtoS)	VEEGMNHINQDMKEAEK	SSDAYK	75	100			8,97E-06	18		
SN25(CtoS)	SN25(CtoS)	VEEGMNHINQDMKEAEK	SSDAYK	75	105	7,52E-04	24	7,25E-08	38		
SN25(CtoS)	SN25(CtoS)	VEEGMNHINQDMKEAEK	KAWGNQDGVVASQPAR	75	106	1,83E-05	25	1,67E-08	58		
SN25(CtoS)	SN25(CtoS)	VEEGMNHINQDMKEAEK	IMEKADSNK	75	187	4,12E-05	39	8,19E-10	105	1,01E-02	3
SN25(CtoS)	SN25(CtoS)	VEEGMNHINQDMKEAEK	ADSNKTR	75	192			2,47E-01	19		
SN25(CtoS)	SN25(CtoS)	NLKDLGK	SSDAYK	82	100	3,29E-10	39	2,45E-09	18		
SN25(CtoS)	SN25(CtoS)	DLGKSSGLFISPSNK	EAEKNLK	86	79			6,43E-04	8		
SN25(CtoS)	SN25(CtoS)	DLGKSSGLFISPSNK	LKSSDAYK	86	99	4,77E-08	129	3,09E-11	75		
SN25(CtoS)	SN25(CtoS)	DLGKSSGLFISPSNK	SSDAYK	86	100	3,15E-08	23	2,26E-08	17		

protein 1	protein 2	sequence 1	sequence 2	residue 1	residue 2	replicate 1		replicate 2		replicate 3	
						score	# spectra	score	# spectra	score	# spectra
SN25(CtoS)	SN25(CtoS)	DLGKSSGLFISPSNK	SSDAYKK	86	105	5,19E-06	74	2,57E-08	53		
SN25(CtoS)	SN25(CtoS)	DLGKSSGLFISPSNK	IMEKADSNK	86	187	2,87E-05	43	4,08E-12	34		
SN25(CtoS)	SN25(CtoS)	DLGKSSGLFISPSNK	ADSNKTR	86	192			4,79E-05	19		
SN25(CtoS)	SN25(CtoS)	SSGLFISPSNK	NLKDLGK	87	82	1,57E-06	32				
SN25(CtoS)	SN25(CtoS)	SSGLFISPSNK	IMEKADSNK	87	187	3,19E-06	12	1,36E-05	6		
SN25(CtoS)	SN25(CtoS)	SSGLFISPSNK	TRIDEANQR	87	193	9,91E-06	12				
SN25(CtoS)	SN25(CtoS)	SSGLFISPSNK	NLKDLGK	93	82	5,93E-08	52				
SN25(CtoS)	SN25(CtoS)	SSGLFISPSNK	IMEKADSNK	93	187	7,75E-05	15	7,03E-06	22		
SN25(CtoS)	SN25(CtoS)	SSGLFISPSNK	NLKDLGK	95	82	5,57E-08	18	6,17E-05	11		
SN25(CtoS)	SN25(CtoS)	SSGLFISPSNK	SSDAYKK	95	105	5,38E-05	3	3,00E-06	3		
SN25(CtoS)	SN25(CtoS)	SSGLFISPSNK	IMEKADSNK	95	187			9,67E-06	3		
SN25(CtoS)	SN25(CtoS)	SSGLFISPSNKLK	EAEKNLK	97	79			4,85E-04	35		
SN25(CtoS)	SN25(CtoS)	SSGLFISPSNKLK	NLKDLGK	97	82	2,78E-08	112	1,65E-06	86		
SN25(CtoS)	SN25(CtoS)	SSGLFISPSNKLK	SSDAYK	97	100	1,00E-06	47	2,68E-07	25		
SN25(CtoS)	SN25(CtoS)	SSGLFISPSNKLK	SSDAYK	97	101	2,31E-04	2				
SN25(CtoS)	SN25(CtoS)	SSGLFISPSNKLK	SSDAYKK	97	105	1,84E-09	77	1,88E-07	61		
SN25(CtoS)	SN25(CtoS)	SSGLFISPSNKLK	IMEKADSNK	97	187	1,72E-07	44	3,62E-05	32		
SN25(CtoS)	SN25(CtoS)	SSGLFISPSNKLK	ADSNKTR	97	192			3,07E-03	15		
SN25(CtoS)	SN25(CtoS)	LKSSDAYK	NLKDLGK	99	82	9,50E-13	73	1,46E-11	56		
SN25(CtoS)	SN25(CtoS)	LKSSDAYK	VTNDAR	99	141			1,43E-06	6		
SN25(CtoS)	SN25(CtoS)	SSDAYKK	NLKDLGK	105	82	9,13E-09	58	4,38E-06	40		
SN25(CtoS)	SN25(CtoS)	SSDAYKK	ADSNKTR	105	192	4,94E-20	46	1,27E-15	5		
SN25(CtoS)	SN25(CtoS)	KAWGNNQDGVVASQPAR	ADQLADESLESTR	106	28			1,25E-02	9		
SN25(CtoS)	SN25(CtoS)	KAWGNNQDGVVASQPAR	MLQLVEESKDAGIR	106	43	2,52E-10	98	1,79E-07	93	1,87E-28	47
SN25(CtoS)	SN25(CtoS)	KAWGNNQDGVVASQPAR	TLVMLDEQGEQLDR	106	49					4,19E-03	2
SN25(CtoS)	SN25(CtoS)	KAWGNNQDGVVASQPAR	EAEKNLK	106	79			4,47E-07	24	9,38E-03	7
SN25(CtoS)	SN25(CtoS)	KAWGNNQDGVVASQPAR	NLKDLGK	106	82	2,05E-10	86	2,08E-08	74	9,60E-13	6
SN25(CtoS)	SN25(CtoS)	KAWGNNQDGVVASQPAR	DLGKSSGLFISPSNK	106	86	6,32E-09	73	6,22E-11	76	5,36E-19	3
SN25(CtoS)	SN25(CtoS)	KAWGNNQDGVVASQPAR	SSGLFISPSNK	106	87	6,02E-09	30	8,35E-07	10		
SN25(CtoS)	SN25(CtoS)	KAWGNNQDGVVASQPAR	SSGLFISPSNK	106	88			2,24E-03	5		
SN25(CtoS)	SN25(CtoS)	KAWGNNQDGVVASQPAR	SSGLFISPSNK	106	93	4,91E-08	46	9,26E-06	27		
SN25(CtoS)	SN25(CtoS)	KAWGNNQDGVVASQPAR	SSGLFISPSNK	106	95	6,08E-07	11	1,62E-05	11		

						replicate 1		replicate 2		replicate 3	
protein 1	protein 2	sequence 1	sequence 2	residue 1	residue 2	score	# spectra	score	# spectra	score	# spectra
SN25(CtoS)	SN25(CtoS)	KAWGNNQDGVVASQPAR	SSGLFISPSNKLK	106	97	4,90E-07	88	3,48E-11	78	2,62E-13	5
SN25(CtoS)	SN25(CtoS)	KAWGNNQDGVVASQPAR	LKSSDAYK	106	99	1,58E-07	84	4,80E-10	77	4,97E-04	19
SN25(CtoS)	SN25(CtoS)	KAWGNNQDGVVASQPAR	SSDAYK	106	100	3,00E-12	44	4,63E-09	26		
SN25(CtoS)	SN25(CtoS)	KAWGNNQDGVVASQPAR	EQMAISGGFIR	106	133	7,02E-05	10				
SN25(CtoS)	SN25(CtoS)	KAWGNNQDGVVASQPAR	IMEKADSNK	106	187	4,82E-05	43	2,53E-08	25	6,99E-04	6
SN25(CtoS)	SN25(CtoS)	KAWGNNQDGVVASQPAR	ADSNKTR	106	192					3,32E-06	5
SN25(CtoS)	SN25(CtoS)	KAWGNNQDGVVASQPAR	ATKMLGSG	106	204			1,98E-08	51		
SN25(CtoS)	SN25(CtoS)	AWGNNQDGVVASQPAR	NLKDLGK	118	82	1,46E-04	16	3,76E-06	7		
SN25(CtoS)	SN25(CtoS)	AWGNNQDGVVASQPAR	LKSSDAYK	118	99	8,81E-07	15	4,06E-05	9		
SN25(CtoS)	SN25(CtoS)	AWGNNQDGVVASQPAR	SSDAYKK	118	105	1,82E-04	7	1,04E-04	7		
SN25(CtoS)	SN25(CtoS)	EQMAISGGFIR	NLKDLGK	133	82			6,90E-03	10		
SN25(CtoS)	SN25(CtoS)	EQMAISGGFIR	SSDAYKK	133	105	4,26E-04	12				
SN25(CtoS)	SN25(CtoS)	ENEMDENLEQVSGIIGNLR	KAWGNNQDGVVASQPAR	157	106					8,51E-11	1
SN25(CtoS)	SN25(CtoS)	ENEMDENLEQVSGIIGNLR	IMEKADSNK	157	187					7,67E-12	4
SN25(CtoS)	SN25(CtoS)	IMEKADSNK	EAEKNLK	187	79			1,76E-05	27		
SN25(CtoS)	SN25(CtoS)	IMEKADSNK	NLKDLGK	187	82	1,07E-09	48	2,05E-12	29	1,55E-12	8
SN25(CtoS)	SN25(CtoS)	IMEKADSNK	LKSSDAYK	187	99	1,02E-07	36	3,06E-14	52		
SN25(CtoS)	SN25(CtoS)	IMEKADSNK	SSDAYKK	187	105	7,33E-07	33	3,07E-10	44		
SN25(CtoS)	SN25(CtoS)	ADSNKTR	NLKDLGK	192	82	1,94E-08	27	3,94E-15	21		
SN25(CtoS)	SN25(CtoS)	ADSNKTR	SSDAYK	192	100	9,37E-11	13				

Supplementary Table 4. Cross-links identified in Stx(1-262). The protein names, the peptide sequences of the cross-linked peptides and the cross-linked residues are given. Cross-linked residues are highlighted (bold) in the peptide sequences. The pLink score and the number of acquired tandem mass spectra are given for each cross-link in each replicate.

protein 1	protein 2	sequence 1	sequence 2	residue 1	residue 2	replicate 1		replicate 2		replicate 3	
						score	# spectra	score	# spectra	score	# spectra
homomultimeric cross-links											
Stx(1-262)	Stx(1-262)	K TQHSTLSR	K TQHSTLSR	120	120	6,81E-09	4	5,69E-07	7	6,36E-10	19
Stx(1-262)	Stx(1-262)	K FVEVMSEYNATQSDYR	K FVEVMSEYNATQSDYR	129	129	1,31E-06	2	3,34E-05	10		
Stx(1-262)	Stx(1-262)	TAKDSDDDDDVTVTVD R	TAKDSDDDDDVTVTVD R	15	15			7,59E-09	21	4,72E-08	42
Stx(1-262)	Stx(1-262)	TAKDSDDDDDVTVTVD R	DSDDDDDVTVTVD R	15	17					1,23E-04	2
Stx(1-262)	Stx(1-262)	HSEI I KLENSIR	HSEI I KLENSIR	207	207	3,56E-10	16	1,18E-06	40	1,06E-07	7
Stx(1-262)	Stx(1-262)	IEYNVEHAVDY V ER	IEYNVEHAVDY V ER	238	238	2,24E-17	7	1,89E-04	20		
Stx(1-262)	Stx(1-262)	AV K YQSK	AV K YQSK	259	259	7,34E-09	11	1,39E-07	35		
Stx(1-262)	Stx(1-262)	AV K YQSK	Y Q SKAR	259	263						
Stx(1-262)	Stx(1-262)	GFID K IAENVEEV K R	GFID K IAENVEEV K	49	49	7,47E-11	3	1,78E-03	5		
Stx(1-262)	Stx(1-262)	GFID K IAENVEEV K	IAENVEEV K R	49	58			3,88E-07	26		
Stx(1-262)	Stx(1-262)	IAENVEEV K R	IAENVEEV K R	58	58			1,22E-08	8		
Stx(1-262)	Stx(1-262)	K H S AILASPNPDE K	K H S AILASPNPDE K	60	60	1,29E-14	32	4,16E-09	16	3,29E-15	17
Stx(1-262)	Stx(1-262)	HSAILASPNPDE K T K	K H S AILASPNPDE K	73	60	2,02E-09	19	5,95E-05	13	5,18E-10	4
Stx(1-262)	Stx(1-262)	K H S AILASPNPDE K	HSAILASPNPDE K	62	62					4,37E-01	1
Stx(1-262)	Stx(1-262)	HSAILASPNPDE K TKEELEELMSDI K	TKEELEELMSDI K	73	75			1,28E-02	4		
Stx(1-262)	Stx(1-262)	TKEELEELMSDI K	TKEELEELMSDI K	75	75			2,58E-05	14		
Stx(1-262)	Stx(1-262)	TKEELEELMSDI K	TKEELEELMSDI K	75	86	2,83E-16	12	3,36E-06	32		
Stx(1-262)	Stx(1-262)	TKEELEELMSDI K	TKEELEELMSDI K	86	86			2,96E-04	20		
Stx(1-262)	Stx(1-262)	TAN K V R	TAN K V R	91	91	1,38E-14	15	2,43E-08	9		
Stx(1-262)	Stx(1-262)	LKSIEQSIEQEEGL N R	LKSIEQSIEQEEGL N R	97	97	2,98E-14	9	7,72E-09	25	1,27E-07	13
Stx(1-262)	Stx(1-262)	LKSIEQSIEQEEGL N R	S IEQSIEQEEGL N R	97	98			9,20E-04	1		
Stx(1-262)	Stx(1-262)	LKSIEQSIEQEEGL N R	S IEQSIEQEEGL N R	98	98			1,46E-02	4	5,22E-02	1
intramolecular cross-links											
Stx(1-262)	Stx(1-262)	K TQHSTLSR	S SADLR	120	112	8,39E-32	18	3,97E-13	48		
Stx(1-262)	Stx(1-262)	K FVEVMSEYNATQSDY R	S SADLR	129	112			1,19E-09	11	2,95E-10	6
Stx(1-262)	Stx(1-262)	HSEI I KLENSIR	S SADLR	207	112			1,56E-08	20	3,46E-04	12
Stx(1-262)	Stx(1-262)	IEYNVEHAVDY V ER	S SADLR	238	112	2,64E-07	4	3,70E-09	23		

protein 1	protein 2	sequence 1	sequence 2	residue 1	residue 2	replicate 1		replicate 2		replicate 3	
						score	# spectra	score	# spectra	score	# spectra
Stx(1-262)	Stx(1-262)	AVKYQSK	SSADLR	259	112	1,24E-36	8	2,72E-10	12		
Stx(1-262)	Stx(1-262)	YQSKAR	SSADLR	263	112	6,46E-09	4	3,66E-08	9		
Stx(1-262)	Stx(1-262)	HSEIIKLENSIR	SSADLR	207	113	3,45E-05	1				
Stx(1-262)	Stx(1-262)	IEYNVEHAVDYVER	SSADLR	238	113			7,50E-05	3		
Stx(1-262)	Stx(1-262)	YQSKAR	SSADLR	263	113	9,90E-08	1				
Stx(1-262)	Stx(1-262)	KFVEVMSEYNATQSDYR	KTQHSTLSR	129	120			5,18E-10	29		
Stx(1-262)	Stx(1-262)	TTTSEELEDMLESGNPAIFASGIIMDSSISKQ ALSEIETR	KTQHSTLSR	192	120			1,92E-03	2	1,81E-03	5
Stx(1-262)	Stx(1-262)	KTQHSTLSR	QALSEIETR	120	196	2,60E-08	4				
Stx(1-262)	Stx(1-262)	HSEIIKLENSIR	KTQHSTLSR	207	120	7,93E-12	33	6,70E-10	29	6,34E-14	178
Stx(1-262)	Stx(1-262)	IEYNVEHAVDYVER	KTQHSTLSR	238	120			4,05E-10	10	6,53E-05	16
Stx(1-262)	Stx(1-262)	IEYNVEHAVDYVER	KTQHSTLSR	246	120			2,12E-03	3		
Stx(1-262)	Stx(1-262)	KTQHSTLSR	AVSDTKK	120	255			2,62E-07	14		
Stx(1-262)	Stx(1-262)	KTQHSTLSR	AVKYQSK	120	259	1,01E-08	8	1,96E-08	11	4,50E-09	5
Stx(1-262)	Stx(1-262)	KFVEVMSEYNATQSDYR	TQHSTLSR	129	121					2,33E-08	20
Stx(1-262)	Stx(1-262)	KTQHSTLSR	QALSEIETR	121	196	1,64E-14	3				
Stx(1-262)	Stx(1-262)	HSEIIKLENSIR	TQHSTLSR	207	121					4,95E-03	14
Stx(1-262)	Stx(1-262)	IEYNVEHAVDYVER	KTQHSTLSR	238	121					8,20E-03	11
Stx(1-262)	Stx(1-262)	KTQHSTLSR	AVSDTK	121	252	6,60E-03	3				
Stx(1-262)	Stx(1-262)	TQHSTLSR	AVSDTKK	121	255			7,24E-04	5		
Stx(1-262)	Stx(1-262)	HSEIIKLENSIR	TQHSTLSR	207	124	2,07E-04	2			4,23E-03	10
Stx(1-262)	Stx(1-262)	TQHSTLSR	AVKYQSK	124	259			1,20E-05	3		
Stx(1-262)	Stx(1-262)	KFVEVMSEYNATQSDYR	HSEIIKLENSIR	129	207	1,24E-14	31	8,03E-09	38	1,84E-17	4
Stx(1-262)	Stx(1-262)	KFVEVMSEYNATQSDYR	IEYNVEHAVDYVER	129	238			1,90E-05	29		
Stx(1-262)	Stx(1-262)	KFVEVMSEYNATQSDYR	AVKYQSK	129	259			2,39E-07	62	3,56E-13	13
Stx(1-262)	Stx(1-262)	KFVEVMSEYNATQSDYR	YQSKAR	129	263			2,00E-04	39	8,73E-07	18
Stx(1-262)	Stx(1-262)	TAKSDDDDDVTVTVDR	SIEQSIEQEEGLNR	15	102					1,26E-05	5
Stx(1-262)	Stx(1-262)	TAKSDDDDDVTVTVDR	SSADLR	15	112			4,12E-13	11	9,62E-10	48
Stx(1-262)	Stx(1-262)	TAKSDDDDDVTVTVDR	KTQHSTLSR	15	120	1,77E-14	36	1,99E-12	38	3,64E-21	172
Stx(1-262)	Stx(1-262)	TAKSDDDDDVTVTVDR	TQHSTLSR	15	121					3,08E-04	7
Stx(1-262)	Stx(1-262)	TAKSDDDDDVTVTVDR	TQHSTLSR	15	124					1,20E-02	7
Stx(1-262)	Stx(1-262)	TAKSDDDDDVTVTVDR	TQHSTLSR	15	125			1,93E-03	2		

protein 1	protein 2	sequence 1	sequence 2	residue 1	residue 2	replicate 1		replicate 2		replicate 3	
						score	# spectra	score	# spectra	score	# spectra
Stx(1-262)	Stx(1-262)	TAKDSDDDDVTVTVDR	TQHSTLSR	15	127			6,50E-04	2		
Stx(1-262)	Stx(1-262)	KFVEVMSEYNATQSDYR	TAKDSDDDDVTVTVDR	129	15	8,85E-17	18	1,09E-10	69	2,58E-16	145
Stx(1-262)	Stx(1-262)	TAKDSDDDDVTVTVDR	HSEIIKLENSIR	15	207			1,48E-08	26	1,69E-14	23
Stx(1-262)	Stx(1-262)	TAKDSDDDDVTVTVDR	IEYNVEHAVDYVER	15	238			1,59E-06	26	2,08E-11	24
Stx(1-262)	Stx(1-262)	TAKDSDDDDVTVTVDR	IEYNVEHAVDYVER	15	246			2,93E-05	18	1,49E-05	7
Stx(1-262)	Stx(1-262)	TAKDSDDDDVTVTVDR	AVSDTKK	15	255			7,03E-06	27	5,20E-09	24
Stx(1-262)	Stx(1-262)	TAKDSDDDDVTVTVDR	KAVKYQSK	15	256			1,10E-06	2		
Stx(1-262)	Stx(1-262)	TAKDSDDDDVTVTVDR	AVKYQSK	15	259	7,99E-11	30	4,86E-10	25	1,99E-14	21
Stx(1-262)	Stx(1-262)	TAKDSDDDDVTVTVDR	YQSKAR	15	263	6,65E-09	16	1,60E-04	16	3,26E-04	8
Stx(1-262)	Stx(1-262)	TAKDSDDDDVTVTVDRDR	GFIDKIAENVEEVKR	15	49	6,83E-14	9	6,18E-11	29	2,17E-07	16
Stx(1-262)	Stx(1-262)	TAKDSDDDDVTVTVDR	IAENVEEVKR	15	58			4,58E-09	21	1,63E-09	18
Stx(1-262)	Stx(1-262)	TAKDSDDDDVTVTVDR	KHSAILASPNDPEK	15	60	6,08E-12	12	1,31E-11	27	1,01E-21	47
Stx(1-262)	Stx(1-262)	TAKDSDDDDVTVTVDR	HSAILASPNDPEK	15	62					4,57E-03	1
Stx(1-262)	Stx(1-262)	TAKDSDDDDVTVTVDR	HSAILASPNDPEKTK	15	73	4,07E-09	9	1,27E-06	13	6,52E-14	6
Stx(1-262)	Stx(1-262)	TAKDSDDDDVTVTVDR	TKEELEELMSDIK	15	75	8,86E-14	16	5,15E-05	22	1,09E-06	6
Stx(1-262)	Stx(1-262)	TAKDSDDDDVTVTVDR	TKEELEELMSDIKK	15	86	5,36E-19	31	1,11E-07	47	3,43E-13	10
Stx(1-262)	Stx(1-262)	TAKDSDDDDVTVTVDR	TANKVR	15	91			3,41E-07	35	1,99E-07	49
Stx(1-262)	Stx(1-262)	TAKDSDDDDVTVTVDR	LKSIEQSIEQEEGLNR	15	97	1,12E-08	9	6,13E-11	45	1,35E-16	36
Stx(1-262)	Stx(1-262)	TAKDSDDDDVTVTVDR	SIEQSIEQEEGLNR	15	98			1,94E-03	3	1,15E-08	6
Stx(1-262)	Stx(1-262)	TTTSEELEDMLESGNPAIFASGIIMDSSISK	HSEIIKLENSIR	164	207			3,26E-03	1		
Stx(1-262)	Stx(1-262)	DSDDDDVTVTVDR	KTQHSTLSR	17	120			3,33E-04	5		
Stx(1-262)	Stx(1-262)	DSDDDDVTVTVDR	KTQHSTLSR	17	121	1,23E-08	3				
Stx(1-262)	Stx(1-262)	KFVEVMSEYNATQSDYR	DSDDDDVTVTVDR	129	17			4,45E-03	5		
Stx(1-262)	Stx(1-262)	DSDDDDVTVTVDR	AVKYQSK	17	259			3,07E-04	4		
Stx(1-262)	Stx(1-262)	DSDDDDVTVTVDR	KHSAILASPNDPEK	17	60			1,02E-03	4		
Stx(1-262)	Stx(1-262)	DSDDDDVTVTVDR	TANKVR	17	91			4,84E-04	6		
Stx(1-262)	Stx(1-262)	TTTSEELEDMLESGNPAIFASGIIMDSSISKQ ALSEIETR	AVKYQSK	192	259			4,06E-03	4		
Stx(1-262)	Stx(1-262)	HSEIIKLENSIR	QALSEIETR	207	196			4,94E-06	16	2,06E-02	7
Stx(1-262)	Stx(1-262)	QALSEIETR	AVKYQSK	196	259	8,28E-08	2				
Stx(1-262)	Stx(1-262)	IEYNVEHAVDYVER	HSEIIKLENSIR	238	207	3,28E-16	16	2,65E-06	16	6,10E-04	6
Stx(1-262)	Stx(1-262)	HSEIIKLENSIR	AVSDTKK	207	255					4,08E-08	68

protein 1	protein 2	sequence 1	sequence 2	residue 1	residue 2	replicate 1		replicate 2		replicate 3	
						score	# spectra	score	# spectra	score	# spectra
Stx(1-262)	Stx(1-262)	HSEIIKLENSIR	AVKYQSK	207	259	2,44E-07	11	2,76E-07	17	6,03E-12	11
Stx(1-262)	Stx(1-262)	HSEIIKLENSIR	YQSKAR	207	263					3,87E-05	16
Stx(1-262)	Stx(1-262)	IEYNVEHAVDYVER	AVSDTK	238	252			5,99E-04	12	5,84E-03	10
Stx(1-262)	Stx(1-262)	IEYNVEHAVDYVER	AVSDTKK	238	255			1,75E-09	26		
Stx(1-262)	Stx(1-262)	IEYNVEHAVDYVER	AVKYQSK	238	259	5,93E-11	8	3,84E-10	31	2,11E-03	10
Stx(1-262)	Stx(1-262)	IEYNVEHAVDYVER	YQSKAR	238	262	8,29E-03	5				
Stx(1-262)	Stx(1-262)	IEYNVEHAVDYVER	YQSKAR	238	263			6,75E-06	11		
Stx(1-262)	Stx(1-262)	IEYNVEHAVDYVER	AVKYQSK	246	259	7,49E-08	5	1,54E-08	22		
Stx(1-262)	Stx(1-262)	DSDDDDDDVT/TVDR	AVKYQSK	24	259			4,62E-05	2		
Stx(1-262)	Stx(1-262)	AVSDTKK	YQSKAR	255	263	4,48E-19	31	3,81E-09	33	4,04E-06	7
Stx(1-262)	Stx(1-262)	GFIDKIAENVEEVKR	KTQHSTLSR	49	120			6,52E-10	43	9,46E-16	20
Stx(1-262)	Stx(1-262)	KFVEVMSEYNATQSDYR	GFIDKIAENVEEVK	129	49	3,96E-13	7	1,53E-05	27		
Stx(1-262)	Stx(1-262)	GFIDKIAENVEEVK	HSEIIKLENSIR	49	207	4,44E-15	19	4,13E-08	22	9,08E-15	3
Stx(1-262)	Stx(1-262)	GFIDKIAENVEEVKR	IEYNVEHAVDYVER	49	238	1,32E-13	5	1,07E-05	17		
Stx(1-262)	Stx(1-262)	GFIDKIAENVEEVK	AVKYQSK	49	259	1,72E-11	24	3,32E-08	43	7,17E-13	2
Stx(1-262)	Stx(1-262)	GFIDKIAENVEEVK	YQSKAR	49	263	5,54E-09	29	6,63E-07	50	9,76E-08	7
Stx(1-262)	Stx(1-262)	GFIDKIAENVEEVKR	KHSAILASPNPDEK	49	60	5,77E-17	20	6,70E-12	54	3,80E-22	28
Stx(1-262)	Stx(1-262)	HSAILASPNPDEKTK	GFIDKIAENVEEVK	73	49	2,19E-12	9	2,32E-03	10		
Stx(1-262)	Stx(1-262)	GFIDKIAENVEEVKR	TKEELEELMSDIKK	49	75	8,62E-19	7	2,30E-06	9		
Stx(1-262)	Stx(1-262)	GFIDKIAENVEEVKR	TKEELEELMSDIKK	49	86	7,58E-15	11	4,02E-08	22		
Stx(1-262)	Stx(1-262)	GFIDKIAENVEEVKR	TANKVR	49	91	6,59E-18	77	9,39E-07	268	2,51E-11	101
Stx(1-262)	Stx(1-262)	LKSIEQSIEQEEGLNR	GFIDKIAENVEEVKR	97	49	2,58E-17	12	1,87E-07	23	7,45E-06	6
Stx(1-262)	Stx(1-262)	IAENVEEVKR	KTQHSTLSR	58	120	4,21E-11	14	1,40E-11	20	7,92E-12	35
Stx(1-262)	Stx(1-262)	KFVEVMSEYNATQSDYR	IAENVEEVKR	129	58			5,98E-09	104	2,83E-17	221
Stx(1-262)	Stx(1-262)	HSEIIKLENSIR	IAENVEEVKR	207	58			2,62E-11	15		
Stx(1-262)	Stx(1-262)	IEYNVEHAVDYVER	IAENVEEVKR	238	58			7,81E-07	27		
Stx(1-262)	Stx(1-262)	IAENVEEVKR	AVKYQSK	58	259	4,98E-11	10	1,06E-09	17		
Stx(1-262)	Stx(1-262)	KHSAILASPNPDEK	IAENVEEVKR	60	58			9,01E-08	10		
Stx(1-262)	Stx(1-262)	TKEELEELMSDIK	IAENVEEVKR	75	58	1,94E-14	22	5,71E-06	23		
Stx(1-262)	Stx(1-262)	LKSIEQSIEQEEGLNR	IAENVEEVKR	97	58			4,64E-06	25	4,66E-08	8
Stx(1-262)	Stx(1-262)	TAKDSDDDDDVT/TVDR	GSHMKDR	15	5					1,49E-09	85
Stx(1-262)	Stx(1-262)	KHSAILASPNPDEK	SSADLR	60	112	3,39E-25	11	3,20E-09	10	2,56E-04	3

protein 1	protein 2	sequence 1	sequence 2	residue 1	residue 2	replicate 1		replicate 2		replicate 3	
						score	# spectra	score	# spectra	score	# spectra
Stx(1-262)	Stx(1-262)	KHSAILASPNPDEK	KTQHSTLSR	60	120	2,36E-12	15	4,32E-13	31	9,09E-23	50
Stx(1-262)	Stx(1-262)	KFVEVMSEYNATQSDYR	KHSAILASPNPDEK	129	60			4,70E-08	43	7,18E-20	13
Stx(1-262)	Stx(1-262)	TTTSEELEDMLESGNPAIFASGIIMDSSISKQ ALSEIETR	KHSAILASPNPDEK	192	60	3,31E-08	3	9,47E-03	2		
Stx(1-262)	Stx(1-262)	KHSAILASPNPDEK	HSEIIKLENSIR	60	207			4,85E-10	20	1,28E-13	25
Stx(1-262)	Stx(1-262)	IEYNVEHAVDYVER	KHSAILASPNPDEK	238	60			3,99E-06	6		
Stx(1-262)	Stx(1-262)	KHSAILASPNPDEK	AVSDTKK	60	255	9,33E-05	20	5,70E-06	20	5,30E-08	18
Stx(1-262)	Stx(1-262)	KHSAILASPNPDEK	AVKYQSK	60	259	4,60E-12	27	1,14E-07	37	4,81E-12	9
Stx(1-262)	Stx(1-262)	KHSAILASPNPDEK	YQSKAR	60	263	7,23E-08	20	4,95E-05	20		
Stx(1-262)	Stx(1-262)	KHSAILASPNPDEK	TKEELEELMSDIK	60	75					1,28E-17	17
Stx(1-262)	Stx(1-262)	TKEELEELMSDIK	KHSAILASPNPDEK	86	60			2,28E-08	59		
Stx(1-262)	Stx(1-262)	KHSAILASPNPDEK	TANKVR	60	91	4,56E-10	37			1,79E-08	23
Stx(1-262)	Stx(1-262)	SKLKSIEQSIEQEEGLNR	RKHSAILASPNPDEK	95	60			5,05E-04	17		
Stx(1-262)	Stx(1-262)	LKSIEQSIEQEEGLNR	KHSAILASPNPDEK	97	60			2,84E-11	52	1,53E-16	20
Stx(1-262)	Stx(1-262)	LKSIEQSIEQEEGLNR	HSAILASPNPDEK	98	62			1,45E-04	2		
Stx(1-262)	Stx(1-262)	HSAILASPNPDEK	KTQHSTLSR	67	120			1,66E-05	2		
Stx(1-262)	Stx(1-262)	HSAILASPNPDEKTK	KTQHSTLSR	73	120	1,23E-09	10	2,69E-08	17	1,91E-04	4
Stx(1-262)	Stx(1-262)	HSAILASPNPDEKTKEELEELMSDIK	KFVEVMSEYNATQSDYR	73	129			2,85E-03	19		
Stx(1-262)	Stx(1-262)	HSAILASPNPDEKTK	HSEIIKLENSIR	73	207			3,10E-05	14		
Stx(1-262)	Stx(1-262)	HSAILASPNPDEKTK	AVKYQSK	73	259	2,61E-09	14	7,81E-05	21		
Stx(1-262)	Stx(1-262)	HSAILASPNPDEKTK	TANKVR	73	91			1,17E-02	38		
Stx(1-262)	Stx(1-262)	HSAILASPNPDEKTKEELEELMSDIK	LKSIEQSIEQEEGLNR	73	97	2,52E-09	2	6,75E-07	20		
Stx(1-262)	Stx(1-262)	IEYNVEHAVDYVER	TKEELEELMSDIK	238	74			1,31E-06	22		
Stx(1-262)	Stx(1-262)	IEYNVEHAVDYVER	TKEELEELMSDIK	246	74			3,74E-05	10		
Stx(1-262)	Stx(1-262)	KFVEVMSEYNATQSDYR	TKEELEELMSDIK	129	75			1,62E-06	21		
Stx(1-262)	Stx(1-262)	TKEELEELMSDIK	HSEIIKLENSIR	75	207	3,17E-17	24	2,93E-10	73	3,18E-18	26
Stx(1-262)	Stx(1-262)	IEYNVEHAVDYVER	TKEELEELMSDIK	238	75			6,94E-06	22		
Stx(1-262)	Stx(1-262)	TKEELEELMSDIK	AVKYQSK	75	259	1,08E-12	17	4,99E-08	65		
Stx(1-262)	Stx(1-262)	TKEELEELMSDIK	YQSKAR	75	263	2,31E-06	11	1,45E-06	57		
Stx(1-262)	Stx(1-262)	TKEELEELMSDIK	TANKVR	75	91	7,34E-07	9	4,21E-05	69		
Stx(1-262)	Stx(1-262)	LKSIEQSIEQEEGLNR	TKEELEELMSDIK	97	75	7,61E-19	10	1,30E-08	26		
Stx(1-262)	Stx(1-262)	TKEELEELMSDIK	KTQHSTLSR	86	120			2,94E-10	47		

protein 1	protein 2	sequence 1	sequence 2	residue 1	residue 2	replicate 1		replicate 2		replicate 3	
						score	# spectra	score	# spectra	score	# spectra
Stx(1-262)	Stx(1-262)	KFVEVMSEYNATQSDYR	TKEELEELMSDIKK	129	86	6,12E-15	10	2,15E-05	35		
Stx(1-262)	Stx(1-262)	ELEEELMSDIKK	HSEIIKLENSIR	86	207	2,95E-15	23	2,71E-08	69	4,65E-15	13
Stx(1-262)	Stx(1-262)	TKEELEELMSDIKK	LENSIR	86	211					9,36E-02	3
Stx(1-262)	Stx(1-262)	IEYNVEHAVDYVER	TKEELEELMSDIKK	238	86	2,11E-16	4	3,34E-05	24		
Stx(1-262)	Stx(1-262)	IEYNVEHAVDYVER	TKEELEELMSDIKK	246	86			8,06E-05	6		
Stx(1-262)	Stx(1-262)	TKEELEELMSDIKK	AVKYQSK	86	259			9,59E-07	40		
Stx(1-262)	Stx(1-262)	TKEELEELMSDIKK	TANKVR	86	88	3,51E-29	14				
Stx(1-262)	Stx(1-262)	TKEELEELMSDIKK	TANKVR	86	91					2,68E-09	68
Stx(1-262)	Stx(1-262)	LKSIEQSIEQEEGLNR	TKEELEELMSDIKK	97	86	7,73E-19	13	3,24E-09	53	1,34E-15	6
Stx(1-262)	Stx(1-262)	TANKVR	SSADLR	91	112	1,11E-16	3				
Stx(1-262)	Stx(1-262)	KTQHSTLSR	TANKVR	120	91	3,22E-12	23	7,19E-04	13		
Stx(1-262)	Stx(1-262)	KFVEVMSEYNATQSDYR	TANKVR	129	91			2,68E-04	47		
Stx(1-262)	Stx(1-262)	HSEIIKLENSIR	TANKVR	207	91	5,50E-07	15	2,09E-04	19	2,04E-07	59
Stx(1-262)	Stx(1-262)	IEYNVEHAVDYVER	TANKVR	238	91			9,48E-05	27	6,25E-03	15
Stx(1-262)	Stx(1-262)	AVSDTKK	TANKVR	255	91	4,47E-20	16	7,26E-06	12		
Stx(1-262)	Stx(1-262)	AVKYQSK	TANKVR	259	91	7,69E-16	20	2,99E-10	30		
Stx(1-262)	Stx(1-262)	YQSKAR	TANKVR	263	91	1,29E-12	21	1,31E-07	13		
Stx(1-262)	Stx(1-262)	LKSIEQSIEQEEGLNR	TANKVR	97	91	8,22E-10	13	1,46E-05	55	9,75E-07	17
Stx(1-262)	Stx(1-262)	SIEQSIEQEEGLNR	TANKVR	98	91	1,18E-08	4				
Stx(1-262)	Stx(1-262)	LKSIEQSIEQEEGLNR	SSADLR	97	112			7,62E-07	5		
Stx(1-262)	Stx(1-262)	LKSIEQSIEQEEGLNR	KTQHSTLSR	97	120			3,21E-12	40	4,59E-22	113
Stx(1-262)	Stx(1-262)	LKSIEQSIEQEEGLNR	TQHSTLSR	97	121			3,62E-10	10	7,77E-09	24
Stx(1-262)	Stx(1-262)	LKSIEQSIEQEEGLNR	TQHSTLSR	97	125					1,39E-02	12
Stx(1-262)	Stx(1-262)	KFVEVMSEYNATQSDYR	LKSIEQSIEQEEGLNR	129	97	1,45E-18	14	1,57E-10	62	2,95E-07	5
Stx(1-262)	Stx(1-262)	LKSIEQSIEQEEGLNR	HSEIIKLENSIR	97	207	4,63E-15	45	1,22E-08	39	6,95E-17	46
Stx(1-262)	Stx(1-262)	LKSIEQSIEQEEGLNR	IEYNVEHAVDYVER	97	238	1,80E-36	13	1,36E-08	27	3,33E-08	17
Stx(1-262)	Stx(1-262)	LKSIEQSIEQEEGLNR	IEYNVEHAVDYVER	97	246			1,13E-08	9	1,97E-08	6
Stx(1-262)	Stx(1-262)	LKSIEQSIEQEEGLNR	AVKYQSK	97	259	5,10E-07	5	3,83E-07	39	4,32E-11	12
Stx(1-262)	Stx(1-262)	LKSIEQSIEQEEGLNR	YQSKAR	97	263	1,08E-05	7				
Stx(1-262)	Stx(1-262)	SIEQSIEQEEGLNR	KTQHSTLSR	98	120			1,72E-04	4	8,24E-04	4
Stx(1-262)	Stx(1-262)	TTTSEELEDMLESGNPAIFASGIIMDSSISK	LKSIEQSIEQEEGLNR	174	98	9,26E-05	1				
Stx(1-262)	Stx(1-262)	SIEQSIEQEEGLNR	HSEIIKLENSIR	98	207			2,84E-06	5		

						replicate 1		replicate 2		replicate 3	
protein 1	protein 2	sequence 1	sequence 2	residue 1	residue 2	score	# spectra	score	# spectra	score	# spectra
Stx(1-262)	Stx(1-262)	SIEQSIEQEEGLNR	AVKYQSK	98	259			5,38E-05	4		

Supplementary Table 5. Cross-links identified in Cpx1. The protein names, the peptide sequences of the cross-linked peptides and the cross-linked residues are given. Cross-linked residues are highlighted (bold) in the peptide sequences. The pLink score and the number of acquired tandem mass spectra are given for each cross-link in each replicate.

protein 1	protein 2	sequence 1	sequence 2	residue 1	residue 2	replicate 1		replicate 2		replicate 3	
						score	# spectra	score	# spectra	score	# spectra
homomultimeric cross-links											
Cpx1	Cpx1	DKYGIK	DKYGIK	72	72	1.26E-03	8	1.28E-06	23	1.59E-10	28
Cpx1	Cpx1	DKYGIKK	DKYGIK	76	72	1.77E-01	2				
Cpx1	Cpx1	DMGKMLGGDEEKDPDAAK	DMGKMLGGDEEKDPDAAK	21	21	5.50E-04	5				
Cpx1	Cpx1	GSHMEFVMK	GSHMEFVMK	1	1	1.66E-06	20				
Cpx1	Cpx1	KEEREAEQAAMEANSEGLTRPK	YGIKKKEER	78	78			4.83E-01	2		
Cpx1	Cpx1	MLGGDEEKDPDAAK	MLGGDEEKDPDAAK	29	29	2.94E-07	12				
Cpx1	Cpx1	MLGGDEEKDPDAAKK	MLGGDEEKDPDAAKK	35	35	7.14E-06	2				
Cpx1	Cpx1	QALGGATKDMGK	QALGGATKDMGK	17	17	7.06E-03	2				
Cpx1	Cpx1	QALGGATKDMGKMLGGDEEKDPDAAK	QALGGATKDMGKMLGGDEEKDPDAAK	17	21	4.73E-03	21	1.68E-03	12		
Cpx1	Cpx1	YAKMEAER	YAKMEAER	57	57	5.33E-05	36			1.32E-06	16
Cpx1	Cpx1	YGIKKKEER	DKYGIK	77	72	2.49E-01	5				
intramolecular cross-links											
Cpx1	Cpx1	AIPPGCGDEPEEEDESILDTVIKYLPGPLQDMFK	DKYGIK	125	72	4.28E-02	1				
Cpx1	Cpx1	DKYGIK	KAKYAK	72	54	2.66E-03	3	8.97E-04	5		
Cpx1	Cpx1	DMGKMLGGDEEK	DPDAAKK	21	35	1.30E-03	37				
Cpx1	Cpx1	DMGKMLGGDEEKDPDAAK	DKYGIK	21	72	9.49E-06	25	2.31E-06	7	2.09E-05	5
Cpx1	Cpx1	DMGKMLGGDEEKDPDAAK	GSHMEFVMK	21	1	3.12E-12	121				
Cpx1	Cpx1	DMGKMLGGDEEKDPDAAK	GSHMEFVMKQALGGATK	21	9	1.45E-08	27				
Cpx1	Cpx1	DMGKMLGGDEEKDPDAAK	KEERQEARL	21	36	5.59E-03	11				
Cpx1	Cpx1	DMGKMLGGDEEKDPDAAK	YAKMEAER	21	57	8.36E-06	12				
Cpx1	Cpx1	EAEAQAAMEANSEGLTR	AKYAKMEAER	93	54	4.27E-02	4	4.27E-02	4		
Cpx1	Cpx1	EAEAQAAMEANSEGLTRPK	KAKYAK	98	54	7.50E-03	4	7.50E-03	4	1.70E-04	2
Cpx1	Cpx1	EAEAQAAMEANSEGLTRPKK	DKYGIK	101	72	1.12E-04	14	1.68E-04	20	3.77E-05	10
Cpx1	Cpx1	EAEAQAAMEANSEGLTRPKK	DKYGIKK	101	76	1.51E-02	7	3.70E-03	4		
Cpx1	Cpx1	EAEAQAAMEANSEGLTRPKK	GSHMEFVMK	101	1	4.04E-03	3				
Cpx1	Cpx1	GSHMEFVMK	DKYGIK	1	72	4.60E-08	41	1.09E-07	16	1.27E-11	15

protein 1	protein 2	sequence 1	sequence 2	residue 1	residue 2	replicate 1		replicate 2		replicate 3	
						score	# spectra	score	# spectra	score	# spectra
Cpx1	Cpx1	GSHMEFVMK	YAKMEAER	1	57	5.57E-07	22	2.41E-09	9		
Cpx1	Cpx1	GSHMEFVMKQALGGATK	AKYAKMEAER	9	57	3.15E-03	5	8.29E-02	2		
Cpx1	Cpx1	GSHMEFVMKQALGGATK	DKYGIK	9	72	1.42E-04	4				
Cpx1	Cpx1	GSHMEFVMKQALGGATK	MLGGDEEKDPDAAK	9	29	9.40E-05	13				
Cpx1	Cpx1	KAIPPGCGDEPEEEDESILDTVIK	DKYGIK	102	72	5.46E-07	107	5.01E-10	124	2.12E-09	33
Cpx1	Cpx1	KAIPPGCGDEPEEEDESILDTVIK	DKYGIKK	102	76	5.26E-05	42				
Cpx1	Cpx1	KAIPPGCGDEPEEEDESILDTVIK	DMGKMLGGDEEKDPDAAK	102	21	6.67E-09	21				
Cpx1	Cpx1	KAIPPGCGDEPEEEDESILDTVIK	EAEAQAAMEANSEGLTR	102	93					2.47E-12	2
Cpx1	Cpx1	KAIPPGCGDEPEEEDESILDTVIK	GSHMEFVMK	102	1	4.93E-10	31	2.22E-06	7		
Cpx1	Cpx1	KAIPPGCGDEPEEEDESILDTVIK	KAKYAK	102	54			4.70E-03	32		
Cpx1	Cpx1	KAIPPGCGDEPEEEDESILDTVIK	MLGGDEEKDPDAAK	102	29	2.06E-06	35	6.58E-12	33	1.13E-04	20
Cpx1	Cpx1	KAIPPGCGDEPEEEDESILDTVIK	MLGGDEEKDPDAAKK	102	35	4.97E-06	32				
Cpx1	Cpx1	KAIPPGCGDEPEEEDESILDTVIK	QALGGATKDMGK	102	17	3.17E-05	45	6.15E-06	23	1.55E-02	13
Cpx1	Cpx1	KAIPPGCGDEPEEEDESILDTVIK	YAKMEAER	102	57	4.96E-08	76	1.84E-11	36	5.15E-07	25
Cpx1	Cpx1	KEERQEALR	DKYGIK	36	72	3.34E-02	1				
Cpx1	Cpx1	KEERQEALR	GSHMEFVMK	36	1	1.27E-06	7				
Cpx1	Cpx1	KEEREAEAQAAMEANSEGLTRPK	DKYGIK	78	72	1.74E-02	19				
Cpx1	Cpx1	KEEREAEAQAAMEANSEGLTRPK	KAKYAK	78	54	2.40E-02	2				
Cpx1	Cpx1	KEEREAEAQAAMEANSEGLTRPK	QGIRDKYGIKK	78	76	2.23E-06	79				
Cpx1	Cpx1	KEEREAEAQAAMEANSEGLTRPK	YAKMEAER	78	57	1.14E-03	1				
Cpx1	Cpx1	MLGGDEEKDPDAAK	DKYGIK	29	72	2.89E-04	14	2.53E-06	20	2.29E-08	15
Cpx1	Cpx1	MLGGDEEKDPDAAK	GSHMEFVMK	29	1	1.24E-08	97	7.67E-07	21		
Cpx1	Cpx1	MLGGDEEKDPDAAK	KAKYAK	29	54	4.08E-02	12	3.07E-01	6		
Cpx1	Cpx1	MLGGDEEKDPDAAK	KEERQEALR	29	36			3.76E-04	14		
Cpx1	Cpx1	MLGGDEEKDPDAAK	YAKMEAER	29	57	2.22E-04	9	7.12E-05	7	4.57E-05	4
Cpx1	Cpx1	MLGGDEEKDPDAAKK	DKYGIK	35	72	9.12E-05	4				
Cpx1	Cpx1	MLGGDEEKDPDAAKK	GSHMEFVMK	35	1	3.41E-07	17				
Cpx1	Cpx1	MLGGDEEKDPDAAKK	QALGGATKDMGK	35	17	4.18E-02	14	2.47E-02	7		
Cpx1	Cpx1	MLGGDEEKDPDAAKK	YAKMEAER	35	57	4.52E-04	8	1.34E-04	3		
Cpx1	Cpx1	MLGGDEEKDPDAAKKEEER	QALGGATKDMGK	29	17	8.72E-05	37	2.95E-04	25		
Cpx1	Cpx1	PKKAIPPGCGDEPEEEDESILDTVIK	KAKYAKMEAER	101	54	1.59E-04	70	1.14E-05	67		
Cpx1	Cpx1	PKKAIPPGCGDEPEEEDESILDTVIK	YAKMEAER	101	57	3.98E-04	33				

						replicate 1		replicate 2		replicate 3	
protein 1	protein 2	sequence 1	sequence 2	residue 1	residue 2	score	# spectra	score	# spectra	score	# spectra
Cpx1	Cpx1	QALGGATKDMGK	DKYGIK	17	72	8.43E-03	6	5.22E-06	8	3.85E-09	16
Cpx1	Cpx1	QALGGATKDMGK	DKYGIKK	17	76	5.97E-02	2				
Cpx1	Cpx1	QALGGATKDMGK	GSHMEFVMK	17	1	4.63E-06	62	2.80E-05	16	4.11E-07	6
Cpx1	Cpx1	QALGGATKDMGK	KAKYAK	17	54	7.67E-01	1				
Cpx1	Cpx1	QALGGATKDMGK	YAKMEAER	17	57	7.42E-05	8	8.24E-03	4		
Cpx1	Cpx1	YAKMEAER	DKYGIK	57	72	2.71E-03	46	3.95E-07	43	2.79E-16	89
Cpx1	Cpx1	YAKMEAER	DKYGIKK	57	76	2.27E-03	5	1.01E-05	8	1.30E-07	4
Cpx1	Cpx1	YLPGPLQDMFK	DKYGIK	126	72	2.51E-07	8	2.51E-07	8		
Cpx1	Cpx1	YLPGPLQDMFK	KAKYAK	126	54	1.93E-04	18	1.93E-04	18		
Cpx1	Cpx1	YLPGPLQDMFKK	DKYGIK	137	72	2.30E-05	33	1.76E-07	23	5.39E-07	6
Cpx1	Cpx1	YLPGPLQDMFK	GSHMEFVMK	126	1	2.58E-06	1	2.58E-06	1		

Supplementary Table 6. Cross-links identified in SNARE:Cpx1 complex. The protein names, the peptide sequences of the cross-linked peptides and the cross-linked residues are given. Cross-linked residues are highlighted (bold) in the peptide sequences. The pLink score and the number of acquired tandem mass spectra are given for each cross-link in each replicate.

protein 1	protein 2	sequence 1	sequence 2	residue 1	residue 2	replicate 1		replicate 2		replicate 3	
						score	# spectra	score	# spectra	score	# spectra
homomultimeric cross-links											
Cpx1	Cpx1	G SHMEFVMK	G SHMEFVMK	1	1	2.71E-04	9				
Cpx1	Cpx1	DM G KMLGGDEEKDPDA A KK	DPDA A KK	21	35	2.52E-01	10				
Cpx1	Cpx1	Y A KME A ER	Y A KME A ER	57	57			4.93E-01	3		
Cpx1	Cpx1	D K Y G IK	D K Y G IK	72	72					2.42E-07	4
SN25(CtoS)	SN25(CtoS)	DL G KSSGLFISPS N K	N L KDL G K	86	82			7.02E-02	1		
SN25(CtoS)	SN25(CtoS)	K AWGNNQDG V VASQ P AR	K AWGNNQDG V VASQ P AR	106	106	1.34E-03	4				
SN25(CtoS)	SN25(CtoS)	IM E K A DS N K	AD S N K TR	187	192			3.37E-02	1		
Stx(1-262)	Stx(1-262)	HSAILASPN P DE K TK	K H S AILASPN P DE K	73	60	1.32E-03	7	5.47E-04	3	1.84E-02	1
Stx(1-262)	Stx(1-262)	L K SIEQ S IEQ E EGL N R	L K SIEQ S IEQ E EGL N R	97	97	1.45E-03	14	1.24E-03	6	1.69E-05	3
Stx(1-262)	Stx(1-262)	K H S AILASPN P DE K	K H S AILASPN P DE K	60	60	8.70E-11	12	3.03E-05	5		
Stx(1-262)	Stx(1-262)	K T Q H S T L S R	K T Q H S T L S R	120	120	1.80E-04	15	2.66E-04	9		
Stx(1-262)	Stx(1-262)	T A K D S D D D D D V T V T V D R	T A K D S D D D D D V T V T V D R	15	15	6.10E-05	33				
Stx(1-262)	Stx(1-262)	T A K D S D D D D D V T V T V D R	D S D D D D D D V T V T V D R	15	17	1.70E-03	4				
Stx(1-262)	Stx(1-262)	T A K D S D D D D D V T V T V D R	D S D D D D D D V T V T V D R	17	17	9.26E-04	2				
Stx(1-262)	Stx(1-262)	T K E E L E E L M S D I K T A N K	T A N K V R	87	91			7.73E-01	1		
Stx(1-262)	Stx(1-262)	K F V E V M S E Y N A T Q S D Y R	K F V E V M S E Y N A T Q S D Y R	129	129	1.67E-05	11				
Syb(1-96)	Syb(1-96)	V N V D K V L E R	V N V D K V L E R	55	55	4.48E-04	23	2.77E-02	11	1.11E-05	7
Syb(1-96)	Syb(1-96)	D Q K L S E L D D R	D Q K L S E L D D R	62	62	1.71E-03	22	4.45E-06	11	6.60E-09	7
Syb(1-96)	Syb(1-96)	ADALQAGASQ F ET S A A K L K R	R K Y W W K	86	90	3.69E-04	28	2.42E-06	39	8.47E-05	5
Syb(1-96)	Syb(1-96)	G SHMSATAATV P PA A PAGE G GP P A PP P N L T S N R	G SHMSATAATV P PA A PAGE G GP P A PP P N L T S N R	1	1	1.26E-09	21				
Syb(1-96)	Syb(1-96)	ADALQAGASQ F ET S A A K L K	ADALQAGASQ F ET S A A K L K	86	86			2.32E-02	5		
intermolecular cross-links											
Cpx1	SN25(CtoS)	QALGGAT K DM G K	N L KDL G K	17	82	3.30E-01	4	9.84E-05	8	2.16E-05	4
Cpx1	SN25(CtoS)	QALGGAT K DM G K	L K SS D A Y K	17	99	1.26E-03	7	5.21E-05	7	4.66E-04	5
Cpx1	SN25(CtoS)	MLGGDEEK D PDA A K	N L KDL G K	29	82	2.83E-02	3	7.32E-03	6		
Cpx1	SN25(CtoS)	Y A KME A ER	N L KDL G K	57	82			7.14E-05	4	3.61E-09	6
Cpx1	SN25(CtoS)	Y A KME A ER	L K SS D A Y K	57	99	4.06E-03	4	2.04E-04	5		

protein 1	protein 2	sequence 1	sequence 2	residue 1	residue 2	replicate 1		replicate 2		replicate 3	
						score	# spectra	score	# spectra	score	# spectra
Cpx1	SN25(CtoS)	YAKMEAER	SSDAYKK	57	105	4.89E-03	7	1.72E-08	7		
Cpx1	SN25(CtoS)	EAEAQAAMEANSEGLTRPKK	SSDAYKK	101	105	8.21E-04	7	2.70E-03	5		
Cpx1	SN25(CtoS)	QALGGATKDMGK	SSDAYKK	17	105	1.12E-02	5				
Cpx1	SN25(CtoS)	DMGKMLGGDEEKDPDAAK	KAWGNQDGVVASQPAR	21	106			1.04E-04	6		
Cpx1	SN25(CtoS)	MLGGDEEKDPDAAK	LKSSDAYK	29	99			5.09E-03	3		
Cpx1	SN25(CtoS)	EAEAQAAMEANSEGLTRPKK	KAWGNQDGVVASQPAR	101	106	1.25E-01	3				
Cpx1	SN25(CtoS)	KAIPPGCGDEPEEEDESILDTVIK	KAWGNQDGVVASQPAR	102	106	7.67E-23	30				
Cpx1	Stx(1-262)	QALGGATKDMGK	TANKVR	17	91	9.23E-02	6	2.27E-03	5	7.87E-02	3
Cpx1	Stx(1-262)	QALGGATKDMGK	KTQHSTLSR	17	120	1.32E-05	10	6.73E-06	9	6.12E-06	8
Cpx1	Stx(1-262)	MLGGDEEKDPDAAK	KTQHSTLSR	29	120	4.90E-05	28	7.81E-08	25	4.00E-07	6
Cpx1	Stx(1-262)	MLGGDEEKDPDAAK	AVKYQSK	29	259	3.60E-03	22	1.27E-06	18	5.75E-04	8
Cpx1	Stx(1-262)	YAKMEAER	AVKYQSK	57	259	1.02E-02	3	1.68E-09	6	2.10E-03	2
Cpx1	Stx(1-262)	KAIPPGCGDEPEEEDESILDTVIK	LKSIEQSIEQEEGLNR	102	97	1.13E-05	2	4.48E-05	1	8.70E-03	1
Cpx1	Stx(1-262)	GSHMEFVMK	YQSKAR	1	263	2.44E-06	12			6.52E-15	13
Cpx1	Stx(1-262)	QALGGATKDMGK	YQSKAR	17	263	4.99E-02	6			1.06E-01	5
Cpx1	Stx(1-262)	DMGKMLGGDEEKDPDAAK	TAKSDDDDDVTVTVDR	21	15	1.58E-05	10	2.50E-05	4		
Cpx1	Stx(1-262)	DMGKMLGGDEEKDPDAAK	KHSAILASPNPDEK	21	60	1.19E-02	4	5.39E-06	3		
Cpx1	Stx(1-262)	DMGKMLGGDEEKDPDAAK	KTQHSTLSR	21	120	8.81E-06	8	6.22E-07	10		
Cpx1	Stx(1-262)	MLGGDEEKDPDAAK	YQSKAR	29	263	3.77E-03	9			2.44E-03	8
Cpx1	Stx(1-262)	YAKMEAER	TANKVR	57	91	1.71E-02	9	5.07E-10	8		
Cpx1	Stx(1-262)	YAKMEAER	YQSKAR	57	263	6.54E-02	4			6.72E-02	4
Cpx1	Stx(1-262)	KAIPPGCGDEPEEEDESILDTVIK	KTQHSTLSR	102	120	6.06E-19	23	2.45E-07	16		
Cpx1	Stx(1-262)	GSHMEFVMK	KTQHSTLSR	1	120	1.11E-06	10				
Cpx1	Stx(1-262)	GSHMEFVMK	AVKYQSK	1	259	2.08E-05	12				
Cpx1	Stx(1-262)	QALGGATKDMGK	AVKYQSK	17	259			8.56E-04	7		
Cpx1	Stx(1-262)	DMGKMLGGDEEKDPDAAK	YQSKAR	21	263	7.56E-03	8				
Cpx1	Stx(1-262)	YAKMEAER	AVSDTKK	57	255					2.86E-02	3
Cpx1	Stx(1-262)	DKYGIK	TANKVR	72	91	6.98E-04	6				
Cpx1	Stx(1-262)	EAEAQAAMEANSEGLTRPKK	KTQHSTLSR	101	120	4.21E-04	6				
Cpx1	Stx(1-262)	EAEAQAAMEANSEGLTRPKK	AVSDTKK	101	255	6.47E-03	7				
Cpx1	Stx(1-262)	KAIPPGCGDEPEEEDESILDTVIK	TAKSDDDDDVTVTVDR	102	15	9.03E-24	25				
Cpx1	Stx(1-262)	KAIPPGCGDEPEEEDESILDTVIK	KFVEVMSEYNATQSDYR	102	129	9.21E-04	1				

protein 1	protein 2	sequence 1	sequence 2	residue 1	residue 2	replicate 1		replicate 2		replicate 3	
						score	# spectra	score	# spectra	score	# spectra
Cpx1	Stx(1-262)	KAIPPGCGDEPEEEDESILDTVIK	HSEIIKLENSIR	102	207	1.65E-02	2				
Cpx1	Stx(1-262)	YLPGPLQDMFKK	YQSKAR	136	263	1.59E-01	6				
Cpx1	Syb(1-96)	MLGGDEEKDPDAAK	YWWKNLK	29	94	5.00E-03	17	1.53E-02	12		
Cpx1	Syb(1-96)	QALGGATKDMGK	YWWKNLK	17	94					1.68E-05	4
SN25(CtoS)	Cpx1	KAWGNQDGVVASQPAR	QALGGATKDMGK	106	17	3.54E-03	9	6.05E-04	9	5.87E-11	7
SN25(CtoS)	Cpx1	KAWGNQDGVVASQPAR	YAKMEAER	106	57	4.27E-05	20	2.06E-05	6	1.42E-04	3
SN25(CtoS)	Cpx1	DLGKSSGLFISPSNK	QALGGATKDMGK	86	17	2.21E-02	3	2.08E-02	4		
SN25(CtoS)	Cpx1	KAWGNQDGVVASQPAR	GSHMEFVMK	106	1	3.85E-06	10				
SN25(CtoS)	Cpx1	KAWGNQDGVVASQPAR	MLGGDEEKDPDAAK	106	29	1.05E-03	4				
SN25(CtoS)	Cpx1	IMEKADSNK	YAKMEAER	187	57			5.03E-05	1		
SN25(CtoS)	Stx(1-262)	MLQLVEESKDAGIR	KTQHSTLSR	43	120	2.29E-04	10	2.33E-04	9	1.86E-04	2
SN25(CtoS)	Stx(1-262)	DLGKSSGLFISPSNK	AVKYQSK	86	259	2.18E-04	15	5.99E-06	16	1.33E-15	10
SN25(CtoS)	Stx(1-262)	KAWGNQDGVVASQPAR	KTQHSTLSR	106	120	8.52E-07	13	9.53E-09	13	3.31E-09	5
SN25(CtoS)	Stx(1-262)	KAWGNQDGVVASQPAR	AVKYQSK	106	259	7.20E-05	10	1.87E-04	4	1.55E-03	2
SN25(CtoS)	Stx(1-262)	DLGKSSGLFISPSNK	YQSKAR	86	263			1.44E-02	5	4.55E-04	6
SN25(CtoS)	Stx(1-262)	LKSSDAYK	AVKYQSK	99	259			3.94E-04	4	1.75E-03	4
SN25(CtoS)	Stx(1-262)	KAWGNQDGVVASQPAR	KHSAILASPNPDEK	106	60	3.28E-05	8	1.50E-04	4		
SN25(CtoS)	Stx(1-262)	KAWGNQDGVVASQPAR	LKSIEQSIEQEEGLNR	106	97	2.86E-07	18	1.15E-07	7		
SN25(CtoS)	Stx(1-262)	KAWGNQDGVVASQPAR	YQSKAR	106	263	2.02E-04	9	2.25E-04	5		
SN25(CtoS)	Stx(1-262)	MLQLVEESKDAGIR	KHSAILASPNPDEK	43	60			3.53E-05	5		
SN25(CtoS)	Stx(1-262)	NLKDLGK	YQSKAR	82	263					3.02E-02	2
SN25(CtoS)	Stx(1-262)	DLGKSSGLFISPSNK	KTQHSTLSR	86	120			7.97E-04	6		
SN25(CtoS)	Stx(1-262)	LKSSDAYK	TANKVR	99	91	1.30E-02	1				
SN25(CtoS)	Stx(1-262)	KAWGNQDGVVASQPAR	GFIDKIAENVEEVK	106	49	1.66E-03	4				
SN25(CtoS)	Stx(1-262)	KAWGNQDGVVASQPAR	TKEELEELMSDIKK	106	86	2.93E-03	6				
SN25(CtoS)	Stx(1-262)	KAWGNQDGVVASQPAR	KTANKVR	106	91	2.80E-02	5				
SN25(CtoS)	Stx(1-262)	KAWGNQDGVVASQPAR	HSEIIKLENSIR	106	207			2.26E-03	5		
SN25(CtoS)	Stx(1-262)	KAWGNQDGVVASQPAR	IEYNVEHAVDYVER	106	238			1.02E-06	6		
SN25(CtoS)	Syb(1-96)	DLGKSSGLFISPSNK	VNVDKVLER	86	55	2.07E-02	2	1.43E-01	1		
SN25(CtoS)	Syb(1-96)	KAWGNQDGVVASQPAR	DQKLSLDDR	106	62	1.78E-05	8	1.78E-04	5		
SN25(CtoS)	Syb(1-96)	MLQLVEESKDAGIR	VNVDKVLER	43	55	1.81E-02	13				
SN25(CtoS)	Syb(1-96)	DLGKSSGLFISPSNK	DQKLSLDDR	86	62	5.39E-02	1				

protein 1	protein 2	sequence 1	sequence 2	residue 1	residue 2	replicate 1		replicate 2		replicate 3	
						score	# spectra	score	# spectra	score	# spectra
SN25(CtoS)	Syb(1-96)	DLGKSSGLFISPSNK	YVWVKNLK	86	94	1.82E-04	2				
SN25(CtoS)	Syb(1-96)	SSGLFISPSNKLK	VNVDKVLER	97	55	4.13E-02	9				
SN25(CtoS)	Syb(1-96)	KAWGNQDGVVASQPAR	VNVDKVLER	106	55	2.83E-01	3				
Stx(1-262)	Cpx1	TAKDSDDDDVTVTVDR	YAKMEAER	15	57	1.36E-05	25	6.82E-07	12	1.70E-19	8
Stx(1-262)	Cpx1	KHSAILASPNPDEK	YAKMEAER	60	57	3.36E-05	11	1.11E-04	6	1.88E-06	2
Stx(1-262)	Cpx1	KTQHSTLSR	YAKMEAER	120	57	8.31E-07	22	4.28E-15	16	2.32E-06	9
Stx(1-262)	Cpx1	KTQHSTLSR	DKYGIK	120	72	1.42E-06	10	1.33E-13	11	3.07E-07	8
Stx(1-262)	Cpx1	KFVEVMSEYNATQSDYR	YAKMEAER	129	57	3.68E-05	23	5.88E-07	8	1.83E-03	2
Stx(1-262)	Cpx1	TAKDSDDDDVTVTVDR	GSHMEFVMK	15	1	9.45E-07	19	6.59E-07	12		
Stx(1-262)	Cpx1	TAKDSDDDDVTVTVDR	QALGGATKDMGK	15	17	9.69E-03	13	8.60E-04	6		
Stx(1-262)	Cpx1	TAKDSDDDDVTVTVDR	MLGGDEEKDPDAAK	15	29	3.46E-06	14	2.48E-04	5		
Stx(1-262)	Cpx1	TAKDSDDDDVTVTVDR	DKYGIK	15	72	7.27E-05	14			8.65E-04	6
Stx(1-262)	Cpx1	KHSAILASPNPDEK	QALGGATKDMGK	60	17	1.69E-02	3	3.06E-03	4		
Stx(1-262)	Cpx1	LKSIEQSIEQEGLNR	GSHMEFVMK	97	1	6.74E-09	11	2.73E-10	7		
Stx(1-262)	Cpx1	LKSIEQSIEQEGLNR	QALGGATKDMGK	97	17	3.83E-04	11	1.37E-02	5		
Stx(1-262)	Cpx1	LKSIEQSIEQEGLNR	YAKMEAER	97	57	3.30E-05	23	1.40E-11	12		
Stx(1-262)	Cpx1	KFVEVMSEYNATQSDYR	QALGGATKDMGK	129	17	3.20E-03	12	1.12E-03	5		
Stx(1-262)	Cpx1	FVEVMSEYNATQSDYR	KAKYAK	135	54	4.54E-02	10			2.73E-02	2
Stx(1-262)	Cpx1	HSEIIKLENSIR	GSHMEFVMK	207	1	7.76E-05	8	1.68E-04	12		
Stx(1-262)	Cpx1	HSEIIKLENSIR	YAKMEAER	207	57			4.87E-03	4	6.52E-04	3
Stx(1-262)	Cpx1	TAKDSDDDDVTVTVDR	DPDAAKK	15	35	4.59E-03	10				
Stx(1-262)	Cpx1	IAENVEEVKR	YAKMEAER	58	57	1.91E-04	4				
Stx(1-262)	Cpx1	TKEELEELMSDIKK	YAKMEAER	86	57	1.83E-04	12				
Stx(1-262)	Cpx1	LKSIEQSIEQEGLNR	DKYGIK	97	72	6.44E-05	20				
Stx(1-262)	Cpx1	KFVEVMSEYNATQSDYR	MLGGDEEKDPDAAK	129	29	2.79E-04	8				
Stx(1-262)	Cpx1	KFVEVMSEYNATQSDYR	DKYGIK	129	72	3.38E-05	12				
Stx(1-262)	Cpx1	FVEVMSEYNATQSDYR	KAKYAK	137	54			1.65E-03	6		
Stx(1-262)	Cpx1	IEYNVEHAVDYVER	QALGGATKDMGK	238	16			2.04E-04	10		
Stx(1-262)	Cpx1	YQSKAR	DKYGIK	263	72			4.58E-02	1		
Stx(1-262)	SN25(CtoS)	TAKDSDDDDVTVTVDR	LKSSDAYK	15	99	9.87E-06	7	1.82E-03	3	5.39E-06	3
Stx(1-262)	SN25(CtoS)	KTQHSTLSR	NLKD LGK	120	82	3.22E-04	9	1.25E-08	8	6.48E-06	6
Stx(1-262)	SN25(CtoS)	KTQHSTLSR	LKSSDAYK	120	99	7.74E-06	10	1.36E-10	10	5.07E-08	9

protein 1	protein 2	sequence 1	sequence 2	residue 1	residue 2	replicate 1		replicate 2		replicate 3	
						score	# spectra	score	# spectra	score	# spectra
Stx(1-262)	SN25(CtoS)	TAKDSDDDDVTVTVDR	NLKDLGK	15	82	5.75E-03	9	2.14E-02	3		
Stx(1-262)	SN25(CtoS)	TAKDSDDDDVTVTVDR	SSGLFISPSNKLK	15	97	7.38E-03	5	1.68E-04	4		
Stx(1-262)	SN25(CtoS)	TAKDSDDDDVTVTVDR	KAWGNQDGVVASQPAR	15	106	2.18E-07	20			2.24E-04	1
Stx(1-262)	SN25(CtoS)	LKSIEQSIEQEEGLNR	LKSSDAYK	97	99	9.47E-06	6	2.83E-04	5		
Stx(1-262)	SN25(CtoS)	KFVEVMSEYNATQSDYR	NLKDLGK	129	82	6.47E-04	11	1.61E-03	5		
Stx(1-262)	SN25(CtoS)	KFVEVMSEYNATQSDYR	KAWGNQDGVVASQPAR	129	106	4.19E-07	7	1.23E-03	2		
Stx(1-262)	SN25(CtoS)	AVKYQSK	NLKDLGK	259	82			7.94E-05	5	4.59E-04	2
Stx(1-262)	SN25(CtoS)	TAKDSDDDDVTVTVDR	MLQLVEESKDAGIR	15	43	1.95E-03	3				
Stx(1-262)	SN25(CtoS)	TAKDSDDDDVTVTVDR	SSDAYKK	15	105	6.16E-03	6				
Stx(1-262)	SN25(CtoS)	KHSAILASPNPDEK	NLKDLGK	60	82			1.27E-02	2		
Stx(1-262)	SN25(CtoS)	KHSAILASPNPDEK	SSDAYKK	60	105	3.23E-03	6				
Stx(1-262)	SN25(CtoS)	LKSIEQSIEQEEGLNR	NLKDLGK	97	82			2.71E-03	4		
Stx(1-262)	SN25(CtoS)	KTQHSTLSR	IMEKADSNK	120	187			1.70E-06	12		
Stx(1-262)	SN25(CtoS)	KFVEVMSEYNATQSDYR	MLQLVEESKDAGIR	129	43	3.34E-03	6				
Stx(1-262)	SN25(CtoS)	KFVEVMSEYNATQSDYR	DLGKSSGLFISPSNK	129	86	7.31E-04	1				
Stx(1-262)	SN25(CtoS)	KFVEVMSEYNATQSDYR	SSGLFISPSNKLK	129	97	1.25E-03	9				
Stx(1-262)	SN25(CtoS)	IEYNVEHAVDYVER	NLKDLGK	238	82			3.06E-03	6		
Stx(1-262)	SN25(CtoS)	IEYNVEHAVDYVER	ADSNKTR	238	192			1.12E-01	2		
Stx(1-262)	Syb(1-96)	KHSAILASPNPDEK	VNVDKVLER	60	55	8.65E-03	6	1.12E-01	6	4.10E-01	2
Stx(1-262)	Syb(1-96)	LKSIEQSIEQEEGLNR	VNVDKVLER	97	55	6.79E-04	11	1.33E-03	5	3.52E-03	6
Stx(1-262)	Syb(1-96)	LKSIEQSIEQEEGLNR	DQKLSLDDR	97	62	2.58E-04	6	1.37E-03	2	6.45E-05	3
Stx(1-262)	Syb(1-96)	TAKDSDDDDVTVTVDR	DQKLSLDDR	15	62	1.83E-04	9	9.75E-03	2		
Stx(1-262)	Syb(1-96)	TAKDSDDDDVTVTVDR	VNVDKVLER	15	55	3.42E-03	7				
Stx(1-262)	Syb(1-96)	KHSAILASPNPDEK	DQKLSLDDR	60	62	2.99E-03	3				
Stx(1-262)	Syb(1-96)	LKSIEQSIEQEEGLNR	YWWKNLK	97	94			7.20E-03	4		
Stx(1-262)	Syb(1-96)	HSEIIKLENSIR	VNVDKVLER	207	55			8.05E-02	3		
Stx(1-262)	Syb(1-96)	IEYNVEHAVDYVER	VNVDKVLER	238	55			3.83E-02	1		
Syb(1-96)	Cpx1	ADALQAGASQFETSAAKLK	MLGGDEEKDPDAKK	86	29	3.82E-04	20	1.86E-03	16		
Syb(1-96)	Cpx1	ADALQAGASQFETSAAKLK	YAKMEAER	86	57	3.53E-03	6	5.31E-03	4		
Syb(1-96)	Cpx1	GSHMSATAATVPPAAPAGEGGP PAPPPNLTNR	KAIPPGCGDEPEEDESILDTVI K	1	102	5.06E-08	14				
Syb(1-96)	Cpx1	VNVDKVLER	YAKMEAER	55	57	1.53E-02	5				

protein 1	protein 2	sequence 1	sequence 2	residue 1	residue 2	replicate 1		replicate 2		replicate 3	
						score	# spectra	score	# spectra	score	# spectra
Syb(1-96)	Cpx1	VNVDKVLER	DKYGIK	55	72			5.89E-05	4		
Syb(1-96)	Cpx1	ADALQAGASQFETSAAKLK	DMGKMLGGDEEKDPDAAK	86	21	8.53E-04	7				
Syb(1-96)	SN25(CtoS)	VNVDKVLER	LKSSDAYK	55	99	1.93E-03	9	4.58E-08	10	6.25E-10	7
Syb(1-96)	SN25(CtoS)	VNVDKVLER	SSDAYKK	55	105	6.32E-03	9	3.19E-07	5	7.74E-15	7
Syb(1-96)	SN25(CtoS)	VNVDKVLER	IMEKADSNK	55	187	3.83E-04	14	2.03E-05	10	6.66E-13	8
Syb(1-96)	SN25(CtoS)	VNVDKVLER	NLKDLGK	55	82	7.88E-03	6	9.27E-03	4		
Syb(1-96)	SN25(CtoS)	DQKSELDDR	NLKDLGK	62	82	1.87E-05	6	5.68E-03	2		
Syb(1-96)	SN25(CtoS)	GSHMSATAATVPPAAPAGEGGP PAPPPNLTSNR	KAWGNQDGVVASQPAR	1	106	1.95E-10	23				
Syb(1-96)	SN25(CtoS)	VNVDKVLER	EAEKNLK	55	79	8.78E-02	4				
Syb(1-96)	SN25(CtoS)	DQKSELDDR	IMEKADSNK	62	187	1.35E-02	1				
Syb(1-96)	SN25(CtoS)	ADALQAGASQFETSAAKLK	NLKDLGK	86	82	1.20E-01	6				
Syb(1-96)	SN25(CtoS)	ADALQAGASQFETSAAKLK	DLGKSSGLFISPSNK	86	86	4.76E-04	4				
Syb(1-96)	SN25(CtoS)	ADALQAGASQFETSAAKLK	LKSSDAYK	86	99	7.65E-03	3				
Syb(1-96)	SN25(CtoS)	ADALQAGASQFETSAAKLK	KAWGNQDGVVASQPAR	86	106	1.11E-03	10				
Syb(1-96)	Stx(1-262)	VNVDKVLER	KTQHSTLSR	55	120	2.24E-04	6	4.64E-04	6	2.29E-05	5
Syb(1-96)	Stx(1-262)	VNVDKVLER	AVKYQSK	55	259	3.73E-02	4	3.19E-07	7	2.68E-06	4
Syb(1-96)	Stx(1-262)	ADALQAGASQFETSAAKLK	AVKYQSK	86	259	1.56E-06	43	7.21E-12	29	3.10E-20	15
Syb(1-96)	Stx(1-262)	VNVDKVLER	YQSKAR	55	263			1.45E-02	5	1.01E-06	6
Syb(1-96)	Stx(1-262)	DQKSELDDR	KTQHSTLSR	62	120	1.33E-03	1	6.17E-05	2		
Syb(1-96)	Stx(1-262)	ADALQAGASQFETSAAKLK	KTQHSTLSR	86	120	1.07E-04	15	4.20E-05	10		
Syb(1-96)	Stx(1-262)	ADALQAGASQFETSAAKLK	YQSKAR	86	263	1.57E-03	23	1.25E-06	22		
Syb(1-96)	Stx(1-262)	GSHMSATAATVPPAAPAGEGGP PAPPPNLTSNR	TAKDSDDDDVTVTVDR	1	15	1.04E-16	23				
Syb(1-96)	Stx(1-262)	GSHMSATAATVPPAAPAGEGGP PAPPPNLTSNR	KHSAILASPNDK	1	60	1.29E-22	70				
Syb(1-96)	Stx(1-262)	GSHMSATAATVPPAAPAGEGGP PAPPPNLTSNR	LKSIEQSIEQEEGLNR	1	97	1.29E-19	38				
Syb(1-96)	Stx(1-262)	GSHMSATAATVPPAAPAGEGGP PAPPPNLTSNR	KFVEVMSEYNATQSDYR	1	129	1.59E-19	39				
Syb(1-96)	Stx(1-262)	GSHMSATAATVPPAAPAGEGGP PAPPPNLTSNR	HSEIIKLENSIR	1	207	2.22E-17	24				
Syb(1-96)	Stx(1-262)	DQKSELDDR	YQSKAR	62	263					2.26E-05	2
Syb(1-96)	Stx(1-262)	ADALQAGASQFETSAAKLK	TAKDSDDDDVTVTVDR	86	15	7.39E-05	11				
Syb(1-96)	Stx(1-262)	ADALQAGASQFETSAAKLK	LKSIEQSIEQEEGLNR	86	97	1.30E-07	10				

						replicate 1		replicate 2		replicate 3	
protein 1	protein 2	sequence 1	sequence 2	residue 1	residue 2	score	# spectra	score	# spectra	score	# spectra
Syb(1-96)	Stx(1-262)	ADALQAGASQFETSAALKL	KFVEVMSEYNATQSDYR	86	129	9.57E-03	4				
intramolecular cross-links											
Cpx1	Cpx1	QALGGATKDMGK	GSHMEFVMK	17	1	1.05E-05	50	6.77E-08	79	5.95E-25	34
Cpx1	Cpx1	QALGGATKDMGK	YAKMEAER	17	57	8.81E-04	9	3.28E-04	13	5.63E-11	7
Cpx1	Cpx1	QALGGATKDMGK	DKYGIK	17	72	4.23E-02	10	7.39E-03	6	3.85E-07	8
Cpx1	Cpx1	YAKMEAER	DKYGIK	57	72	1.51E-13	13	2.40E-09	13	5.92E-18	14
Cpx1	Cpx1	GSHMEFVMK	YAKMEAER	1	57	3.57E-06	16	8.27E-16	31		
Cpx1	Cpx1	GSHMEFVMK	DKYGIK	1	72	4.21E-04	4			8.44E-19	3
Cpx1	Cpx1	DMGKMLGGDEEKDPDAAK	GSHMEFVMK	21	1	2.64E-06	25	9.32E-12	83		
Cpx1	Cpx1	DMGKMLGGDEEKDPDAAK	YAKMEAER	21	57	1.42E-04	12	2.42E-05	10		
Cpx1	Cpx1	MLGGDEEKDPDAAKKEEER	QALGGATKDMGK	29	17	6.06E-03	39	8.32E-05	34		
Cpx1	Cpx1	MLGGDEEKDPDAAK	YAKMEAER	29	57	1.06E-04	9	6.21E-04	7		
Cpx1	Cpx1	DMGKMLGGDEEKDPDAAK	GSHMEFVMKQALGGATK	21	9			3.05E-06	4		
Cpx1	Cpx1	MLGGDEEKDPDAAK	GSHMEFVMK	29	1	6.41E-05	33				
Cpx1	Cpx1	MLGGDEEKDPDAAK	DKYGIK	29	72			2.14E-03	3		
Cpx1	Cpx1	EAEAQAAMEANSEGLTRPK	KAKYAK	98	54	3.25E-01	2				
Cpx1	Cpx1	EAEAQAAMEANSEGLTRPKK	YAKMEAER	101	57			1.15E-04	5		
Cpx1	Cpx1	KAIPPGCGDEPEEEDESILDTVIK	YAKMEAER	102	57	2.58E-04	22				
Cpx1	Cpx1	KAIPPGCGDEPEEEDESILDTVIK	DKYGIK	102	72	5.12E-04	41				
SN25(CtoS)	SN25(CtoS)	MLQLVEESKDAGIR	NLKDLGK	43	82	9.37E-04	28	7.69E-05	23	3.08E-04	14
SN25(CtoS)	SN25(CtoS)	DLGKSSGLFISPSNK	LKSSDAYK	86	99	2.37E-06	40	4.78E-08	34	3.65E-22	16
SN25(CtoS)	SN25(CtoS)	DLGKSSGLFISPSNK	SSDAYK	86	105	9.07E-05	22	6.64E-07	12	8.28E-06	9
SN25(CtoS)	SN25(CtoS)	SSGLFISPSNK	NLKDLGK	87	82	6.98E-03	8	7.27E-03	10	3.08E-05	11
SN25(CtoS)	SN25(CtoS)	SSGLFISPSNK	NLKDLGK	93	82	3.91E-02	9	3.43E-02	15	3.53E-03	5
SN25(CtoS)	SN25(CtoS)	SSGLFISPSNKLK	SSDAYK	97	105	2.65E-08	55	3.36E-08	41	5.79E-20	44
SN25(CtoS)	SN25(CtoS)	KAWGNQDGVVASQPAR	EAEKNLK	106	79	1.63E-03	17	1.89E-05	7	2.37E-16	5
SN25(CtoS)	SN25(CtoS)	KAWGNQDGVVASQPAR	NLKDLGK	106	82	4.96E-07	38	7.70E-08	26	4.64E-16	25
SN25(CtoS)	SN25(CtoS)	KAWGNQDGVVASQPAR	SSGLFISPSNKLK	106	97	3.79E-07	55	7.02E-08	35	5.00E-16	7
SN25(CtoS)	SN25(CtoS)	KAWGNQDGVVASQPAR	LKSSDAYK	106	99	1.88E-09	57	1.12E-09	32	2.29E-21	24
SN25(CtoS)	SN25(CtoS)	KAWGNQDGVVASQPAR	IMEKADSNK	106	187	1.42E-05	25	1.83E-05	10	3.88E-11	4
SN25(CtoS)	SN25(CtoS)	IMEKADSNK	NLKDLGK	187	82	1.36E-02	7	8.57E-04	6	1.86E-03	4
SN25(CtoS)	SN25(CtoS)	IMEKADSNK	LKSSDAYK	187	99	1.77E-04	12	1.67E-06	10	1.88E-03	2

protein 1	protein 2	sequence 1	sequence 2	residue 1	residue 2	replicate 1		replicate 2		replicate 3	
						score	# spectra	score	# spectra	score	# spectra
SN25(CtoS)	SN25(CtoS)	MLQLVEESKDAGIR	SSDAYKK	43	105	4.42E-03	13	3.28E-05	12		
SN25(CtoS)	SN25(CtoS)	MLQLVEESKDAGIR	IMEKADSNK	43	187	5.94E-03	15	1.54E-03	14		
SN25(CtoS)	SN25(CtoS)	MLQLVEESKDAGIR	ADSNKTR	43	192	2.55E-01	7	9.94E-02	6		
SN25(CtoS)	SN25(CtoS)	NLKDLGK	SSDAYK	82	100			2.61E-03	3	7.32E-05	4
SN25(CtoS)	SN25(CtoS)	DLGKSSGLFISPSNK	MLQLVEESKDAGIR	86	43	8.51E-05	16	1.14E-05	3		
SN25(CtoS)	SN25(CtoS)	DLGKSSGLFISPSNK	IMEKADSNK	86	187	4.97E-03	11	8.24E-04	4		
SN25(CtoS)	SN25(CtoS)	SSGLFISPSNK	LKSSDAYK	87	99	1.53E-03	11	1.23E-05	7		
SN25(CtoS)	SN25(CtoS)	SSGLFISPSNKLK	NLKDLGK	97	82	2.37E-08	54	6.35E-09	44		
SN25(CtoS)	SN25(CtoS)	SSGLFISPSNKLK	SSDAYK	97	100			7.48E-05	9	6.43E-05	8
SN25(CtoS)	SN25(CtoS)	LKSSDAYK	EAEKNLK	99	79	2.60E-03	9	1.29E-07	9		
SN25(CtoS)	SN25(CtoS)	LKSSDAYK	NLKDLGK	99	82			5.87E-10	24	5.34E-28	32
SN25(CtoS)	SN25(CtoS)	KAWGNQDGVVASQPAR	MLQLVEESKDAGIR	106	43	5.36E-05	31	2.53E-05	16		
SN25(CtoS)	SN25(CtoS)	IMEKADSNK	SSDAYKK	187	105	1.29E-03	26	5.31E-05	7		
SN25(CtoS)	SN25(CtoS)	MLQLVEESKDAGIR	EAEKNLK	43	79	2.08E-02	18				
SN25(CtoS)	SN25(CtoS)	MLQLVEESKDAGIR	SSGLFISPSNKLK	43	97	1.74E-03	19				
SN25(CtoS)	SN25(CtoS)	VEEGMNHINQDMKEAEK	MLQLVEESKDAGIR	75	43	4.04E-06	30				
SN25(CtoS)	SN25(CtoS)	VEEGMNHINQDMKEAEK	NLKDLGK	75	82	1.24E-02	81				
SN25(CtoS)	SN25(CtoS)	VEEGMNHINQDMKEAEK	DLGKSSGLFISPSNK	75	86	1.20E-04	16				
SN25(CtoS)	SN25(CtoS)	VEEGMNHINQDMKEAEK	SSDAYKK	75	105	5.78E-05	10				
SN25(CtoS)	SN25(CtoS)	VEEGMNHINQDMKEAEK	KAWGNQDGVVASQPAR	75	106	4.48E-08	27				
SN25(CtoS)	SN25(CtoS)	VEEGMNHINQDMKEAEK	ATKMLGSG	75	204	8.80E-03	10				
SN25(CtoS)	SN25(CtoS)	SSGLFISPSNK	LKSSDAYK	93	99	1.17E-01	2				
SN25(CtoS)	SN25(CtoS)	SSGLFISPSNKLK	EAEKNLK	97	79	5.51E-04	16				
SN25(CtoS)	SN25(CtoS)	SSGLFISPSNKLK	SSDAYK	97	104			1.74E-02	9		
SN25(CtoS)	SN25(CtoS)	SSDAYKK	NLKDLGK	105	82					6.27E-16	15
SN25(CtoS)	SN25(CtoS)	KAWGNQDGVVASQPAR	SSGLFISPSNK	106	93			5.95E-03	1		
SN25(CtoS)	SN25(CtoS)	KAWGNQDGVVASQPAR	SSDAYK	106	100	1.91E-06	18				
SN25(CtoS)	SN25(CtoS)	KAWGNQDGVVASQPAR	ADSNKTR	106	192			2.75E-01	5		
SN25(CtoS)	SN25(CtoS)	ADSNKTR	NLKDLGK	192	82			4.28E-02	2		
Stx(1-262)	Stx(1-262)	TAKDSDDDDDVTVTVD R	GFIDKIAENVEEVK	15	49	4.23E-06	13	1.09E-05	5	1.10E-07	2
Stx(1-262)	Stx(1-262)	TAKDSDDDDDVTVTVD R	KHSAILASPND E K	15	60	1.04E-07	22	2.81E-07	12	8.72E-09	8
Stx(1-262)	Stx(1-262)	TAKDSDDDDDVTVTVD R	TKEELEELMSDIK K	15	86	2.88E-06	26	1.52E-05	16	8.01E-06	11

protein 1	protein 2	sequence 1	sequence 2	residue 1	residue 2	replicate 1		replicate 2		replicate 3	
						score	# spectra	score	# spectra	score	# spectra
Stx(1-262)	Stx(1-262)	TAKDSDDDDVTVTVDR	LKSIEQSIEQEEGLNR	15	97	4.94E-29	75	1.47E-08	13	9.29E-15	8
Stx(1-262)	Stx(1-262)	TAKDSDDDDVTVTVDR	SSADLR	15	112	7.08E-06	4	2.50E-03	5	6.66E-04	3
Stx(1-262)	Stx(1-262)	TAKDSDDDDVTVTVDR	KTQHSTLSR	15	120	5.56E-18	61	6.99E-21	44	8.58E-25	31
Stx(1-262)	Stx(1-262)	TAKDSDDDDVTVTVDR	AVKYQSK	15	259	1.20E-05	8	5.10E-07	8	8.79E-17	5
Stx(1-262)	Stx(1-262)	TAKDSDDDDVTVTVDR	YQSKAR	15	263	7.90E-04	13	8.87E-03	5	1.70E-03	5
Stx(1-262)	Stx(1-262)	GFIDKIAENVEEVKR	KHSAILASPNPDEK	49	60	1.60E-36	52	2.54E-12	52	3.81E-21	14
Stx(1-262)	Stx(1-262)	GFIDKIAENVEEVKR	TANKVR	49	91	2.73E-06	197	1.37E-11	162	2.90E-19	93
Stx(1-262)	Stx(1-262)	KHSAILASPNPDEK	TKEELEELMSDIK	60	75	8.86E-07	15	8.26E-10	28	5.52E-11	8
Stx(1-262)	Stx(1-262)	KHSAILASPNPDEK	TANKVR	60	91	1.08E-03	17	2.44E-03	13	2.21E-03	9
Stx(1-262)	Stx(1-262)	KHSAILASPNPDEK	KTQHSTLSR	60	120	9.78E-07	15	1.47E-09	12	1.60E-09	6
Stx(1-262)	Stx(1-262)	KHSAILASPNPDEK	HSEIIKLENSIR	60	207	4.43E-05	16	4.70E-07	13	9.78E-03	6
Stx(1-262)	Stx(1-262)	KHSAILASPNPDEK	AVKYQSK	60	259	2.66E-03	8	4.13E-04	7	4.69E-06	2
Stx(1-262)	Stx(1-262)	LKSIEQSIEQEEGLNR	KHSAILASPNPDEK	97	60	3.26E-14	29	5.88E-10	11	2.56E-03	7
Stx(1-262)	Stx(1-262)	LKSIEQSIEQEEGLNR	TKEELEELMSDIKK	97	86	7.66E-27	18	1.11E-08	43	5.39E-20	22
Stx(1-262)	Stx(1-262)	LKSIEQSIEQEEGLNR	TANKVR	97	91	1.77E-05	69	3.02E-04	49	3.08E-13	42
Stx(1-262)	Stx(1-262)	LKSIEQSIEQEEGLNR	KTQHSTLSR	97	120	9.17E-17	118	8.66E-19	93	8.89E-47	79
Stx(1-262)	Stx(1-262)	LKSIEQSIEQEEGLNR	TQHSTLSR	97	121	1.09E-05	15	3.47E-11	15	1.09E-14	10
Stx(1-262)	Stx(1-262)	LKSIEQSIEQEEGLNR	TQHSTLSR	97	125	3.52E-04	33	9.15E-06	33	6.83E-08	21
Stx(1-262)	Stx(1-262)	LKSIEQSIEQEEGLNR	HSEIIKLENSIR	97	207	2.98E-06	31	1.66E-07	25	2.41E-13	17
Stx(1-262)	Stx(1-262)	LKSIEQSIEQEEGLNR	AVKYQSK	97	259	6.92E-05	13	3.39E-05	10	8.63E-19	6
Stx(1-262)	Stx(1-262)	KTQHSTLSR	SSADLR	120	112	3.00E-06	25	2.77E-04	31	1.05E-09	14
Stx(1-262)	Stx(1-262)	KFVEVMSEYNATQSDYR	GSHMKDR	129	5	4.31E-04	27	5.77E-05	42	1.66E-11	31
Stx(1-262)	Stx(1-262)	KFVEVMSEYNATQSDYR	KHSAILASPNPDEK	129	60	3.90E-13	22	1.87E-07	10	1.54E-05	5
Stx(1-262)	Stx(1-262)	KFVEVMSEYNATQSDYR	TANKVR	129	91	5.52E-03	24	1.15E-03	14	2.10E-03	8
Stx(1-262)	Stx(1-262)	KFVEVMSEYNATQSDYR	KTQHSTLSR	129	120	4.30E-07	40	1.65E-09	28	1.05E-07	20
Stx(1-262)	Stx(1-262)	KFVEVMSEYNATQSDYR	AVKYQSK	129	259	3.93E-05	15	2.86E-06	13	9.28E-23	8
Stx(1-262)	Stx(1-262)	KFVEVMSEYNATQSDYR	YQSKAR	129	263	3.59E-03	30	3.75E-03	18	3.78E-06	17
Stx(1-262)	Stx(1-262)	HSEIIKLENSIR	KTQHSTLSR	207	120	2.03E-06	20	2.20E-08	18	7.53E-28	14
Stx(1-262)	Stx(1-262)	HSEIIKLENSIR	QALSEIETR	207	196	1.49E-01	6	1.14E-04	17	6.14E-05	4
Stx(1-262)	Stx(1-262)	IEYNVEHAVDYVER	AVKYQSK	238	259	2.90E-01	1	4.45E-08	16	3.35E-05	5
Stx(1-262)	Stx(1-262)	TAKDSDDDDVTVTVDR	GSHMKDR	15	5	2.11E-03	28	1.20E-05	44		
Stx(1-262)	Stx(1-262)	TAKDSDDDDVTVTVDR	TQHSTLSR	15	121			3.18E-04	1	4.43E-02	3

protein 1	protein 2	sequence 1	sequence 2	residue 1	residue 2	replicate 1		replicate 2		replicate 3	
						score	# spectra	score	# spectra	score	# spectra
Stx(1-262)	Stx(1-262)	TAKDSDDDDVTVTVDR	TQHSTLSR	15	125			2.79E-02	4	1.56E-01	2
Stx(1-262)	Stx(1-262)	GFIDKIAENVEEVK	KTQHSTLSR	49	120	6.45E-07	26	9.88E-08	17		
Stx(1-262)	Stx(1-262)	HSAILASPNPDEKTK	TANKVR	73	91	3.63E-02	5	1.71E-02	3		
Stx(1-262)	Stx(1-262)	HSAILASPNPDEKTK	KTQHSTLSR	73	120	4.99E-04	6	2.86E-04	5		
Stx(1-262)	Stx(1-262)	TKEELEELMSDIK	HSEIIKLENSIR	75	207	1.13E-04	3	2.54E-07	9		
Stx(1-262)	Stx(1-262)	TKEELEELMSDIKK	KHSAILASPNPDEK	86	60	4.56E-05	17	3.11E-07	25		
Stx(1-262)	Stx(1-262)	TKEELEELMSDIKK	KTQHSTLSR	86	120	4.45E-06	18	1.73E-08	26		
Stx(1-262)	Stx(1-262)	LKSIEQSIEQEEGLNR	GFIDKIAENVEEVK	97	49	2.20E-06	3	2.40E-03	1		
Stx(1-262)	Stx(1-262)	LKSIEQSIEQEEGLNR	TQHSTLSR	97	127	3.74E-03	12	1.09E-05	13		
Stx(1-262)	Stx(1-262)	LKSIEQSIEQEEGLNR	IEYNVEHAVDYVER	97	238	1.58E-05	4	1.19E-09	5		
Stx(1-262)	Stx(1-262)	SIEQSIEQEEGLNR	TANKVR	98	91	6.33E-03	10	1.87E-02	7		
Stx(1-262)	Stx(1-262)	KTQHSTLSR	AVKYQSK	120	259	1.06E-07	6	1.26E-05	1		
Stx(1-262)	Stx(1-262)	KFVEVMSEYNATQSDYR	TAKDSDDDDVTVTVDR	129	15	5.84E-31	208	2.78E-08	6		
Stx(1-262)	Stx(1-262)	KFVEVMSEYNATQSDYR	IAENVEEVKR	129	58	3.43E-28	321	1.23E-11	206		
Stx(1-262)	Stx(1-262)	KFVEVMSEYNATQSDYR	TKEELEELMSDIKK	129	86			8.51E-07	7	8.04E-07	3
Stx(1-262)	Stx(1-262)	KFVEVMSEYNATQSDYR	LKSIEQSIEQEEGLNR	129	97	8.78E-31	47			7.56E-04	2
Stx(1-262)	Stx(1-262)	KFVEVMSEYNATQSDYR	HSEIIKLENSIR	129	207	1.81E-05	21	1.33E-06	11		
Stx(1-262)	Stx(1-262)	HSEIIKLENSIR	SSADLR	207	112			4.58E-03	3	5.42E-06	2
Stx(1-262)	Stx(1-262)	HSEIIKLENSIR	AVKYQSK	207	259			3.28E-03	5	3.64E-03	5
Stx(1-262)	Stx(1-262)	IEYNVEHAVDYVER	TKEELEELMSDIKK	238	86			2.18E-05	4	8.31E-11	2
Stx(1-262)	Stx(1-262)	TAKDSDDDDVTVTVDR	TANKVR	15	91	5.25E-03	20	5.50E-02	10		
Stx(1-262)	Stx(1-262)	TAKDSDDDDVTVTVDR	IEYNVEHAVDYVER	15	238	3.65E-05	1	3.08E-08	7		
Stx(1-262)	Stx(1-262)	KHSAILASPNPDEK	AVSDTKK	60	255			6.63E-02	5	4.45E-04	2
Stx(1-262)	Stx(1-262)	TAKDSDDDDVTVTVDR	IAENVEEVKR	15	58	5.27E-04	14				
Stx(1-262)	Stx(1-262)	TAKDSDDDDVTVTVDR	HSAILASPNPDEKTK	15	73	4.44E-06	8				
Stx(1-262)	Stx(1-262)	TAKDSDDDDVTVTVDR	SIEQSIEQEEGLNR	15	98	3.07E-03	3				
Stx(1-262)	Stx(1-262)	TAKDSDDDDVTVTVDR	SIEQSIEQEEGLNR	15	102	4.97E-02	2				
Stx(1-262)	Stx(1-262)	TAKDSDDDDVTVTVDR	SSADLR	15	113	3.95E-05	10				
Stx(1-262)	Stx(1-262)	TAKDSDDDDVTVTVDR	TQHSTLSR	15	124	2.98E-02	6				
Stx(1-262)	Stx(1-262)	TAKDSDDDDVTVTVDR	HSEIIKLENSIR	15	207			8.34E-05	2		
Stx(1-262)	Stx(1-262)	TAKDSDDDDVTVTVDR	AVSDTK	15	252	2.56E-01	1				
Stx(1-262)	Stx(1-262)	TAKDSDDDDVTVTVDR	AVSDTKK	15	255	1.11E-04	11				

protein 1	protein 2	sequence 1	sequence 2	residue 1	residue 2	replicate 1		replicate 2		replicate 3	
						score	# spectra	score	# spectra	score	# spectra
Stx(1-262)	Stx(1-262)	DSDDDDDDVT/TVDR	KTQHSTLSR	17	120	8.08E-04	2				
Stx(1-262)	Stx(1-262)	GFIDKIAENVEEVK	GSHMKDR	49	5			1.82E-03	9		
Stx(1-262)	Stx(1-262)	GFIDKIAENVEEVK	YQSKAR	49	263	2.94E-02	6				
Stx(1-262)	Stx(1-262)	IAENVEEVK KRK	TQHSTLSR	58	121	1.50E-03	9				
Stx(1-262)	Stx(1-262)	KHSAILASPNPDEK	GSHMKDR	60	5	1.38E-02	7				
Stx(1-262)	Stx(1-262)	KHSAILASPNPDEK	YQSKAR	60	263	2.15E-03	10				
Stx(1-262)	Stx(1-262)	KHSAILASPNPDEK	TQHSTLSR	62	121			7.99E-03	7		
Stx(1-262)	Stx(1-262)	TKEELEELMSDIKK	GSHMKDR	86	5			1.31E-04	14		
Stx(1-262)	Stx(1-262)	TKEELEELMSDIKK	TANKVR	86	91			2.27E-06	250		
Stx(1-262)	Stx(1-262)	TKEELEELMSDIKK	HSEIIKLENSIR	86	207			3.14E-06	20		
Stx(1-262)	Stx(1-262)	LKSIEQSIEQEEGLNR	GSHMKDR	97	5			2.86E-06	26		
Stx(1-262)	Stx(1-262)	LKSIEQSIEQEEGLNR	HSAILASPNPDEKTK	97	73	1.62E-04	7				
Stx(1-262)	Stx(1-262)	LKSIEQSIEQEEGLNR	KTANKVR	97	87			3.18E-01	1		
Stx(1-262)	Stx(1-262)	KTQHSTLSR	TANKVR	120	91	2.80E-06	5				
Stx(1-262)	Stx(1-262)	KTQHSTLSR	QALSEIETR	120	196			2.17E-02	4		
Stx(1-262)	Stx(1-262)	TTTSEELEDMLESGNPAIFASGII MDSSISKQALSEIETR	TKEELEELMSDIKK	192	86	5.29E-21	2				
Stx(1-262)	Stx(1-262)	HSEIIKLENSIR	TANKVR	207	91	2.11E-01	9				
Stx(1-262)	Stx(1-262)	IEYNVEHAVDYVER	KTQHSTLSR	238	120			4.42E-10	1		
Syb(1-96)	Syb(1-96)	VNVDKVLER	YWWKNLK	55	94	6.39E-05	32	4.35E-04	20	1.32E-05	13
Syb(1-96)	Syb(1-96)	DQKSELDDR	VNVDKVLER	62	55	6.86E-11	65	7.53E-06	50	1.17E-15	31
Syb(1-96)	Syb(1-96)	ADALQAGASQFETSAAKLK	VNVDKVLER	86	55	3.85E-03	25	5.18E-04	10	6.33E-04	7
Syb(1-96)	Syb(1-96)	DQKSELDDR	YWWKNLK	62	94	4.05E-04	14	1.49E-07	9		
Syb(1-96)	Syb(1-96)	ADALQAGASQFETSAAKLK	YWWKNLK	86	94	5.47E-04	19			2.11E-08	11
Syb(1-96)	Syb(1-96)	GSHMSATAATVPPAAPAGEGGP PAPPPNLTNR	VNVDKVLER	1	55			3.78E-04	8		
Syb(1-96)	Syb(1-96)	GSHMSATAATVPPAAPAGEGGP PAPPPNLTNR	DQKSELDDR	1	62	2.01E-14	42				
Syb(1-96)	Syb(1-96)	VNVDKVLER	LSELDDR	55	64	6.49E-01	1				
Syb(1-96)	Syb(1-96)	ADALQAGASQFETSAAKLK	DQKSELDDR	86	62			1.85E-05	7		

Acknowledgment

First and foremost, I would like to express my sincere gratitude to Carla for her guidance, unwavering support and mentorship throughout my doctoral journey. Her inspiring enthusiasm for our research, her encouragement and valuable feedback were indispensable in shaping both my research and personal development. I am deeply grateful for her trust and the patience she had with me. The combination of scientific curiosity and the positive atmosphere created an environment that made this research not only successful but truly enjoyable. Thank you!

I also want to thank the second and third reviewer of this thesis for their reviews.

I am especially thankful to all my former and present group members for the supporting atmosphere, thoughtful discussions and funny breaks to keep the long lab days less long. Thank you for all the enjoyable ice cream, cake and sparkling wine breaks, Christmas and doctoral hat parties, retreats, conferences and tons of 'motivase'. It was and still is a pleasure to work with you. Special thanks go to Julian for never getting tired of answering my questions even after leaving the group, to Til for all his data analysis support and to Rita for helping me to reproduce the floatation and lipid overlay assays.

I also want to thank Reinhard Jahn for sharing the plasmids encoding the SNARE proteins and Cpx1 as well as discussing the data shown in this thesis. I am greatly thankful for the help of Bruno Voigt and Ralph Golbik with the circular dichroism measurements and the interpretation of the spectra. I gratefully acknowledge the financial support from Deutsche Forschungsgemeinschafts and Joachim Herz Stiftung, which was essential for the success of this project. Furthermore, I would like to acknowledge the scientific network of the RTG2467 about intrinsically disordered proteins. I am thankful to all RTG2467 students, post-docs and PIs for fruitful discussions and the great collaborations emerging from it. Special thanks go to Jochen Balbach and Maria Ott of my thesis advisory committee for their time and advice during my time at the Martin Luther University. I am also deeply grateful for being part of the HALOmem research centre including the groups of Milton T. Stubbs, Jochen Balbach, Kirsten Bacia and Panagiotis Kastritis. Thank you for the amazing and supportive environment and the awesome retreats.

Lastly, I would like to thank my family and friends for their continuous encouragement and understanding. Without their unconditional support, completing this journey would not have been possible. My deepest gratitude goes to my beloved husband, Janis. There are no words to describe how grateful I am to have you by my side.

Curriculum vitae

Name: Julia Bieber (geb. Hesselbarth)

Date of birth:

Place of birth:

Nationality:

Education

Since 10/2022

Doctoral candidate

Department for Chemistry – Biochemistry

Johannes Gutenberg University, Mainz (Germany)

Thesis: *Characterisation of synaptic proteins and their complexes using structural mass spectrometry*

Advisor: Prof. Dr. Carla Schmidt

07/2019 – 09/2022

Doctoral candidate

Institute for Biochemistry and Biotechnology, Research Training Group 2467, Martin Luther University, Halle (Germany)

Advisor: Prof. Dr. Carla Schmidt

10/2016 – 01/2019

Master of Science, Biochemistry

Institute for Biochemistry and Biotechnology

Martin Luther University, Halle (Germany)

Thesis: *Analyse von SNARE-Komplexintermediaten mittels struktureller Massenspektrometrie*

10/2010 – 10/2016

Bachelor of Science, Biochemistry

Institute for Biochemistry and Biotechnology

Martin Luther University, Halle (Germany)

Thesis: *Herstellung von homogenem spDltDtr mit C-terminalem Hexahistidin-tag*

Work

Since 10/2022	Research associate, Department for Chemistry – Biochemistry Johannes Gutenberg University, Mainz (Germany)
07/2019 – 09/2022	Research associate, Institute for Biochemistry and Biotechnology, Martin Luther University, Halle (Germany)
03/2019 – 06/2019	Research assistant, Institute for Biochemistry and Biotechnology, Martin Luther University, Halle (Germany)
06/2017 – 12/2017 11/2013 – 04/2016	Research assistant, Fraunhofer Centre for Silicon Photovoltaic CSP, Halle (Germany)

Awards and Grants

11/2023	Add on Fellowship for Interdisciplinary Life Science 2023 of the Joachim Herz Stiftung
09/2023	Travel grant of the EMBO Workshop ‘Mechanisms of membrane fusion’
12/2022	ASMS Sanibel Student Stipend award 2022
07/2022	Poster award of the Gordon Research Conference on Intrinsically Disordered Proteins 2022
03/2020	Poster award of the 53rd Annual Conference of the DGMS 2020

Publication list

- (6.) **J. Bieber** and C. Schmidt, *A critical reflection: Characterisation of Synaptobrevin-2-lipid interactions by native mass spectrometry using detergent-lipid micelles*. **Manuscript in preparation**
5. J. Bender, T. Kundlacz, L.S.P. Rudden, M. Frick, **J. Bieber**, M.T. Degiacomi, Carla Schmidt. *Ca²⁺-dependent lipid preferences shape synaptotagmin-1 C2A and C2B dynamics: Insights from experiments and simulations*. *Structure* (2024), doi: 10.1016/j.str.2024.07.017
4. B. Voigt, T. Bhatia, **J. Hesselbarth**, M. Baumann, C. Schmidt, M. Ott, J. Balbach. *The Prenucleation Equilibrium of the Parathyroid Hormone Determines the Critical Aggregation Concentration and Amyloid Fibril Nucleation*. *ChemPhysChem* (2023), doi.org/10.1002/cphc.202300439
3. **J. Hesselbarth** and C. Schmidt. *Mass spectrometry uncovers intermediates and off-pathway complexes for SNARE complex assembly*. *Communications Biology* (2023), doi: 10.1038/s42003-023-04548-0
2. L. Piersimoni, M. Abd el Malek, T. Bhatia, J. Bender, C. Brankatschk, J. Calvo Sánchez, G.W. Dayhoff, A. Di Ianni, J. O. Figueroa Parra, D. Garcia-Martinez, **J. Hesselbarth**, J. Köppen, L.M. Lauth, L. Lippik, L. Machner, S. Sachan, L. Schmidt, R. Selle, I. Skalidis, O. Sorokin, D. Ubbiali, B. Voigt, A. Wedler, A. An Jung Wie, P. Zorn, A. K. Dunker, M. Köhn, A. Sinz, V.N. Uversky. *Lighting up Nobel Prize-winning studies with protein intrinsic disorder*. *Cellular and Molecular Life Sciences* (2022), doi: 10.1007/s00018-022-04468-y
1. **J. Hesselbarth** and C. Schmidt. *Disorder-to-order transition of Synaptobrevin-2: Tracing the conformational diversity of a synaptic SNARE protein*. *Journal of structural biology* (2021), doi: 10.1016/j.jsb.2021.107824

Oral presentations

9. **GBM Compact: Focus on Proteomics**, Frankfurt am Main (05.09.-06.09.2023), Short talk, SNARE complex regulation by Complexin-1 - a structural mass spectrometry study
8. **33rd Sanibel Conference on Mass Spectrometry: Membrane Proteins and Their Complexes**, St. Pete Beach, Florida (USA) (19.01.-23.01.2023), Flash talk, SNARE complex regulation by Complexin-1 - a structural mass spectrometry study
7. **Sino-German MegaSyn Symposium 2022**, Frankfurt am Main (10.-12.10.2022), Flash talk, SNARE complex regulation by Complexin-1 - a structural mass spectrometry study
6. **RTG2467 Students Retreat 2022**, Weißenfels (04.05.-06.05.2022), Analysis of Synaptobrevin-2 lipid interactions
5. **HALOmem Retreat 2021**, Wittenberg (15.-17.07.2021), Synaptobrevin-2 – key player in neuronal signal transmission
4. **RTG2467 Students Retreat 2021**, online (28.-29.05.2021), Complexin-1 – Regulator of SNARE assembly
3. **RTG2467 Retreat 2020**, online (19.-21.11.2020), Native Mass Spectrometry
2. **HALOmem Statusseminar 2020**, online (12.11.2020), Regulation of SNARE complex assembly by Complexin-1
1. **RTG2467 Retreat 2019**, Wittenberg (22.-23.11.2019), Purification and characterisation of the soluble synaptobrevin-2 (1-96) domain – first insights

Poster presentations

14. **72nd ASMS Conference on Mass Spectrometry and Allied Topics**, Anaheim, California (USA) (02.06.-06.06.2024), Analysing lipid binding of Synaptobrevin-2 and Complexin-1: a preference for negatively charged lipids
13. **55th Annual Meeting of the DGMS**, Freising (10.03.-13.03.2024), Analysing lipid binding of Synaptobrevin-2 and Complexin-1: a preference for negatively charged lipids
12. **EMBO workshop - Mechanism of membrane fusion**, Göttingen (18.09.-22.09.2023), SNARE complex regulation by Complexin-1 - a structural mass spectrometry study
11. **GBM Compact: Focus on Proteomics**, Frankfurt am Main (05.09.-06.09.2023), SNARE complex regulation by Complexin-1 - a structural mass spectrometry study
10. **33rd Sanibel Conference on Mass Spectrometry: Membrane Proteins and Their Complexes**, St. Pete Beach, Florida (USA) (19.01.-23.01.2023), SNARE complex regulation by Complexin-1 - a structural mass spectrometry study
9. **Sino-German MegaSyn Symposium 2022**, Frankfurt am Main (10.-12.10.2022), SNARE complex regulation by Complexin-1 - a structural mass spectrometry study
8. **2st HALOmem International Meeting on Membrane Structure and Dynamics**, Halle (15.09.-16.09.2022), SNARE complex regulation by Complexin-1 - a structural mass spectrometry study
7. **Gordon Research Seminar & Conference - Intrinsically disordered proteins**, Les Diablerets (Switzerland) (25.06.-01.07.2022), SNARE complex regulation by Complexin-1 - a structural mass spectrometry study
6. **EMBO workshop - Recent Advances in Structural Biology of Membrane Proteins**, online (29.11.-01.12.2021), SNARE complex regulation by Complexin-1 - a structural mass spectrometry study

5. **65th Biophysical Society Annual Meeting**, online (22.-26.02.2021), SNARE complex assembly and its regulation by Complexin-1 - a CD spectroscopy and native mass spectrometry study
4. **53rd Annual Meeting of the DGMS**, Münster (01.-04.03.2020), Analysis of SNARE complex intermediates by structural mass spectrometry
3. **1st HALOmem International Meeting on Membrane Structure and Dynamics**, Halle (14.-15.11.2019), Analysis of SNARE complex intermediates by structural mass spectrometry
2. **9th Symposium on Structural Proteomics**, Berlin (03.-06.11.2019), Analysis of SNARE complex intermediates by structural mass spectrometry
1. **EMBO workshop - Tools for Structural Biology of Membrane Proteins**, Hamburg (07.- 09.10.2019), Analysis of SNARE complex intermediates by structural mass spectrometry

Affidavit

I hereby declare that this thesis was written independently and with no other sources and aids than quoted. Parts directly or indirectly obtained from foreign sources are indicated. In addition, material provided, or experiments performed by other persons are indicated. The submitted written version of the thesis corresponds to that on the electronic storage medium. Furthermore, I assure that this doctoral thesis has not been submitted as a thesis elsewhere. I have not submitted any other doctoral thesis before this thesis.

Mainz, 09.12.2024

Julia Bieber

Eidesstattliche Erklärung

Hiermit versichere ich, dass ich die vorliegende Arbeit selbstständig und ohne fremde Hilfe angefertigt und keine anderen als die angegebenen Quellen und Hilfsmittel verwendet habe. Die aus fremden Quellen direkt oder indirekt übernommenen Stellen sind als solche kenntlich gemacht. Ebenfalls sind alle von anderen Personen bereitgestellten Materialien oder erbrachten Experimente als solche gekennzeichnet. Die eingereichte schriftliche Fassung der Arbeit entspricht der auf dem elektronischen Speichermedium. Weiterhin versichere ich, dass die vorliegende Promotionsarbeit noch nicht als Abschlussarbeit an anderer Stelle eingereicht wurde. Ich habe vor dieser Arbeit keine andere Promotionsarbeit eingereicht.

Mainz, 09.12.2024

Julia Bieber